EXPERIMENTAL AND THEORETICAL ASPECTS OF HYDROCARBON ACTIVATION BY TRANSITION METAL IONS IN THE GAS PHASE

Thesis by

J. Bruce Schilling

In Partial Fulfillment of the Requirements

for the Degree of

Doctor of Philosophy

California Institute of Technology

Pasadena, California

1987

Submitted May 20, 1987

FOR MY PARENTS

AND ESPECIALLY FOR

NANCY

Acknowledgments

There have been a large number of people who have made my graduate stay at Caltech more pleasant and who have also contributed to the research presented in this thesis. I would especially like to thank my research advisor, Jack Beauchamp, for all of his help, both from the standpoint of financial support as well as his encouragement and almost constant stream of research ideas. Bill Goddard also deserves my thanks for allowing me to work on theoretical problems associated with my experimental research as well as for his insights into the nature of chemical bonding.

Past and present members of both the Beauchamp and Goddard groups have been good friends. They have provided fellowship as well as expertise in their various areas of work. John Low, Marv Goodgame, Emily Carter, and Mark Brusich deserve thanks for all of the discussions either dealing with chemistry or computers or both. Linda Halle and Mary Mandich first introduced me to the world of metal ion chemistry and ion beam spectroscopy. They, along with Maureen Hanratty, Jocelyn Schultz, Heonin Kang, Gary Kruppa, Dave Dearden, Karl Irikura, Seung Koo Shin, Bob Sweeney, and of course Maggie Tolbert, always kept things interesting both in the lab and the office. Maggie Tolbert deserves special thanks. While she was a member of the group, nothing was ever dull. Maggie also made lab work a little more enjoyable and was always there to discuss any part of the chemistry we were involved with.

I would also like to thank other members of the Caltech community, especially Tom Dunn, Tony Stark, and Guy Duremberg who were always there to help and never ran out of ideas. Thanks also to Adria McMillan for help in typing some of the theoretical portions of this thesis.

Lastly, I thank my mother and father for their support from the very beginning and also my wife, Nancy, who has definitely stood behind me through all of this work. Thank you very much for all of your love and support, even though it has taken longer than you ever thought it would.

Abstract

The reactions of several gas-phase metal cations with small hydrocarbons have been studied using ion beam mass spectrometric techniques. We also present several theoretical studies into the sigma bonding between the first and second row transition metal ions and H and CH_3.

Chapter II discusses the three cations, europium, praseodymium, and gadolinium in an attempt to understand the role of f electrons in the reactivity of gas-phase lanthanide ions. Eu^+ and Pr^+ are found to be unreactive with alkanes while Gd^+ readily activates both C–H and C–C bonds. The unreactive metals have only one non-4f valence electron. Oxidative addition of a C–H bond to these metals requires a strong bond to an f electron. Gd^+, with two non-4f valence electrons need not use the 4f electrons and is seen to be very reactive. This reactivity behavior indicates that the 4f electrons of the lanthanides play little role in alkane activation due to the formation of weak sigma bonds.

In Chapter III and VI, we discuss the reasons for the unreactivity of gas-phase chromium ions. Molybdenum ions which have a very similar electrons structure are found to activate C–H bonds of alkanes. The metal ions are studied from the standpoint of gas-phase reactivity as well as the theoretical description of the bonding in the hydride and dihydride ions. The two metals are found to differ greatly in the strength of the sigma bonds that they form to hydrogen. The oxidative addition of C–H and C–C bonds to Cr^+ is endothermic due to the extremely weak bonds formed to the metal ion.

Chapters IV and V report systematic, ab initio, generalized valence bond and configuration interaction calculations on the first and second row transition metal hydrides. The bonding in these systems is seen to depend on a number of factors including: (1) the electronic structure of the metal ions; (2) the sizes of the metal s and d orbitals and the effect on the intrinsic strength of the metal–hydrogen bond; and (3) the mediation of the intrinsic bond strengths by the loss of high spin exchange energy.

Chapter VII presents a theoretical comparison between the metal hydride ions and metal methyl ions. The present theoretical study indicates that for a variety of metal systems, the metal–hydrogen and metal–carbon bonds are very similar, both from the standpoint of metal orbital hybridization as well as bond dissociation energy.

TABLE OF CONTENTS

Dedication ii

Acknowledgements iii

Abstract iv

Chapter I. Introduction 1

References 5

Chapter II. Hydrocarbon Activation by Gas-Phase Lanthanide Cations: Interaction of Pr^+, Eu^+, and Gd^+ with Small Alkanes, Cycloalkanes, and Alkenes 8

References 54

Chapter III. What's Wrong with Gas-Phase Chromium? A Comparison of the Unreactive Cr^+ Cation with the Alkane Activating Molydenum Cation 57

References 89

Chapter IV. Theoretical Studies of Transition Metal Hydrides: II. CaH^+ through ZnH^+ 92

References 127

Chapter V. Theoretical Studies of Transition Metal Hydrides: III. SrH^+ through CdH^+ 129

References 174

Chapter VI. Theoretical Studies of Transition Metal Hydrides: IV. Comparison of the Transition Metal Dihydride Ions CrH_2^+ and MoH_2^+ 176

References 211

Chapter VII. Theoretical Studies of Transition Metal Methyl Ions, MCH_3^+: M = Sc, Cr, Mn, Zn, Y, Mo, Tc, Pd, and Cd . 214

References 247

CHAPTER I

INTRODUCTION

Much has been learned about the reactivity of atomic, gas-phase metal cations with hydrocarbons since it was first reported that Fe^+ activates C–H and C–C bonds of alkanes.[1] Ion cyclotron resonance, fourier transform mass spectrometry (FTMS), and ion beam mass spectrometry have been used to study the reactivity of an ever increasing number of metal ions. These include Group 8–10 metal ions of the first row (Fe^+, Co^+, and Ni^+),[2–11] the early first row metals (Ti^+ and V^+),[7,12,13] the second row Group 8–10 metals (Ru^+, Rh^+, and Pd^+),[14–16] the Group 3 metals (Sc^+, Y^+, and La^+),[17–18] and the third row metal ion, Ta^+.[19]

Very different product distributions have been observed for the ions depending upon the accessible electronic states and the metal bonding characteristics. The first row Group 8–10 metals[2–11] have been shown to yield metal–alkene products in processes which involve cleavage of both C–H and C–C bonds of alkanes and elimination of hydrogen or small alkanes such as methane and ethane. In contrast, the second row metals, Ru^+ and Rh^+, yield almost exclusively, products resulting from elimination of one or more molecules of hydrogen.[14–16] At the time of its publication, the reactivity of Sc^+ was seen to be unique in the fact that metal–dialkyl complexes were formed as products.[17] An example of this is the formation of $Sc(CH_3)_2^+$ in the reaction with n-butane. Recently published results of products formed on reaction of Y^+ and La^+ with alkanes[18] also show the dialkyl products for these metals, although multiple dehydrogenation becomes increasingly important proceeding from the first to the third row.

The proposed reaction pathways for the reaction of the bare, gas-phase metal ions involve the initial formation of an ion-molecule interaction complex, insertion of the metal into either a C–H or C–C bond of the hydrocarbon, β–hydrogen or β–alkyl shift onto the metal center and elimination of a small neutral molecule such as hydrogen, an alkane, or an alkene. In all of these processes, an important feature is the strength of the bonds formed between the metal ion and either hydrogen, alkyl groups, or the π systems of alkenes. An understanding

of the bond strengths and the types of metal orbitals necessary to form strong bonds is essential for prediction of reactivity, understanding the reaction pathways, and explaining the product distributions. Ion beam mass spectroscopy has been a valuable tool for studying the thermodynamic aspects of metal ion reactions. Determination of thresholds for endothermic reactions has led to values of bond dissociation energies for the metal hydrides, methyls, methylenes, and oxides.[12,20-30] Recent photodissociation studies using FTMS have also yielded estimates for various metal bond dissociation energies.[31-32] There have also been several recent theoretical studies of metal ion species.[33-40] Theoretical calculations are useful in providing a check on the bond dissociation energies which have been determined experimentally as well as for their insight into the nature of the bonds formed to the metal ions. In this light, we present in Chapters IV–VII, theoretical studies into the nature of sigma bonds between metal ions and H and CH_3, model systems for the larger alkane interactions. The systematic studies of the first and second row metal hydrides should be useful for the continued refinement of the experimental results, especially in deconvoluting the reaction cross sections between excited state and ground state metal ions.

The experimental work presented here involves two parts: a comparison of the reactivity of the first and second row metals, Cr^+ and Mo^+; and the first look at the reactivity of the gas-phase lanthanide cations. In both cases, the energetics of C–H insertion play a crucial role. Cr^+ is found to be extremely unreactive while the electronically similar Mo^+ activates the C–H bonds of alkanes. This comparison of reactive versus unreactive species points out the importance of the strength of metal sigma bonds and the initial insertion step in the metal ion reactions. Cr^+ is found to be unreactive due to the very weak bonds it forms, causing the oxidative addition of a C–H bond to the metal center to be endothermic.

Recent condensed phase studies have shown that several lanthanide complexes are very active olefin polymerization catalysts.[41-42] $Cp^*_2LuCH_3$

($Cp^* = C_5Me_5$) has also been observed to activate many types of C–H bonds, including those in methane.[42] We have thus studied the reaction of three gas-phase lanthanide ions with alkanes and alkenes in an effort to determine both the reactivity of the lanthanides as well as the role of the f electrons in their reactions. Pr^+ ($4f^36s^1$) and Eu^+ ($4f^76s^1$), with ground state electron configurations representative of most of the lanthanides, are very unreactive with alkanes. Gd^+ ($4f^75d^16s^1$) readily activates C–H and C–C bonds in alkanes and shows product distributions which are quite similar to Sc^+. The unreactivity of metals which must use f electrons in bonding indicates that sigma bonds formed to these orbitals are weak and that the initial insertion into C–H or C–C bonds is endothermic. The reactivity of Gd^+ is thus mostly due to the 5d and 6s electrons and the metal reacts in a very similar fashion to the Group 3 metals which contain two valence electrons.

References

(1) Allison, J.; Freas, R. B.; Ridge, D. P. *J. Am. Chem. Soc.* **1979**, *101*, 1332.

(2) Armentrout, P. B.; Halle, L. F.; Beauchamp, J. L. *J. Am. Chem. Soc.* **1981**, *103*, 6624.

(3) Armentrout, P. B.; Beauchamp, J. L. *J. Am. Chem. Soc.* **1981**, *103*, 6628.

(4) Halle, L. F.; Houriet, R.; Kappes, M. M.; Staley, R. H.; Beauchamp, J. L. *J. Am. Chem. Soc.* **1982**, *104*, 6293.

(5) Halle, L. F.; Armentrout, P. B.; Beauchamp, J. L. *Organometallics* **1982**, *1*, 963.

(6) Houriet, R.; Halle, L. F.; Beauchamp, J. L. *Organometallics* **1983**, *2*, 1818.

(7) Byrd, G. D.; Burnier, R. C.; Freiser, B. S. *J. Am. Chem. Soc.* **1982**, *104*, 3565.

(8) Jacobson, D. B.; Freiser, B. S. *J. Am. Chem. Soc.* **1983**, *105*, 736.

(9) Jacobson, D. B.; Freiser, B. S. *J. Am. Chem. Soc.* **1983**, *105*, 5197.

(10) Jacobson, D. B.; Freiser, B. S. *J. Am. Chem. Soc.* **1983**, *105*, 7484.

(11) Jacobson, D. B.; Freiser, B. S. *J. Am. Chem. Soc.* **1983**, *105*, 7492.

(12) (a) Aristov, N.; Armentrout, P. B. *J. Am. Chem. Soc.* **1984**, *106*, 4065. (b) Aristov, N.; Armentrout, P. B. *J. Am. Chem. Soc.* **1986**, *108*, 1806.

(13) Tolbert, M. A.; Beauchamp, J. L. *J. Am. Chem. Soc.* **1986**, *108*, 7509.

(14) Byrd, G. D.; Freiser, B. S. *J. Am. Chem. Soc.* **1982**, *104*, 5944.

(15) Jacobson, D. B.; Freiser, B. S. *J. Am. Chem. Soc.* **1984**, *106*, 1159.

(16) Tolbert, M. A.; Mandich, M. L.; Halle, L. F.; Beauchamp, J. L. *J. Am. Chem. Soc.* **1986**, *108*, 5675.

(17) Tolbert, M. A.; Beauchamp, J. L. *J. Am. Chem. Soc.* **1984**, *106*, 8117.

(18) Huang, Y.; Wise, M. B.; Jacobson, D. B.; Freiser, B. S. *Organometallics* **1987**, *6*, 346.

(19) (a) Wise, M. B.; Jacobson, D. B.; Freiser, B. S. *J. Am. Chem. Soc.* **1985**, *107*, 1590. (b) Wise, M. B.; Jacobson, D. B.; Freiser, B. S. *J. Am. Chem. Soc.* **1985**, *107*, 6744.

(20) Armentrout, P. B.; Beauchamp, J. L.*Chem. Phys.* **1980**, *50*, 37.

(21) Armentrout, P. B.; Beauchamp, J. L. *J. Chem. Phys.* **1981**, *74*, 2819.

(22) Armentrout, P. B.; Halle, L. F.; Beauchamp, J. L. *J. Am. Chem. Soc.* **1981**, *103*, 6501.

(23) Armentrout, P. B.; Halle, L. F.; Beauchamp, J. L. *J. Chem. Phys.* **1982**, *76*, 2449.

(24) Mandich, M. L.; Halle, L. F.; Beauchamp, J. L. *J. Am. Chem. Soc.* **1984**, *106*, 4403.

(25) Georgiadis, R.; Armentrout, P. B. *J. Am. Chem. Soc.* **1986**, *108*, 2119.

(26) Elkind, J. L.; Armentrout, P. B. *Inorg. Chem.* **1986**, *25*, 1078.

(27) Elkind, J. L.; Armentrout, P. B. *J. Chem. Phys.* **1986**, *84*, 4862.

(28) Elkind, J. L.; Armentrout, P. B. *J. Phys. Chem.* **1985**, *89*, 5626.

(29) Elkind, J. L.; Armentrout, P. B. *J. Phys. Chem.* **1986**, *90*, 6576.

(30) Sunderlin, L.; Aristov, N.; Armentrout, P. B. *J. Am. Chem. Soc.* **1987**, *109*, 78.

(31) Hettich, R. L.; Freiser, B. S. *J. Am. Chem. Soc.* **1986**, *108*, 2537.

(32) Hettich, R. L.; Freiser, B. S. *J. Am. Chem. Soc.* **1986**, *108*, 5086.

(33) Schilling, J. B.; Goddard, W. A., III; Beauchamp, J. L. *J. Am. Chem. Soc.* **1986**, *108*, 582.

(34) Carter, E. A.; Goddard, W. A., III *J. Phys. Chem.* **1984**, *88*, 1485.

(35) Carter, E. A.; Goddard, W. A., III *J. Am. Chem. Soc.* **1986**, *108*, 2180.

(36) Carter, E. A.; Goddard, W. A., III *J. Am. Chem. Soc.* **1986**, *108*, 4746.

(37) Alvarado-Swaisgood, A. E.; Allison, J.; Harrison, J. F. *J. Phys. Chem.* **1985**, *89*, 2517.

(38) Alvarado-Swaisgood, A. E.; Harrison, J. F. *J. Phys. Chem.* **1985**, *89*, 5198.

(39) Mavridis, A.; Alvarado-Swaisgood, A. E.; Harrison, J. F. *J. Phys. Chem.* **1986**, *90*, 2584.

(40) Harrison, J. F. *J. Phys. Chem.* **1986**, *90*, 3313.

(41) (a) Jeske, G.; Lauke, H.; Mauermann, H.; Swepston, P. N.; Schumann, H.; Marks, T. J. *J. Am. Chem. Soc.* **1985**, *107*, 8091. (b) Jeske, G.; Schock, L. E.; Swepston, P. N.; Schumann, H.; Marks, T. J. *J. Am. Chem. Soc.* **1985**, *107*, 8103. (c) Jeske, G.; Lauke, H.; Mauermann, H.; Schumann, H.; Marks, T. J. *J. Am. Chem. Soc.* **1985**, *107*, 8111.

(42) Watson, P. L.; Parshall, G. W. *Acc. Chem. Res.* **1985**, *18*, 51, and references therein.

CHAPTER II

HYDROCARBON ACTIVATION BY GAS-PHASE LANTHANIDE CATIONS: INTERACTION OF Pr^+, Eu^+, and Gd^+ WITH SMALL ALKANES, CYCLOALKANES, AND ALKENES

Hydrocarbon Activation by Gas-Phase Lanthanide Cations: Interaction of Pr^+, Eu^+, and Gd^+ with Small Alkanes, Cycloalkanes, and Alkenes

J. Bruce Schilling and J. L. Beauchamp

Contribution No. 7590 from the

Arthur Amos Noyes Laboratory of Chemical Physics

California Institute of Technology, Pasadena, CA 91125

Abstract

We describe ion beam studies of the interaction of gas-phase lanthanide ions, praseodymium (Pr^+), europium (Eu^+), and gadolinium (Gd^+), with small alkanes, cycloalkanes, alkenes, and several oxygen-containing compounds. Only Gd^+ is seen to activate C–H and C–C bonds of alkanes. The ground state electronic configuration of Gd^+ ($4f^7 5d^1 6s^1$) is different from that of Pr^+ ($4f^3 6s^1$) and Eu^+ ($4f^7 6s^1$) leading to the conclusion that the f electrons play little part in the metal ion reactivity. Gd^+ can be thought of as having two valence electrons and indeed it reacts similarly to Sc^+ and the other Group 3 metal ions Y^+ and La^+ yielding products corresponding to elimination of hydrogen, alkanes, and alkenes. The elimination of neutral alkenes in the reaction of Gd^+ with alkanes results in the formation of metal dialkyl or hydrido-alkyl complexes. This finding leads to estimates for the sum of two Gd^+ sigma bond dissociation energies of between 110–130 kcal/mol. Gd^+ and Pr^+ react readily with alkenes yielding mostly dehydrogenation products along with smaller amounts of C–C bond cleavage products. Reactions of Gd^+ and Pr^+ with oxygen containing species such as nitric oxide, formaldehyde, acetaldehyde, and acetone yield primarily the metal oxide ions and provide a lower limit for $D(M^+–O)$ of 179 kcal/mol, in good agreement with literature values of $D(Pr^+–O) = 188.4 \pm 5.2$ kcal/mol and $D(Gd^+–O) = 181.0 \pm 4.4$ kcal/mol. In keeping with the strong metal sigma bonds, Gd^+ is also seen to readily react with formaldehyde to eliminate CO and form GdH_2^+.

Introduction

Studies of gas-phase atomic transition metal ions have shown that many of these systems are very reactive in the activation of both C–H and C–C bonds in small alkanes, cycloalkanes, alkenes, and other organic molecules. While studies have expanded to include most of the first[1–6] and second[7–9] row metals and a few of the third row transition series,[9–11] the reactivity of many of the heavier metals is still unknown. Both experimental[12] and theoretical[13–15] studies are gradually detailing the types of metal orbitals necessary to form strong metal ion–ligand bonds as well as the electronic structures best suited for activation of C–C and C–H bonds.

To further these basic investigations, the present paper details experiments involving three lanthanide ions, praseodymium (Pr^+), europium (Eu^+), and gadolinium (Gd^+), which, show a wide range of reactivity. The intent of the present study was to examine the role of f orbitals in the reactivity of the metal ions with organic molecules. Although the reactions of La^+ with hydrocarbons have recently been described,[9] no systematic gas-phase studies of the bare lanthanide series ions have been reported. Solution phase results for various $Cp^*_2MCH[Si(CH_3)_3]_2$ and $[Cp^*_2MH]_2$ (Cp^* = pentamethylcyclopentadiene; M = La, Nd, Sm, and Lu)[16] species along with $Cp^*_2LuCH_3$[17] have shown that these lanthanide complexes are very active ethylene polymerization catalyts. The $Cp^*_2LuCH_3$ species has also been shown to activate a variety of C–H bonds including alkyl–H, phenyl–H, benzyl–H, vinyl–H, and even the C–H bonds in methane.[17]

The most common ground state valence electronic structure of the lanthanide cations is $4f^{n-1}6s^1$ where n is the total number of valence electrons.[18] Ce^+ ($4f^15d^2$), Gd^+ ($4f^75d^16s^1$), and Lu^+ ($4f^{14}6s^2$) are exceptions to this. We have chosen two metal ions, Pr^+ ($4f^36s^1$) and Eu^+ ($4f^76s^1$), with the standard lanthanide configuration, one with three f electrons and one with a half full f shell. The f orbitals of the heavier lanthanides would be expected to participate

less in bonding to hydrogen or carbon due to the orbital contraction which occurs in moving from left to right along the row (the f orbitals contract faster than the 5d and 6s orbitals). The effects of the so-called "lanthanide contraction" can be seen by the examining the size of the orbitals of La^+ and Hf^+, as shown in Table I. We have also chosen to study Gd^+ which has a half full f shell and two non-f valence orbitals. Reactivity differences in these three metal ions should serve to detail the possible role of f electrons in the activation of small molecules by lanthanide ions.

Experimental Details

The ion beam apparatus has been described previously.[19] Briefly, bare metal cations are produced in the source as described below. The ions are accelerated, collimated into an ion beam, mass and energy selected, and injected into a collision cell holding a neutral reactant gas. The gas is at ambient temperature and is held at a constant pressure of two millitorr or less. This pressure range allows study of the reactions under single-collision conditions. Product ions scattered in the forward direction as well as unreacted metal ions are extracted from the collision cell and injected into a quadrupole mass spectrometer. The mass selected ions are then detected using a conversion dynode coupled with a channeltron electron multiplier. Ion counting as well as quadrupole control are achieved using an IBM-PC XT computer.

The metal ions in this study were produced by the process of surface ionization. A metal salt is heated in a small oven to $\sim$ 650° C, vaporized onto a hot rhenium ribbon filament, and surface ionized at a temperature between 2200 and 2400 K. The metal salts used in the present study were the metal trichlorides for all three of the metals studied. Praseodymium chloride was purchased as an anhydrous salt while the other two metal chlorides were obtained as hydrates. The two hydrates were placed in an oven at 120° C for several hours before use.

It is generally assumed that the ions resulting from surface ionization have

Table I

Selected Ionic Radii[a]

Ion	State	Configuration	R_s[b] (Å)	R_d[c] (Å)
Sc^+	^3D	$3d^14s^1$	2.02	1.01
Ti^+	^4F	$3d^24s^1$	1.89	0.87
Y^+	^3D	$4d^15s^1$	2.14	1.38
Zr^+	^4F	$4d^25s^1$	2.00	1.21
La^+	^3D	$5d^16s^1$	2.38	1.59
Hf^+	^4F	$5d^26s^1$	1.90	1.30

[a] Root mean square radii from Hartree-Fock calculations on the atomic ions, taken from reference 13. [b] R_s is the radius of the valence s orbital. [c] R_d is the radius of the valence d_{z^2} orbital.

an internal temperature equivalent to the surface temperature of the filament. A Maxwell-Boltzmann distribution over electronic energy levels thus gives an approximate distribution of the ions in the ground and low-lying excited electronic states. Table II presents some of the low-lying electronic states for the three metal ions, Pr^+, Eu^+, and Gd^+, along with the state splittings and an estimate of the beam population at a temperature of 2300 K. For Eu^+, only three states are present in any significant amount. The $a^9S°$ ($4f^76s^1$) and $a^7S°$ ($4f^76s^1$) states amount to over 99% of the beam while the $a^9D°$ ($4f^75d^1$) state accounts for over 0.5%. For Gd^+, a few more states contribute to the overall population of the beam. The $^{10}D°$ and $^8D°$ states ($4f^75d^16s^1$) make up approximately 89% of the beam, while $^{10}F°$ ($4f^75d^2$, 7.3%) and $^8S°$ ($4f76s^2$, 2.5%) are the other significant contributers to the remainder. Pr^+ has a large number of low-lying electronic excited states. Table II, which is by no means a complete list of electronic states represented in the beam, lists some of the more significant levels. It is likely that reactions of excited states will be observed in the experiments involving Pr^+.

Results and Discussion

Interaction of Eu^+ and Pr^+ with Alkanes and Cycloalkanes. We have looked at the low energy interaction (< 1 eV in the center-of-mass) of praseodymium and europium ions with a number of alkanes including propane, n-butane, and 2-methylpropane. Pr^+ was also studied with hexane, 2,3-dimethylbutane, heptane, and 2,4-dimethylpentane. With Eu^+, no reaction products are observed in the three cases examined. In addition, only very small amounts of adduct are observed (at maximum pressures which are lower than 2 mtorr). The praseodymium ion is also seen to be quite unreactive with all of the alkanes studied, although very small amounts of multiple hydrogen loss products are seen at low energies for almost all of the species. The product reaction cross sections are, however, all much less than 1 $Å^2$. The cross section versus energy data tend to indicate that there is a very small amount of product

Table II

Low-Lying M^+ Electronic States[a] and Beam Populations

Ion	Configuration	Term	E_{rel}(Low J)[b] (eV)	E_{rel}(Ave. J)[c] (eV)	Ion Beam Population[d] (%)
Eu^+	$4f^76s^1$	$a^9S°$	0.00	0.00	78.07
	$4f^76s^1$	$a^7S°$	0.21	0.21	21.37
	$4f^75d^1$	$a^9D°$	1.23	1.31	0.55
	$4f^75d^1$	$a^7D°$	2.09	2.11	0.01
	$4f^76p^1_{1/2}$	(7/2, 1/2)	2.95	2.98	0.00
	$4f^76p^1_{3/2}$	(7/2, 3/2)	3.24	3.31	0.00
Gd^+	$4f^75d^16s^1$	$^{10}D°$	0.00	0.00	78.64
	$4f^75d^16s^1$	$^8D°$	0.35	0.36	10.38
	$4f^76s^2$	$^8S°$	0.43	0.30	2.47
	$4f^75d^2$	$^{10}F°$	0.50	0.55	7.33
	$4f^86s^1$	^8F	0.99	1.11	0.44
	$4f^75d^16s^1$	$^8D°$	1.06	0.99	0.40
	$4f^86s^1$	^6F	1.23	1.33	0.10
	$4f^75d^16s^1$	$^6D°$	1.25	1.17	0.12
	$4f^75d^2$	$^{10}P°$	1.31	1.26	0.08
	$4f^75d^2$	$^8F°$	1.57	1.52	0.04
Pr^+	$4f^36s^1_{1/2}$	(9/2, 1/2)°	0.00	0.00	46.50
	$4f^36s^1_{1/2}$	(11/2, 1/2)°	0.20	0.18	22.34
	$4f^36s^1_{1/2}$	(13/2, 1/2)°	0.37	0.36	10.31
	$4f^35d^1$	$^5L°$	0.48	0.81	6.08
	$4f^35d^1$	$^5K°$	0.51	0.81	4.89
	$4f^36s^1_{1/2}$	(15/2, 1/2)°	0.55	0.56	4.52
	$4f^25d^2$	^5L	0.73	0.70	0.89
	$4f^25d^2$	^5I	0.90	0.87	0.26
	$4f^35d^1$	$^3I°$	0.92	0.96	0.46
	$4f^35d^1$	$^5I°$	0.92	1.21	0.53
	$4f^35d^1$	^5H	0.96	1.22	0.44

[a] Electronic state information taken from reference 18. [b] Relative energy determined using the splitting between the lowest j level for each state. [c] Relative energy determined using a weighted average over j levels for each state. [d] Populations determined using a Maxwell-Boltzman distribution over the energy levels at a temperature of 2300 K.

formed exothermically and to this is added endothermic processes as the energy is increased. The extremely low apparent cross sections for what appear to be exothermic processes indicate that the reactivity is probably due to one or more of the excited states in the Pr^+ beam.

Pr^+ has also been reacted with the cyclic alkanes, cyclopropane, cyclobutane, and cyclohexane. Cyclopropane reacts with Pr^+ to form two products $Pr(C_3H_4)^+$ and $PrCH_2^+$, both of which appear to be formed in endothermic processes with threshold energies below 0.25 eV. Reaction of Pr^+ with cyclohexane also shows a slightly endothermic reaction, the elimination of three molecules of H_2 and formation of $Pr(C_6H_6)^+$ (presumably a Pr^+–benzene complex). Reaction with cyclobutane produces $Pr(C_4H_6)^+$ in what is apparently an exothermic reaction. Since the apparent cross section at a collision energy of 0.25 eV is only 2.4 $Å^2$ it is again possible that this product is formed by reaction of Pr^+ excited states. A second product, $Pr(C_4H_4)^+$, is also observed but with endothermic behavior.

The only cyclic alkane that we have studied with Eu^+ is cyclopropane, expected to be one of the more reactive of the cycloalkanes due to its highly strained nature and weak C–C bonds. As with the linear alkanes, no reaction products are observed. Thus, both Eu^+ and Pr^+ are quite unreactive with cycloalkanes.

There are several possible explanations for the unreactive behavior of Pr^+ and Eu^+ with the smaller alkanes and cycloalkanes. The first step in a gas-phase ion-molecule reaction is presumably formation of a loose collision complex held together by interaction of the ion with either a permanent dipole or an ion-induced-dipole. Adduct formation may result if the interaction of the metal ion and neutral results in the formation of a complex which is sufficiently long-lived to undergo a stabilizing collision with another neutral gas molecule. In the Pr^+ experiments, the amount of adduct is seen to increase with the increasing size of the neutral hydrocarbon (Table III), consistent with an increase of the neutral polarizability and the subsequent increase in the ion induced dipole interaction

Table III

Adduct Production in the Reactions of

Pr^+ with Alkenes

Alkane	Apparent Adduct Cross Section[a] ($Å^2$)
Propane	0.00
n-Butane	0.04
2-Methylpropane	0.06
n-Hexane	0.26
2,3-Dimethylbutane	0.59
n-Heptane	2.46
2,4-Dimethylpentane	2.33

[a] From experiments at a center-of-mass collision energy of ~0.25 eV and neutral pressures between 1.2 and 1.6 mtorr.

with the metal ion. It is the chemical activation gained from this ion-molecule association which allows many ion-molecule reactions to proceed with no appreciable barrier to reaction. This is illustrated in Figure 1. Curve (a) shows a hypothetical interaction between a neutral metal and alkane with an activation barrier, E_a, for the insertion process. Curve (c) shows the same insertion process for a metal ion, where we assume that the barrier height remains constant. This barrier height is now measured with respect to the energy of the collision complex, $M(RH)^+$, which is lower in energy than the reactants due to the ion-molecule interaction energy. This chemical activation lowers the effective barrier to below the total energy of the reacting molecules, allowing the ion-molecule reaction to proceed as if no barrier existed. The early third row metals are fairly large (Table I). An estimate for the size of Eu^+ is given by averaging the 6s orbitals sizes of La^+ and Hf^+, giving 2.14 Å. Pr^+ would be expected to be closer to the size of La^+. Since the energy of association is due to electrostatic interactions, one might expect that for a large ion such as Pr^+ or Eu^+, the ion-neutral distance could be such that the energy lowering is not enough to decrease the barrier height to below the total energy of the system (a case such as this is shown as curve (b) in Figure 2).

A second possible explanation centers around the presence of the metal 6s electron in the ground electronic state (the ground state configurations are $4f^36s^1$ for Pr^+ and $4f^76s^1$ for Eu^+) as well as some of the low-lying states (see Table II). Armentrout et al., in work on the reactions of first row transition metal ions, have produced a set of rules predicting the metal ion reactivity based on the electronic configuration.[12] After the initial ion-molecule association, the reactions probably proceed via insertion into a C–H bond (C–C bond insertion is also possible). Assuming that insertion into a C–H bond involves donation of the C–H sigma electrons into an empty metal sigma orbital and also back-donation from a metal $d\pi$ orbital into the C–H σ^* orbital, metals with empty s or $d\sigma$ orbitals and occupied $d\pi$ orbitals would be expected to be more reactive.

Figure 1: Illustration of the effects of chemical activation in ion-molecule reactions, using a hypothetical insertion of either a neutral metal or metal ion into a C–H bond. Path (a) shows the neutral reaction with an activation barrier, Ea. Path (c) shows the effects of the interaction of the ionic charge with an induced dipole in the neutral, effectively lowering the barrier below the total energy of the reactants. Path (b) represents the situation when the chemical activation is not large enough to effectively overcome the activation barrier.

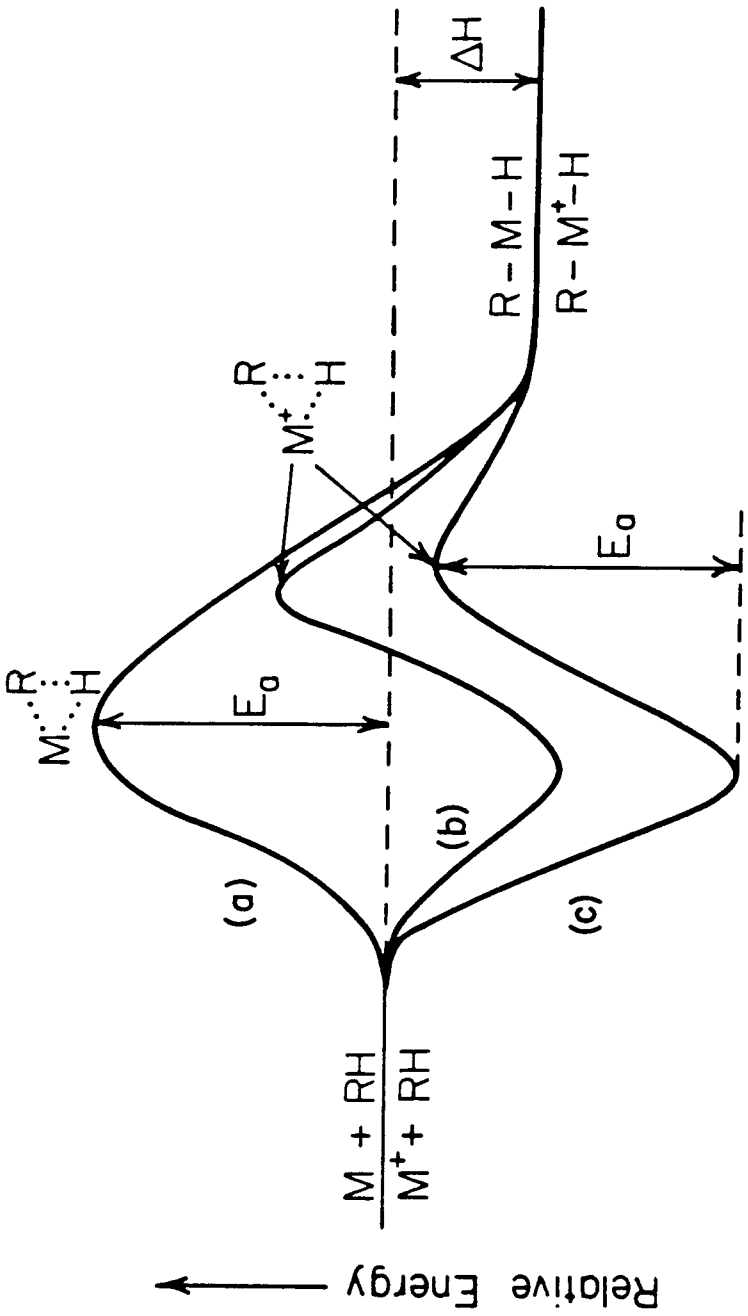
Relative Energy
M + RH
M+ + RH
(a)
(b)
(c)
R
M
H
Eo
R
M+
H
Eo
R-M-H
R-M+-H
ΔH

Occupied valence s orbitals, as on Pr^+ and Eu^+, would be expected to raise the energy of the system due to electron-electron repulsion with the C–H sigma bonding electrons. Thus, electronic states of the ions with an empty 6s orbital or empty 6s *and* $5d_{z^2}$ orbitals, will probably be more reactive than the ground electronic state which has the detriment of having an occupied 6s orbital.

For the C–H insertion process to be feasible, the sum of the M^+–C and M^+–H bond dissociation energies must of necessity be larger than the bond energy of the C–H bond being broken. Since almost all of the low-lying electonic states represented in the beam (for Pr^+ and Eu^+) have either an $4f^{n-1}6s^1$ or $4f^{n-1}5d^1$ valence electronic configuration, one of the metal sigma bonds must be made with a 4f electron. There are several drawbacks to bonding to f orbitals. First, the 4f orbitals are quite small and compact spatially when compared to the 5d and 6s orbitals. This is due to the lower principal quantum number of the f orbitals (making access to the orbitals difficult). Second, the six-lobed nature of the f orbitals could lower the strength of sigma bonds due to the smaller amount of electron density along any one bond axis (the f_{z^3} orbital would prove best for forming σ bonds just as the d_{z^2} orbital is best of the d orbitals for forming σ bonds).[20] Third, as the number of high-spin coupled f electrons increases, bond energies will decrease due to the loss of high-spin exchange energy between the electrons. Effects of this type are seen for the first row transition metals where the bonding choice is between the 4s orbital and the much smaller 3d orbitals. Bonding is preferentially to the s orbital, especially in the later metals which have very compact d orbitals.[13] Weak bonds are seen to metals such as Cr^+ (^6S, d^5) where $\sim$ 36 kcal/mol of exchange energy is lost on bonding to one of the d electrons. Similar effects, possibly even more pronounced, should be expected with the lanthanides. Thus, because of the nature of the f orbitals, one would not expect strong M^+–H or M^+–C bonds to be formed using electrons in these metal orbitals. Also, backbonding between f orbitals and σ^* or π^* orbitals would not be expected. Although one strong bond can possibly be formed to an s or

d orbital, without the formation of two strong metal sigma bonds, the oxidative addition of a C–H bond cannot take place and the metal ion will be seen to be unreactive. Higher energy states of the metals with more than one non-f valence electron should be reactive since they no longer must depend on forming a strong bond with an f electron.

Reactions of Gd^+ with Alkanes. Gadolinium ions form a striking contrast to the other two lanthanides, praseodymium and europium. While Pr^+ and Eu^+ are both very unreactive, Gd^+ is quite reactive with alkanes and shows a fairly wide spectrum of products, including activation of both C–H and C–C bonds with the elimination of hydrogen, alkanes, and alkenes. Table IV lists the reactions products, product distributions, and total reaction cross sections for the reaction of Gd^+ with C_1–C_6 alkanes. The reactivity of Gd^+ and the recently observed reactivity of La^+ helps to answer the question of why Pr^+ and Eu^+ are unreactive. Clearly, all of these ions are similar in size and thus a lowering of the ion-molecule association energy cannot totally explain the unreactivity. The very small amount of adduct ions formed by the unreactive ions tends to indicate that the adducts are not very long-lived (possibly indicating a small interaction energy), however, the *larger* La^+ ion *is* reactive. We thus conclude that the difference in reactivity is due to the fact that Gd^+ possesses two non-4f valence electrons and thus does not need to form sigma bonds utilizing f electrons. The $4f^7$ shell of electrons probably has little to do with the ion reactivity. Gd^+ can thus be considered to possess a valence electron configuration with two electrons (s^1d^1), very similar to the Group 3 metal ions, Sc^+, Y^+, and La^+. We have included the reaction product distributions for these three metals in Table IV.

Methane, Ethane, and Propane. Gadolinium follows the general trend of the transition metals in its unreactivity toward methane. Gd^+ does, however, react with ethane, although the reaction cross section is small (0.96 $Å^2$ at a collision energy of 0.09 eV). Two products are observed, as indicated in reactions (1) and

Table IV

Product Distributions for the Reactions of Gd^+ and Group 3 M^+ with Alkanes

Alkane	Total Reaction Cross Section ($Å^2$)[a]		Neutral(s) Lost	Product Ion	Relative Product Intensities (%)				
					Ion Beam		FTMS[c]		
	Gd^+	Sc^+[b]			Gd^+	Sc^+[b]	Sc^+	Y^+	La^+
CH_4			N.R.	N.R.					
C_2H_6	0.3	1.4	H_2	$M(C_2H_4)^+$	62		71	100	100
			$2H_2$	$M(C_2H_2)^+$	38		29		
C_3H_8[e]	6	11	H_2	$M(C_3H_6)^+$	69	68	73	75	85
			$2H_2$	$M(C_3H_4)^+$	4	5		25	15
			CH_4	$M(C_2H_4)^+$	28	27	27		
n-C_4H_{10}	110	151	H_2	$M(C_4H_8)^+$	34	44	54	12	4
			$2H_2$	$M(C_4H_6)^+$	27	16	16	47	77
			$3H_2$	$M(C_4H_4)^+$	tr[d]				
			CH_4	$M(C_3H_6)^+$	tr[d]	2			
			CH_4, H_2	$M(C_3H_4)^+$	tr[d]	2	2	3	
			C_2H_4	$M(C_2H_6)^+$	38	32	28	35	19
			C_2H_6	$M(C_2H_4)^+$	tr[d]	4			
			C_3H_6	$M(CH_4)^+$				3	
i-C_4H_{10}	105	152	H_2	$M(C_4H_8)^+$	50	69	86	17	
			$2H_2$	$M(C_4H_6)^+$	37	16	9	66	86
			CH_4	$M(C_3H_6)^+$	tr[d]	1			
			CH_4, H_2	$M(C_3H_4)^+$	tr[d]	1		5	
			C_2H_4	$M(C_2H_6)^+$	12	13	5	12	14
n-C_5H_{12}	172	429	H_2	$M(C_5H_{10})^+$	23	32	19	4	
			$2H_2$	$M(C_5H_8)^+$	26	7	8	34	75
			$3H_2$	$M(C_5H_6)^+$	tr[d]			6	3
			CH_4	$M(C_4H_8)^+$	1	8	9		
			CH_4, H_2	$M(C_4H_6)^+$	13	13	13	14	5
			C_2H_4	$M(C_3H_8)^+$	27	34	51	12	4
			C_2H_6	$M(C_3H_6)^+$	1	1		16	3
			C_2H_6, H_2	$M(C_3H_4)^+$		1		2	
			C_3H_6	$M(C_2H_6)^+$	8	4		10	10
			C_3H_8	$M(C_2H_4)^+$		tr[d]			
			C_3H_8, H_2	$M(C_2H_2)^+$				2	

Alkane	Total Reaction Cross Section ($Å^2$)[a]		Neutral(s) Lost	Product Ion	Relative Product Intensities (%)				
					Ion Beam		FTMS[c]		
	Gd^+	Sc^+[b]			Gd^+	Sc^+[b]	Sc^+	Y^+	La^+
i-C_5H_{12}	132		H_2	$M(C_5H_{10})^+$	9				
			$2H_2$	$M(C_5H_8)^+$	64				
			CH_4	$M(C_4H_8)^+$	2				
			CH_4, H_2	$M(C_4H_6)^+$	12				
			C_2H_4	$M(C_3H_8)^+$	4				
			C_3H_6	$M(C_2H_6)^+$	8				
neo-C_5H_{12}	1.5	129	H_2	$M(C_5H_{10})^+$	34	70	71	12	
			CH_4	$M(C_4H_8)^+$		17	14		
			CH_4, H_2	$M(C_4H_6)^+$	31	11	15	65	72
			$CH_4, 2H_2$	$M(C_4H_4)^+$	19				
			C_3H_6	$M(C_2H_6)^+$	16	2		23	28
n-C_6H_{14}	232	381	H_2	$M(C_6H_{12})^+$	5	1		1	
			$2H_2$	$M(C_6H_{10})^+$	19	9	22	10	12
			$3H_2$	$M(C_6H_8)^+$	10	4	2	30	53
			$4H_2$	$M(C_6H_6)^+$	12			3	
			CH_4	$M(C_5H_{10})^+$	tr[d]	2	4		
			CH_4, H_2	$M(C_5H_8)^+$	9	6		7	6
			$CH_4, 2H_2$	$M(C_5H_6)^+$	tr[d]			4	2
			C_2H_4	$M(C_4H_{10})^+$	8	20	7	2	2
			C_2H_6	$M(C_4H_8)^+$	11	28	36	14	4
			C_2H_6, H_2	$M(C_4H_6)^+$	12	14	20	8	5
			C_3H_6	$M(C_3H_8)^+$	11	14	9	6	7
			C_3H_8	$M(C_3H_6)^+$	tr[d]			6	4
			C_4H_8	$M(C_2H_6)^+$	2			8	3
			C_4H_{10}	$M(C_2H_4)^+$				1	
			C_4H_{10}, H_2	$M(C_2H_2)^+$					2

[a] Reaction cross sections measured at a center-of-mass collision energy of approximately 0.25 eV. [b] Reference 1. [c] Reference 9. [d] Trace amount of this product observed (less than 1%). [e] Some $Gd(CD_4)^+$ product is observed in the reaction with C_3D_8 although large changes in product distributions on deuteration (and the GdO^+ product) make it impossible to estimate the amount of $Gd(CH_4)^+$ formed in the reaction with C_3H_8.

(2).

$$Gd^+ + C_2H_6 \xrightarrow{62\%} Gd(C_2H_4)^+ + H_2 \quad (1)$$

$$\xrightarrow{38\%} Gd(C_2H_2)^+ + 2H_2 \quad (2)$$

These are suggested to be the single and double dehydrogenation products Gd^+–ethylene and Gd^+–acetylene, indicating that the bond energies for the two are greater than or equal to 33 and 75 kcal/mol, respectively.[21]

Gd^+ is more reactive with propane than with ethane (a total reaction cross section of 6.2 Å^2 at a collision energy of 0.25 eV versus 0.3 Å^2 for ethane at the same energy). Again, products are seen which correspond to loss of both one and two molecules of H_2, $Gd(C_3H_6)^+$ and $Gd(C_3H_4)^+$. The latter may be either a propyne or allene complex. Formation of propyne and allene from propane is endothermic by 69.2 and 70.5 kcal/mol, respectively. Reaction with propane-2,2-d_2 (Table V) yields an almost statistical ratio of H_2, HD, and D_2 loss products, indicating very rapid scrambling of the hydrogen atoms. In addition to the two hydrogen loss products, Gd^+–ethylene is formed via elimination of methane. This process can take place either through initial insertion into a terminal C–H bond followed by β–CH_3 transfer and reductive elimination of CH_4 or through initial C–C insertion followed by β–H transfer and methane elimination. With the labeled propane, an almost equal amount of CH_4 and CH_3D loss products are observed. Again, this indicates that some scrambling is taking place since the two mechanisms above predict loss of only CH_4.

As pointed out in the experimental details section, GdO^+ is formed in a reaction with the background oxygen. With normal propane, this obscures any $Gd(CH_4)^+$ product formed. Experiments using propane-d_8 show formation of $GdCD_4^+$. Reaction with propane-2,2-d_2 yields a 6:1 ratio of $GdCDH_3^+$ and $GdC_2H_2^+$. Any $GdCH_4^+$ product is obscured by the GdO^+ peak. The deuterated products are observed to be about as intense as the $Gd(C_2H_4)^+$ product. The overall product distributions are dependent on the extent of deuteration and it

Table V

Product Distributions in the Reactions of Gd^+ and Sc^+ with Deuterium-Labeled Alkanes

Neutral(s) Lost	Product Distribution (%)					
	Propane-2,2-d_2		2-Methylpropane-2-d_1		n-Butane-1,1,1,4,4,4-d_6	
	Gd^+[a]	Sc^+[b]	Gd^+[a]	Sc^+[b]	Gd^+[a]	Sc^+[b]
H_2	26.6	21	30.2	41	2.3	
HD	25.8	33	13.2	27	26.4	38
$2H_2$ (D_2)	7.0	2	26.0	10	1.8	4
H_2 + HD	8.6	3	16.7	6	1.8	
2HD (H_2 + D_2)	2.3	2			15.9	13
HD + D_2			1.1			
$2D_2$			0.5			
CH_4		17				7.0
CH_3D		12				6.2
C_2H_4	6.3		6.2	5	27.5	28
C_2H_3D	14.1	3	7.7	11	4.9	3
$C_2H_2D_2$	*[c]	7			1.8	3
C_2HD_3					13.3	8
C_2D_4					0.6	3

[a] Distributions measured at a collision energy of ~0.25 eV. [b] Distributions measured at a collision energy of ~0.5 eV, reference 1. [c] Information about the formation of $Gd(CH_4)^+$ is obscured by the presence of GdO^+.

is thus difficult to estimate the amount of $GdCH_4^+$ formed in reaction of C_3H_8. There are several possible structures, I–III, for the $Gd(CH_4)^+$ product.

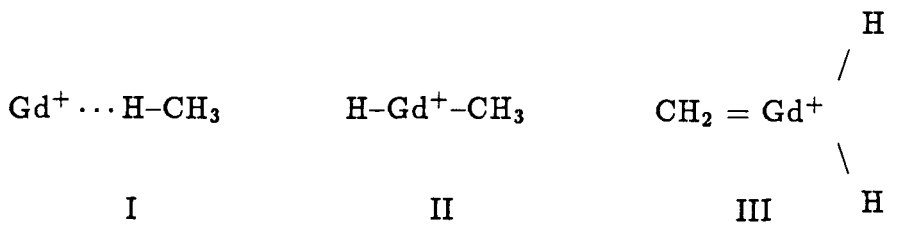

Formation of methane and ethylene from propane is endothermic by 19 kcal/mol. We can estimate the interaction energy of Gd^+ and methane. An estimate for the Gd^+ 6s orbital radius is 2.14 Å (as mentioned earlier for Eu^+). For second row metal hydrides, the metal–hydrogen bond length in a covalent bond is about 0.17 Å shorter than this.[12] Coupling this shortest Gd^+–H distance with the C–H bond distance (0.94 Å)[22] gives a minimum interaction distance of ~3 Å. Ion induced dipole interaction energies are given by equation (3),

$$V(r) = -\frac{e^2\alpha}{2R^4} = -\frac{166\alpha}{R_o^4} \text{ kcal/mol} \qquad (3)$$

where R_o is the internuclear separation in Å, α is the ligand polarizability in $Å^3$, and e is the unit charge of the electron.[23] Using the methane polarizability[24] of 2.60 $Å^3$, the interaction energy is calculated to be only a little over 5 kcal/mol, effectively ruling out structure I (bonding interaction between the metal ion and H could lower the energy slightly). For structure III to be feasible, the strength of two metal–hydrogen bonds plus the metal-methylene bond would have to be over 222 kcal/mol.[25] Considering that Gd^+ has only two non-f valence electrons to bond to the three species, this is highly unlikely. Thus, we feel that the $Gd(CH_4)^+$ species is a hydrido-methyl complex. The presence of this product at low energy gives an estimate for the sum of the Gd^+–H and Gd^+–CH_3 bonds. The process of producing C_2H_4, H, and CH_3 from propane is endothermic by 124.5 kcal/mol. The sum of the two sigma bonds must be greater than or equal to this value.

n-Butane and 2-Methylpropane. Figure 2 shows the reactions cross sections as a function of collision energy (at low interaction energies) for the reaction of Gd^+ with n-butane. The cross sections show the general behavior for exothermic reactions–decreasing as the collision energy increases. In experiments of Tolbert and Beauchamp on the reactions of Sc^+ with alkanes,[1] it was shown that Sc^+ forms products that involve sigma bonding two alkyl groups to the metal in addition to the normal metal–olefin products seen with other metals. This same process has also recently been seen in the other Group 3 metal ions Y^+ and La^+.[9] The reaction products for the reaction of Gd^+ with n-butane and 2-methylpropane (the distributions for 2-methylpropane are shown in parentheses) are shown in eq 4-6.

$$Gd^+ + C_4H_{10} \xrightarrow{34\%(50\%)} Gd(C_4H_8)^+ + H_2 \quad (4)$$

$$\xrightarrow{27\%(37\%)} Gd(C_4H_6)^+ + 2H_2 \quad (5)$$

$$\xrightarrow{38\%(12\%)} Gd(C_2H_6)^+ + C_2H_4 \quad (6)$$

As with Sc^+, Y^+, and La^+, a product is seen with the general formula $M(C_2H_6)^+$ which, for Sc^+ has been shown to be Sc^+–dimethyl. As with propane, reaction with deuterium labeled n-butane also shows a very small amount of the hydrido–methyl product (although this product appears to be much less important for the butane case). The other major products observed correspond to loss of one and two molecules of H_2.

With observation of the $Gd(CH_4)^+$ product in the reaction of propane, it is not surprising that "dialkyl" products are also observed with butane and the higher alkanes. As has been pointed out for other metals, the $Gd(C_2H_6)^+$ product could have several possible structures (IV–VI).

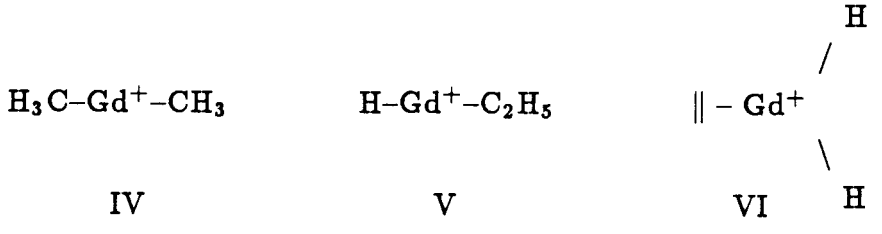

IV V VI

Figure 2: Low energy products in the reaction of Gd^+ with n-butane. The product reaction cross sections are plotted as a function of the center-of-mass collision energy between the metal ion and neutral.

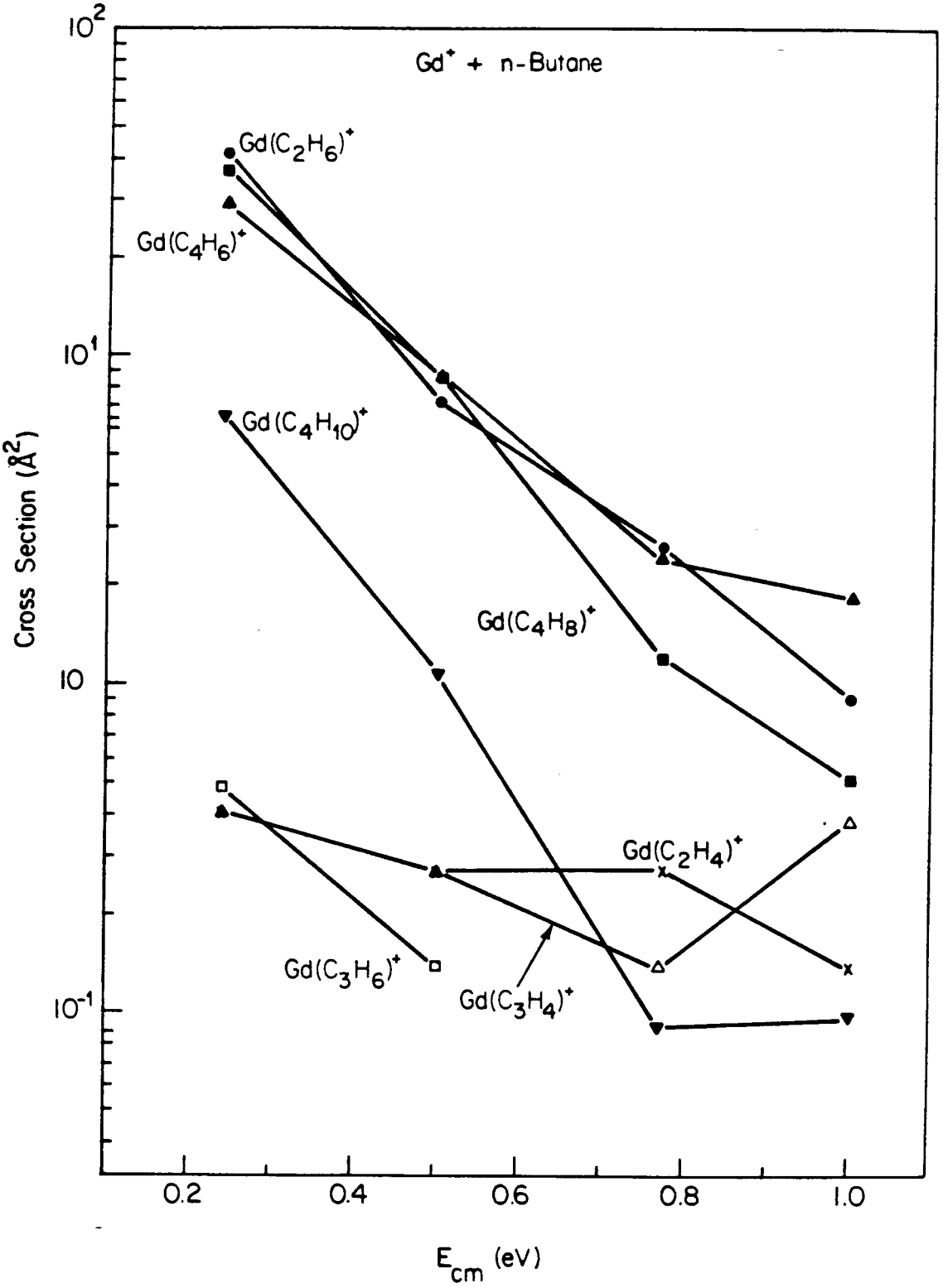
Gd+ + n-Butane
Gd(C2H6)+
Gd(C4H6)+
Gd(C4H10)+
Gd(C4H8)+
Gd(C2H4)+
Gd(C3H6)+
Gd(C3H4)+
Cross Section (Å2)
10^2
10^1
10
10^-1
0.2
0.4
0.6
0.8
1.0
Ecm (eV)

Structures V and VI were ruled out for Sc^+ due to energy considerations. Equations 7–9 show the energy requirements for the dissociation of butane to the respective fragments.

$$C_4H_{10} \longrightarrow 2CH_3 + C_2H_4 \qquad \Delta H^\circ = 113.0 \text{ kcal/mol} \qquad (7)$$

$$\longrightarrow H + C_2H_5 + C_2H_4 \qquad \Delta H^\circ = 121.6 \text{ kcal/mol} \qquad (8)$$

$$\longrightarrow 2H + 2C_2H_4 \qquad \Delta H^\circ = 159.5 \text{ kcal/mol} \qquad (9)$$

We can probably rule out structure VI. The formation of strong metal-ethylene bonds to the early transition metals is usually through the formation of a metallacyclopropane.[26] With the hydrogen atoms bound to the metal through the two valence electrons, none are left over for bonding to the C_2H_4 fragment and formation of the metallacycle. Structures IV and V are probably both possible from an energetic standpoint. Table V gives the product distributions seen for reaction with butane-1,1,1,4,4,4-d_6 and 2-methylpropane-2-d_2. The major neutrals lost giving the dialkyl type product are C_2H_4 and C_2HD_3 for n-butane and C_2H_4 and C_2H_3D for 2-methylpropane. Schemes I and II show possible mechanisms (including both C–H and C–C insertion processes) for the production of the major products for the two neutrals. The products seen to be most abundant can be produced in very straightforward mechanisms. The second major product in both cases is produced by scrambling of the hydrogens. Scheme III shows possible mechanisms for production of a hydrido-ethyl complex from butane. This results in the loss of $C_2H_2D_2$ which is seen as only a minor product in the spectra. Thus, as for Sc^+, the $Gd(C_2H_6)^+$ product is probably the dimethyl species. We will call products of this sort "dialkyl" products although it should be kept in mind that the hydrido-alkyl structures are also possible. With the larger alkanes, a larger number of possible structures exist and we will not attempt to detail them all. Comparison of n-butane to 2-methylpropane indicates that the amount of the dialkyl product observed for n-butane is greater. Formation of $Gd(C_2H_6)^+$ from 2-methylpropane is uphill two kcal/mol compared to

Scheme I

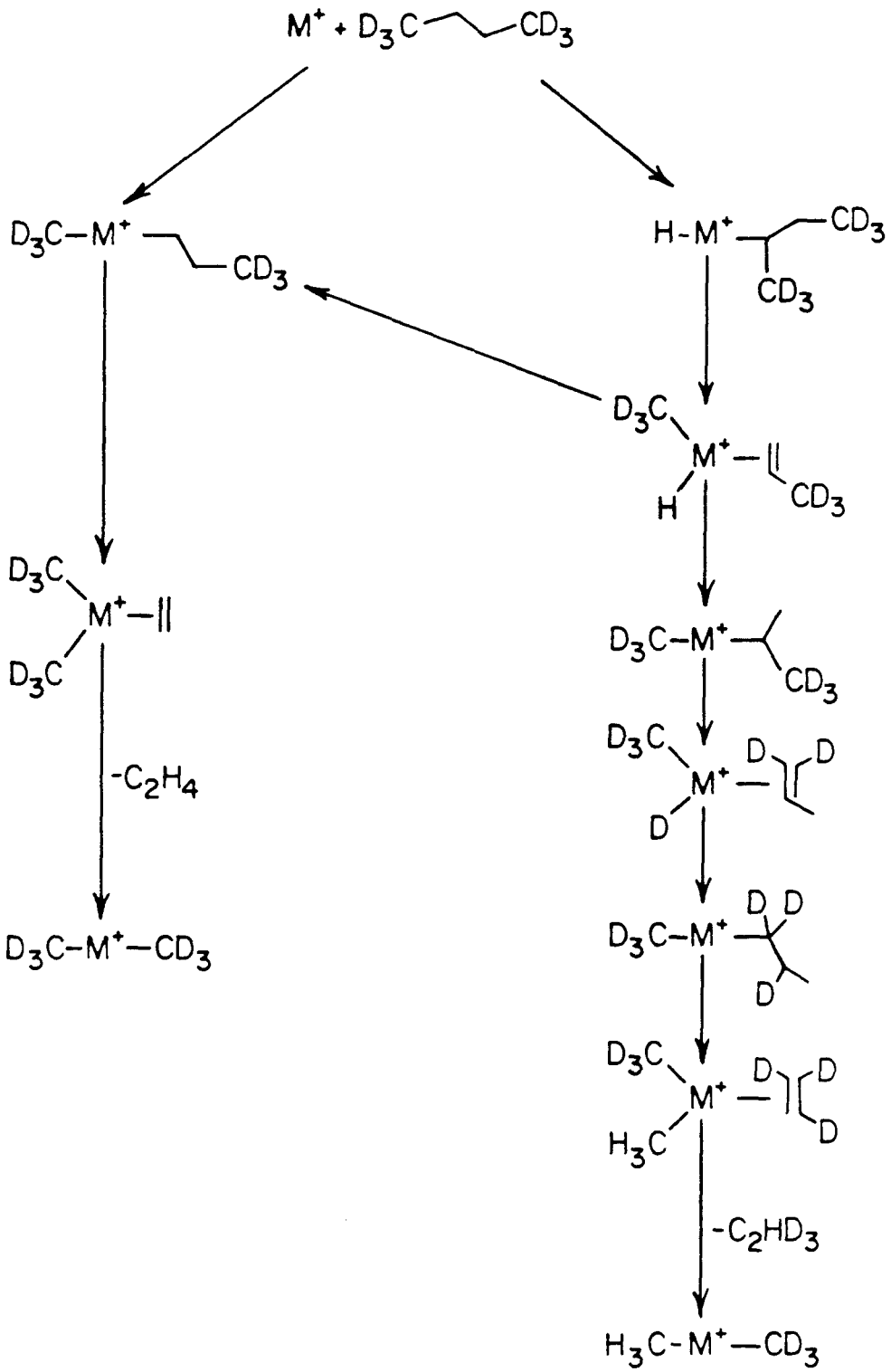
M+ + D3C CD3
D3C–M+ CD3
H–M+ CD3 CD3
D3C M+ H CD3
D3C M+ D3C
-C2H4
D3C–M+–CD3
D3C–M+ CD3
D3C M+ D D D
D
D3C–M+ D D D
D3C M+ H3C D D D
-C2HD3
H3C–M+–CD3

Scheme II

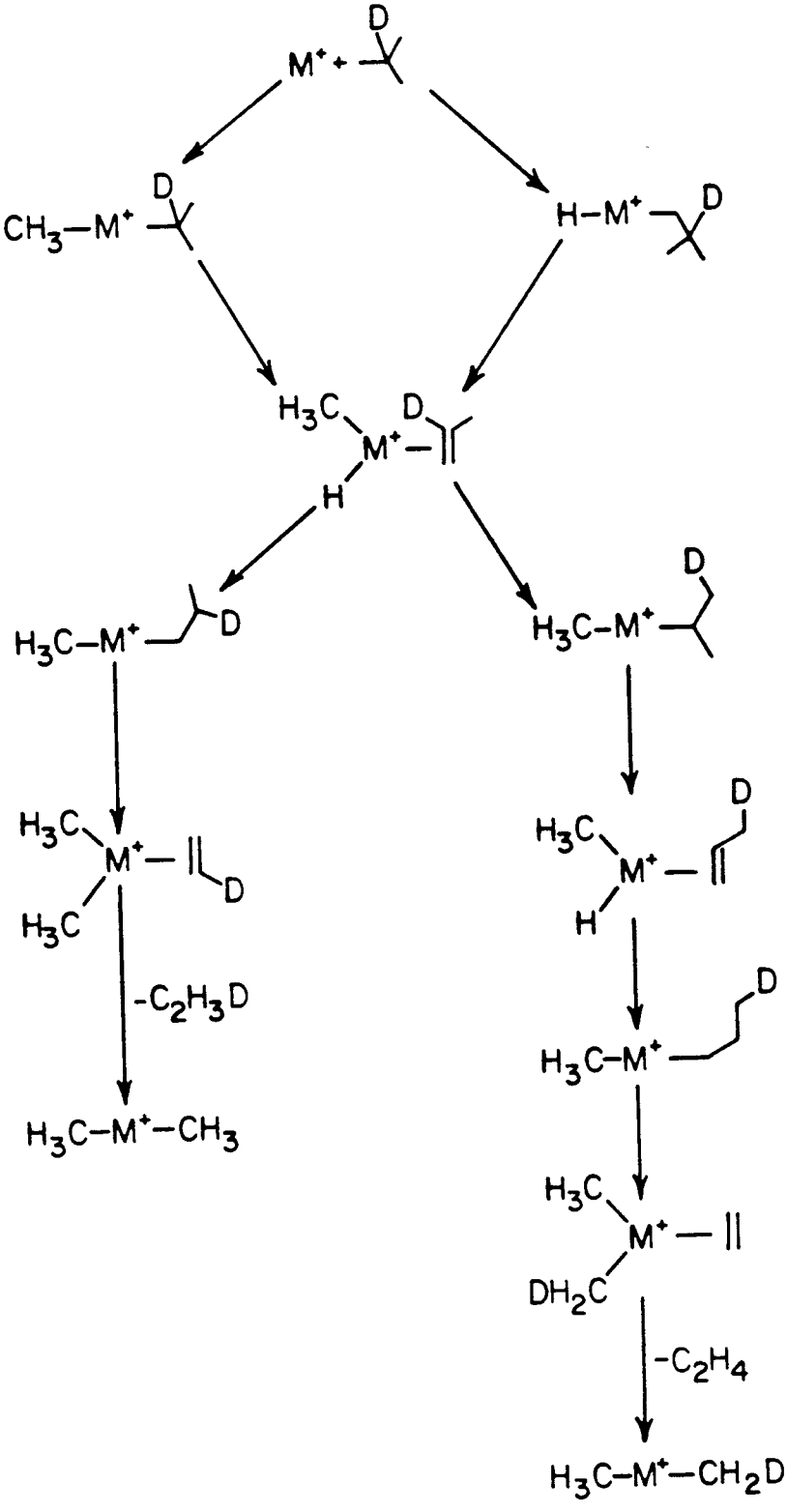
M+ + D
CH3–M+ D
H–M+ D
H3C D
M+
H
H3C–M+ D
H3C–M+ D
H3C
M+
D
H3C
-C2H3D
H3C–M+–CH3
H3C
M+
H
D
H3C–M+ D
H3C
M+
DH2C
-C2H4
H3C–M+–CH2D

Scheme III

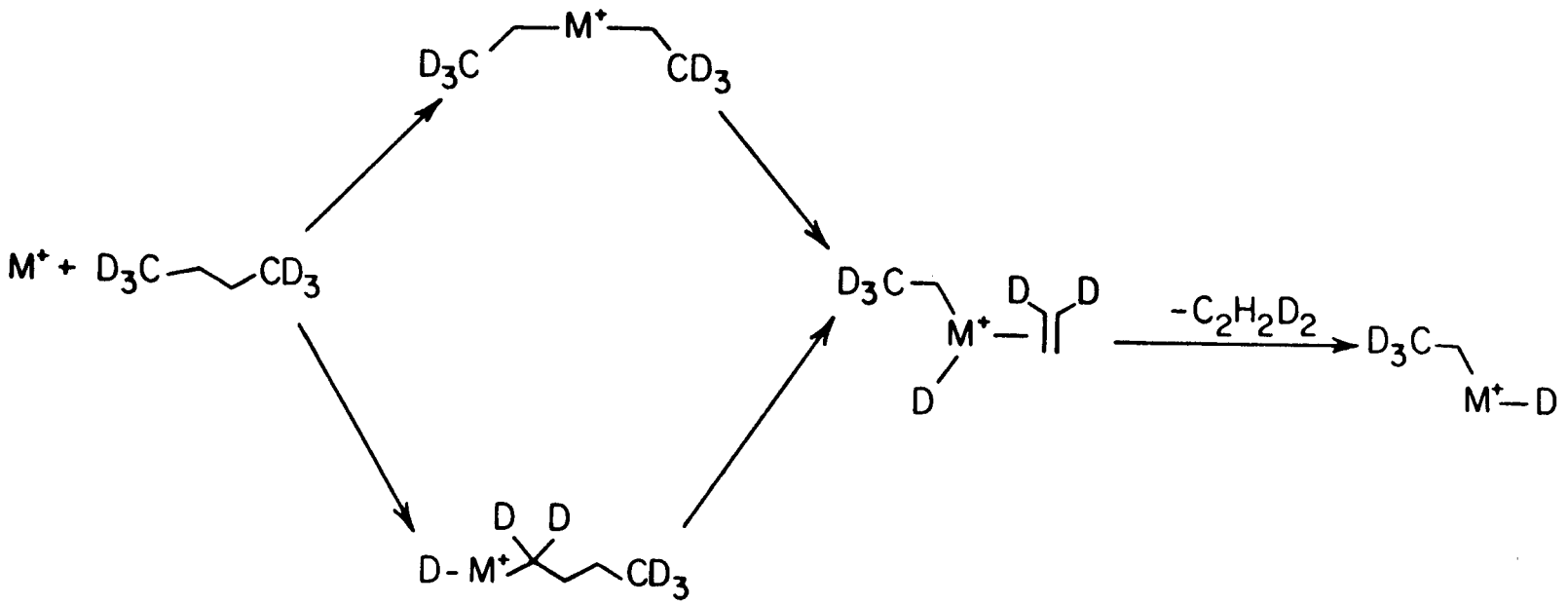

the similar process with n-butane. This would place a lower limit on the sum of the two metal–carbon sigma bonds of 115 kcal/mol.

n-Pentane, 2-Methylbutane, and 2,2-Dimethylpropane. The major products seen in the reaction of Gd^+ with n-pentane are shown in equations 10–16.

$$Gd^+ + \text{n-}C_5H_{12} \xrightarrow{23\%(9\%)} Gd(C_5H_{10})^+ + H_2 \quad (10)$$

$$\xrightarrow{26\%(64\%)} Gd(C_5H_8)^+ + 2H_2 \quad (11)$$

$$\xrightarrow{2\%(3\%)} Gd(C_4H_8)^+ + CH_4 \quad (12)$$

$$\xrightarrow{13\%(12\%)} Gd(C_4H_6)^+ + CH_4 + H_2 \quad (13)$$

$$\xrightarrow{27\%(4\%)} Gd(C_3H_8)^+ + C_2H_4 \quad (14)$$

$$\xrightarrow{1\%} Gd(C_3H_6)^+ + C_2H_6 \quad (15)$$

$$\xrightarrow{8\%(8\%)} Gd(C_2H_6)^+ + C_3H_6 \quad (16)$$

Again, elimination of one and two molecules of H_2 accounts for a significant percentage of the products although other unsaturated products such as Gd^+–butadiene are also seen arising from elimination of both methane and hydrogen. The other major products are dialkyl products. With the lengthening of the alkane chain, two dialkyls are seen, $Gd(C_3H_8)^+$ and $Gd(C_2H_6)^+$. The process of forming CH_3, C_2H_5, and C_2H_4 from n-pentane costs 109 kcal/mol while forming two methyl groups and propene requires 110 kcal/mol. The energy requirements of both processes are just slightly less than forming two methyl groups and ethylene from n-butane.

The product percentages for the Gd^+ reaction with 2-methylbutane are shown in parentheses in equations 10-16 for comparison with n-pentane. The major differences between the two are the large increase in double dehydrogenation and decrease in $Gd(C_3H_8)^+$ on changing the neutral to 2-methylbutane. Insertion of the metal into a C–C bond provides the most straightforward mechanisms for formation of the dialkyl-type products, although mechanisms involving initial C–H insertion (involving more extensive rearrangement) can also be drawn.

Schemes IV and V show possible mechanisms for the reactions with n-pentane and 2-methylbutane depending upon which C–C bond is initially cleaved. We see that for 2-methylbutane, formation of $Gd(C_3H_8)^+$ would necessarily call for initial insertion into the C_2–C_3 bond, the most sterically hindered C–C bond of the molecule. Insertion into the other C–C bonds leads to the $Gd(C_2H_6)^+$ product. For n-pentane, insertion into the C_1–C_2 bond leads to $Gd(C_3H_8)^+$ while insertion into the other C–C bond can lead to both products. It is normally assumed that the larger alkyl groups form stronger bonds due to better stabilization of the metal positive charge. This is a possible explanation for the predominance of the heavier product with n-pentane.

An even more drastic change is seen when 2-methylbutane is replaced with 2,2-dimethylpropane. The differences in reaction cross section for the three isomers are (at a collision energy of 0.25 eV) 171.7 $Å^2$ for n-pentane, 132.0 $Å^2$ for 2-methylbutane, and 1.5 $Å^2$ for 2,2-dimethylpropane. Thus, the reactivity of Gd^+ with 2,2-dimethylpropane is very low. Dehydrogenation of butane-1,1,1,4,4,4-d_6 by Sc^+ shows mostly loss of HD. This coupled with the facile dehydrogenation of 2,2-dimethylpropane and the strong sigma bonds formed by Sc^+ led to the proposal that the dehydrogenation was by a 1,3 process forming a metallacyclobutane product. Gd^+ also dehydrogenates labeled butane to give predominantly HD loss. However, the unreactivity with 2,2-dimethylpropane tends to indicate that the dehydrogenation process is by a 1,2 mechanism rather than the 1,3 mechanism evidenced by Sc^+. The studies on the reactivity of Y^+ and La^+ also suggest that the 1,3 dehydrogenation is less important for these metals as well.

n-Hexane. The reaction products observed in the reaction of Gd^+ with n-hexane are given in Table IV. The distribution is fairly evenly spread between ten major products with several minor products also seen. Dehydrogenation products account for almost 50% of the reaction. Elimination of from one to four molecules of H_2 are seen, the latter possibly forming a complex between

Scheme IV

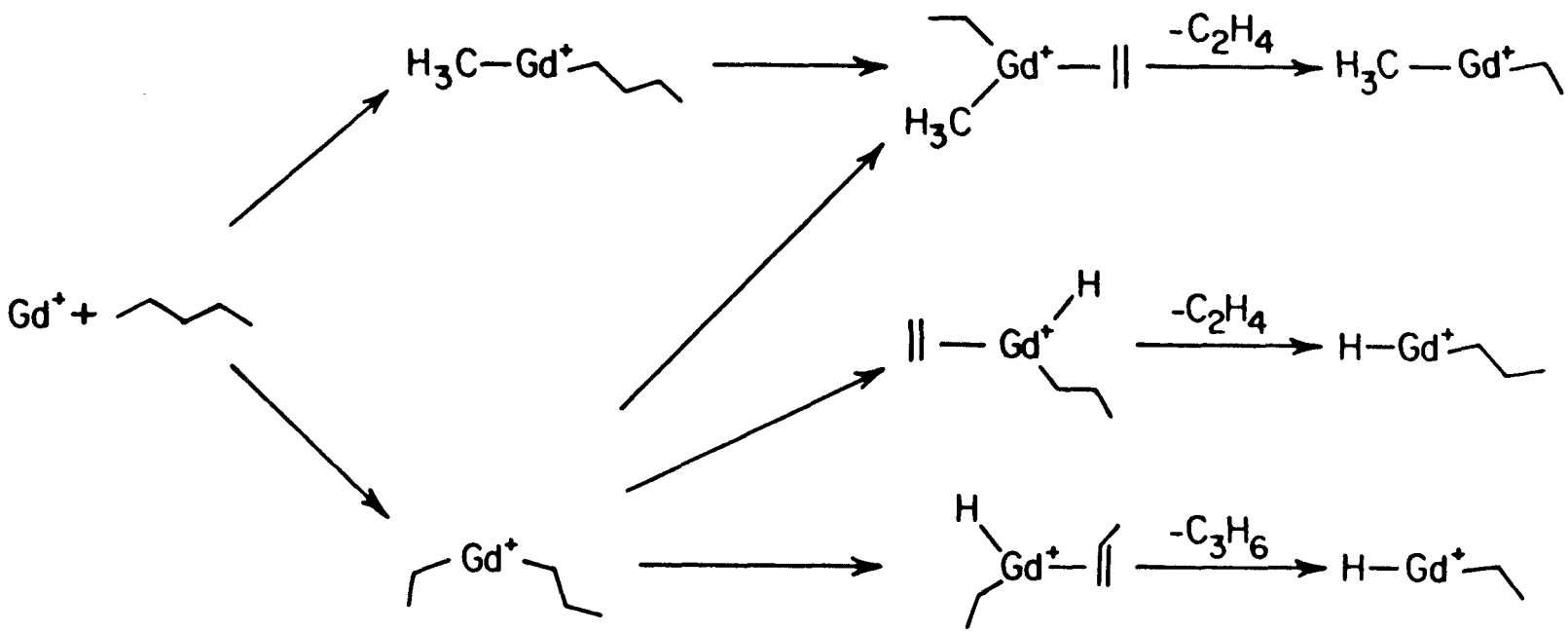

Scheme V

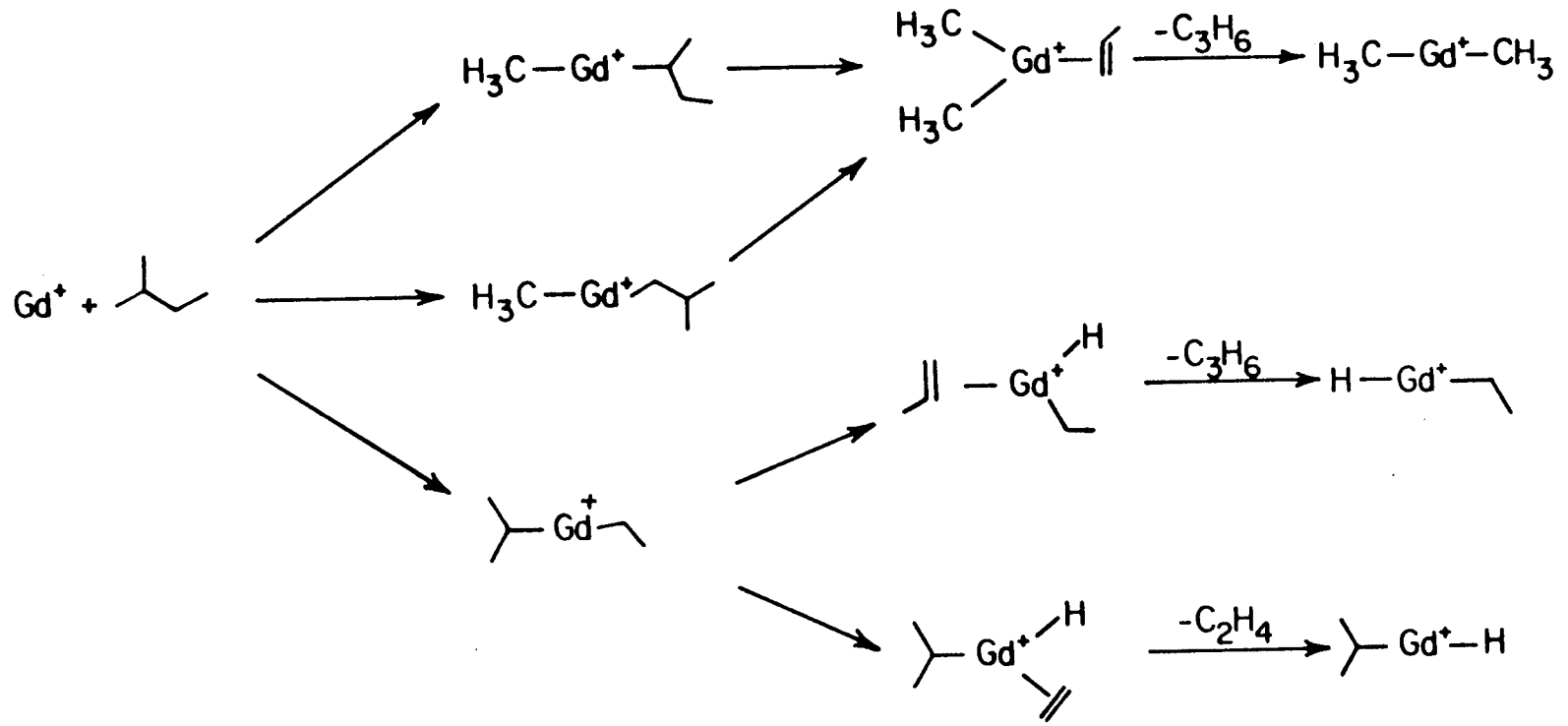
Gd+ +
H3C—Gd+
H3C—Gd+
H3C
Gd+
H3C
-C3H6
H3C—Gd+—CH3
Gd+
H
-C3H6
H—Gd+
Gd+
H
-C2H4
Gd+—H

Gd^+ and benzene. If this is occurring, the energetics yield a lower bound of 60 kcal/mol for the Gd^+–benzene interaction energy. Dialkyl products are again in evidence including $Gd(C_4H_{10})^+$, $Gd(C_3H_8)^+$, and $Gd(C_2H_6)^+$. The dialkyl products decrease, as a percentage of the overall product distribution, as the size of the reacting alkane increases and the number of competing pathways increases.

Reaction of Gd^+ with Cycloalkanes. Table VI lists the reaction products, product distributions, and cross sections for the reactions between Gd^+ and the C_3–C_6 cycloalkanes. The product distributions from FTMS studies of Sc^+, Y^+, and La^+ are also contained in Table VI for comparison with the present results.

Cyclopropane and Cyclobutane. The reaction of Gd^+ with cyclopropane yields the products shown in Table VI. Elimination of H_2 is by far the major reaction pathway. CID experiments on the $M(C_3H_4)^+$ products in the reactions of Y^+ and La^+ with cyclopropane show these products to be very similar to those formed from propane and propene, suggesting that the ring has been opened. The C–C bond is clearly the weakest bond in the molecule while the C–H bonds of cyclopropane are exceptionally strong (106 kcal/mol).[25b] The pathway of choice would thus seem to be insertion into one of the ring C–C bonds. Condensed-phase experiments by Periana and Bergman[26] indicate that the reaction of reaction of $Cp^*(L)Rh$ ($Cp^* = \eta^5$-C_5Me_5; $L = PMe_3$) with cyclopropane proceeds first through oxidative addition of a cyclopropyl–H bond to the metal and then intramolecular rearrangement gives the metallacyclobutane. Either mechanism would result in the cleavage of the cyclopropane ring. Two β–H transfers and reductive elimination of H_2 would then yield the product. Small amounts of other ring cleavage products, $Gd(C_2H_2)^+$ and $GdCH_2^+$ are also seen. Formation of the metal–methylene product requires a metal–carbon double bond strength which is greater than 93 kcal/mol.

Hydrogen loss products are the principal reaction products observed in the reaction with cyclobutane, although small amounts of C–C bond cleavage prod-

Table VI

Product Distributions for the Reactions of Gd^+ and Group 3 M^+ with Cycloalkanes

Alkane	Total Reaction Cross Section ($Å^2$)[a] Gd^+	Neutral(s) Lost	Product Ion	Relative Product Intensities (%) Ion Beam Gd^+	FTMS[b] Sc^+	FTMS[b] Y^+	FTMS[b] La^+
Cyclopropane	62	H_2	$M(C_3H_4)^+$	93	97	100	31
		CH_4	$M(C_2H_2)^+$	3	3		
		C_2H_4	$M(CH_2)^+$	4			69
Cyclobutane	133	H_2	$M(C_4H_6)^+$	62	27	30	7
		$2H_2$	$M(C_4H_4)^+$	31	41	28	81
		CH_4	$M(C_3H_4)^+$			4	
		C_2H_2	$M(C_2H_6)^+$	1			
		C_2H_4	$M(C_2H_4)^+$	3	16		
		C_2H_6	$M(C_2H_2)^+$	3	16	38	12
Cyclopentane	202	H_2	$M(C_5H_8)^+$	1			
		$2H_2$	$M(C_5H_6)^+$	99	100	100	100
Cyclohexane	203	$2H_2$	$M(C_6H_8)^+$	9	11		
		$3H_2$	$M(C_6H_6)^+$	91	89	100	100

[a] Reaction cross sections measured at a center-of-mass collision energy of approximately 0.25 eV. [b] Reference 9.

ucts are also seen (eq 17–21).

$$Gd^+ + \text{c-}C_4H_8 \xrightarrow{62\%} Gd(C_4H_6)^+ + H_2 \quad (17)$$

$$\xrightarrow{31\%} Gd(C_4H_4)^+ + 2H_2 \quad (18)$$

$$\xrightarrow{1\%} Gd(C_2H_6)^+ + C_2H_2 \quad (19)$$

$$\xrightarrow{3\%} Gd(C_2H_4)^+ + C_2H_4 \quad (20)$$

$$\xrightarrow{3\%} Gd(C_2H_2)^+ + C_2H_6 \quad (21)$$

A trace amount of methane loss is also observed in the reaction. As with cyclopropane, these products probably result from initial insertion into one of the C–C bonds. H_2 loss then occurs through successive β–H transfers and reductive elimination. Further elimination of H_2 yields the $Gd(C_4H_4)^+$ product. Both of these hydrogen loss products could be produced without ring cleavage through C–H insertion and successive hydrogen transfer and elimination. The C–H bond strength is not excessively strong (96.5 kcal/mol) as it is in cyclopropane. The reactions of Y^+ and La^+ have been proposed[9] to differ in that Y^+ is thought to initially cleave the ring while La^+ is thought to interact with the cyclobutane C–H bonds. The C–C bond cleavage products can be thought of as coming from initial formation of a metallacyclopentane and then symmetric ring cleavage followed by elimination of neutral product molecules.

Cyclopentane and Cyclohexane. No ring cleavage products are observed in the reaction of Gd^+ or the three Group 3 metal ions with cyclopentane and cyclohexane. Dehydrogenation is the only process involved in these reactions, with the major product ions arising from loss of two (cyclopentane) and three (cyclohexane) molecules of hydrogen. These are believed to correspond to Gd^+–cyclopentadiene and Gd^+–benzene complexes. Formation of cyclopentadiene and hydrogen from cyclopentane is endothermic by 50 kcal/mol. This is a lower bound for the binding energy to Gd^+. It is noted above that that Gd^+–benzene may be bound by at least 60 kcal/mol. Formation of benzene from cyclohexane is

endothermic by 49 kcal/mol, so that formation of Gd^+–benzene is consistent with the earlier result.

Reactions of Gd^+ and Pr^+ with Alkenes. Activation of C–C and C–H bonds in alkanes requires formation of two strong sigma bonds by the metal. In contrast, activation of C–H and C–C bonds in alkenes is enhanced by the interaction of the alkene π system with the metal ion. First row metals are seen to bind alkenes with a bond energy on the order of 40–50 kcal/mol.[27] The need for strong metal sigma bonding in the inserted product is thus not as great. The reactivity of Pr^+ with alkenes and not with alkanes is an example of this. Eu^+, on the other hand, has an extremely stable, half-filled f shell (f^7). We have tested the reactivity of Eu^+ with cyclohexene, a fairly reactive alkene, and observe only adduct formation and no elimination products. Table VII presents the reaction data for the reaction of Gd^+ and Pr^+ with cyclohexene and the linear alkenes from ethene to 1-hexene.

Ethene and Propene. Gd^+, as was discussed earlier, doubly dehydrogenates ethane. It is thus expected that dehydrogenation of ethene will take place and this is indeed what is observed. The same process is also seen for Pr^+, although with extremely low efficiency ($\sigma_{rxn} = 0.9$ Å^2 at a collision energy of 0.25 eV). Three products are observed in the reaction of propene with Gd^+ (Pr^+), equations 22–24.

$$M^+ + C_3H_6 \xrightarrow{99\%(97.7\%)} M(C_3H_4)^+ + H_2 \quad (22)$$

$$\xrightarrow{0.6\%(0.3\%)} M(C_2H_2)^+ + CH_4 \quad (23)$$

$$\xrightarrow{0.4\%(2.0\%)} M(CH_2)^+ + C_2H_4 \quad (24)$$

The major product in both cases is elimination of one molecule of H_2. The process can take place via interaction of the metal ion with the weakest C–H bonds in the molecule, the allylic C–H bonds. After formation of a metal–hydrido–allyl complex, hydrogen transfer and H_2 elimination yields a metal–allene product. The presence of the MCH_2^+ product at low energy provides an

Table VII

Product Distributions for the Reactions of Gd^+ and Pr^+ with Alkenes

Alkene	Total Reaction Cross Section ($Å^2$)[a]		Neutral(s) Lost	Product Ion	Relative Product Intensities (%)	
	Gd^+	Pr^+			Gd^+	Pr^+
Ethene	44	0.9	H_2	$M(C_2H_2)^+$	100.0	100.0
Propene	230	30	H_2	$M(C_3H_4)^+$	99.0	97.7
			CH_4	$M(C_2H_2)^+$	0.6	0.3
			C_2H_4	$M(CH_2)^+$	0.4	2.0
1-Butene	406	223	H_2	$M(C_4H_6)^+$	95.5	98.2
			$2H_2$	$M(C_4H_4)^+$	0.7	0.2
			CH_4	$M(C_3H_4)^+$	1.6	0.6
			C_2H_4	$M(C_2H_4)^+$	0.3	0.2
			C_2H_6	$M(C_2H_2)^+$	1.8	0.5
			C_3H_6	$M(CH_2)^+$	0.1	0.3
1-Pentene	454	273	H_2	$M(C_5H_8)^+$	33.6	85.7
			$2H_2$	$M(C_5H_6)^+$	35.8	9.2
			CH_2	$M(C_4H_8)^+$	0.3	0.1
			CH_4	$M(C_4H_6)^+$	7.8	1.0
			CH_4, H_2	$M(C_4H_4)^+$	0.2	
			C_2H_2	$M(C_3H_8)^+$	0.1	
			C_2H_4	$M(C_3H_6)^+$	1.7	0.9
			C_2H_6	$M(C_3H_4)^+$	20.0	2.7
			C_3H_4	$M(C_2H_6)^+$	0.1	
			C_3H_6	$M(C_2H_4)^+$	0.1	0.1
			C_3H_8	$M(C_2H_2)^+$	0.3	0.1
			C_4H_8	$M(CH_2)^+$		0.2

Alkene	Total Reaction Cross Section ($Å^2$)[a]		Neutral(s) Lost	Product Ion	Relative Product Intensities (%)	
	Gd^+	Pr^+			Gd^+	Pr^+
1-Hexene	452	167	H_2	$M(C_6H_{10})^+$	7.3	21.2
			$2H_2$	$M(C_6H_8)^+$	62.1	65.3
			$3H_2$	$M(C_6H_6)^+$	5.6	2.0
			CH_2	$M(C_5H_{10})^+$	0.2	
			CH_4	$M(C_5H_8)^+$	1.1	0.5
			CH_4, H_2	$M(C_5H_6)^+$	9.2	2.8
			$CH_4, 2H_2$	$M(C_5H_4)^+$	0.1	
			C_2H_4	$M(C_4H_8)^+$	0.8	0.5
			C_2H_6	$M(C_4H_6)^+$	10.0	5.9
			C_3H_6	$M(C_3H_6)^+$	0.5	0.4
			C_3H_8	$M(C_3H_4)^+$	2.0	1.1
			C_4H_6	$M(C_2H_6)^+$	1.0	0.1
			C_4H_8	$M(C_2H_4)^+$		0.1
			C_4H_{10}	$M(C_2H_2)^+$	0.1	
			C_5H_{10}	$M(CH_2)^+$		0.1
Cyclohexene	313	340	H_2	$M(C_6H_8)^+$	0.4	0.5
			$2H_2$	$M(C_6H_6)^+$	99.2	99.5
			C_6H_8	$M(H_2)^+$	0.4	

[a] Reaction cross sections measured at a center-of-mass collision energy of approximately 0.25 eV.

estimate of the strength of the metal–carbon double bond of greater than or equal to 101 kcal/mol.

The formation of $PrCH_2^+$ from propene and cyclopropane, the first being exothermic and the second appearing endothermic, poses a dilemma. Exothermic production from propene requires a bond strength of greater than 101 kcal/mol while endothermic production from cyclopropane would indicate that the bond energy is less than 93 kcal/mol. Two explanations exist for the discrepancy between the two results. First, the production of $PrCH_2^+$ from propene could be due to reaction of excited state Pr^+. Secondly, if we look more closely at the reactions of the two systems we see that there is another reaction product, $Pr(C_3H_4)^+$, that the two have in common. Again, the product is formed in an exothermic reaction with propene and a seemingly endothermic reaction with cyclopropane. The formation of C_3H_4 and H_2 from propene is 7.9 kcal/mol more endothermic than formation from cyclopropane. If the reaction with cyclopropane does indeed proceed via ring cleavage and β–H transfer, than the two processes proceed through a common intermediate. This indicates that there is possibly a thermodynamic barrier on the potential surface for interaction of Pr^+ with cyclopropane. The exact nature of the metal-methylene bonding is not known at this time.

1-Butene and 1-Pentene. As the size of the alkene increases the number of products observed also increases. Seven products are observed in the reaction of Gd^+ with 1-butene and 13 with 1-pentene. Pr^+ exhibits slightly lower reactivity and slightly fewer products. The product intensities for those products with abundances of 0.1% or larger are shown in Table VII. Dehyrogenation is again the major reaction pathway, representing over 95% of the product intensity for both metals in the reaction with 1-butene. Minor amounts of carbon–carbon bond cleavage products are also observed.

Scheme VI shows possible reaction mechanisms accounting for the major products observed with 1-pentene. These involve insertion of the metal into

Scheme VI

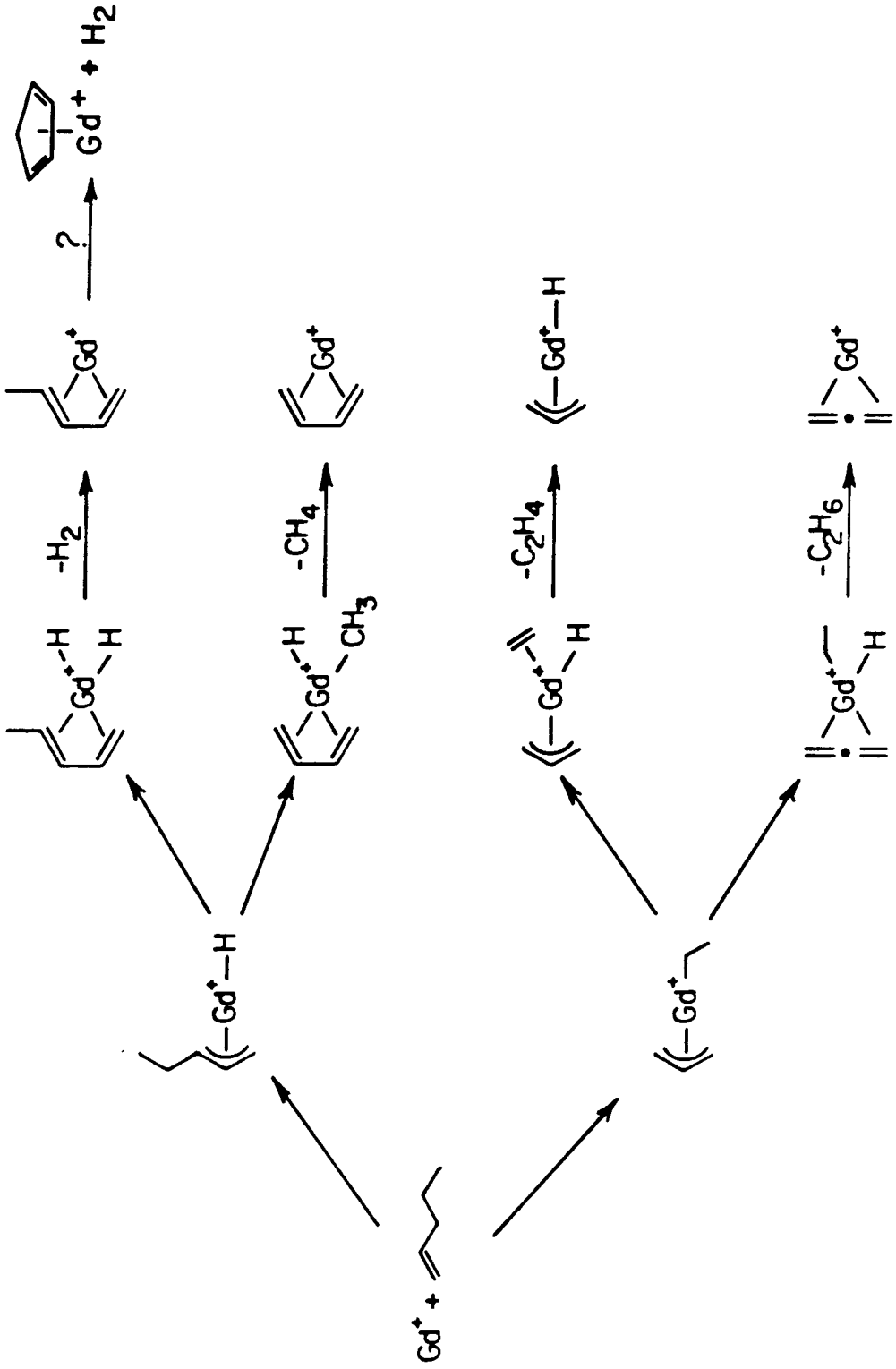

either an allylic C–H or C–C bond. C–C insertion leads to the $M(C_3H_6)^+$ and $M(C_3H_4)^+$ products while C–H insertion would lead to the dehydrogenation products and also loss of CH_4.

1-Hexene and Cyclohexene. Eighteen different products are observed at low energy in the reaction of Gd^+ with 1-hexene, while thirteen are observed in the reaction involving Pr^+. 75% and 88% of the product abundance, for Gd^+ and Pr^+, respectively, is due to single and multiple dehydrogenation processes. Smaller amounts are seen in chain cleavage processes. Again, the major products can be predicted by mechanisms involving initial insertion into allylic bonds followed by β–H or β–alkyl transfer and reductive elimination of the neutral species. We will not attempt to account for the processes producing all eighteen products.

The reactions of cyclohexene are quite a contrast to those of 1-hexene. A total of only three low energy products are seen. Both Gd^+ and Pr^+ doubly dehydrogenate cyclohexene to produce M^+–benzene, a product which accounts for over 99% of the total product distribution. In the reaction with Gd^+, an endothermic process is also seen with a threshold at very low energy. This process produces GdH_2^+ and either cyclohexadiene or benzene and hydrogen. The latter process is the most energetically favorable. It is uphill 125 kcal/mol to produce benzene, hydrogen, and two H atoms. The threshold for production of GdH_2^+ appears to be less than 0.25 eV (5.8 kcal/mol). This would put an upper limit on the sum of the two Gd^+–H sigma bonds somewhere between 119 and 125 kcal/mol.

Reaction of Gd^+ and Pr^+ with Oxygen Containing Compounds. The two ions have been reacted with nitric oxide, formaldehyde, acetaldehyde, and acetone. As mentioned earlier, Gd^+ readily reacts with any O_2 in the system. Pr^+ is also seen to form the oxide when any oxygen is present. Table VIII lists the products observed at low collision energy for these systems. The principal

Table VIII

Product Distributions for the Reactions of Gd^+ and Pr^+ with Oxygen Containing Compounds

Alkene	Total Reaction Cross Section ($Å^2$)[a]		Neutral(s) Lost	Product Ion	Relative Product Intensities (%)	
	Gd^+	Pr^+			Gd^+	Pr^+
Nitric Oxide	4.8	16	N	MO^+	100.0	100.0
Formaldehyde	86	43	CH_2	MO^+	29.1	100.0
			CO	MH_2^+	70.9	
Acetaldehyde	614	319	H_2	$M(C_2H_2O)^+$	1.4	
			C_2H_2	$M(OH_2)^+$	0.2	
			C_2H_4	MO^+	98.1	100.0
			CO	$M(CH_4)^+$	0.3	
Acetone	352	385	H_2	$M(C_3H_4O)^+$	2.4	
			CH_3	$M(C_2H_3O)^+$	0.1	
			CH_4	$M(C_2H_2O)^+$	0.3	
			CO	$M(C_2H_6)^+$	0.2	
			C_3H_4	$M(OH_2)^+$	0.5	0.1
			C_3H_6	MO^+	96.5	99.9

[a] Reaction cross sections measured at a center-of-mass collision energy of approximately 0.25 eV.

product in almost all of the reactions (eqs 25–28) is MO^+.

$$M^+ + NO \longrightarrow MO^+ + N \tag{25}$$

$$M^+ + (CH_3)_2CO \longrightarrow MO^+ + C_3H_6 \tag{26}$$

$$M^+ + CH_3CHO \longrightarrow MO^+ + C_2H_4 \tag{27}$$

$$M^+ + CH_2O \longrightarrow MO^+ + :CH_2 \tag{28}$$

Small amounts of other products are also seen. In the reaction with acetone, both metal ions produce $M(OH_2)^+$ with the loss of C_3H_4. Other products observed in the reaction of Gd^+ with acetone involve elimination of H_2, CH_3, CH_4, and CO. Elimination of CO yields the metal–dimethyl ion (the sum of the two bonds must be greater than or equal to 95.7 kcal/mol). Gd^+ reacts with acetaldehyde to give, in addition to GdO^+, $Gd(C_2H_2O)^+$, $Gd(OH_2)^+$, and $Gd(CH_4)^+$. The presence of a small amount of the hydrido–methyl species was determined using CH_3CDO and CD_3CDO to sort this product out from the oxide and water complexes. Formation of the hydrido–methyl complex requires that the sum of the metal–hydrogen and metal–methyl bonds be greater than or equal to 100.5 kcal/mol. The other important non-oxide product observed in these reactions is GdH_2^+, formed in the reaction with formaldehyde. The large reaction cross section indicates that the two metal–hydrogen bonds are much more stable than the 103.7 kcal/mol necessary for formation of the product. This is in keeping with the earlier result of $\sim$ 120 kcal/mol from the endothermic production from cyclohexene. GdH_2^+ is therefore stable with respect to reductive elimination of H_2.

An interesting result which was observed in the reaction of Gd^+ with acetone and acetaldehyde involves the secondary reaction of the product oxide. The reaction to produce GdO^+ is very efficient and a large enough population is built up in the cell that many GdO^+–neutral collisions are seen to take place. These secondary collisions serve to produce secondary reaction products, the primary one being the dehydration of the neutral to give $GdO(OH_2)^+$. One

other secondary product, $Gd(O_2)^+$, is also observed.

For thermodynamic purposes, the neutral decomposition pathways and energetics for production of O atom from the various species are given in Table IX. Reaction with formaldehyde, reaction 31, is seen for both metal ions. For a reaction to take place between M^+ and CH_2O to produce MO^+, the M^+–O bond dissociation energy must be greater than or equal to 179 kcal/mol. Reaction with acetaldehyde and acetone can thus produce either the neutral alkenes or the corresponding methyl and dimethyl carbene. Metal ions show considerable diversity in their reactions with acetone depending upon the strength of the metal oxide bond. The Group 8–10 metal ions form much weaker bonds to oxygen.[29] The Group 8–10 metals of the first row (Fe^+, Co^+, and Ni^+),[30] along with Pd^+,[7] react to give primarily the metal–dimethyl product, $M(CH_3)_2^+$, with smaller amounts of the metal carbonyl, MCO^+. Group 8–9 metals of the second row (Ru^+ and Rh^+)[7] yield $M(CH_2O)^+$ and $M(C_2H_4)^+$ products as well as $M(CH_3)_2^+$ and MCO^+. Mo^+ reacts with acetone predominantly by a dehydrogenation pathway[31] to give presumably $Mo(CO)(C_2H_4)^+$. Sc^+, on the other hand, with an oxide bond energy of about 159 kcal/mol, behaves similarly to Pr^+, producing only the oxide product.[1] $D(Sc^+–O)$, however, is not large enough to produce the oxide from formaldehyde due to the high heat of formation of methylene.

The present results for $D(Pr^+–O)$ and $D(Gd^+–O)$, giving a lower limit of 179 kcal/mol, compare very well with calculations of the bond energies from known quantities for neutral MO.[32] Using the MO bond energies of 177.6 ± 4.0 kcal/mol and 169.7 ± 3.0 kcal/mol for Pr^+ and Gd^+, respectively, the MO ionization potentials of 4.90 ± 0.1 eV and 5.75 ± 0.1 eV, and the metal atom IP's of 5.37 ± 0.1 eV and 6.24 ± 0.1 eV, one can calculate (using the thermodynamic cycle shown

Table IX

Heats of Dissociation for Gaseous Oxygen Containing Molecules

Reaction	ΔH°_{298} (kcal/mol)
$O_2 \longrightarrow O + O$	117
$NO \longrightarrow O + N$	151
$(CH_3)_2CO \longrightarrow O + H_2C{=}CHCH_3$	116
$\longrightarrow O + :C(CH_3)_2$	174
$CH_3CHO \longrightarrow O + H_2C{=}CH_2$	112
$\longrightarrow O + :CHCH_3$	177
$CH_2O \longrightarrow O + :CH_2$	179

[a] Individual heats of formation from references 21, 25, and 28.

in eq 36)

$$\begin{array}{ccc} MO^+ + e^- & \xrightarrow{D(M^+-O)} & M^+ + O + e^- \\ {\scriptstyle IP(MO)}\uparrow & & \uparrow{\scriptstyle IP(M)} \\ MO & \xrightarrow[D(M-O)]{} & M + O \end{array} \qquad (36)$$

the metal oxide cation bond dissociation energies. Values of 188.4 ± 5.2 kcal/mol and 181.0 ± 4.4 kcal/mol are calculated for $D(Pr^+-O)$ and $D(Gd^+-O)$, respectively, slightly greater than the lower limit set by the present experiments. A similar calculation for Eu^+ using $D(Eu-O) = 114.5 \pm 4.0$ kcal/mol, $IP(EuO) = 6.48 \pm 0.1$ eV, and $IP(Eu) = 5.68 \pm 0.1$ eV, yield an EuO^+ bond dissociation energy of 96.1 ± 5.2 kcal/mol, explaining why no EuO^+ product was seen due to background oxygen in the system.

Conclusion

The results presented show that those lanthanide cations which, of necessity, must involve the f electrons in bonding, are unable to activate the C–H or C–C bonds of saturated hydrocarbons. This supports the contention that bonds formed utilizing the f electrons are inherently weak. On the other hand, where two non-f valence electrons are available for use in bonding, the metal ion is very reactive. Gd^+, with a ground state derived from the $4f^7 5d^1 6s^1$ configuration, exhibits reactivity simialr to that of the Group 3 transition metal cations. Product distributions are fairly similar to Sc^+, although more multiple dehydrogenation products are seen for Gd^+. As with Sc^+, Gd^+ is capable of forming two strong sigma bonds to carbon and hydrogen. An estimate of the sum of the two bonds in GdH_2^+ is 120 ± 5 kcal/mol. $Gd(CH_3)(H)^+$ is produced in the reaction with propane indicating that the sum of the bonds is around 125 kcal/mol. Although the reactions yielding $Gd(C_2H_6)^+$ yield an estimate of 115 kcal/mol for the sum of the bond energies, it is also likely to be over 120 kcal/mol.

By looking at the electronic states of the other lanthanide cations, one can try to make predictions of reactivity. Ce^+ and Lu^+ are the other two ions with

two non-f valence electrons, however, Lu^+ has a closed shell $f^{14}s^2$ configuration. An $f^{14}d^1s^1$ configuration which would be necessary for bonding is at over 1.5 eV. Ce^+ has two 5d electrons, like La^+, and should be quite reactive in its ground state. The other lanthanide cations only have one non-f valence electron. Except for Tb^+, which has a state at approximately 0.4 eV with a $4f^85d^16s^1$ configuration, the reactive excited states are fairly high in energy and it can be expected that these ions will all be unreactive.

Acknowledgement. We thank the National Science Foundation (Grant No. CHE84-07857) for partial support of this work.

References

(1) Tolbert, M. A.; Beauchamp, J. L. *J. Am. Chem. Soc.* **1984**, *106*, 8117.

(2) Tolbert, M. A.; Beauchamp, J. L. *J. Am. Chem. Soc.* **1986**, *108*, 7508.

(3) Byrd, G. D.; Burnier, R. C.; Freiser, B. S. *J. Am. Chem. Soc.* **1982**, *104*, 3565.

(4) (a) Halle, L. F.; Armentrout, P. B.; Beauchamp, J. L. *Organometallics* **1982**, *1*, 963. (b) Houriet, R.; Halle, L. F.; Beauchamp, J. L. *Organometallics* **1983**, *2*, 1818. (c) Jacobson, D. B.; Freiser, B. S. *J. Am. Chem. Soc.* **1983**, *105*, 5197.

(5) (a) Armentrout, P. B.; Halle, L. F.; Beauchamp, J. L. *J. Am. Chem. Soc.* **1981**, *103*, 6624. (b) Jacobson, D. B.; Freiser, B. S. *J. Am. Chem. Soc.* **1983**, *105*, 7484. (c) Peake, D. A.; Gross, M. L.; Ridge, D. P. *J. Am. Chem. Soc.* **1984**, *106*, 4307.

(6) (a) Armentrout, P. B.; Beauchamp, J. L. *J. Am. Chem. Soc.* **1981**, *103*, 6628. (b) Jacobson, D. B.; Freiser, B. S. *J. Am. Chem. Soc.* **1983**, *105*, 7492.

(7) Tolbert, M. A.; Mandich, M. L.; Halle, L. F.; Beauchamp, J. L. *J. Am. Chem. Soc.* **1986**, *108*, 5675.

(8) Byrd, G. D.; Freiser, B. S. *J. Am. Chem. Soc.* **1982**, *104*, 5944.

(9) Huang, Y.; Wise, M. B.; Jacobson, D. B.; Freiser, B. S. *Organometallics* **1987**, *6*, 346.

(10) (a) Wise, M. B.; Jacobson, D. B.; Freiser, B. S. *J. Am. Chem. Soc.* **1985**, *107*, 1590. (b) Wise, M. B.; Jacobson, D. B.; Freiser, B. S. *J. Am. Chem. Soc.* **1985**, *107*, 6744.

(11) Weil, D. A.; Wilkins, C. L. *J. Am. Chem. Soc.* **1985**, *107*, 7316.

(12) Armentrout, P. B. in "Structure/Reactivity and Thermochemistry of Ions," Ausloos, P. J.; Lias, S. G. Ed., NATO ASI Series C, Reidel, Dordrect, 1987, and references therein.

(13) (a) Schilling, J. B.; Beauchamp, J. L.; Goddard, W. A., III *J. Am. Chem.*

Soc. **1986**, *108*, 582. (b) Schilling, J. B.; Beauchamp, J. L.; Goddard, W. A., III, submitted for publication. (c)Schilling, J. B.; Beauchamp, J. L.; Goddard, W. A., III *J. Am. Chem. Soc.* , in press. (d) Schilling, J. B.; Beauchamp, J. L.; Goddard, W. A., III *J. Phys. Chem.* , in press.

(14) (a) Carter, E. A.; Goddard, W. A., III *J. Phys. Chem.* **1984**, *88*, 1485. (b) Carter, E. A.; Goddard, W. A., III *J. Am. Chem. Soc.* **1986**, *108*, 2180. (c) Carter, E. A.; Goddard, W. A., III *J. Am. Chem. Soc.* **1986**, *108*, 4746.

(15) (a) Alvarado-Swaisgood, A. E.; Allison, J.; Harrison, J. F. *J. Phys. Chem.* **1985**, *89*, 2517. (b) Alvarado-Swaisgood, A. E.; Harrison, J. F. *J. Phys. Chem.* **1985**, *89*, 5198. (c) Mavridis, A.; Alvarado-Swaisgood, A. E.; Harrison, J. F. *J. Phys. Chem.* **1986**, *90*, 2584. (d) Harrison, J. F. *J. Phys. Chem.* **1986**, *90*, 3313.

(16) (a) Jeske, G.; Lauke, H.; Mauermann, H.; Swepston, P. N.; Schumann, H.; Marks, T. J. *J. Am. Chem. Soc.* **1985**, *107*, 8091. (b) Jeske, G.; Schock, L. E.; Swepston, P. N.; Schumann, H.; Marks, T. J. *J. Am. Chem. Soc.* **1985**, *107*, 8103. (c) Jeske, G.; Lauke, H.; Mauermann, H.; Schumann, H.; Marks, T. J. *J. Am. Chem. Soc.* **1985**, *107*, 8111.

(17) Watson, P. L.; Parshall, G. W. *Acc. Chem. Res.* **1985**, *18*, 51, and references therein.

(18) Martin, W. C.; Zalubas, R.; Hagan, L. "Atomic Energy Levels–The Rare-Earth Elements," National Bureau of Standards, Washington D.C., 1978.

(19) (a) Armentrout, P. B.; Beauchamp, J. L. *Chem. Phys.* **1980**, *50*, 21. (b) Armentrout, P. B.; Beauchamp, J. L. *J. Chem. Phys.* **1981**, *74*, 2819.

(20) Steigerwald, M. L.; *Ph.D. Thesis*, California Institute of Technology, Pasadena, California (1984).

(21) Heat of formation values for stable organic molecules obtained from: Cox, J. D.; Pilcher, G. "Thermochemistry of Organic and Organometallic Compounds," Academic Press, New York, 1970.

(22) Herzberg, G. "Molecular Spectra and Molecular Structure. III. Electronic Spectra of Polyatomic Molecules," Van Nostrand Reinhold, New York, 1966.

(23) Benson, S. W. "Thermochemical Kinetics," Wiley, New York, 1976.

(24) Chan, S. C.; Rabinovitch, B. S.; Bryant, J. T.; Spicer, L. D.; Fujimoto, T.; Lin, Y. N.; Pavlou, S. P. *J. Phys. Chem.* **1970**, *74*, 3160.

(25) Unless otherwise noted, thermochemical values for radicals and carbenes are taken from: (a) Wagman, D. D.; Evans, W. H.; Parker, V. B.; Schumm, R. H.; Halow, I.; Bailey, S. M.; Churney, K. L.; Nuttall, R. L. *J. Phys. Chem. Ref. Data* **1982**, *11*, Supp. 2. (b) McMillen, D. F.; Golden, D. M. *Annu. Rev. Phys. Chem.* **1982**, *33*, 493.

(26) Steigerwald, M. L.; Goddard, W. A., III *J. Am. Chem. Soc.* **1985**, *107*, 5027.

(26) Periana, R. A.; Bergman, R. G. *J. Am. Chem. Soc.* **1986**, *108*, 7346.

(27) (a) Aristov, N.; Armentrout, P. B. *J. Am. Chem. Soc.* **1986**, *108*, 1806. (b) Hanratty, M. A.; Beauchamp, J. L.; Illies, A. J.; van Koppen, P.; Bowers, M. T., in press.

(28) The heat of formation of $(CH_3)_2C$ and $(CH_3)HC$ were obtained from: Liu, K.; Parson, J. M. *J. Phys. Chem.* **1979**, *83*, 970.

(29) (a) Armentrout, P. B.; Halle, L. F.; Beauchamp, J. L. *J. Chem. Phys.* **1982**, *76*, 2449. (b) Armentrout, P. B.; Halle, L. F.; Beauchamp, J. L. *J. Am. Chem. Soc.* **1981**, *103*, 6501.

(30) (a) Burnier, R. C.; Byrd, G. D.; Freiser, B. S. *J. Am. Chem. Soc.* **1981**, *103*, 4360. (b) Halle, L. F.; Crowe, W. E.; Armentrout, P. B.; Beauchamp, J. L. *Organometallics* **1984**, *3*, 1694.

(31) Schilling, J. B.; Beauchamp, J. L., manuscript in preparation.

(32) (a) Pedley, J. B.; Marshall, E. M. *J. Phys. Chem. Ref. Data* **1983**, *12*, 967. (b) Ackerman, R. J.; Rauh, E. G.; Thorn, R. J. *J. Chem. Phys.* **1976**, *65*, 1027.

CHAPTER III

WHAT'S WRONG WITH GAS-PHASE CHROMIUM? A COMPARISON OF THE UNREACTIVE Cr^+ CATION WITH THE ALKANE ACTIVATING MOLYBDENUM CATION

What's Wrong with Gas-Phase Chromium? A Comparison of the Unreactive Cr^+ Cation with the Alkane Activating Molybdenum Cation.

J. Bruce Schilling and J. L. Beauchamp*

Contribution No. 7591 from the

Arthur Amos Noyes Laboratory of Chemical Physics

California Institute of Technology, Pasadena, CA 91125

Abstract

We have studied the interaction of gas-phase Cr^+ and Mo^+ with small alkanes, cycloalkanes, and alkenes using ion beam mass spectrometric techniques. Although the two Group 6 metal ions have the same ground electronic state (^6S, d^5) and similar excitation energies to the first excited electronic state (^6D, d^4s^1 with state splittings of 1.52 eV and 1.59 eV for Cr^+ and Mo^+, respectively) they behave quite differently. Unlike a majority of the metal ions which have been studied, Cr^+ ions are extremely unreactive. Cr^+ does not react with C_1–C_6 alkanes, cycloalkanes and alkenes. Even though the reaction cross sections are quite small, Mo^+, on the other hand, reacts with all alkanes except methane, to give dehydrogenation products. Reactions of Mo^+ with the strained cycloalkanes, cyclopropane and cyclobutane, and with most alkenes are quite facile. This difference in reactivity is attributed to the difference in size of the Mo^+ orbitals with respect to Cr^+. The larger size of the d orbitals reduces the d-d exchange energy and increases the sigma bond energies between the metal and carbon or hydrogen, allowing exothermic insertion into C–H and C–C bonds.

I. Introduction

A growing number of experiments have shown that the unsaturated, gas-phase transition metal cations are very reactive when it comes to activation of C–H and C–C bonds of alkanes and other small hydrocarbons. The largest number of studies have involved the first row Group 8–10 metal ions Fe^+, Co^+, and Ni^+,[1] although more recently, the early first row metals[2–4] as well as several second[5–7] and third[7–9] row species (Ru^+, Rh^+, Pd^+, Y^+, and La^+) have been investigated. Comparison of the reactivity of the second row metals with their counterparts in the first row has shown some surprising differences. As one moves down a given column, dehydrogenation increases in importance relative to C–C bond cleavage processes. This is especially noticeable with Ru^+ and Rh^+ where dehydrogenation products are almost exclusively formed compared to Fe^+ and Co^+, where C–C bond cleavage products dominate. The present paper is another study of the differences encountered between similar metals of the first and second transition metal series. Previous work has shown that, although excited state Cr^+ is reactive with alkanes[10] (even reacting exothermically with methane), ground state Cr^+ is quite unreactive. This unreactivity is fairly unusual for a gas-phase metal cation. Theoretical calculations have indicated that differences in bonding and bond dissociation energies between Cr^+ and Mo^+ could be significant enough that Mo^+ would react exothermically with small hydrocarbons.[11] The present study confirms this hypothesis and we discuss the differences between the two Group 6 metal ions.

Experimental Section

The ion beam mass spectrometer used in this study of transition metal ion reactivity has been described previously.[12] Briefly, singly-charged, atomic metal ions are formed by thermal vaporization of a metal-containing compound and surface ionization on a hot rhenium ribbon filament. Cr^+ ions were formed from $Cr(CO)_6$ at approximately 1800 K while Mo^+ ions were formed using $[CpMo(CO)_3]_2$ (Cp = cyclopentadienyl) and an approximate filament temperature of 2500 K. It is generally assumed that the internal temperature of the ions is the same as the filament surface temperature. It is thus possible, using a Maxwell-Boltzmann distribution, to estimate the population of ions in the ground and low-lying excited electronic states. Table I lists several of the low-lying electronic states for Cr^+ and Mo^+ along with their relative energies[13] (determined by two methods: from lowest J level to lowest J level of each state; and using weighted averages over the J levels for each state, the latter being useful for discussion of theoretical results pertinent to the present experiments) and relative populations at the filament temperatures used. Both ions have similar ground states (^6S, d^5) with the lowest excited state (^6D, d^4s^1) ~1.5 eV higher in energy. The Cr^+ ions are formed with greater than 99.9% of the ions in the ground electronic state. For Mo^+, greater than 99.5% of the ions are in the ground state. Thus, any reactions observed are likely to be reactions of ground state metal ions.

After the metal ions are produced on the filament, they are accelerated, collimated into a beam, mass analyzed, and injected into a collision chamber containing the neutral reaction gas. The gas is at ambient temperature with a pressure which is maintained at less than two millitorr to yield single-collision conditions. By varying the kinetic energy of the ion beam, it is possible to study the reaction products as a function of the center-of-mass interaction energy between the ion and neutral. Unreacted ions and forward scattered products are extracted from the collision chamber and injected into a quadrupole mass spec-

Table I

Low-Lying M^+ Electronic States[a] and Beam Populations

Ion	Configuration	Term	E_{rel}(Low J)[b] (eV)	E_{rel}(Ave. J)[c] (eV)	Ion Beam Population[d] (%)
Cr^+	$3d^5$	a^6S	0.00	0.00	99.97
	$3d^44s^1$	a^6D	1.48	1.52	0.03
	$3d^44s^1$	a^4D	2.42	2.46	0.00
	$3d^5$	a^4G	2.54	2.54	0.00
	$3d^5$	a^4P	2.70	2.71	0.00
Mo^+	$4d^5$	a^6S	0.00	0.00	99.52
	$4d^45s^1$	a^6D	1.46	1.59	0.34
	$4d^5$	a^4G	1.88	1.91	0.08
	$4d^5$	a^4P	1.94	1.95	0.02
	$4d^5$	a^4D	2.08	2.11	0.02

[a] Electronic state information taken from reference 13. [b] Relative energy determined using the splitting between the lowest j level for each state. [c] Relative energy determined using a weighted average over j levels for each state. [d] Populations determined using a Maxwell-Boltzmann distribution over the energy levels at a temperature of 1800 K for Cr^+ and 2500 K for Mo^+.

trometer for mass analysis. The ions are detected using a channeltron electron multiplier and pulse counting electronics. The quadrupole and ion detection circuits are controlled by an IBM-PC XT computer.

Results

Interaction of Cr^+ and Mo^+ with Alkanes. Previous experiments in our labs,[10] coupled with the present work, have shown that Cr^+ is unable to exothermically activate the C–H and C–C bonds of alkanes. These experiments have involved a variety of alkanes varying in size from methane to the C_7 hydrocarbons n-heptane and 2,4-dimethylpentane. Although many of these systems exhibit extensive adduct formation at collision energies of less than 1 eV and pressures of 1-2 mtorr (indicating long-lived interaction complexes are being formed), no reaction products are observed.

In marked contrast to Cr^+, Mo^+ reacts with alkanes larger than methane. Table II gives product distributions and total cross sections for these reactions measured at a center-of-mass collision energy of approximately 0.25 eV. It should be noted that the reaction cross sections for these processes are quite small, similar to those seen for reaction of V^+ in the first row,[3] indicating that Mo^+ is not as reactive as many of the other transition metal ions which have been studied.

Methane, Ethane, and Propane. Very few metal ions have been observed to react with methane exothermically, and Mo^+ is no exception. Gas-phase reactions under single-collision conditions require formation of a neutral product to satisfy momentum and energy constraints. The most favorable pathway for reaction with methane is shown in equation 1.

$$M^+ + CH_4 \longrightarrow MCH_2^+ + H_2 \qquad (1)$$

For this reaction to be exothermic, the bond dissociation energy, $D(M^+–CH_2)$ must exceed 111 kcal/mol[14] (this is seen to be the case for Ta^+).[8]

Table II

Product Distributions for the Reactions of Mo^+ with Alkanes and Cycloalkanes

Neutral Reactant	Percentages of Neutral Products[a]							Cross Section (Å²)	
	H_2	$2H_2$	$3H_2$	$4H_2$	$CH_4 + H_2$	$CH_4 + 2H_2$	C_2H_4	Products[b]	Adduct[c]
Ethane	83	17						0.4	0.0
Propane	46	54						0.7	0.8
n-Butane		100						3.0	15.8
2-Methylpropane	37	63						1.2	6.9
n-Pentane	6	80	14					4.7	20.5
2,2-Dimethylpropane	23	63			12	5		3.4	51.2
n-Hexane	10	51	24	15				18.7	44.6
Cyclopropane	100							54.8	0.0
Cyclobutane	40	5					55	60.6	2.9
Cyclopentane	3	97						26.8	2.5
Cyclohexane	5	13	82					6.9	17.1

[a] Observed at a center-of-mass collision energy of approximately 0.25 eV. [b] Total reaction cross section for all observed products. [c] Apparent cross section observed for formation of adduct species. The neutral reaction gas pressure ranges from 1–1.5 mtorr.

Mo^+ does react with ethane to eliminate both one and two molecules of H_2 This requires that the Mo^+–ethylene and Mo^+–acetylene bonds be greater than 32.7 kcal/mol and 74.6 kcal/mol, respectively. Similarly, reaction with propane also generates products corresponding to loss of one and two molecules of hydrogen, $Mo(C_3H_6)^+$ and $Mo(C_3H_4)^+$, the latter is either a metal–allene or a metal–propyne complex (the energetics of formation of allene and propyne from propane are 70.5 and 69.2 kcal/mol, respectively).

n-Butane and 2-Methylpropane. As with the smaller molecules, Mo^+ reacts with n-butane and 2-methylpropane by dehydrogenation. $Mo(C_4H_6)^+$ is the only reaction product from n-butane while both $Mo(C_4H_8)^+$ and $Mo(C_4H_6)^+$ are formed in the reaction with 2-methylpropane. Formation of a metal–1,3-butadiene complex from 2-methylpropane requires rearrangement of the carbon skeleton. This structural rearrangement could account for the difference in product distribution for the two isomers. Reaction with n-butane to produce 1,3-butadiene can proceed with no rearrangement of the carbon skeleton. These reactions yield a lower limit for the molybdenum–butadiene bond energy of 58.5 kcal/mol.

n-Pentane, n-Hexane, and 2,2-Dimethylpropane. As the size of the alkane increases, the amount of dehydrogenation is also seen to increase. The reaction of Mo^+ with n-pentane, eq 2–4,

$$Mo^+ + \text{n-}C_5H_{12} \xrightarrow{6\%} Mo(C_5H_{10})^+ + H_2 \quad (2)$$

$$\xrightarrow{80\%} Mo(C_5H_8)^+ + 2H_2 \quad (3)$$

$$\xrightarrow{14\%} Mo(C_5H_6)^+ + 3H_2 \quad (4)$$

produces products corresponding to loss of up to three molecules of H_2, the latter possibly involving cyclization of the carbon chain to produce a Mo^+–cyclopentadiene complex with an interaction energy which must be $\geq$ 67 kcal/mol. In a similar fashion, reaction with n-hexane, eq 5–8,

$$Mo^+ + \text{n-}C_6H_{14} \xrightarrow{10\%} Mo(C_6H_{12})^+ + H_2 \quad (5)$$

$$\xrightarrow{51\%} Mo(C_6H_{10})^+ + 2H_2 \quad (6)$$

$$\xrightarrow{24\%} Mo(C_6H_8)^+ + 3H_2 \quad (7)$$

$$\xrightarrow{15\%} Mo(C_6H_6)^+ + 4H_2 \quad (8)$$

produces dehydrogenation of hexane with the loss of up to four molecules of hydrogen in one ion-molecule encounter. The cross section versus collision energy data are shown in Figure 1. The products show the typical exothermic behavior with cross sections decreasing with increasing collision energy. If loss of four molecules of H_2 produces a metal–benzene complex, the reaction places a lower bound on the Mo^+–benzene interaction energy of 59.7 kcal/mol.

As seen in Table II, the products from reaction with 2,2-dimethylpropane are distinguished from the linear alkanes by the appearance of C–C bond cleavage processes. 1,2 H_2 elimination, which is prevalent in the reactions of many metal ions, is impossible. After initial insertion into a C–H bond, there are no β–hydrogens. Sc^+ is seen to undergo a very facile H_2 elimination reaction with 2,2-dimethylpropane,[2] part of the evidence put forth in support of a 1,3 dehydrogenation mechanism for that metal ion. For metals which do not react via this 1,3 mechanism, extensive rearrangement must take place before dehydrogenation and this allows other reaction pathways to compete, such as the elimination of CH_4 and H_2, as seen here.

Interaction with Cycloalkanes. Cr^+ is unreactive with the C_3–C_6 cycloalkanes, as it is with the corresponding linear and branched alkanes. Table II contains the product distributions for the reactions of Mo^+ with cycloalkanes at a center-of-mass collision energy of approximately 0.25 eV.

Cyclopentane and Cyclohexane. These two reactive systems exhibit chemistry similar to that described for the linear alkanes. Both react via dehydrogenation and form almost exclusively $Mo(C_5H_6)^+$ and $Mo(C_6H_6)^+$, products which are also obtained with the loss of three and four molecules of hydrogen from the linear alkanes. The sequential dehydrogenation process favors formation of

Figure 1: Reaction cross section versus center-of-mass collision energy, E_{CM}, for the reaction between Mo^+ and n-hexane. The neutral hexane pressure was approximately 1.4 mtorr. The most abundant product at low energy is the metal adduct, $Mo(C_6H_{14})^+$, with the four dehydrogenation products at lower intensity. All products show exothermic behavior. Solid lines are a simple extrapolation between data points.

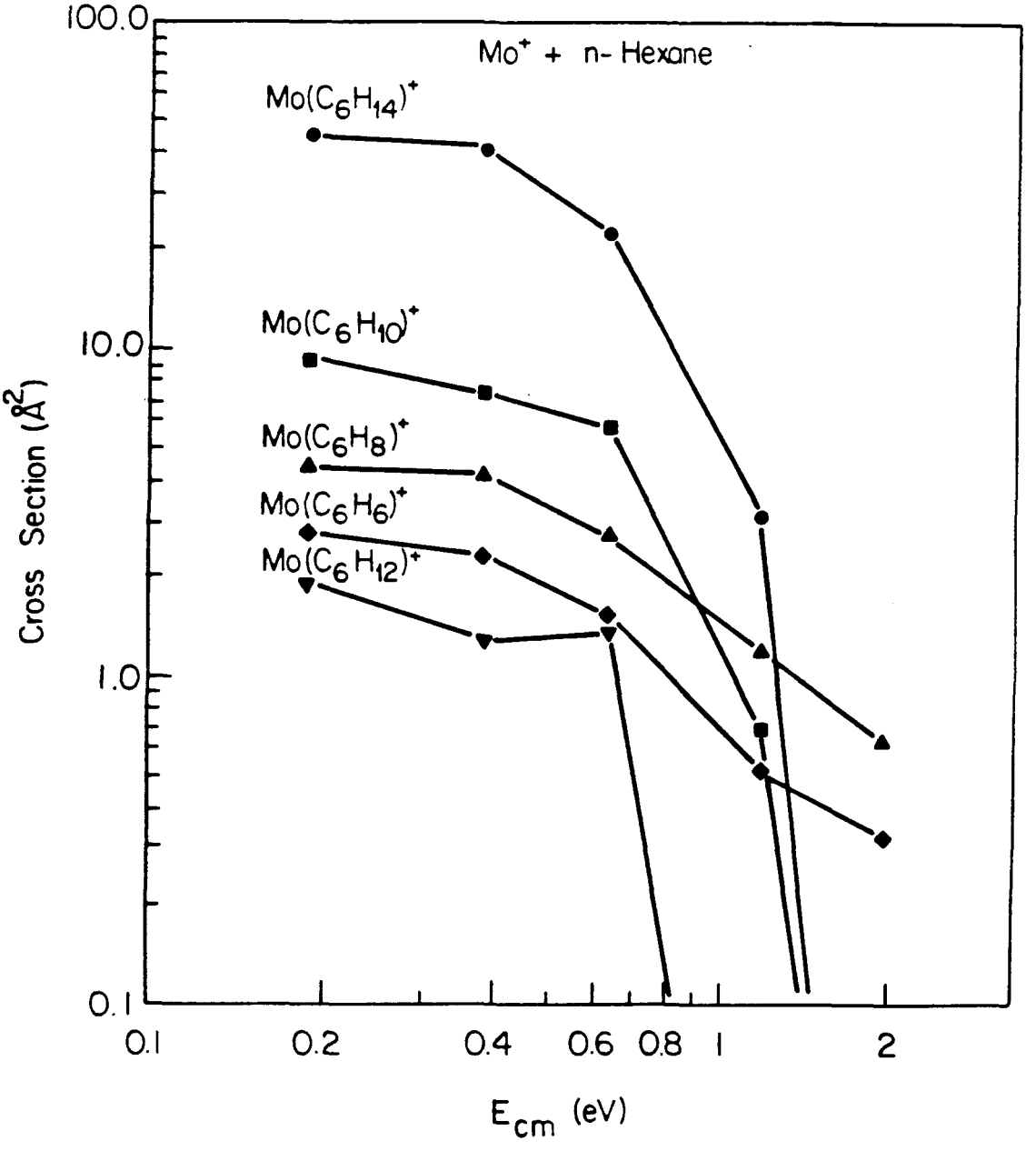
Mo+ + n- Hexane
Mo(C6H14)+
Mo(C6H10)+
Mo(C6H8)+
Mo(C6H6)+
Mo(C6H12)+
Cross Section (Å2)
100.0
10.0
1.0
0.1
0.1
0.2
0.4
0.6
0.8
1
2
Ecm (eV)

$Mo(C_6H_6)^+$ from $Mo(C_6H_8)^+$ due to the −5.5 kcal/mol enthalpic change on conversion of 1,3-cyclohexadiene to benzene and hydrogen.

Cyclopropane and Cyclobutane. The ring strain in these two cycloalkanes is seen to increase their reactivity over that of cyclopentane and cyclohexane. Although dehydrogenation products are seen for both of these molecules, it is unlikely that these products arise from a process involving initial C–H insertion, at least not for cyclopropane. The C–H bond strengths of cyclopropane and cyclobutane are 106.3 and 96.5 kcal/mol, respectively, while the C–C bonds are much weaker, being only approximately 54 and 55 kcal/mol.[15] Schemes I and II show the expected pathways for production of $Mo(C_3H_4)^+$ from cyclopropane and the three products, eq. 9–11,

$$Mo^+ + c\text{-}C_4H_8 \xrightarrow{40\%} Mo(C_4H_6)^+ + H_2 \quad (9)$$

$$\xrightarrow{5\%} Mo(C_4H_4)^+ + 2H_2 \quad (10)$$

$$\xrightarrow{55\%} Mo(C_2H_4)^+ + C_2H_4 \quad (11)$$

formed in the reaction with cyclobutane. We also show the C–H insertion process for cyclobutane since this process could account for the dehydrogenation products. Reaction with both cycloalkanes could proceed through initial insertion into a C–C bond to form a metallacycle. Two β–H transfers and H_2 elimination yield Mo^+–allene and Mo^+–butadiene complexes. Subsequent loss of H_2 from $Mo(C_4H_6)^+$ would yield Mo^+–cyclobutadiene. $Mo(C_2H_4)^+$ can come from symmetric cleavage of the metallacyclopentane to give a bis-ethylene complex and then elimination of C_2H_4. This is a major product pathway and tends to indicate that the metal does indeed insert into one of the C–C bonds.

Interaction of Cr^+ and Mo^+ with Alkenes. Table III shows the product distributions for the reactions between Mo^+ with several small alkenes. Product cross sections are much larger than in the comparable alkane reactions. Although Mo^+ is much more reactive with alkenes than alkanes, Cr^+ remains unreactive. Reaction is only seen with cyclohexene, where very small amounts of $Cr(C_6H_8)^+$

Scheme I

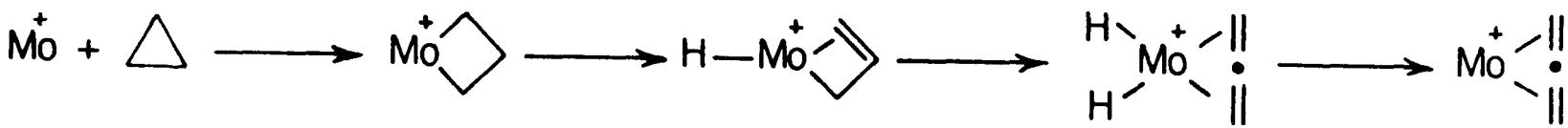

Scheme II

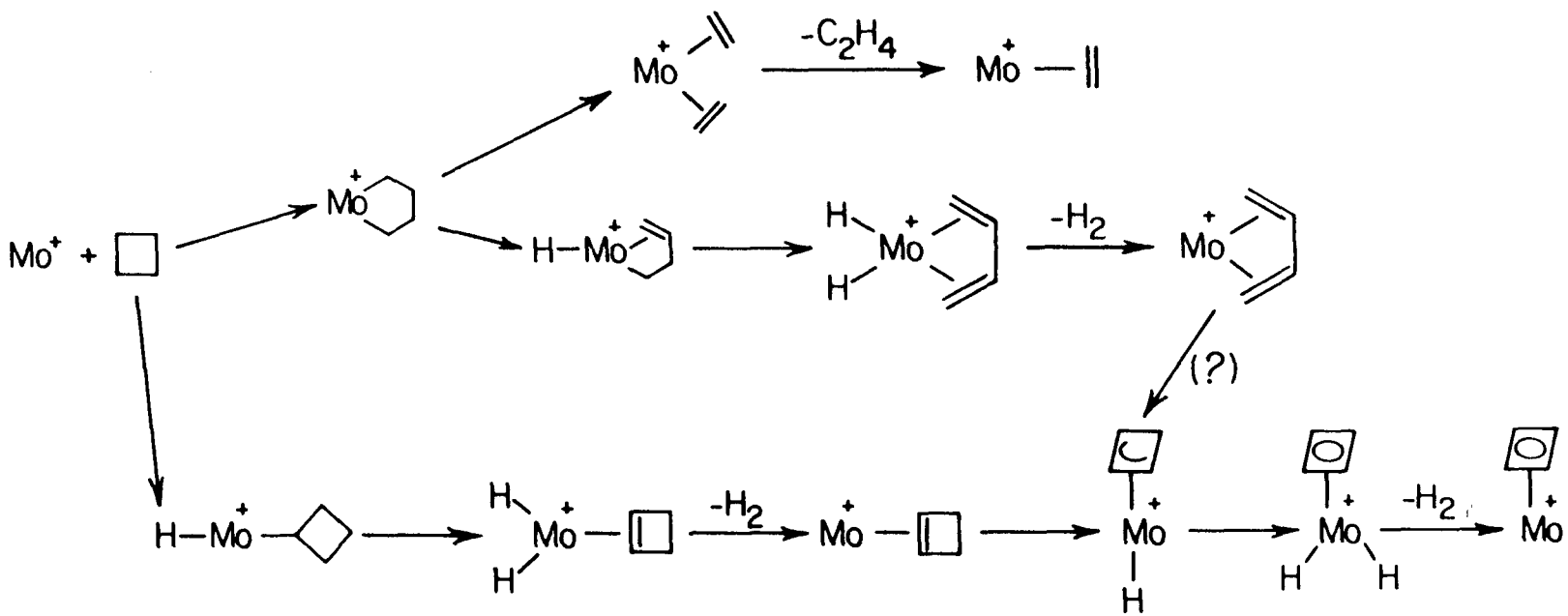

Table III

Product Distributions for the Reactions of Mo^+ with Alkenes

Neutral Reactant	Percentages of Neutral Products[a]							Reaction Cross Section ($Å^2$)[b]
	H_2	$2H_2$	$3H_2$	CH_4	$CH_4 + H_2$	C_2H_4	C_2H_6	
Ethylene	100							0.5
Propene	100							46.5
1-Butene	100							115.0
cis-2-Butene	100							119.0
1-Pentene	73	25		1		1	tr[c]	133.9
1-Hexene	14	81	2		2		1	288.9
Cyclohexene	7	93						216.2

[a] Observed at a center-of-mass collision energy of approximately 0.25 eV. [b] Total reaction cross section for all observed products. [c] Trace amount (<1%) observed.

and $Cr(C_6H_6)^+$ are observed.

Ethylene and Propene. Mo^+ was seen to double dehydrogenate ethane. Thus, it is no surprise that dehydrogenation of ethylene also takes place. The overall reaction cross section for the process is very small (0.5 $Å^2$ at a collision energy of 0.25 eV). The generally accepted pathway for reaction of metal ions with alkenes[16] involves an initial metal insertion into one of the allylic C–H or C–C bonds. With ethylene this is not possible and the metal must interact with the stronger vinylic C–H bonds. Reaction of Mo^+ with propene *can* proceed through initial allylic C–H insertion to yield a hydrido-allyl complex. Subsequent β–H transfer to the metal and reductive elimination of H_2 gives Mo^+–allene. The cross section is approximately a hundred times greater than that for the ethylene reaction as well as the related reaction with propane.

1-Butene and cis-2-Butene. Reaction of Mo^+ with butane yielded Mo^+–butadiene as the only product. Reaction with the two butene isomers also gives this single product by elimination of H_2. Reaction cross sections for the two isomers are very similar and the two reaction processes probably involve the same hydridoallyl intermediate, Scheme III, after allylic C–H insertion.

1-Pentene, 1-Hexene, and Cyclohexene. Similar to the other cases already discussed, Mo^+ reacts with the C_5 and C_6 alkenes to give predominantly H_2 loss products. Contrary to the reactions with the comparable alkanes, however, there are also small amounts of C–C bond cleavage products. Scheme IV shows possible mechanisms for the products observed in the reaction with 1-pentene. Products are produced by either initial insertion into an allylic C–H bond followed by β–H or β–CH_3 shifts and elimination of H_2 or CH_4 or through initial allylic C–C bond insertion. An H shift from either the allyl ligand or the ethyl group then leads to elimination of either C_2H_4 or C_2H_6. In contrast to 1-pentene and 1-hexene, the reaction of Mo^+ with cyclohexene yields only dehydrogenation products (Scheme V).

Scheme III

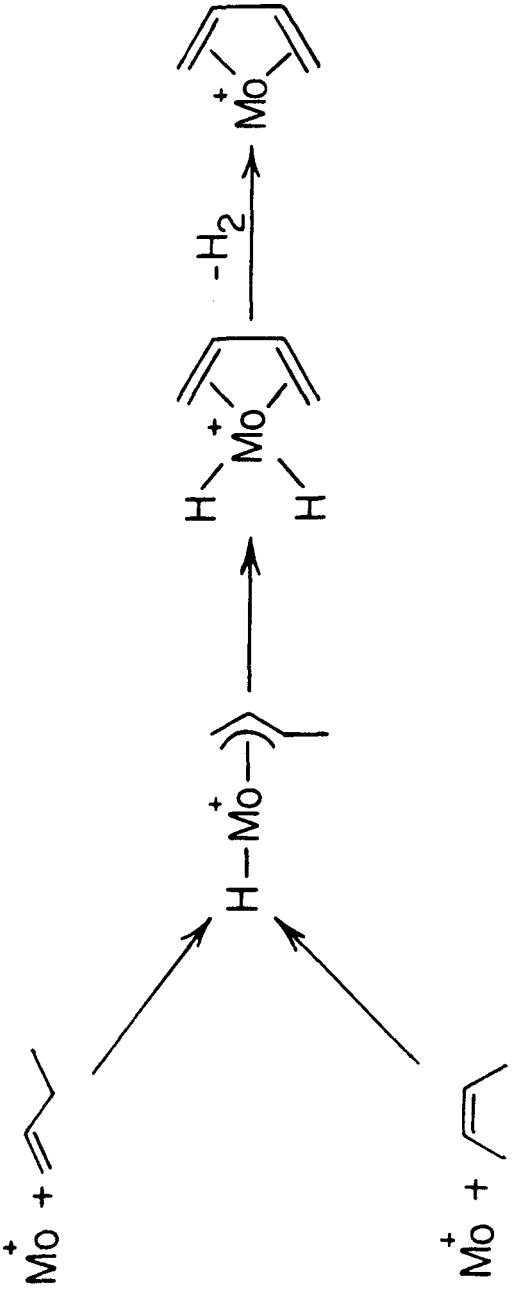

Scheme IV

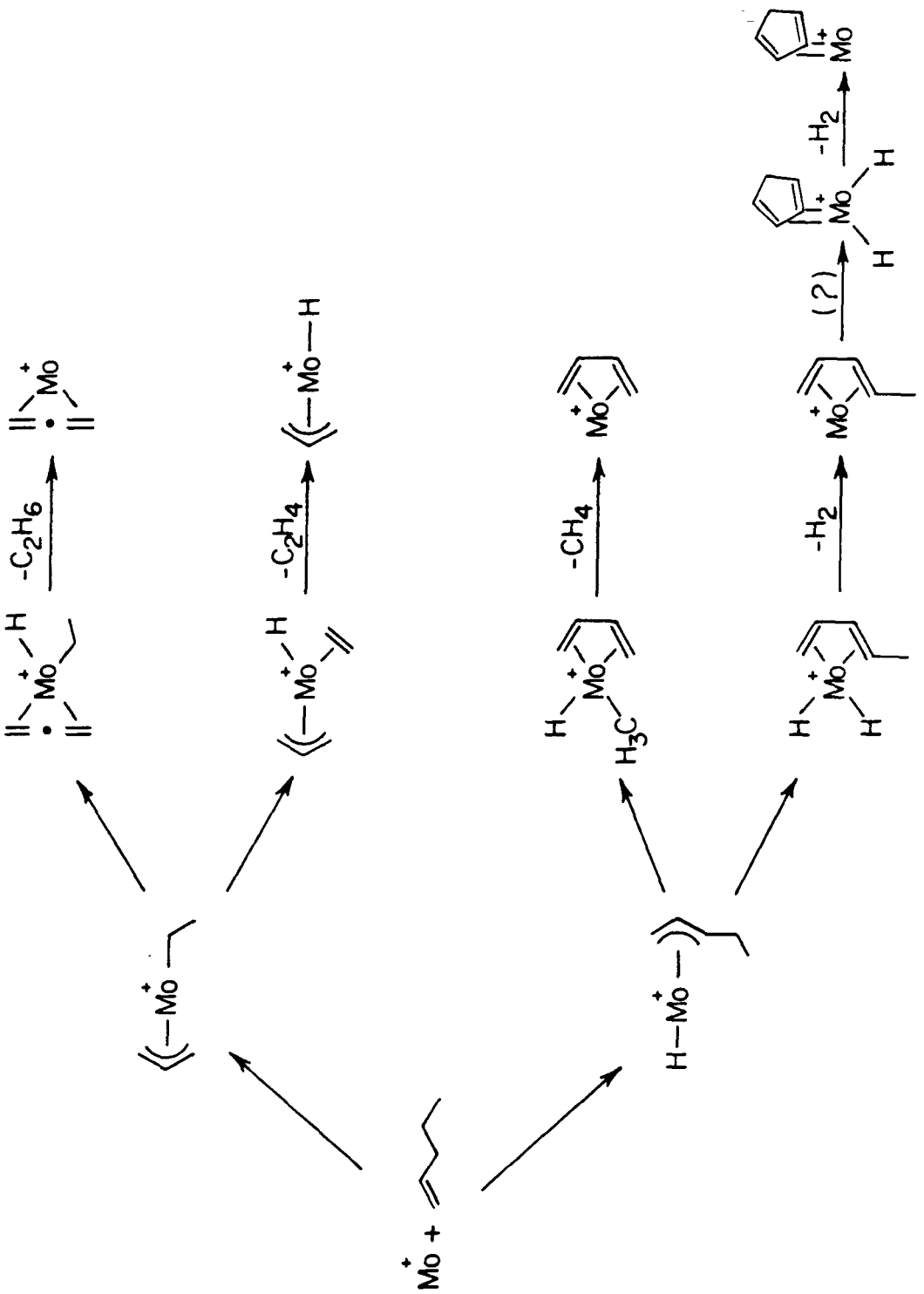

Scheme V

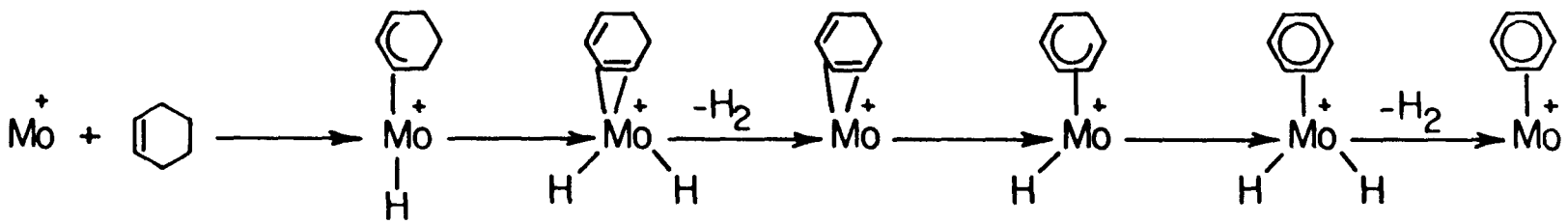

Discussion

Reactivity differences between first and second row transition metal congeners is not a fact unique to Cr^+ and Mo^+. Although the reaction types are similar, the Group 3 metal ions, Sc^+, Y^+, and La^+, to a certain extent, exhibit quite different product distributions.[2,7] The differences displayed by the Group 8 (Fe^+ and Ru^+) and Group 9 (Co^+ and Rh^+) metal ions is much greater than for Sc^+ and its congeners, with very different types of products.[5] While products in which C–C bonds are cleaved are prevalent with Fe^+ and Co^+, the interaction of Ru^+ and Rh^+ with hydrocarbons leads to almost exclusive elimination of one or more molecules of H_2. In all cases studied thus far, congeners are distinguished by differences in the relative importance of different reaction pathways. In the present case there is a difference in overall reactivity, where Cr^+ is totally unreactive while Mo^+ activates C–C and C–H bonds. For an explanation of this behavior, we must understand the differences between the metals in terms of: (1) electronic structure; (2) bonding characteristics; and (3) the overall reaction mechanism for hydrocarbon activation. These points are by no means independent and all interact to produce the observed results.

As an example of the alkane activation process, we will consider the reaction of a metal ion with n-butane (Scheme VI) to give 1,2 H_2 elimination and a M^+–2-butene product (eq 12).

$$M^+ + C_4H_{10} \longrightarrow M(C_4H_8)^+ + H_2 \qquad (12)$$

In the gas phase, for the reaction to occur and exhibit exothermic behavior, the final product as well as all points on the reaction pathway must be lower in energy than the initial reactants. Figure 2 shows a recently proposed simplified potential energy diagram for the dehydrogenation of butane by V^+ along with the proposed reaction intermediates.[3] The 1,2 mechanism for dehydrogenation of butane is assumed to take place in four steps. Initial approach of the metal ion induces a diple in the neutral butane. Interaction of this dipole with the

Scheme VI

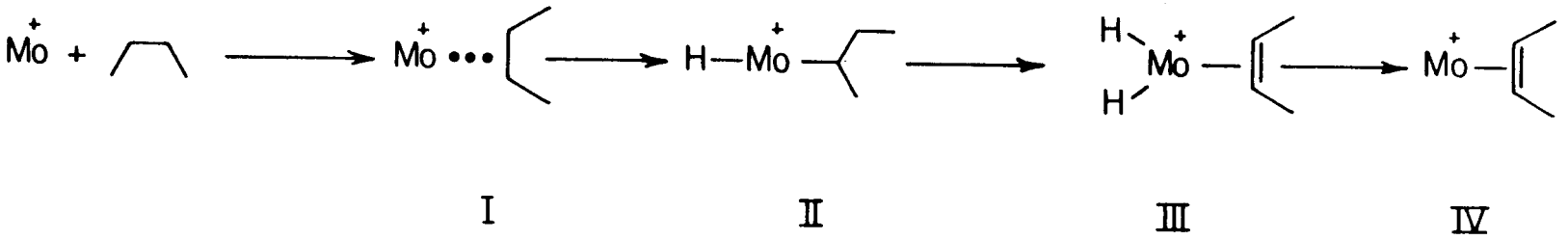

Figure 2: Simplified potential energy diagram for the reaction of M^+ with n-butane to form a metal–2-butene product and H_2. The diagram follows the reaction pathway of Scheme VI. The diagram was taken from reference 3 as proposed for the reaction of V^+.

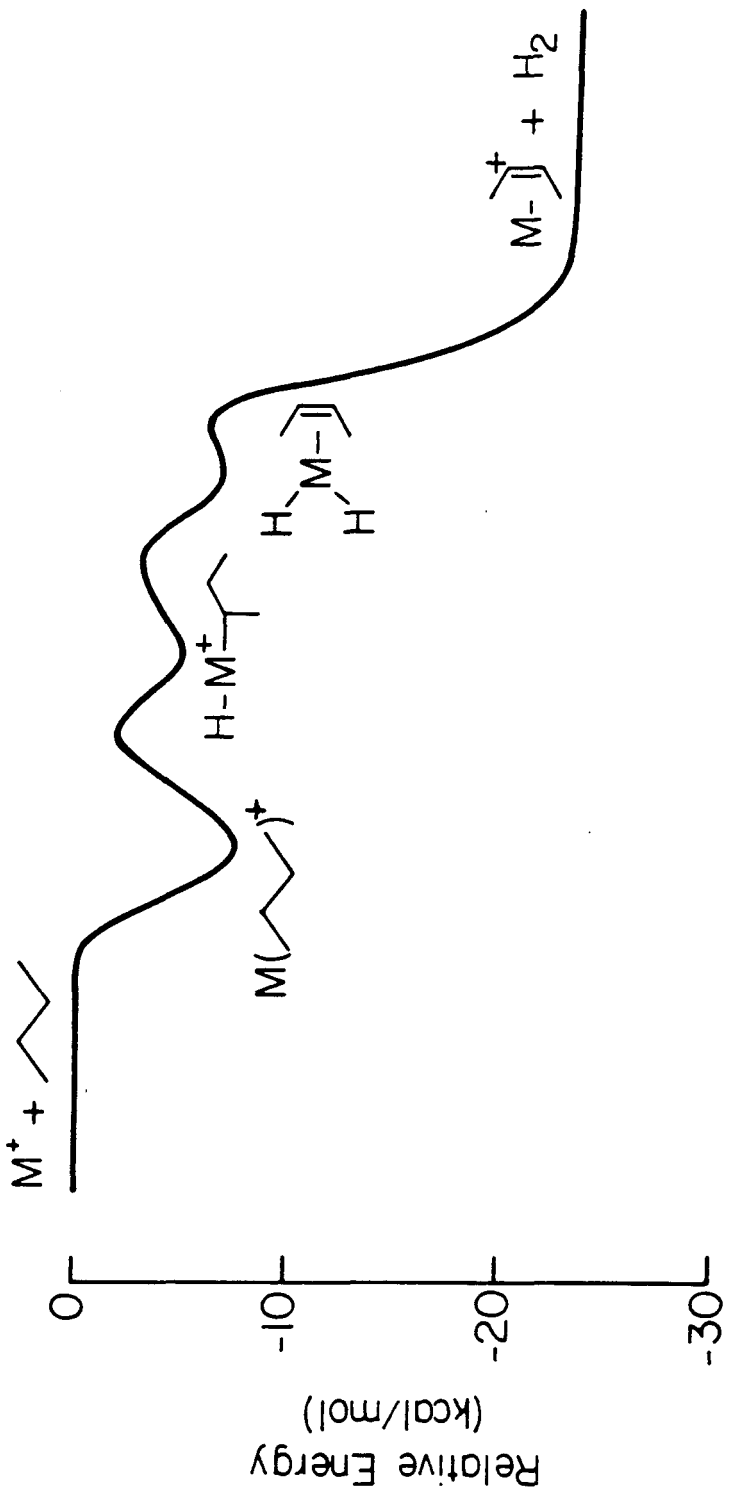
Relative Energy
(kcal/mol)
0
-10
-20
-30
M+ +
M(
)+
H-M+
H
M
H
M-
+ H2

metal ion allows formation of a loose collision complex (I in Scheme VI) with an interaction energy of possibly 10–15 kcal/mol. In many ion–molecule reactions, this interaction energy is sufficient to overcome any intrinsic barrier to further reaction. The second step involves insertion of the metal ion into one of the C–H bonds to produce new metal–carbon and metal–hydrogen bonds in place of the original C–H bond (II). Thirdly, transfer of a β–hydrogen to the metal center forms a dihydrido–metal–butene complex (III). Reductive elimination of H_2 then gives the final metal–butene product (IV).

Equations 16–18 give the overall energetics for production of the alkyl and hydrogen fragments in the two inserted intermediates and the final product.

$$C_4H_{10} \longrightarrow C_4H_9 + H \qquad \Delta H = 96 \text{ kcal/mol} \qquad (13)$$

$$\longrightarrow C_4H_8 + 2H \qquad = 132 \text{ kcal/mol} \qquad (14)$$

$$\longrightarrow C_4H_8 + H_2 \qquad = 27 \text{ kcal/mol} \qquad (15)$$

Thus, for the initial insertion step to be exothermic, the sum of the metal–carbon and metal–hydrogen bonds must be greater than 96 kcal/mol. For the next step, the sum of the two metal–hydrogen bonds plus the metal–alkene bond must be greater than 132 kcal/mol. Lastly, for the overall reaction to be exothermic, the metal–2-butene bond energy must be greater than 27 kcal/mol. Several estimates have been made on the bond strength between bare metal ions and ethylene. It has been estimated that the Sc^+–ethylene bond strength is on the order of 40 kcal/mol.[2] Aristov and Armentrout have indicated that V^+ binds ethylene with an energy of approximately 50 kcal/mol.[4] The M^+–ethylene bond strength has also been estimated, from kinetic energy release data for the reactions of the first row Group 8–10 metals, as being between 40 and 45 kcal/mol.[17] We can thus assume that the metal–butene interaction is also this strong and that the overall dehydrogenation reaction of butane by Cr^+ and Mo^+ is exothermic. If we also assume that $D(H_2M^+–C_4H_8) = 50$ kcal/mol, then the sum of the two M^+–H bonds in the reaction intermediate must be greater than 82 kcal/mol.

If, as we have suggested, the overall dehydrogenation reaction is exothermic, then either the initial insertion step or the β–hydrogen transfer step must be endothermic for the reaction of Cr^+ and the difference between Cr^+ and Mo^+ must lie in the strengths of the bonds formed to the two metals. As shown in Table I, the ground and first excited electronic states for Cr^+ and Mo^+ are the same with almost identical state splittings. These two states have been shown to be important in the bonding between the metal ions and hydrogen.[11] The superficial similarity between the electronic states of the two metal ions might lead one to assume that the bonding in equivalent compounds would be very similar. This, however, is not the case. One must also take other factors into consideration such as the size of the orbitals, the intrinsic bond strengths of hydrogen and carbon to various orbitals, and the exchange energy between the high spin electrons. Elkind and Armentrout[18] have determined, using guided ion beam techniques, bond energies for the diatomic metal hydride ions, CrH^+ and MoH^+, of $D_{298}(M^+ - H) = 28.6 \pm 2$ kcal/mol and 42 ± 3 kcal/mol, respectively, a fairly substantial difference. Ab initio theoretical calculations on the two molecules[11] also indicate significant differences in the hybridizations of the bonding orbitals used by the two metals. In CrH^+, the metal bond orbital is hybridized 40.6% s, 12.5% p, and 46.9% d, building in a substantial amount of the ^6D excited state. For MoH^+, on the other hand, the hybridization is 19.7% s, 7.0% p, and 73.3% d, with a much greater amount of d (ground state) character.

How does one account for the differences in bonding to the two metals? The major difference is in the principal quantum numbers for the valence electrons. The Mo^+ orbitals are larger than the corresponding Cr^+ orbitals. Hartree-Fock calculations[11] indicate a difference of $\sim$0.29 Å in the radii of the 3d and 4d orbitals (0.75 Å versus 1.04 Å) and a 0.14 Å difference between the 4s and 5s orbitals (1.73 Å versus 1.87 Å). Calculations designed to show the trends in "intrinsic" bond energy of hydrogen to pure s or d orbitals indicate that the optimal size s orbital is smaller than that of Zn^+, 1.49 Å, and that the optimum size d orbital

is larger than the 4d orbitals of Y^+, 1.47 Å. Thus, the intrinsic bond strengths predict stronger s-bonding for Cr^+ and stronger d-bonding for Mo^+.

Exchange energy losses are another important consideration. For unpaired electrons in orthogonal orbitals, high spin coupling is best (Hund's rule) due to the energy stabilization from electron exchange. When one of these high spin electrons is spin paired to another electron to form a bond, it is essentially high spin coupled to the other metal electrons only one half of the time, causing a loss of one half of the high spin exchange stabilization due to that electron. For ^6S Cr^+, the average d–d exchange energy, K_{dd}, is 16.5 kcal/mol, while for ^6D Cr^+, K_{sd} = 5.1 kcal/mol and K_{dd} = 18.2 kcal/mol. The exchange terms are inversely proportional to the distance between the electrons. Thus, for Mo^+, with larger d orbitals and a smaller s–d size difference, K_{dd} is smaller than for Cr^+, 13.4 and 14.2 kcal/mol (^6S and ^6D states, respectively), while K_{sd} is larger, 8.5 kcal/mol. Since the electronic states of the two metal ions are the same, the number of exchange terms lost on bonding is also the same. Exchange arguments yield the same trends as the intrinsic bonding arguments, supporting more d-bonding in Mo^+ compounds and more s-bonding in Cr^+ compounds. For Cr^+, however, s-bonding has the unfortunate energy penalty of involving an electronic state 1.52 eV above the ground state. Thus, exchange energy losses are high on bonding to the ground state and promotion energy losses are high on bonding to the excited state, all of which causes the Cr^+–H bond energy to be quite weak. Mo^+, on the other hand, loses less energy bonding with its ground state and forms stronger sigma bonds.

All the reaction intermediates we are dealing with involve not one, but two sigma bonds to the metal ion. Experiments have not yielded bond energies for the second metal bond and we must thus estimate the differences in the first and second bond dissociation energies. The simplest such case is the metal dihydride. We have previously published a theoretical study on the bonding in the two metal dihydrides CrH_2^+ and MoH_2^+.[11d] The second metal–hydrogen bond

in the molybdenum case is very similar to the first from the standpoint of metal orbital hybridization. Since the number of high spin coupled electrons is less, the second bond dissociation energy is found to be slightly higher than the first. In CrH_2^+, from an energy standpoint, the second bond can be thought of as being to an almost pure metal d orbital (although mixing creates two equivalent Cr^+–H bonds). As we have just discussed, d-bonding in Cr^+ is not strong, and the second metal–hydrogen bond in chromium dihydride is indeed seen to be weaker than the first by up to 7 kcal/mol.

Activation of the C–H bonds in ethane by Mo^+ indicates that the sum of the metal–hydrogen and metal–ethyl bond energies is at least 98 kcal/mol. The very small cross section for this reaction suggests that the process may be very nearly thermoneutral. If we assume a difference of 7 kcal/mol in the bond energies of two metal–hydrogen bonds (the difference in exchange energy lost on bonding), this would yield a sum of 91 kcal/mol for two M^+–H bonds.[19] We must assume, then, that a metal–alkyl bond is on the order of 7–10 kcal/mol stronger than a metal hydrogen bond. Making similar assumptions for Cr^+ leads to a sum of metal–hydrogen and metal–alkyl bond energies of approximately 59 kcal/mol, much below the C–C and C–H bond energies of alkanes. Thus, from a bond energy standpoint, the Mo^+ bond energies are just strong enough to activate C–H bonds and the reactions are seen to be exothermic with small cross sections. The bonds formed by Cr^+ are much too weak for the metal to be reactive with hydrocarbons. Estimated potential energy curves for the interaction of both Cr^+ and Mo^+ with n-butane are shown in Figure 3. A previous study[10b] supports the estimated energetics for the Cr^+–butane interaction. Collision induced dissociation of Cr^+–n-butane and Cr^+–2-methylpropane complexes yield, almost exclusively, Cr^+ and the neutral alkane. This indicates that the neutrals are only loosely bound to the metal ion and that the dissociation pathway is lower in energy than reaction pathways.

Replacing n-butane by 1-butene in the dehydrogenation reaction with Mo^+

Figure 3: Estimated potential energy diagrams for the reactions of Cr^+ and Mo^+ with n-butane to produce H_2 and a metal–2-butene product, using the bond energies discussed in the text. The large endothermicity for insertion of Cr^+ into C–H bonds explains the ions unreactivity with alkanes.

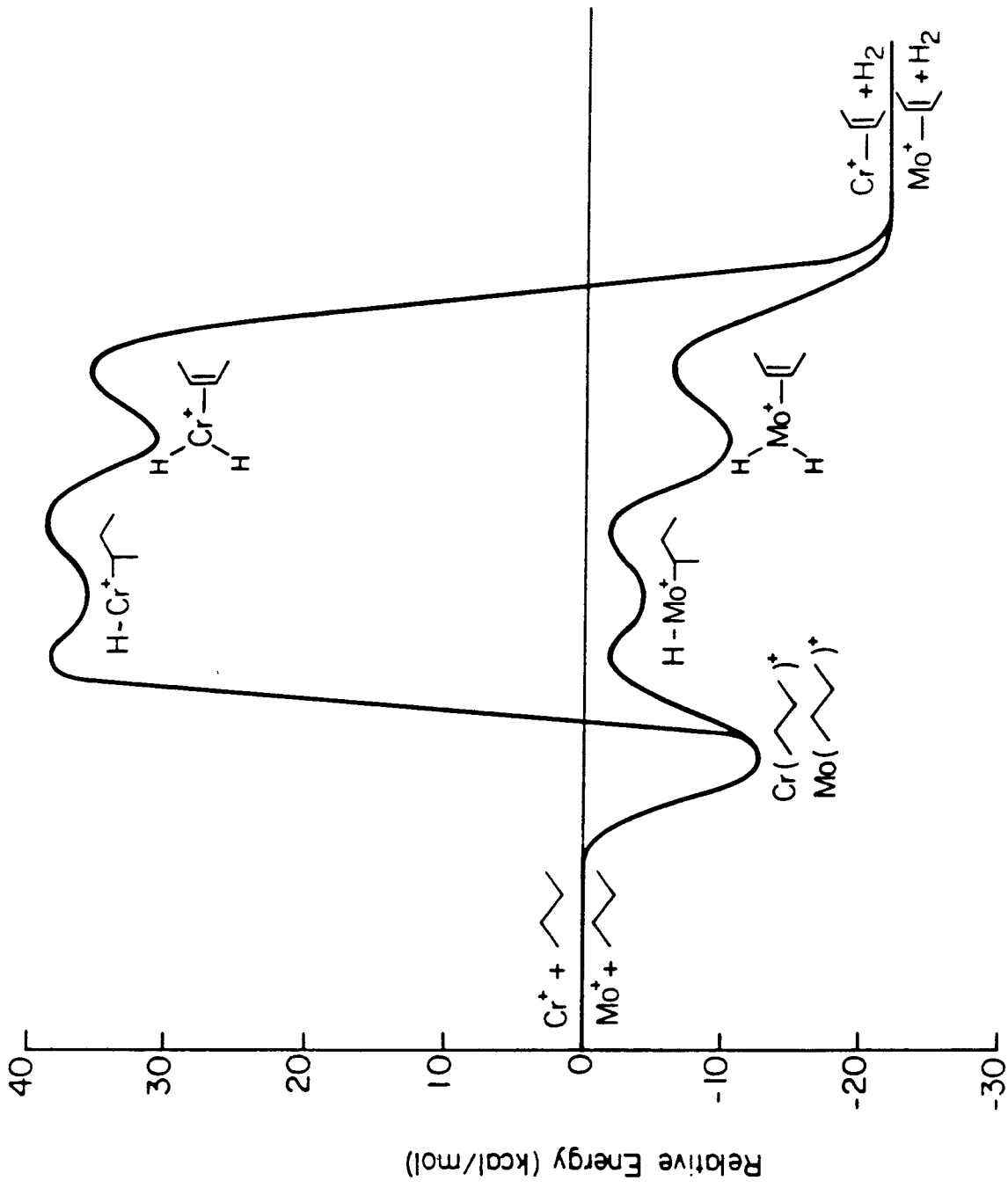
Relative Energy (kcal/mol)
40
30
20
10
0
-10
-20
-30
Cr+ +
Mo+ +
H-Cr+
H-Mo+
Cr(
Mo(
)+
)+
Cr+—
Mo+—
+H2
+H2

is seen to make a large change in the reaction cross section (the cross section increases by a factor of almost 40). This change is brought about by the increased interaction energy between the ion and neutral due to the presence of the π system. We have seen that metal–ethylene bonds are on the order of 40–50 kcal/mol. Thus, the initial metal–butene interaction as well as the bonds in the hydrido–allyl metal insertion complex lower the energy of these species on the reaction surface and make the reaction more facile. Again, for Cr^+, the bond strengths must be too weak for the insertion process to take place.

The types of reaction products observed with Mo^+ are similar to those found in the reactions of Ru^+ and Rh^+, almost exclusive elimination of hydrogen and formation of metal–alkene complexes. First row Group 8–10 metals are seen to form many products which result from cleavage of C–C bonds. In all cases studied so far, as one proceeds down a column in the periodic table, the amount of dehydrogenation increases and the amount of C–C bond cleavage products decrease. It has been argued by Tolbert and Beauchamp that for the case of Ru^+ and Rh^+, this is not due to a difference in the bond dissociation energies to the metals but to the types of orbitals involved in bonding. If one assumes an initial interaction with and insertion into a C–H bond, then hydrogen loss products and alkane loss products must come from a competition between β–hydrogen versus β–alkyl migrations onto the metal followed by reductive elimination. The first row metals are seen to use much more s character in bonding than the corresponding second row metals. It is postulated that the highly directional nature of the second row metal d bonds favor transfer of a spherically symmetric, non-directional hydrogen atom while the less directional, s-containing, bonds of the first row metals allow transfer of alkyl groups with their more directional carbon p orbitals. Mo^+, with its largely d-like bonds falls into the same category as Ru^+ and Rh^+ and is seen to favor insertion into C–H bonds along with β–hydrogen transfer and formation of hydrogen loss products.

Summary

Previous studies have shown that excited state Cr^+ is reactive, even with methane. The present work shows that ground state Cr^+ is very unreactive with small hydrocarbons including alkenes. Mo^+, although quite similar to Cr^+ from the standpoint of low-lying electronic states, is seen to activate C–H bonds of alkanes, cycloalkanes, and alkenes. The reaction products are similar to those seen with other second row metal ions, Rh^+ and Ru^+, although the overall reactivity is not as great. Theoretical calculations on CrH^+, MoH^+, CrH_2^+, and MoH_2^+ indicate that the differeces observed between the two metal ions are the result of the very weak sigma bonds formed by Cr^+, causing the insertion of Cr^+ into C–H bonds to be endothermic. The larger size of the d orbitals of Mo^+, and the resultant decrease in the d–d exchange energy lost on forming sigma bonds to the metal, result in stronger bonds to Mo^+, just strong enough to activate the C–H bonds of alkanes.

Acknowledgement. We thank the National Science Foundation (Grant No. CHE84-07857) for partial support of this work.

References

(1) See for example: (a) Halle, L. F.; Armentrout, P. B.; Beauchamp, J. L. *Organometallics* **1982**, *1*, 963. (b) Houriet, R.; Halle, L. F.; Beauchamp, J. L. *Organometallics* **1983**, *2*, 1818. (c) Jacobson, D. B.; Freiser, B. S. *J. Am. Chem. Soc.* **1983**, *105*, 5197. (d) Larsen, B. S.; Ridge, D. P. *J. Am. Chem. Soc.* **1984**, *106*, 1912. (e) Jacobson, D. B.; Freiser, B. S. *J. Am. Chem. Soc.* **1983**, *105*, 7492. (f) Armentrout, P. B.; Beauchamp, J. L. *J. Am. Chem. Soc.* **1981**, *103*, 6628.

(2) Tolbert, M. A.; Beauchamp, J. L. *J. Am. Chem. Soc.* **1984**, *106*, 8117.

(3) Tolbert, M. A.; Beauchamp, J. L. *J. Am. Chem. Soc.* **1986**, *108*, 7508.

(4) Aristov, N.; Armentrout, P. B. *J. Am. Chem. Soc.* **1986**, *108*, 1806.

(5) Tolbert, M. A.; Mandich, M. L.; Halle, L. F.; Beauchamp, J. L. *J. Am. Chem. Soc.* **1986**, *106*, 5675.

(6) Byrd, G. D.; Freiser, B. S. *J. Am. Chem. Soc.* **1982**, *104*, 5944.

(7) Huang, Y.; Wise, M. B.; Jacobson, D. B.; Freiser, B. S. *Organometallics* **1987**, *6*, 346.

(8) (a) Wise, M. B.; Jacobson, D. B.; Freiser, B. S. *J. Am. Chem. Soc.* **1985**, *107*, 1590. (b) Wise, M. B.; Jacobson, D. B.; Freiser, B. S. *J. Am. Chem. Soc.* **1985**, *107*, 6744.

(9) Weil, D. A.; Wilkins, C. L. *J. Am. Chem. Soc.* **1985**, *107*, 7316.

(10) (a) Halle, L. F.; Armentrout, P. B.; Beauchamp, J. L. *J. Am. Chem. Soc.* **1981**, *103*, 962. (b) Freas, R. B.; Ridge, D. P. *J. Am. Chem. Soc.* **1980**, *102*, 7129.

(11) (a) Schilling, J. B.; Beauchamp, J. L.; Goddard, W. A., III *J. Am. Chem. Soc.* **1986**, *108*, 582. (b) Schilling, J. B.; Beauchamp, J. L.; Goddard, W. A., III , submitted for publication. (c) Schilling, J. B.; Beauchamp, J. L.; Goddard, W. A., III *J. Am. Chem. Soc.* , in press. (d) Schilling, J. B.; Beauchamp, J. L.; Goddard, W. A., III *J. Phys. Chem.* , in press.

(12) (a) Armentrout, P. B.; Beauchamp, J. L. *Chem. Phys.* **1980**, *50*, 21. (b)

Armentrout, P. B.; Beauchamp, J. L. *J. Chem. Phys.* **1981**, *74*, 2819.

(13) Moore, C. E. "Atomic Energy Levels," National Bureau of Standards, Washington D.C., 1971, Vol. II and III.

(14) Thermodynamic quantities used in this paper are taken from: (a) Cox, J. D.; Pilcher, G. "Thermochemistry of Organic and Organometallic Compounds," Academic Press, New York, 1970. (b) McMillen, D. F.; Golden, D. M. *Annu. Rev. Phys. Chem.* **1982**, *33*, 493.. (c) Rosenstock, H. M.; Draxl, K.; Steiner, B. W.; Herron, J. T. *J. Phys. Chem. Ref. Data* **1977**, *6*, Supp. 1. (d) Wagman, D. D.; Evans, W. H.; Parker, V. B.; Schumm, R. H.; Halow, I.; Bailey, S. M.; Churney, K. L.; Nuttall, R. L. *J. Phys. Chem. Ref. Data* **1982**, *11*, Supp. 2.

(15) The cyclopropane and cyclobutane C–C bond energies are determined as outlined in Benson, S. W. "Thermochemical Kinetics," Wiley, New York, 1976. Heats of formation of the diradical formed on ring opening are determined using the terminal C–H bond dissociation energy for the corresponding linear alkane, assuming that breaking the C–H bonds at either end of the molecule are equivalent and that there is no interaction between the resulting radical electrons.

(16) (a) Armentrout, P. B.; Halle, L. F.; Beauchamp, J. L. *J. Am. Chem. Soc.* **1981**, *103*, 6624. (b) Jacobson, D. B.; Freiser, B. S. *J. Am. Chem. Soc.* **1983**, *105*, 7484. (c) Peake, D. A.; Gross, M. L.; Ridge, D. P. *J. Am. Chem. Soc.* **1984**, *106*, 4307.

(17) Hanratty, M. A.; Beauchamp, J. L.; Illies, A. J.; van Koppen, P.; Bowers, M. T., in press.

(18) Elkind, J. L.; Armentrout, P. B.*Inorg. Chem.* **1986**, *25*, 1080.

(19) The calculated bond dissociation energy for MoH^+ is $D_e(M^+ - H) = 33.8$ kcal/mol, which is over 8 kcal/mol weaker than the experimentally determined value. The bond energy, $D_e(HM^+ - H)$, is calculated to be 35.1 kcal/mol, yielding a sum for the two metal–hydrogen bonds of 68.9 kcal/mol.

This value is not consistent with the observed reactivity of Mo^+ and we thus use experimental estimates for the bond strengths.

CHAPTER IV

THEORETICAL STUDIES OF TRANSITION METAL HYDRIDES:

II. CaH^+ THROUGH ZnH^+

Theoretical Studies of Transition Metal Hydrides:

II. CaH^+ through ZnH^+

J. Bruce Schilling, William A. Goddard III, and J. L. Beauchamp

Contribution No. 7550 from the

Arthur Amos Noyes Laboratory of Chemical Physics

California Institute of Technology, Pasadena, CA 91125

Abstract

We present consistent ab initio calculations (generalized valence bond plus configuration interaction) of the spectroscopic parameters for the ground and low-lying electronic states of the diatomic transition metal hydrides CaH^+ through ZnH^+. We examine, in detail, the competing factors affecting metal hydride bonding: (1) the relative energies of the metal low-lying electronic states; (2) the intrinsic bond strength of H to various size 4s, 3d, or hybridized metal orbitals; and (3) the loss of high-spin metal exchange energy on bonding.

I. Introduction

In the past few years, an ever increasing number of experiments have been carried out to determine the bond dissociation energies of the first-row transition metal hydride cations. The various techniques include high pressure proton transfer,[1] ion cyclotron resonance,[2] and ion beam mass spectrometry.[3] Recent investigations by Elkind and Armentrout [4] using "guided" ion beam methods have produced the most accurate, consistent and complete set of M^+–H bond energies. However, in some cases there remain significant inconsistencies

Additional experiments have been carried out to study the gas phase activation, at transition metal centers (using atomic metal ions), of alkanes, alkenes, and cycloalkanes.[5] Most of the proposed mechanisms for the observed reactions involve insertion of the metal ion into either C–C or C–H bonds of the neutral species. The reaction intermediates and sometimes the products thus involve metal systems with metal-ligand σ bonds. Studies have also been carried out on the reactions of the metal hydride ions for the first-row metals of Groups 8–10.[6]

In order to help understand the reactions of the metal hydrides and of the bare metal ions, we have carried out theoretical studies of the metal-hydride bonding in the case of CaH^+ through ZnH^+, with the emphasis on bond dissociation energies and spectroscopic properties.

The ground states, geometries, vibrational frequencies, and bond dissociation energies have been summarized previously.[7] In this paper, we will examine the competing factors affecting metal hydride bonding in some detail. A detailed description of the calculational methods (including how the level of elctronic correlation in the wavefunction affects the calculated bond dissociation energies) is also presented. Some low-lying electronic states of the metal hydride ions are also described.

Results and Discussion

Calculated total energies for MH^+ (at R_e), M^+, and H are presented in Table I and the resultant MH^+ bond dissociation energies in Table II. Table III summarizes the configurations, bond lengths, vibrational frequencies, and excitation energies for various ground and excited state species. A major point of this paper will be to explain the dramatic variations of the bond energies and excitation energies in terms of the atomic states and bond character.

Low-Lying Electronic States. The simplest way to understand the bonding in the first row metal-hydride cations, MH^+, is to start with the $4s^1 3d^{n-1}$ configuration of M^+ and to spin pair the 4s orbital of M^+ with the 1s orbital of H. The n−1 electrons in d orbitals are then partitioned among the five nonbonding orbitals (predominately d-like) which we will denote as $d\sigma$, $d\pi$, and $d\delta$ and this d^{n-1} configuration is coupled high spin. In this way, one can predict and understand the symmetry of the ground and low-lying electronic states.

Thus, for ScH^+, there is one nonbonding electron and it can be $d\delta$ (leading to the $^2\Delta$ state), $d\pi$ (leading to the $^2\Pi$ state), or $d\sigma$ (leading to the $^2\Sigma^+$ state). The ordering of states is $^2\Delta < {}^2\Pi < {}^2\Sigma^+$, which can be understood on the basis of simple electrostatic and orthogonality considerations. Thus, the electrostatic repulsion between the electron in a d orbital and the electrons in the bond is lowest for $d\delta$ and highest for $d\sigma$. In addition, an electron in $d\sigma$ must be orthogonalized to the orbitals in the bond pair which destabilizes $d\sigma$ even more. The net result is an excitation energy from $^2\Delta$ to $^2\Pi$ of 5.1 kcal/mol and to $^2\Sigma^+$ of 8.0 kcal/mol (see Table III).

Based on the orbital ordering in ScH^+ ($d\delta < d\pi < d\sigma$), one might expect that the ground state of TiH^+ would be $(d\delta)^2$ (leading to a $^3\Sigma^-$ state). However, the electron repulsion between two electrons in $d\delta$ orbitals is too high (more than one electron is localized in the xy plane) and the best energy is achieved with a $(d\pi)^1(d\delta)^1$ configuration. This configuration leads to both $^3\Phi$ and $^3\Pi$ states but the $^3\Phi$ state is lower in energy due to lower electron-electron repulsion resulting

Table I

Total Energies for Ground State MH^+ (R_e), M^+, and H

Species	State	Total Energy (hartrees)[a]		
		GVB-PP	DCCI-GEOM	DCCI
CaH^+	$^1\Sigma^+$	−676.35376	−676.36760	−676.36760
Ca^+	^2S	−675.79379	−675.79379	−675.79379
ScH^+	$^2\Delta^\pm$	−759.23792	−759.24271	−759.25453
Sc^+	^3D	−758.66317	−758.66317	−758.66365
TiH^+	$^3\Phi^\pm$	−847.80648	−847.82324	−847.82788
Ti^+	^4F	−847.23803	−847.23809	−847.23867
VH^+	$^4\Delta^\pm$	−942.15893	−942.17786	−942.18614
V^+	^5D	−941.60584	−941.60584	−941.61338
CrH^+	$^5\Sigma^+$	−1042.48981	−1042.51595	−1042.52762
Cr^+	^6S	−1041.97641	−1041.97641	−1041.98550
MnH^+	$^6\Sigma^+$	−1148.90683	−1148.92728	−1148.93267
Mn^+	^7S	−1148.36628	−1148.36628	−1148.36685
FeH^+	$^5\Delta^\pm$	−1261.37204	−1261.39378	−1261.40462
Fe^+	^6D	−1260.82309	−1260.82415	−1260.82664
CoH^+	$^4\Phi^\pm$	−1380.21703	−1380.24028	−1380.25658
Co^+[b]	^5F	−1379.66373	−1379.66559	−1379.66836
NiH^+	$^3\Delta^\pm$	−1505.54170	−1505.56404	−1505.59710
Ni^+[b]	^4F	−1504.98306	−1504.984130	−1504.99697
CuH^+	$^2\Sigma^+$	−1637.49155	−1637.51731	−1637.58045
Cu^+[b]	^3D	−1636.92328	−1636.92427	−1636.94055
ZnH^+	$^1\Sigma^+$	−1776.12985	−1776.14322	−1776.14797
Zn^+	^2S	−1775.55652	−1775.55678	−1775.56091
H	^2S	−0.49928	−0.49928	−0.49928

[a] For MH^+ the total energies are for the calculation levels shown while the M^+ and H total energies are for the calculation levels to which these MH^+ molecules dissociate (see Calculational Details Section of text). [b]For these metals, MH^+ dissociates to an excited state of M^+ as shown.

Table II

Bond Dissociation Energies[a]

Molecule	State	This Work		Literature		
				Experiment		Theory
		$D_e(M^+–H)$	$D_0(M^+–H)$	$D_0(M^+–H)$[b]	$D_0(M^+–H)$[c]	$D_e(M^+–H)$
CaH^+	$^1\Sigma^+$	46.8	44.7	45.9 ±2.0		49.9[d],81.6[e],100.4[e]
ScH^+	$^2\Delta^\pm$	57.5	55.2	55.3±2.0	53±4	54.8[f],54.7[g]
TiH^+	$^3\Phi^\pm$	56.4	54.0	55.1±2.0		
VH^+	$^4\Delta^\pm$	46.1	43.6	47.3±1.4		
CrH^+	$^5\Sigma^+$	26.9	24.3	27.7±2.0	34±4	25.1[f]
MnH^+	$^6\Sigma^+$	41.8	39.6	47.5±3.4	52±3	40.8[h]
FeH^+	$^5\Delta^\pm$	49.4	47.0	48.9±1.4	57±5	
CoH^+	$^4\Phi^\pm$	45.9	43.6	45.5±2.3	51±4	
NiH^+	$^3\Delta^\pm$	38.2	35.7	38.5±1.4	42±2	
CuH^+	$^2\Sigma^+$	23.5	20.9	21.8±2.1	29±3	
ZnH^+	$^1\Sigma^+$	55.1	52.4	57.7[i]	57±7[j]	35.1[e]

[a]All bond energies in kcal/mol. [b]Reference 4 unless noted. [c]Reference 3 unless noted. D_{298} values have been lowered by 0.9 kcal/mol to give D_0 values. [d]Reference 12. [e]Reference 11. [f]Reference 16. [g]Reference 15. [h]Reference 14. [i]Reference 18. [j]Reference 2.

Table III
Relative Energies for Some Low-Lying
Metal Hydride Electronic States

Molecule	State	Nonbonding Configuration $d\sigma$ $d\pi$ $d\delta$	R_e (Å)	ω_e (cm^{-1})	Force Constant[a] (hartrees/Å^2)	Relative Energy (kcal/mol)
CaH^+	$^1\Sigma^+$	0 0 0	1.940	1467	0.2859	0.0
ScH^+	$^2\Delta^\pm$	0 0 1	1.810	1631	0.3571	0.0
	$^2\Pi^\pm$	0 1 0	1.798	1599	0.3405	5.1
	$^2\Sigma^+$	1 0 0	1.822	1591	0.3373	8.0
TiH^+	$^3\Phi^\pm$	0 1 1	1.730	1696	0.3868	0.0
	$^3\Sigma^-$	0 2 0 0 0 2	1.731	1686	0.3794	2.9
	$^3\Pi^\pm$	0 1 1 1 1 0	1.739	1666	0.3703	3.9
	$^3\Delta^\pm$	1 0 1	1.751	1619	0.3497	11.6
VH^+	$^4\Delta^\pm$	0 2 1	1.662	1749	0.4115	0.0
	$^4\Pi^\pm$	0 1 2 1 1 1	1.690	1700	0.3863	4.5
	$^4\Sigma^-$	1 2 0 1 0 2	1.750	1570	0.3295	12.1
	$^4\Phi^\pm$	1 1 1	1.735	1537	0.3156	13.8
CrH^+	$^5\Sigma^+$	0 2 2	1.602	1818	0.4448	0.0
MnH^+	$^6\Sigma^+$	1 2 2	1.702	1570	0.3321	0.0
FeH^+	$^5\Delta^\pm$	1 2 3	1.653	1657	0.3702	0.0
	$^5\Pi^\pm$	1 3 2	1.641	1629	0.3552	2.1
	$^5\Sigma^+$	2 2 2	1.663	1581	0.3345	10.0
CoH^+	$^4\Phi^\pm$	1 3 3	1.606	1631	0.3590	0.0
	$^4\Sigma^-$	1 4 2 1 2 4	1.602	1619	0.3512	1.3
	$^4\Pi^\pm$	1 3 3 2 3 2	1.615	1631	3590	6.4
	$^4\Delta^\pm$	2 2 3	1.696	1616	0.3498	14.4
	$^2\Delta^\pm$	0 4 3	1.460	1992	0.5317	17.6
NiH^+	$^3\Delta^\pm$	1 4 3	1.561	1728	0.4029	0.0
	$^3\Pi^\pm$	1 3 4 2 3 3	1.586	1680	0.3779	8.7
	$^1\Sigma^+$	0 4 4	1.442	1980	0.5250	9.1
	$^3\Sigma^-$	2 2 4 2 4 2	1.664	1662	0.3698	18.4
	$^3\Phi^\pm$	2 3 3	1.652	1642	0.3610	18.9
CuH^+	$^2\Sigma^+$	1 4 4	1.513	1793	0.4341	0.0
ZnH^+	$^1\Sigma^+$	2 4 4	1.545	1868	0.4713	0.0

[a] Multiply by 4.359 to obtain mdyne/Å or by 627.5 to obtain (kcal/mol)/Å^2.

from the higher angular momentum. To understand this better, consider the states of a free Ti^+ ion having two electrons in the d shell. The best state (for the d shell) is a spin triplet (high spin, Hund's rule) but there are $(5 \times 4)/2 = 10$ triplet states for d^2. Of these, seven (^3F) have low energy (less electron-electron repulsion) and three (^3P) have high energy (more electron-electron repulsion). Writing the seven states of ^3F in terms of real d orbitals leads to

$$\Phi^+ : \quad \left[d_{xz}d_{x^2-y^2} - d_{yz}d_{xy}\right] \tag{1}$$

$$\Phi^- : \quad \left[d_{xz}d_{xy} + d_{yz}d_{x^2-y^2}\right] \tag{2}$$

$$\Delta^+ : \quad \left[d_{z^2}d_{x^2-y^2}\right] \tag{3}$$

$$\Delta^- : \quad \left[d_{z^2}d_{xy}\right] \tag{4}$$

$$\Pi^+ : \quad \left\{(3/5)^{1/2}\left[d_{xz}d_{x^2-y^2} + d_{yz}d_{xy}\right] + (2/5)^{1/2}\left[d_{z^2}d_{xz}\right]\right\} \tag{5}$$

$$\Pi^- : \quad \left\{(3/5)^{1/2}\left[d_{xz}d_{xy} - d_{yz}d_{x^2-y^2}\right] + (2/5)^{1/2}\left[d_{z^2}d_{yz}\right]\right\} \tag{6}$$

$$\Sigma^- : \quad \left\{(4/5)^{1/2}\left[d_{xz}d_{yz}\right] + (1/5)^{1/2}\left[d_{x^2-y^2}d_{xy}\right]\right\} \tag{7}$$

all with the same energy. We are using the superscripts $^+$ or $^-$ to indicate state reflection symmetry or antisymmetry with respect to the xz plane. Of these pure ^3F atom states, only $^3\Phi$ and $^3\Sigma^-$ include no dσ electrons. Coupled with the previous arguments $^3\Phi$ is thus seen to be lower in energy than either $^3\Pi$ or $^3\Sigma^-$.

In VH^+ the nonbonding configuration is d^3 which for a free ion would lead to a ^4F ground state for the d shell:

$$\Phi^+ : \quad \left\{d_{z^2}\left[d_{xz}d_{x^2-y^2} - d_{yz}d_{xy}\right]\right\} \tag{8}$$

$$\Phi^- : \quad \left\{d_{z^2}\left[d_{xz}d_{xy} + d_{yz}d_{x^2-y^2}\right]\right\} \tag{9}$$

$$\Delta^+ : \quad \left[d_{xz}d_{yz}d_{xy}\right] \tag{10}$$

$$\Delta^- : \quad \left[d_{xz}d_{yz}d_{x^2-y^2}\right] \tag{11}$$

$$\Pi^+ : \quad \left\{(3/5)^{1/2}\left[d_{z^2}\left[d_{xz}d_{x^2-y^2} + d_{yz}d_{xy}\right]\right] + (2/5)^{1/2}\left[d_{yz}d_{x^2-y^2}d_{xy}\right]\right\} \quad (12)$$

$$\Pi^- : \quad \left\{(3/5)^{1/2}\left[d_{z^2}\left[d_{xz}d_{xy} - d_{yz}d_{x^2-y^2}\right]\right] + (2/5)^{1/2}\left[d_{xz}d_{x^2-y^2}d_{xy}\right]\right\} \quad (13)$$

$$\Sigma^- : \quad \left\{(4/5)^{1/2}\left[d_{z^2}d_{x^2-y^2}d_{xy}\right] + (1/5)^{1/2}\left[d_{z^2}d_{xz}d_{yz}\right]\right\} \quad (14)$$

The only pure ^{4}F state not involving dσ is of Δ symmetry and, indeed, the ground state of VH^+ is $^4\Delta$. Similarly, CrH^+ leads to $^5\Sigma^+$ with a $d\pi_{xz}d\pi_{yz}d\delta_{x^2-y^2}d\delta_{xy}$ nonbonded configuration, leaving dσ empty.

The above analysis of MH^+ is oversimplified. As indicated in Table IV, M^+–H bond pairs have both s and d character. Thus, for ScH^+, the configuration on Sc^+ (including both the bonding and nonbonding valence electrons) is sd for an s electron in the bond and d^2 for a d electron in the bond. This is reasonable since the ground state for Sc^+ has a s^1d^1 configuration and the lowest electronic state with a d^2 configuration is only 0.30 eV higher in energy.[8] In order for d^2 to participate in bond formation, one of the occupied d orbitals *must* be dσ (for bonding to the H). This *requires* that the nonbonding orbital be dδ or dπ. A bond orbital with both s and d character could be formed in the $^2\Sigma^+$ state by taking linear combinations of the metal 4s and 3dσ orbitals. In this case it is not necessary to add in excited state character to add d character to the bond. However, this is not a large enough energy saving to offset repulsion between an electron in a non-bonding sigma orbital and the electrons in the bond pair. The same analysis for TiH^+ leads to a mixture of s^1d^2 and d^3 configurations where d^3 must contain an occupied dσ orbital for the TiH^+ bond pair. [The ground state for Ti^+ is ^{4}F ($4s^13d^2$) with the ^{4}F ($3d^3$) state just 0.107 eV higher.][8] Consequently, there is a strong bias for the nonbonding d^2 configurations to *not* use the dσ orbital and the lowest three states of TiH^+ are seen to use only dπ and dδ orbitals for the nonbonding electrons. For V^+ the exchange stabilization for high-spin coupled d electrons leads to a d^n ground state configuration, ^{5}D ($3d^4$), with the first excited state, ^{5}F ($4s^13d^3$), at 0.337 eV above the ground state.[8]

Table IV

Hybridization of Metal Bonding Orbital[a]

Molecule	State	Character of Metal Bonding Orbital		
		%s	%p	%d
CaH^+	$^1\Sigma^+$	60.0	16.3	23.7
ScH^+	$^2\Delta^\pm$	46.2	13.5	40.3
TiH^+	$^3\Phi^\pm$	46.6	14.7	38.7
VH^+	$^4\Delta^\pm$	48.5	14.1	37.4
CrH^+	$^5\Sigma^+$	40.6	12.5	46.9
MnH^+	$^6\Sigma^+$	76.3	12.5	11.2
FeH^+	$^5\Delta^\pm$	73.1	12.8	14.1
CoH^+	$^4\Phi^\pm$	74.5	12.1	13.4
NiH^+	$^3\Delta^\pm$	76.5	11.0	12.5
CuH^+	$^2\Sigma^+$	70.2	10.5	19.3
ZnH^+	$^1\Sigma^+$	90.7	8.9	0.4

[a] Results based on the GVB-PP wavefunction.

However, again, the nonbonding electrons for the lowest two states of VH^+ avoid $d\sigma$.

The four systems, ScH^+, TiH^+, VH^+, and CrH^+, all have significant d character in the MH^+ bond. In contrast, the rest of the transition metal hydrides, MnH^+ through NiH^+ have only about 13%. The reason is that for high spin s^1d^{n-1} the latter four systems must have at least one nonbonding electron in $d\sigma$ [e.g. MnH^+ is $(d\sigma)^1(d\pi)^2(d\delta)^2$] and hence the $d\sigma$ orbital is not freely available for mixing with the bond orbital (this would presumably lead to s character in the nonbonding orbital and a loss in exchange energy). As a result, the lowest configurations for the hydrides of Mn, Fe, Co, Ni, and Cu are constructed by adding $(d\sigma)^1(d\pi)^2(d\delta)^2$ to the lowest configurations of Ca, Sc, Ti, V, and Cr.

The Metal-Hydrogen Bond. ***Low-lying Metal Atomic States.*** The two main atomic states involved in the bonding of the first row metal ions to hydrogen have $3d^n$ and $4s^13d^{n-1}$ configurations. Figure 1 shows the relative ordering of the lowest states with $3d^n$ and $4s^13d^{n-1}$ configurations for Ca^+–Cu^+. Zn^+ is not included since its 11 valence electrons preclude it from having a $3d^n$ configuration. The trends seen can be explained by several effects. First, as nuclear charge increases, the 3d orbitals are preferentially stabilized with respect to the 4s orbital, due to the difference in principal quantum number and to differential shielding effects. Second, the d^n configuration is stabilized due to large exchange energy stabilization arising from the interaction of d electrons of the same spin. Third, the two effects stabilizing the d^n configuration are counteracted to some extent in the late transition metals by the electron-electron repulsion due to two d electrons in the same orbital.

The relative energies of these two states are an important factor in the M^+–H bonding. There are, however, other effects that must also be considered in analyzing the metal-hydrogen bonding.

Metal Orbital Sizes. The intrinsic strength of a two electron metal-hydrogen bond is strongly affected by the type of metal orbital (s,d, or hybridized) and the

Figure 1: Metal ion dependence of the energy difference between the lowest metal electronic states with $3d^n$ and $3d^{n-1}4s$ configurations. $\Delta E = E_{d^n} - E_{d^{n-1}s^1}$.

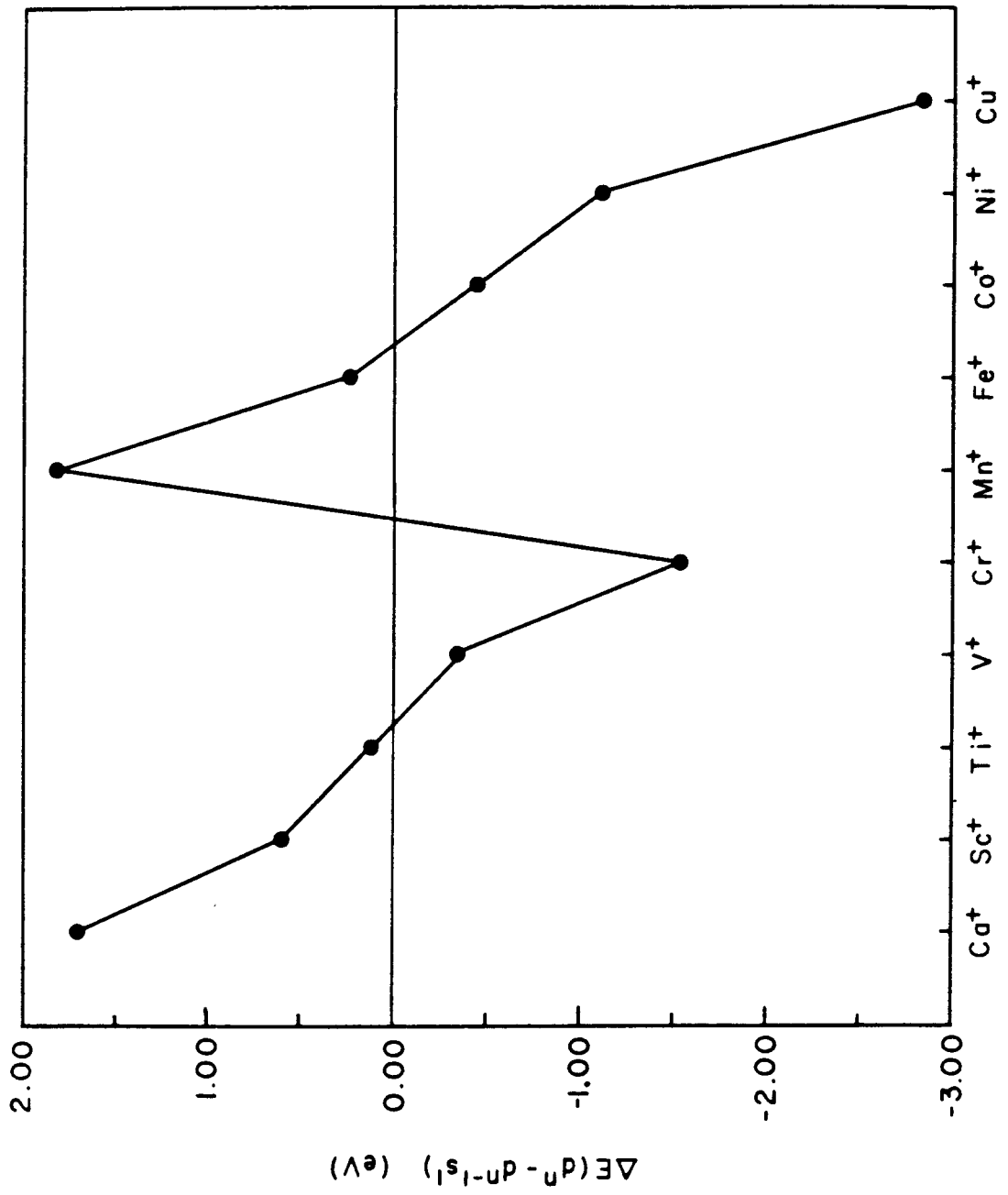
2.00
1.00
0.00
-1.00
-2.00
-3.00
ΔE (dⁿ - dⁿ⁻¹s¹) (eV)
Ca+ Sc+ Ti+ V+ Cr+ Mn+ Fe+ Co+ Ni+ Cu+

relative size of the orbital. We thus expect significant differences in the intrinsic bond strengths to s or d orbitals due to their differences in size as well as to the differences in spatial orientation, directionality and ionizability. There can also be significant differences for the intrinsic bond strengths to the same type of orbital due to orbital sizes which differ from one metal to another.

Table V gives the average sizes for the 4s and 3d metal orbitals. The radii are found by taking the square root of the sum of the second moments for the various Hartree-Fock orbitals of the metal ions. As can be seen from the table, the 4s orbitals are from 1.5 to 3 times larger than the 3d orbitals. Both s and d orbitals contract as one goes from left to right across the periodic table but the 3d orbitals decrease in size much faster than the 4s orbitals. For example, the 3d orbital on Ca^+ is 2.5 times larger than the 3d orbital on Ni^+ while the Ca^+ 4s orbital is only 1.4 times larger than the Ni^+ 4s orbital. This occurs because the d orbitals have a lower principal quantum number and hence decrease in size more rapidly as the effective nuclear charge increases.

Intrinsic Bond Strengths. When we speak of an intrinsic s or d bond we mean a bond formed to a pure s or d orbital with no interaction with any other electrons in the molecule and no hybridization of the metal bonding orbital. In practice it is impossible to calculate this intrinsic bonding. We therefore approximate it by restricting, as much as possible, the orbital hybridization and by adding back into the bond dissociation energy the amount of energy lost due to exchange and promotion effects. As described in the calculational details section, we carried out calculations designed to ensure essentially pure s bonds or pure d bonds (the ***intrinsic*** bonds) to hydrogen with the results indicated in Table VI. The trends for these intrinsic bonds are shown graphically in Figure 2. The essential characteristic of the intrinsic s bond is that it is basically independent of metal from ScH^+ to CuH^+, being about 32 kcal/mol. [The slight discontinuity between CrH^+ and MnH^+ may be due either to the presence of the occupied d_{z^2} orbital for Mn^+ and metals to the right or a slight change in the calculational method at that

Table V

Valence Orbital Sizes (Å) for First Row Transition Metal Ions

Ion	R(4s)[a]	R(3d)[a]			
		$3d^{n-1}4s^1$		$3d^n$	
		$(1e^-)^b$	$(2e^-)^b$	$(1e^-)^b$	$(2e^-)^b$
Ca^+	2.10			1.57	
Sc^+	2.02	1.01		1.15	
Ti^+	1.89	0.87		1.00	
V^+	1.80	0.78		0.89	
Cr^+	1.73	0.70		0.81	
Mn^+	1.68	0.67		0.74	0.81
Fe^+	1.62	0.63	0.66	0.69	0.73
Co^+	1.59	0.60	0.62	0.66	0.69
Ni^+	1.55	0.57	0.58	0.62	0.64
Cu^+	1.52	0.54	0.55		0.60
Zn^+	1.49		0.50		

[a] $R = \sqrt{\langle\phi|r^2|\phi\rangle}$

[b] $1e^-$ and $2e^-$ indicate singly and doubly occupied orbitals.

Table VI

Intrinsic Bond Dissociation Energies

Molecule	s-Bond (kcal/mol)	d-Bond (kcal/mol)
CaH^+	27.1	76.9
ScH^+	32.8	55.0
TiH^+	31.1	49.4
VH^+	31.7	44.7
CrH^+	33.8	32.6
MnH^+	28.2	18.8
FeH^+	31.1	15.1
CoH^+	32.0	17.0
NiH^+	33.3	11.8
CuH^+	36.0	0.0
ZnH^+	46.6	0.0

Figure 2: Intrinsic bond strengths of H to metal 4s (circles) and 3d (squares) orbitals from GVB-PP(1/2) calculations. The intrinsic bond energies are the diabatic bond dissociation energies of the complex adding back in any exchange energy lost on bonding. The trends seen should be a direct result of the changing size of the metal bonding orbitals.

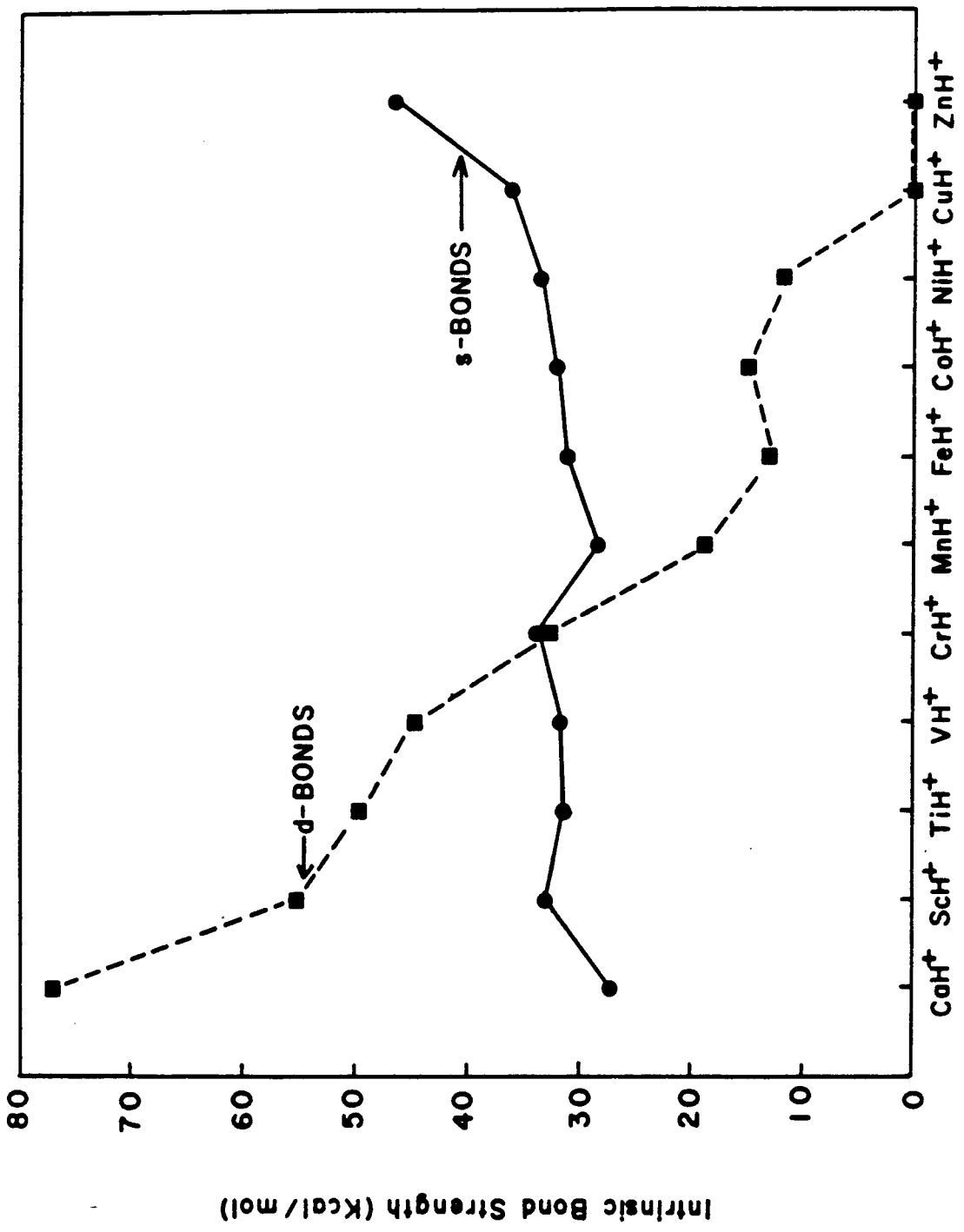
Intrinsic Bond Strength (Kcal/mol)
80
70
60
50
40
30
20
10
0
d-BONDS
s-BONDS
CaH+ ScH+ TiH+ VH+ CrH+ MnH+ FeH+ CoH+ NiH+ CuH+ ZnH+

point.] The slight increase in bond strength from CaH^+ to ZnH^+ is associated with a decrease in the size of the 4s orbital, indicating that the optimum size for a 4s orbital bonding to H is smaller than the Zn 4s orbital (1.49 Å). The 3d bonds show dramatically different trends. The intrinsic bond strength drops from 77 to 12 kcal/mol from CaH^+ to NiH^+ indicating that the optimum size 3d orbital for bonding to H is $\geq$ 1.56 Å. Thus the optimum size for both 4s and 3d orbitals seem to be around 1.5–1.6 Å.

Exchange Energy Considerations. Exchange stabilization plays an important role in determining the ground configuration of transition metal ions and the modification of the exchange energies is comparably important in determining the bonding in the metal hydrides. Bonding to a singly occupied metal orbital that is high spin coupled to other metal d electrons causes a loss of exchange energy on the metal center. The bonded electron is now up-spin only half the time, leading to a loss of half of the exchange energy between it and the other high spin metal electrons. The larger the exchange stabilization (closer to half-full shells) the more important the effect (which weakens the bond). The exchange energy between two orbitals is inversely proportional to the average distance between the electrons in the two orbitals, and thus, the d-d exchange energies (K_{dd}) are much larger than the s-d exchange energies (K_{sd}). Since the sizes of the various orbitals varies dramatically, so also do the exchange energies.

The exchange integrals (and coulomb integrals) for various d orbitals depend to some extent on which orbitals are occupied (see Table VII for the variations on Mn^+). For the purpose of the following analysis we use the exchange terms suitable for the particular metal electron configuration in question. The exchange energies used were determined by Hartree-Fock calculations on the metal ions.

Table VIII shows the effect of loss of exchange energy on the intrinsic s and d bonds. As expected, the effect is largest for the d bonds as well as for those systems which have the highest number of unpaired electrons. As an extreme example, d-bonded CrH^+ loses 32.2 kcal/mol of exchange energy on bonding.

Table VII

4s–3d and 3d–3d Exchange Energies for Mn^+

Orbitals	^6S ($4s^1 3d^5$)		^4D ($3d^6$)	
	# of Terms	K (kcal/mol)	# of Terms	K (kcal/mol)
s–d	5	4.81	0	
Ave. d–d	10	19.81	6	18.10
$d\sigma$–$d\pi$	2	15.02	2	13.76
$d\sigma$–$d\delta$	2	24.60	1	22.46
$d\pi$–$d\pi$	1	21.40	1	19.62
$d\pi$–$d\delta$	4	21.40	2	19.50
$d\delta$–$d\delta$	1	11.83	0	

Table VIII

Intrinsic Bond Strengths after Correction for Exchange Energy Losses

Molecule	s-bond			d-bond		
	Exchange Loss		$D_s(M^+ - H)$[a]	Exchange Loss		$D_d(M^+ - H)$[b]
	K_{sd} Terms	Energy (kcal/mol)	(kcal/mol)	K_{dd} Terms	Energy (kcal/mol)	(kcal/mol)
CaH^+	0	0.0	27.1	0	0.0	76.9
ScH^+	$\frac{1}{2}$	3.6	29.2	$\frac{1}{2}$	7.1	47.9
TiH^+	1	5.7	25.2	1	14.4	35.0
VH^+	$1\frac{1}{2}$	8.2	23.5	$1\frac{1}{2}$	22.5	22.2
CrH^+	2	10.2	23.6	2	33.2	-0.6
MnH^+	$2\frac{1}{2}$	12.0	16.2	$1\frac{1}{2}$	25.0	-6.2
FeH^+	2	9.7	21.4	1	19.0	-3.9
CoH^+	$1\frac{1}{2}$	7.2	24.8	$\frac{1}{2}$	12.8	4.2
NiH^+	1	4.6	28.7	0	0.0	11.8
CuH^+	$\frac{1}{2}$	2.2	33.8	0	0.0	0.0
ZnH^+	0	0.0	46.6	0	0.0	0.0

[a] $D_s(M^+–H)$ = (intrinsic s-bond energy) – (Exchange energy lost on bonding to s orbital).

[b] $D_d(M^+–H)$ = (intrinsic d-bond energy) – (Exchange energy lost on bonding to dσ orbital).

Species such as Ca^+, Zn^+, and d^9 Ni^+ lose no exchange energy due to the presence of only one unpaired electron on the metal.

Metal Orbital Hybridization. Can the hybridization of the metal bonding orbital be predicted from corrections to the calculated intrinsic bonding? The corrections due to loss of exchange energy have been presented. The other major correction to the intrinsic bond is to subtract out the excitation energy necessary to promote the metal ion to the state required to form the particular bond (s or d). The resulting s and d bond energies are shown in Table IX, along with the actual bond dissociation energies (allowing hybridization) from GVB-PP(1/2) calculations. The actual metal orbital hybridization (%s, %p, and %d character) from the GVB Perfect Pairing wave function is shown in Table IV.

From Table IX, we find, as one would expect, a larger bond dissociation energy using hybridized metal bond orbitals than predicted for either pure s or pure d bonds. However, the overall trends seen in the pure s and d bonding are in reasonable agreement with what is actually seen allowing the orbitals to hybridize.

Table IV does show some unexpected results after analyzing the trends in pure s and d bonding. For CaH^+–CrH^+ and NiH^+, the d-bond strength is seen to be greater than the s-bond strength. Yet, when the orbitals are allowed to hybridize, the optimum combination for all of the molecules in the row, except CrH^+, includes more s character than d character. Thus, even when the intrinsic energy of bonding hydrogen to a metal d orbital is much higher than bonding to a metal s orbital, as is the case at the beginning of the row, the influences of the metal excitation energy and loss of exchange energy and finally the orbital shape changes involved in hybridization all combine to give an optimum orbital which is more s in character than d or p.

Two cases, NiH^+ and CuH^+, differ in metal hybridization from the other metal hydrides. As shown in Table IV, both have over 70% s character in the GVB-PP(1/2) wave function. At this level of calculation, NiH^+ has a very weak

Table IX

Comparison of s, d, and Hybridized Bonding in MH^+

Molecule	Intrinsic Bond Energies After Corrections for Exchange and Promotion Energies[a]		Calculated Bond Energies[b] (no restrictions) (kcal/mol)
	s-bond (kcal/mol)	d-bond (kcal/mol)	
CaH^+	27.1	37.7	38.1
ScH^+	29.2	34.1	47.4
TiH^+	25.4	32.5	43.7
VH^+	15.7	22.2	33.8
CrH^+	-11.5	-0.6	8.9
MnH^+	16.2	-47.9	25.9
FeH^+	21.4	-9.7	31.2
CoH^+	14.9	4.2	24.1
NiH^+	3.6	11.8	12.1
CuH^+	-31.0	0.0	-21.5
ZnH^+	46.6		44.4

[a] Bond Energy = (Intrinsic Bond Strength) − (Exchange Energy Lost on Bonding) − (Applicable Metal Promotion Energy). [b]GVB Perfect Pairing wavefunction with no restrictions on orbital hybridization.

bond while CuH^+ is actually unbound. At the DCCI level of calculation, a substantial change is found in the character of the two wave functions. This change involves the excitation of one of the bond pair electrons into the d_{z^2} orbital on the metal. This, in effect, mixes the metal $3d^n$ configuration into the $d^{n-1}s^1$ bonding configuration. The wave functions are thus a mixture of a configuration with a covalent bond between the metal 4s orbital and the hydrogen 1s (with a singly occupied $d\sigma$ nonbonding electron) and a configuration with a doubly occupied $d\sigma$ metal orbital and a singly occupied hydrogen 1s orbital. This mixing is extremely important for CuH^+ where the excitation energy to the ^3D state ($4s^13d^9$) is 2.81 eV, which is larger than any of the bond energies seen for the first row metal hydrides. Thus, for any bound states to exist for CuH^+, they must involve some amount of ground state Cu^+ character (d^{10}). Analysis of the Mulliken populations over basis functions for the CI wavefunctions shows an increase in the d character to 37% for NiH^+ and 66% for CuH^+.

Comparison with Other Theoretical Calculations. There has been only a limited number of theoretical studies of the metal hydride ions, mostly dealing with CaH^+ and ZnH^+. Floating Spherical Gaussian Orbital (FSGO) calculations on CaH^+ by Ray and Mehandru[9] and by Ray and Switalski[10] give bond lengths of 2.05 and 2.13 Å. Dirac-Fock One Center Expansion (DFOCE) relativistic calculations of Pyykkö[11] give bond lengths of 1.86 and 1.93 Å and bond energies of 82 and 100 kcal/mol. Probably the best CaH^+ calculation other than the present study is by McFarland et al.[12] They performed a Hartree-Fock times singles and doubles CI with excitations from the valence and first core level orbitals. They obtained an R_e of 1.881 Å, a D_e of 49.9 kcal/mol, and a vibrational frequency of 1504.4 cm^{-1}. This compares to an R_e of 1.940 Å from this work along with a D_e of 46.8 kcal/mol, and a vibrational frequency of 1467 cm^{-1}.

Calculations on ZnH^+ include DFOCE calculations of Pyykkö[11] yielding an R_e of 1.67 Å and a D_e of 35 kcal/mol. Hartree-Fock calculations of Klimenko

et al.[13] yield a bond length of 1.56 Å and a vibrational frequency of 1945 cm^{-1}. These numbers can be compared to the present results of an R_e of 1.545 Å, a D_e of 55.1 kcal/mol and a frequency of 1868 cm^{-1}.

For other metal hydrides of the first row, bond energy values have been published for MnH^+, ScH^+, and CrH^+. Vincent, Yoshioka, and Schaefer[14] calculate the bond energy of MnH^+ as 40.8 kcal/mol (Hartree-Fock times singles and doubles with Davidson's correction). Anglada et al.[15] performed MRD-CI calculations on ScH^+ and TiH^+ and report a bond dissociation energy of 54.7 kcal/mol for ScH^+. High level MCSCF plus singles and doubles calculations of Alverado-Swaisgood et al.[16] yield for ScH^+ a bond length of 1.822 Å and a bond dissociation energy of 54.8 kcal/mol. The sigma bond is found to be polarized slightly toward the hydrogen and the metal orbital hybridization is 68% sp and 32% dσ. Calculations also show the $^2\Pi$ state to be 4.8 kcal/mol higher in energy than the $^2\Delta$ state and the $^2\Sigma^+$ to be 5.9 kcal/mol above the $^2\Delta$ state. For CrH^+, Alverado-Swaisgood *et al* have found a bond length of 1.63 Å and a bond energy of 25.1 kcal/mol. The bond is found to be covalent (slightly polarized toward Cr^+) with a metal orbital hybridization of 61% sp and 39% d character. These values are fairly consistent with the present results. The bond lengths for the two species are slightly longer (1.810 Å and 1.602 Å in the present work) with a correspondingly larger amount of sp character and lower vibrational frequency. The differences in D_e are only 2.7 and 1.8 kcal/mol for ScH^+ and CrH^+. All of the theoretically determined bond dissociation energies are compared in Table II.

Recent calculations on ScH^+ through CuH^+ have been performed by Pettersson et al.[17] They find the same ground states for all species and the bond dissociation energies are in good agreement with those of the present work.

Comparison With Experiment. A comparison of the present theoretical results with experimental values has been presented previously.[7] Recent work by Elkind and Armentrout[4] has begun to sort out the contributions to ion beam cross sections from ground and excited state metal ions. This has allowed more

accurate bond dissociation energies to be obtained. Table II compares these new values to the theoretical results. Practically all of the experimental values have decreased from those listed in the previous paper. The average difference between theoretical and experimental bond dissociation energies is 2.5 kcal/mol. Spectroscopic values[18] for ZnH^+ lead to an experimental bond length which is 0.03 Å shorter than the calculated value and a vibrational frequency which is about 5% larger than calculated. Similar magnitudes of error would be expected for the other cases as well.

Calculational Details

Electron Correlation. As described previously[7], the equilibrium geometries were determined at a level of calculation which involves starting with the three configurations of the GVB wavefunction and allowing all double excitations from the bond pair *plus* all single excitations out of the nonbonding valence orbitals [RCI(1/2)×(D_σ+S_{val}]. For purposes of discussion, this calculational level is labeled DCCI-GEOM. The calculation dissociates to single excitations from the metal nonbonding valence orbitals. The bond dissociation energy calculations start with the three configurations of the GVB wavefunction and allow all single and double excitations out of the bond pair *simultaneous with* all single excitations out of the nonbonding valence orbitals. This calculational level will be referred to as DCCI (for **D**issociation **C**onsistent **C**onfiguration **I**nteraction). The molecular calculation dissociates to a limit involving simultaneous single excitations out of the nonbonding orbitals and the metal σ bonding orbital. The bond character for the two systems NiH^+ and CuH^+, as discussed earlier, changes substantially in the larger CI calculations. In order to allow the orbital shape changes necessary in these systems, the DCCI-GEOM and DCCI calculations were both modified to include a complete CI in the valence sigma space.

For molecules where the state splittings are not accurately described, the bond dissociation energies are obtained as follows. The molecule is dissociated

diabatically to H atom and metal ion, whether this is the metal ion ground state or an excited electronic state. If the molecule diabatically dissociates to the metal ion ground electronic state, this dissociation energy is taken to be the bond dissociation energy. If the molecule dissociates diabatically to a metal ion excited state the bond dissociation energy is calculated by subtracting the experimental state splitting (between the particular excited state and the ground state) from the diabatic dissociation energy. Thus, for all cases, the molecule is dissociated consistently so that any basis set errors for a particular metal electronic configuration will cancel (since they should be similar in both the molecule and the metal ion) and where necessary, the correct metal ion state splittings are used to give the dissociation energy to ground state fragments.

MnH^+ was used as a test case to compare the changes in the bond dissociation energy to changes in the basis set and in the level of electron correlation. Table X lists the bond dissociation energy as a function of calculation level. The bond energies obtained at the DCCI-GEOM and DCCI calculations are the largest of all the calculation levels examined. These two calculations allow for a large amount of correlation between the two bonding electrons and also some correlation between the bonding electrons and the nonbonding valence electrons. They have thus been used in this study in preference to the other levels. No effort was made to correlate the nonbonding electrons with one another since this has relatively little effect on the bond energies calculated.

Basis Sets. As described in the original paper in this series, the calculations discussed here involve all-electron ab initio wave functions using a basis consisting of an optimized valence double ζ contraction on the metal (5 d primitives)[19] and the Dunning/Huzinaga double ζ basis for H (4s/2s)[20] supplemented with one set of p polarization functions optimized for MnH^+ ($\alpha = 0.50$). Table XI shows a comparison of the theoretical and experimental state splittings obtained with these basis sets. The differences between experiment and theory are not extremely large until one reaches Mn^+. From Mn^+ to the right, the metal states

Table X

Electronic Correlation Effects on $D_e(Mn^+–H)$

Calculation Level	Total Energy (au)	Bond Energy[a] (kcal/mol)
Hartree Fock	−1148.887281	13.6
GVB-PP(1/2)	−1148.906828	25.9
GVB-RCI(1/2)	−1148.910192	28.0
GVB-RCI(1/2) × Singles from the d Orbitals	−1148.912038	29.1
GVB-RCI(1/2) × Singles from the Valence Orbitals	−1148.915426	31.3
GVB-PP(1/5)	−1148.918042	32.9
GVB-RCI(1/5)	−1148.920959	34.8
GVB-PP(1/2) × Singles and Doubles from the Bond Pair	−1148.925431	37.6
DCCI-GEOM	−1148.927276	38.7
DCCI	−1148.932669	41.8

[a] The bond dissociation energy for all calculational levels except DCCI were determined by dissociating to the Hartree-Fock atomic limit: Mn^+ −1148.366284 au and H −0.499277 au. The Mn^+ DCCI atomic limit (Hartree-Fock × singles from the 3d orbitals × singles from the 4s orbital) has an energy of −1148.366850 au.

Table XI

Metal Low-lying $4s^13d^{n-1}$ and $3d^n$ States:

Experimental and Theoretical State Splittings

Ion	$4s^13d^{n-1}$		$3d^n$				
	State	Configuration	State	Configuration	Relative Energy (eV)[a]		
					Exptl[b]	HF	DCCI
Ca^+	^2S	$4s^1$	^2D	$3d^1$	1.70	2.35	2.35
Sc^+	^3D	$4s^13d^1$	^3F	$3d^2$	0.60	0.46	0.15
Ti^+	^4F	$4s^13d^2$	^4F	$3d^3$	0.11	0.30	-0.04
V^+	^5F	$4s^13d^3$	^5D	$3d^4$	-0.34	-0.32	-0.51
Cr^+	^6D	$4s^13d^4$	^6S	$3d^5$	-1.52	-1.59	-1.82
Mn^+	^7S	$4s^13d^5$	^5D	$3d^6$	1.81	2.94	2.59 1.06[c]
Fe^+	^6D	$4s^13d^6$	^4F	$3d^7$	0.25	1.27	0.89 0.41[c]
Co^+	^5F	$4s^13d^7$	^3F	$3d^8$	-0.43	1.01	0.53 -0.69[c]
Ni^+	^4F	$4s^13d^8$	^2D	$3d^9$	-1.09	0.25	0.05 -0.71[c]
Cu^+	^3D	$4s^13d^9$	^1S	$3d^{10}$	-2.81	-1.69	-2.60[c]
Zn^+	^2S	$4s^13d^{10}$					

[a] Relative Energy of the $3d^n$ state with respect to the $4s^13d^{n-1}$ state. [b]Reference 8. The energies were calculated using a weighted average over J levels for each state. [c]DCCI state splitting with two electrons in the d_{z^2} orbital. This is relevant for mixing of the d^n state into the ground state metal-hydrogen bond.

involve doubly occupied d orbitals, with the d^n configurations containing one more doubly occupied d orbital than the metal s^1d^{n-1} configurations. Hartree-Fock calculations do not correctly describe the correlations between the electrons in the doubly occupied orbitals Thus, the d^n configurations are not described, theoretically, as well as the s^1d^{n-1} configurations.

Table XII shows the effects on the bond dissociation energy of MnH^+, of adding polarization functions. One set of f polarization functions on Mn^+ ($\alpha = 0.25$) and one set of p polarization functions on H ($\zeta = 0.5$) were optimized at the DCCI-GEOM level. The effect of p functions on H is seen to be more pronounced than f functions on the metal. At the DCCI level, f functions are seen to give an increase of 1.4 kcal/mol in the bond dissociation energy. One might expect similar changes for the other metal hydrides.

Intrinsic Bond Dissociation Energies. To obtain intrinsic bond energies to metal s and d orbitals we carried out calculations in which little or no mixing of the metal s and dσ orbitals was allowed. The calculational method differs somewhat depending on the position of the metal in the row. For the species CaH^+–CrH^+, s-bonding requires an empty d_{z^2} orbital while d-bonding necessarily involves an empty metal 4s orbital. This was accomplished by carrying out calculations where either the metal 4s or d_{z^2} symmetry vectors were removed such that those particular basis functions could not be used in the bonding. The optimum energy was then found for this level of calculation by varying the bond length. The bond energy was found by dissociation to fragments where the same symmetry vectors were removed from the metal ion calculation.

The s-bonding for MnH^+–CuH^+ is complicated by the fact that the d_{z^2} orbital is occupied by one electron, and the d_{z^2} basis functions cannot be removed from the calculation. Some d character is used in the bond orbitals depending on the amount of sd hybridization. This sd hybridization process can be be partially eliminated by forcing the nonbonding σ electron to use a pure d_{z^2} orbital and freezing this orbital in the predetermined shape while the other orbitals on the

Table XII

Polarization Function Effects on the Mn^+–H Bond Dissociation Energy

Basis Set	DCCI-GEOM[a]	DCCI[a]
VDZ[b]	31.9	
VDZ + f[c]	35.0	
VDZ + p[d]	38.7	41.8
VDZ + f,p[e]	40.5	43.2

[a]Bond energies in kcal/mol. [b]Valence Double Zeta basis with no polarization functions. [c]Valence Double Zeta basis with one set of f functions on Mn^+. [d]Valence Double Zeta basis with one set of p functions on H. [e]Valence Double Zeta basis with polarization functions on both Mn^+ and H.

molecule are allowed to vary. This d_{z^2} orbital shape was determined from a Hartree-Fock calculation on the metal ion. The molecule thus has one electron in a pure d_{z^2} orbital, and the bonding orbitals are forced to use the metal 4s orbital. For MnH^+–CuH^+, the d-bond strengths are determined by calculating the bonding of H to the d^n configuration of the metal. For the most part, the 4s orbital is not involved in the bonding since bonding to the 4s orbital leads to states of different spin.

The intrinsic s-bonding in ZnH^+ is taken from a normal GVB-PP(1/2) calculation. The full d shells in the ground state configurations of Zn^+ and Cu^+ precludes any d contribution to the metal-hydrogen bond and the intrinsic d-bonds to these species are considered to be 0 kcal/mol. For all the species discussed here, the calculations are performed on the lowest-lying electronic state possible for either s- or d-bonds. The actual intrinsic bond dissociation energies given are determined by obtaining the dissociation consistent bond energy and adding to that the total amount of s–d or d–d exchange energy lost on bonding (determined from the metal ion exchange energies and the metal electronic configuration).

Excited States. The relative energies of the low-lying electronic states of the metal hydride ions are determined by the difference in bond dissociation energies calculated for the various states. For molecular states which dissociate to the same state of the metal ion, the bond energies were obtained with DCCI-GEOM calculations. For comparison of molecular states which dissociate to different states of the metal ions, bond energies were determined at the DCCI level. The relative bond dissociation energies were used as a measure of energy differences for the electronic state since the dissociation consistent nature of these calculations helps to remove errors inherent in the basis set representations of the metal ion states.

For TiH^+, VH^+, CoH^+, and NiH^+ slightly different calculational techniques were used to determine the state splittings. All of these molecules have a set of 7 low-lying states which are formed by bonding to one particular metal ion

electronic state. Only two of these seven states can be represented by single-configuration wavefunctions. The others are mixtures of two or three configurations. To allow for correct mixing of these various configurations, the SCF calculations used average field techniques placing an average number of electrons in each d orbital in order to produce cylindrically symmetric sets of d orbitals. The DCCI-GEOM calculations then used all ten possible d orbital occupations as starting configurations for the CI's. For TiH^+ and VH^+ the calculations involved placing electron density in the d_{z^2} orbital at the SCF level since several of the molecular states involved three σ electrons. The DCCI-GEOM calculations were performed using a complete CI in the σ space to compensate for orbital shape changes necessary in those states for which there are only two σ electrons. Due to the nature of the SCF calculations for these four metal hydrides, the excited state calculations can discriminate slightly against certain electronic states. For the splitting between the Φ and Σ^- states of TiH^+ and CoH^+ the calculations were performed using the correct number of $d\sigma$ electrons and should thus be more accurate than the other splittings listed for those molecules. All the excited state calculations should give a correct representation of the state ordering although one would expect some error in the actual quantitative splitting energies.

Conclusion

The present theoretical results should prove useful in a variety of ways for present and future experimental work. Photoelectron spectroscopy of anionic[21] and neutral[22] transition metal molecules allows one to obtain information on low-lying states and possibly bond lengths and vibrational frequencies of the corresponding neutral and ionic species. Future work with neutral MH species will give experimental results for the MH^+ ions. Collisional activation studies are also being used to study low-lying excited electronic states of metal cationic species.[23] These experimental techniques will provide a necessary check on the present results and vice versa. Bond dissociation energies and electronic state splittings will also be useful in analyses of the various gas-phase hydrocarbon

activation studies.

We have presented a consistent ab initio study of the hydrides of the first row transition metals. For almost all systems the calculated bond dissociation energies agree very well with recent guided ion beam studies. The bonding patterns result from several effects including: (1) the relative ordering of the low-lying metal electronic states; (2) the intrinsic bond strength of H to various size 4s, 3d, or hybridized metal orbitals; and (3) the effects of loss of high-spin metal exchange energy on bonding.

The early transition metals bond with orbitals which are approximately 60% s and 40% d in character. This is facilitated by small differences in energy of the low-lying metal electronic states with s^1d^{n-1} and d^n configurations and a smaller discrepancy in s and d orbital sizes when compared to the late metals. CaH^+ has a small bond energy due to the more inaccessible d^1 configuration. As one moves to the right from ScH^+ toward CrH^+ the bond energy drops due to an increasing energy penalty both to add in s character (due to metal promotion energies) and d character (due to loss of exchange energy). For MnH^+ and metals to the right the bond is mostly s in character due to first a loss of exchange energy in bonding to the metal d orbital and second to the small intrinsic bond energies to the very small 3d orbitals. The combination of all these factors produces the oscillations seen in the metal hydride bond dissociation energies and all must be considered in order to predict the bonding in transition metal systems.

Acknowledgement. We thank the National Science Foundation (Grant Nos. CHE83-18041 and CHE84-07857) for partial support of this work.

References

(1) Po, P. L.; Radus, T. P.; Porter, R. P. *J. Phys. Chem.* **1978**, *82*, 520.

(2) (a) Bartmess, J. E.; Kester, J. D. *Inorg. Chem.* **1984**, *23*, 1877. (b) Stevens, A. E.; Beauchamp, J. L. *Chem. Phys. Lett.* **1981**, *78*, 291.

(3) (a) Armentrout, P. B.; Beauchamp, J. L. *Chem. Phys.* **1980**, *50*, 37; *J. Am. Chem. Soc.* **1981**, *103*, 784. (b) Armentrout, P. B.; Halle, L. F.; Beauchamp, J. L. *Ibid.* **1981**, *103*, 6501. (c) Tolbert, M. A.; Beauchamp, J. L. *Ibid.* **1984**, *106*, 8117.

(4) Elkind, J. L.; Armentrout, P. B. *Inorg. Chem.* **1986**, *25*, 1078.

(5) See for example: (a) Armentrout, P. B.; Halle, L. F.; Beauchamp, J. L. *J. Am. Chem. Soc.* **1981**, *103*, 6624. (b) Armentrout, P. B.; Beauchamp, J. L. *Ibid.* **1981**, *103*, 6628. (c) Houriet, R.; Halle, L. F.; Beauchamp, J. L. *Organometallics* **1983**, *2*, 1818. (d) Jacobson, D. B.; Freiser, B. S. *J. Am. Chem. Soc.* **1983**, *105*, 5197. (e) Jacobson, D. B.; Freiser, B. S. *Ibid.* **1983**, *105*, 7492. (f) Peake, D. A.; Gross, M. L.; Ridge, D. P. *Ibid.* **1984**, *106*, 4307. (g) Larsen, B. S.; Ridge, D. P. *Ibid.* **1984**, *106*, 1912. (h) Aristov, N.; Armentrout, P. B. *Ibid.* **1986**, *108*,1806.

(6) (a) Calin, T. J.; Sallans, L.; Cassady, C. J.; Jacobson, D. B.; Freiser, B. S. *J. Am. Chem. Soc.* **1983**, *105*, 6320. (b) Halle, L. F.; Klein, F. S.; Beauchamp, J. L. *Ibid.* **1984**, *106*, 2543.

(7) Schilling, J. B.; Goddard, W. A., III; Beauchamp, J. L. *J. Am. Chem. Soc.* **1986**, *108*, 582.

(8) Moore, C. E. "Atomic Energy Levels"; National Bureau of Standards: Washington, D.C., 1971; Vol. I and II.

(9) Ray, N. K.; Mehandru, S. P. *Pramana* **1978**, *10*, 201.

(10) Ray, N. K.; Switalski, J. *Theoret. Chim. Acta. (Berl.)* **1976**, *41*, 329.

(11) Pyykkö, P. *J. Chem. Soc., Faraday Trans. 2* **1979**, *75*, 1256.

(12) McFarland, R. H.; Schlachter, A. S.; Stearns, J. W.; Liu, B.; Olson, R. E. *Phys. Rev. A* **1982**, *26*, 775.

(13) Klimenko, N. M.; Musaev, D. G.; Zyubin, A. S. *Russ. J. Inorg. Chem.* **1984**, *29*, 352.

(14) Vincent, M. A.; Yoshioka, Y.; Schaefer, H. F., III *J. Phys, Chem.* **1982**, *86*, 3905.

(15) (a) Anglada, P.; Bruna, P. J.; Peyerimhoff, S. D.; Buenker, R. J. *J. Mol. Struc. (Theochem)* **1983**, *93*, 299. (b) Anglada, P.; Bruna, P. J.; Peyerimhoff, S. D.; Buenker, R. J. *Ibid.* **1984**, *107*, 163.

(16) (a) Alverado-Swaisgood, A. E.; Allison, J.; Harrison, J. F. *J. Phys. Chem.* **1985**, *89*, 2517. (b) Alverado-Swaisgood, A. E.; Harrison, J. F. *Ibid.* **1985**, *89*, 5198.

(17) Pettersson, L. G. M.; Bauschlicher, C. W., Jr.; Langhoff, S. R.; Partridge, H., private communication.

(18) Huber, K. P.; Herzberg, G. "Constants of Diatomic Molecules"; Van Nostrand Reinhold Co.; New York, 1979.

(19) (a) Rappé, A. K.; Goddard, W. A., III, to be published. (b) Rappé, A. K.; Smedley, T. A.; Goddard, W. A., III *J. Phys. Chem.* **1981**, *85*, 260.

(20) (a) Huzinaga, S. *J. Chem. Phys.* **1965**, *42*, 1293. (b) Dunning, T. H., Jr. *Ibid.* **1970**, *53*, 2823.

(21) (a) Miller, A. E. S.; Feigerle, C. S.; Lineberger, W. C. *J. Chem. Phys.* **1986**, *84*, 4127. (b) Leopold, D. G.; Miller, T. M.; Lineberger, W. C. *J. Am. Chem. Soc.* **1986**, *108*, 178.

(22) (a) Dyke, J. M.; Gravenor, B. W. J.; Josland, G. D.; Lewis, R. A.; Morris, A. *Mol. Phys.* **1984**, *53*, 465. (b) Dyke, J. M.; Gravenor, B. W.; Hastings, M. P.; Morris, A. *J. Phys. Chem.* **1985**, *89*, 4613.

(23) Hanratty, M. A.; Carter, E. A.; Beauchamp, J. L.; Goddard, W. A., III; Illies, A. J.; Bowers, M. T. *Chem. Phys. Lett.* **1986**, *128*, 239

CHAPTER V

THEORETICAL STUDIES OF TRANSITION METAL HYDRIDES:

III. SrH^+ THROUGH CdH^+

Theoretical Studies of Transition Metal Hydrides: III. SrH^+ through CdH^+

J. Bruce Schilling, William A. Goddard III*, and J. L. Beauchamp

Contribution No. 7551 from the

Arthur Amos Noyes Laboratory of Chemical Physics,

California Institute of Technology, Pasadena, CA 91125

Abstract

Generalized valence bond plus configuration interaction calculations have been carried out on the monopositive diatomic metal hydride ions of the second transition metal series (YH^+–CdH^+, including SrH^+). We analyze the trends in bond energies, equilibrium geometries, vibrational frequencies and metal orbital hybridizations. The trends in these quantities can be understood in terms of (1) the low-lying electronic states of the metal; (2) the orbital sizes of the metal; (3) the loss of exchange energy on bonding to the high-spin metal; and (4) the intrinsic bond strengths of bonding H to metal 5s and 4d electrons. We also present bond lengths, vibrational frequencies, and relative energies for selected MH^+ excited states.

I. Introduction

Recent studies of gas phase transition metal ion chemistry have focused on determination of the differences in reactivity of the various metal ions with small organic and inorganic molecules,[1] structural determination of reaction products,[2] investigation of reaction mechanisms,[3] and attempts to unravel the differences in reactivity between ground and excited state species.[4] Central to analyzing such chemical reactivity studies is an understanding of various thermodynamic quantities, particularly the metal-ligand bond dissociation energies. In order to determine the factors affecting sigma bonding in metal ion systems, we have performed systematic theoretical studies of the bonding in the first and second row transition metal hydride ions. Presented here are the results for the second row systems, the first row results having been published previously.[5]

II. Results and Discussion

Character of the Wavefunction. Figures 1 and 2 show the generalized valence bond (GVB) bond orbitals for SrH^+ through CdH^+ (excluding AgH^+). The GVB orbitals for the bond pairs involve an orbital with one electron centered on the metal ion and an orbital with one electron located on the hydrogen. Figure 3 shows the nonbonding valence σ orbitals present in the YH^+ and TcH^+ (singly occupied s–d_{z^2} hybrids) and CdH^+ (doubly occupied d_{z^2} orbital) molecules. The metal hydrogen bonds of all second-row elements are fairly covalent with an average transfer of 0.08 electrons to hydrogen. The electron transfer ranges from +0.25 electrons transfered to hydrogen in SrH^+ and YH^+ to −0.12 electrons in PdH^+, thus there is a fair increase in electronegativity from Y^+ to Pd^+.

The first row metals bond to hydrogen predominantly with their 4s orbital rather than the 3d orbitals.[5] In contrast, the second row transition metals tend to bond with 4d rather than 5s electrons (see Table I). AgH^+ is not included in the table due to the fact that the AgH^+ bond arises from an ion-dipole type

Figure 1: GVB bond orbitals (at Re) for: (a) $^1\Sigma^+$ SrH^+; (b) $^2\Sigma^+$ YH^+; (c) $^3\Phi$ ZrH^+; (d) $^4\Delta$ NbH^+; and (e) $^5\Sigma^+$ MoH^+. Solid lines indicate positive amplitude, dotted lines indicate negative amplitude, and long dashed lines indicate zero amplitude. The spacing between contours is 0.05 au. The contours are plotted in the xz plane with the M^+–H bond axis along the z axis. The plot limits are -2.0 to 3.5 Å for the z axis and -2.0 to 2.0 Å for the x axis.

a) Sr^+-H

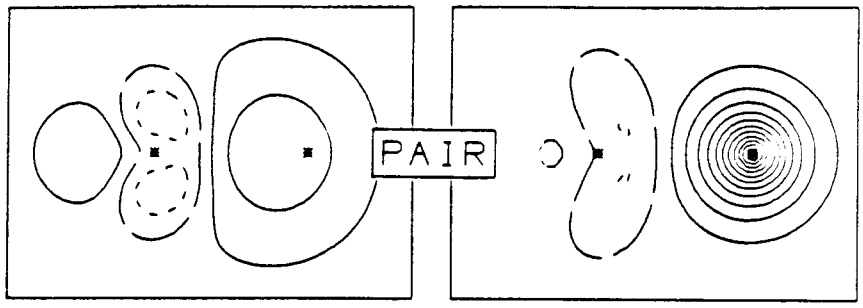

b) Y^+-H

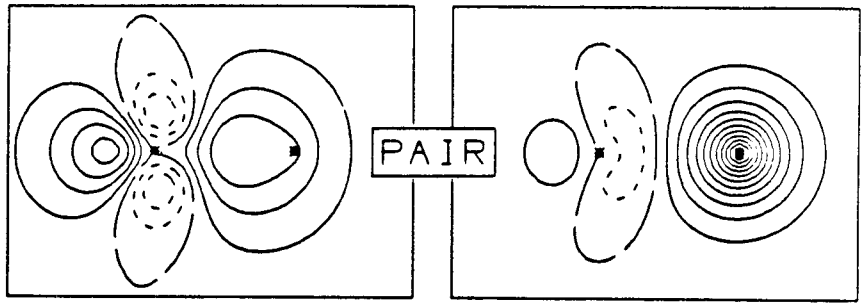

c) Zr^+-H

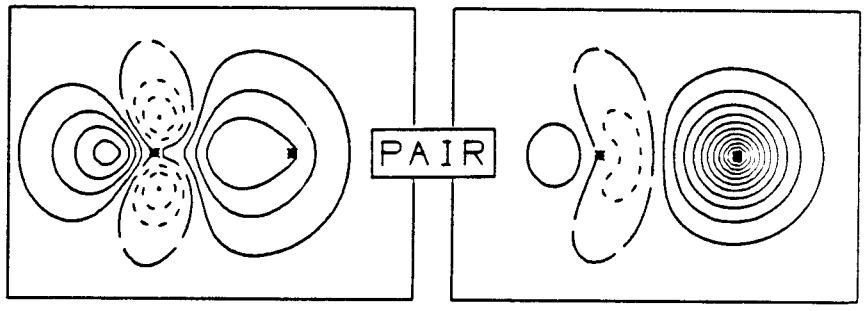

d) Nb^+-H

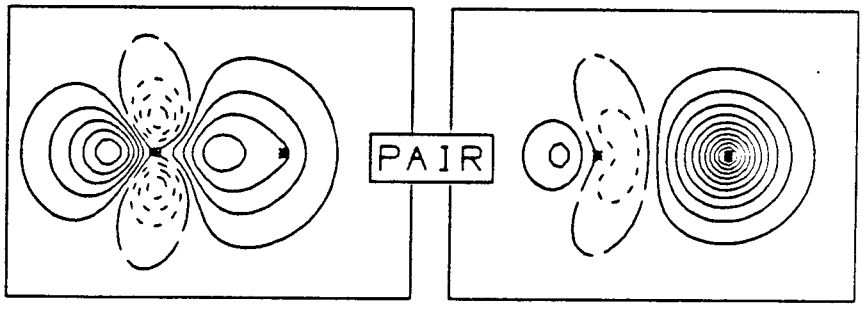

e) Mo^+-H

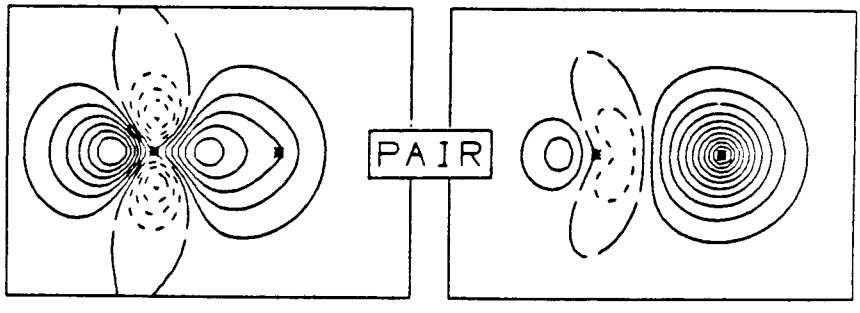

Figure 2: GVB bond orbitals (at R_e) for: (a) $^6\Sigma^+$ TcH^+; (b) $^3\Sigma^-$ RuH^+; (c) $^2\Delta$ RhH^+; (d) $^1\Sigma^+$ PdH^+; and (e) $^1\Sigma^+$ CdH^+. All plotting parameters are the same as in Figure 1.

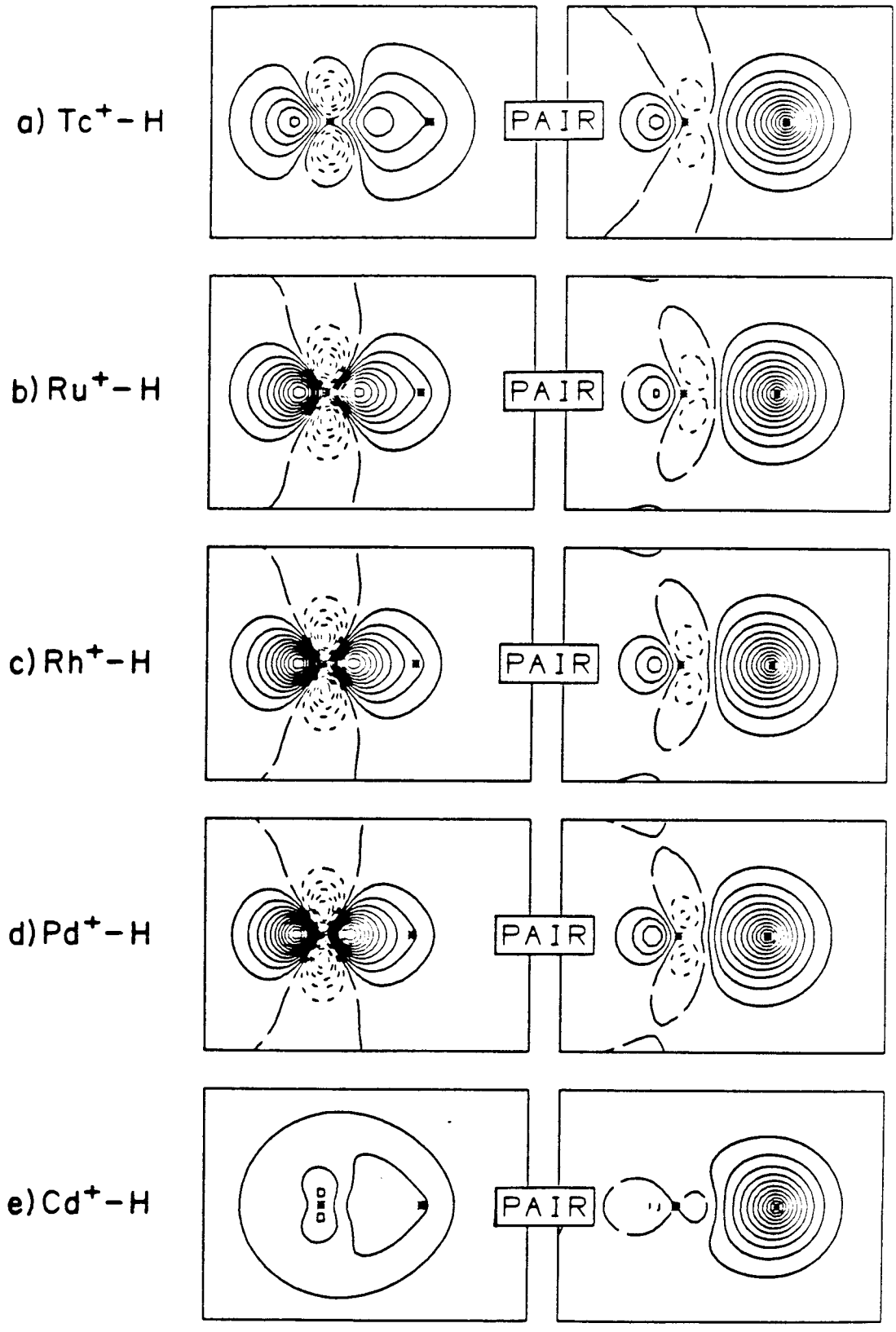
a) $Tc^+ - H$
PAIR
b) $Ru^+ - H$
PAIR
c) $Rh^+ - H$
PAIR
d) $Pd^+ - H$
PAIR
e) $Cd^+ - H$
PAIR

Figure 3: Nonbonding sigma orbitals for: (a) $^2\Sigma^+$ YH^+ (66.9% s, 2.9% p, and 30.2% d); (b) $^6\Sigma^+$ TcH^+ (31.5% s, 0.4% p, and 68.1% d); and (c) $^1\Sigma^+$ CdH^+ (0.8% s, 0.1%p, and 99.1% d). All plotting parameters are the same as in Figures 1 and 2.

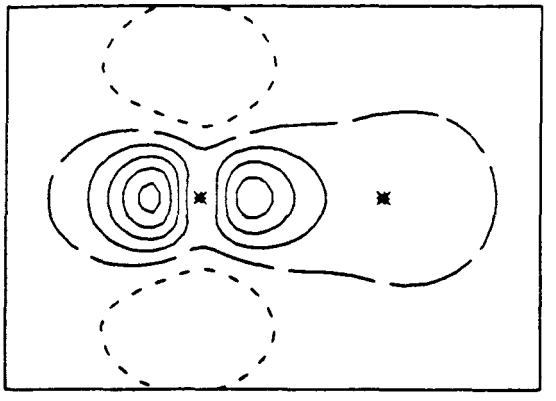

a) Y^+–H SINGLY OCCUPIED σ ORBITAL

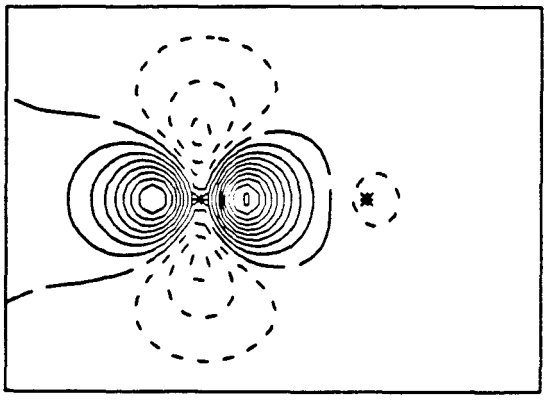

b) Tc^+–H SINGLY OCCUPIED σ ORBITAL

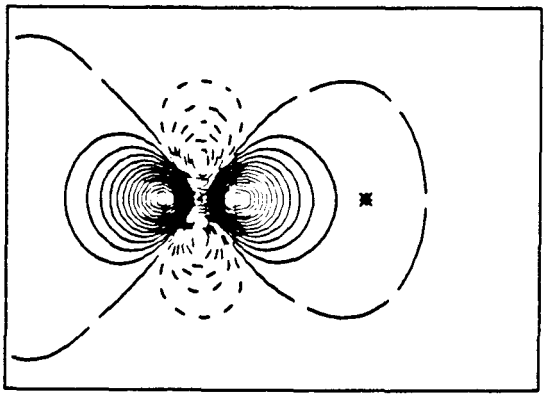

c) Cd^+–H DOUBLY OCCUPIED d_{z^2} ORBITAL

Table I

Character of Wave Functions for MH^+
(from GVB-PP Calculations)

Molecule[a]	State	Character of Metal Bonding Orbital			Overlap	Charge Transfer
		%s	%p	%d		to H
SrH^+ (d^0)	$^1\Sigma^+$	56.3	14.2	29.5	0.755	0.25
YH^+ (d^1)	$^2\Sigma^+$	31.9	10.2	57.9	0.760	0.25
ZrH^+ (d^2)	$^3\Phi^\pm$	36.0	10.6	53.4	0.757	0.17
NbH^+ (d^3)	$^4\Delta^\pm$	30.0	9.3	60.7	0.743	0.13
MoH^+ (d^4)	$^5\Sigma^+$	19.7	7.0	73.3	0.703	0.09
TcH^+ (d^5)	$^6\Sigma^+$	40.5	7.0	52.5	0.751	0.11
RuH^+ (d^6)	$^3\Sigma^-$	9.0	3.9	87.1	0.622	−0.05
RhH^+ (d^7)	$^2\Delta^\pm$	7.0	3.0	90.0	0.595	−0.09
PdH^+ (d^8)	$^1\Sigma^+$	5.1	2.1	92.8	0.572	−0.12
CdH^+ (d^{10})	$^1\Sigma^+$	90.4	9.2	0.4	0.674	0.04

[a] Nonbonded d orbital occupation given in parentheses

interaction which does not lead to a "normal" pair of bonding electrons. With the exception of SrH^+ and CdH^+ all species studied have over 50% d character in the metal bonding orbital (92.8% in the case of PdH^+).

Electronic Configuration. In order to understand the trends it is important to keep in mind the number of nonbonding d electrons on the metal, and we will thus indicate the nonbonding orbital occupation in parentheses. Thus, TcH^+ (d^5) indicates five electrons in nonbonding orbitals (coupled high spin). For $ZrH^+(d^2)$ through $PdH^+(d^8)$, all but one case have the nonbonding d electrons in $d\pi$ or $d\delta$ orbitals (see Table IX) so that the metal $d\sigma$ and s orbitals are free to mix in forming the bond pair. The exception is $TcH^+(d^5)$, where the exchange coupling stabilizes the high-spin state having a nonbonding $d\sigma$ electron. $AgH^+(d^9)$ necessarily has a $d\sigma$ orbital. $YH^+(d^1)$ also has a $d\sigma$ nonbonding electron for reasons discussed below.

Spectroscopic Properties. The spectroscopic properties calculated for the metal hydrides (bond length, vibrational frequency, ground state symmetry, and bond dissociation energies) are given in Table II.

Bond Lengths. The trend in bond lengths for the second row metal hydrides (Table III) parallels that for the first row metal hydrides[5] (with the exception of AgH^+). The bond lengths decrease a total of 0.5 Å as one moves from SrH^+ to PdH^+. As indicated in Table III, this follows the trend of decreasing size in the metal orbitals. Indeed, the MH^+ bond length is systematically about 0.17 Å smaller than the M^+ 5s orbital. Three exceptions to this decreasing bond length are TcH^+ (d^5), CdH^+ (d^{10}), and AgH^+ (d^9). The increase in bond length upon reaching Tc^+ and Cd^+ is due to the completion of stable half-full or completely full 4d shells (of nonbonding electrons) and the concomitant large increase in s character in the bond. For Ag^+, the d^{10} configuration of the ion is so stable that AgH^+ does not make a covalent bond in its ground state and thus does not fit into the bonding trends. Rather, AgH^+ makes an ion-dipole bond, 50% longer than the bond in PdH^+.

Table II

Spectroscopic Properties of Ground State MH^+

Molecule	State	Bond Length R_e (Å)	Force Constant (hartree/Å^2)[g]	Vibrational Frequency ω_e (cm^{-1})	Bond Energies (kcal/mol)				
					Theory[a]			Experiment	
					D_e	D_0	D_{298}	D_0^b	D_0^c
SrH^+	$^1\Sigma^+$	2.079	0.2457	1346	46.0	44.1	45.0		
YH^+	$^2\Sigma^+$	1.892	0.3645	1639	60.1	57.8	58.7		58±3
ZrH^+	$^3\Phi^\pm$	1.857	0.3731	1658	57.0	54.6	55.5		54±3
NbH^+	$^4\Delta^\pm$	1.764	0.4425	1805	51.3	48.7	49.6		53±3
MoH^+	$^5\Sigma^+$	1.708	0.4530	1826	33.8	31.2	32.1		41±3
TcH^+	$^6\Sigma^+$	1.719	0.4099	1737	48.8	46.3	47.2		
RuH^+	$^3\Sigma^-$	1.581	0.5361	1986	34.5	31.7	32.6	40±3.5	
RhH^+	$^2\Delta^\pm$	1.539	0.6138	2125	37.8	34.8	35.7	41±3.5	
PdH^+	$^1\Sigma^+$	1.512	0.6323	2127	43.7	40.6	41.5	44±3.5	53±3
AgH^+	$^2\Sigma^+$	2.428	0.0186	372	2.6	2.1	3.0		15±3
CdH^+	$^1\Sigma^+$	1.709[d]	0.3912	1696[e]	44.4	42.0	42.9		49.3[f]

[a] Present work (GVB-DCCI). [b]Reference 9. D_{298} values have been decreased by 0.9 kcal/mol to give D_0 values. [c]Reference 10. [d]Experimental value 1.67 Å. Reference 8. [e]Experimental value 1771 cm^{-1}. Reference 8. [f]Reference 8. [g] Multiply by 4.359 to obtain mdyne/Å or by 627.5 to obtain (kcal/mol)/Å^2.

Table III

Valence Orbital Sizes (Å) for Second Row Transition Metal Ions, $R = \sqrt{\langle\phi|r^2|\phi\rangle}$

Ion	R(5s)	R(4d)				Change on Bonding MH^+	
		$4d^{n-1}5s^1$		$4d^n$			
		$(1e^-)^a$	$(2e^-)^a$	$(1e^-)^a$	$(2e^-)^a$	$R_e - R(5s)$	$R_e - R(4d)$
Sr^+	2.37			1.93		−0.29	0.15
Y^+	2.14	1.38		1.47		−0.25	0.42
Zr^+	2.00	1.21		1.30		−0.14	0.56
Nb^+	1.94	1.11		1.17		−0.18	0.59
Mo^+	1.87	1.02		1.06		−0.16	0.65
Tc^+	1.79	0.95		0.99	1.04	−0.07	0.73
Ru^+	1.72	0.88	0.91	0.93	0.96	−0.14	0.65
Rh^+	1.68	0.84	0.85	0.87	0.89	−0.14	0.67
Pd^+	1.64	0.80	0.80	0.82	0.85	−0.13	0.69
Ag^+	1.64	0.75	0.76		0.80	0.79	
Cd^+	1.60		0.73			0.11	

[a] $1e^-$ and $2e^-$ indicate singly and doubly occupied orbitals.

Theoretical calculations have been previously reported for SrH^+ and CdH^+ (Dirac-Fock One Center Expansion)[6] yielding bond lengths 2.10 Å and 1.82 Å respectively in reasonable agreement with our values of 2.08 and 1.71 Å. For AgH^+ Preuss et al.[7] (using a one valence electron effective core potential for Ag, but allowing for core polarization effects) calculate a bond length for AgH^+ of 2.24 Å (we obtain 2.43 Å). Only for CdH^+ is there an experimental bond length,[8] 1.667 Å, in comparison with our value of 1.709 Å and the Pyykkö value of 1.82 Å. The calculated bond length should decrease as further electron correlation is included, and our theoretical values are probably generally about 0.03 Å too long.

Vibrational Frequencies. The vibrational frequency for a bond is often considered to increase with bond strength; however no such correlation is seen between various transition metal hydrides. The vibrational frequencies do follow an inverse correlation with the length of the metal-hydrogen bond. Proceeding from SrH^+ (d^0) (2.079 Å, 1346 cm^{-1}), the vibrational frequency increases as the bond length decreases, reaching a maximum for PdH^+ (d^8) (1.512 Å, 2127 cm^{-1}). Again, discontinuities in the smooth increase of the vibrational frequencies are seen for TcH^+ (d^5), AgH^+ (d^9), and CdH^+ (d^{10}), corresponding to the bond length discontinuities. Thus, higher vibrational frequencies are seen for shorter bonds, not necessarily for stronger ones. As with the bond lengths, the vibrational frequency is known experimentally for only CdH^+.[8] The spectroscopic value of 1772 cm^{-1} is 4.5% larger than the theoretical value of 1691 cm^{-1} (consistent with the shorter experimental bond length). It is reasonable to assume that our theoretical vibrational frequencies are also 5% too low for the other systems.

Bond Dissociation Energies. Total energies for the metal hydrides (at Re) for three calculation levels (GVB-PP(1/2), DCCI-GEOM, and DCCI) are shown in Table IV. Comparisons of the present theoretical results and the available experimental bond dissociations energies are shown in Table II and in Figure 4.

Table IV

Total Energies for Ground State MH^+ (at R_e), M^+, and H

Species	State	Total Energy (hartrees)[a]		
		GVB-PP	DCCI-GEOM	DCCI
SrH^+	$^1\Sigma^+$	−30.48147	−30.49560	−30.49560
Sr^+	^2S	−29.92310	−29.92310	−29.92310
YH^+	$^2\Sigma^+$	−37.85232	−37.86748	−37.87067
Y^+[b]	^3D	−37.26855	−37.26855	−37.26974
ZrH^+	$^3\Phi^\pm$	−46.35635	−46.37277	−46.37720
Zr^+	^4F	−45.78547	−45.78569	−45.78714
NbH^+	$^4\Delta^\pm$	−56.02195	−56.94132	−56.04840
Nb^+	^5D	−55.46008	−55.46008	−55.46732
MoH^+	$^5\Sigma^+$	−67.20265	−67.22531	−67.23292
Mo^+	^6S	−66.67212	−66.67212	−66.67981
TcH^+	$^6\Sigma^+$	−79.70781	−79.73303	−79.74350
Tc^+	^7S	−79.16302	−79.16302	−79.16644
RuH^+	$^3\Sigma^-$	−93.39360	−93.43920	
Ru^+	^4F	−92.88143	−92.88407	−92.89714
RhH^+	$^2\Delta^\pm$	−108.99231	−109.01912	−109.03192
Rh^+	^3F	−108.45712	−108.45803	−108.47233
PdH^+	$^1\Sigma^+$	−126.17678	−126.20089	−126.21456
Pd^+	^2D	−125.62886	−125.62941	−125.64562
AgH^+	$^2\Sigma^+$	−145.16705		−145.16806
Ag^+	^1S	−144.66317		−144.66460
CdH^+	$^1\Sigma^+$	−46.85635	−46.87106	−46.88990
Cd^+	^2S	−46.29916	−46.30065	−46.31982
H	^2S	−0.49928	−0.49928	−0.49928

[a] For MH^+ the total energies are for the calculation levels shown while the M^+ and H total energies are for the calculation levels to which these MH^+ molecules dissociate (see Calculational Details Section of text). [b]The $^2\Sigma^+$ state of YH^+ does not dissociate to ground state Y^+ (^1S) but to ^3D Y^+ as shown here.

Figure 4: Comparison of experimental and theoretical bond dissociation energies [$D_e(M^+-H)$]: present work (circles); Mandich, Halle, and Beauchamp—reference 9 (triangles); Elkind and Armentrout—reference 10 (closed squares); and Huber and Herzberg—reference 8 (open square).

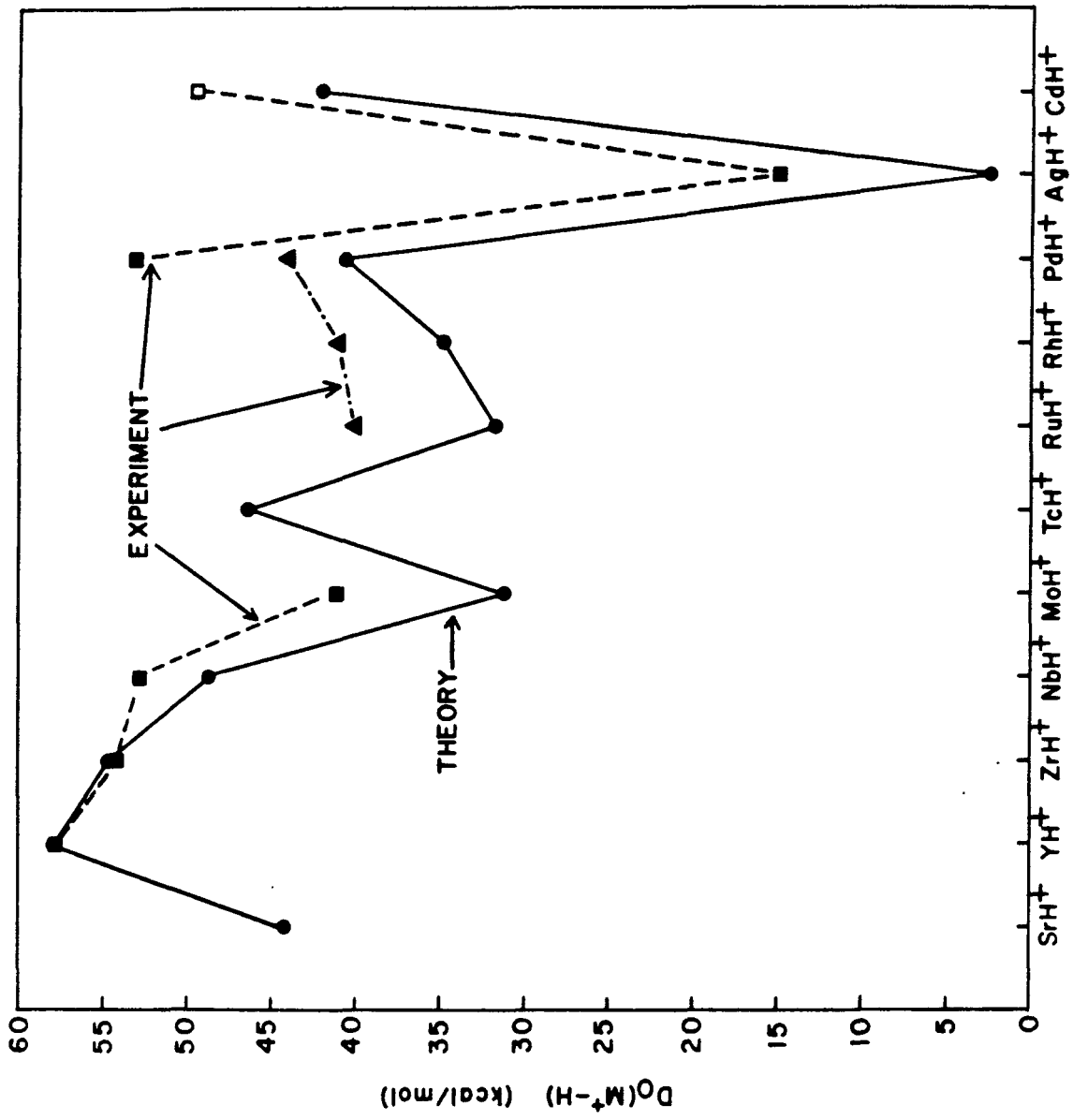
EXPERIMENT
THEORY
$D_0(M^+-H)$ (kcal/mol)
0
5
10
15
20
25
30
35
40
45
50
55
60
SrH^+ YH^+ ZrH^+ NbH^+ MoH^+ TcH^+ RuH^+ RhH^+ PdH^+ AgH^+ CdH^+

Just as for the first row metal hydrides, the trend in the bond energies can be understood in terms of the balance between s and d bonding and the character of the ground state, however these trends are *not* obvious from a plot such as Figure 4. The highest bond energies occur for the very early metals Y^+ (d^1), Zr^+ (d^2), and Nb^+ (d^3) where (i) the s and d orbitals are close in size and energy and readily hybridized and (ii) there is little exchange energy lost on bonding. The smallest bond energy is found for AgH^+ due to the closed shell d^{10} configuration of Ag^+ and the high promotional energy just to obtain a state (s^1d^9 configuration) with singly occupied orbitals. The bonding thus results from small ion-dipole interactions rather than normal covalent bonding. The bond energies of other systems oscillate between these two extremes.

For the first row metal hydrides[5], our theoretical bond dissociation energies compare very well with the ion beam results of Elkind and Armentrout[10] with an average difference of 2.5 kcal/mol. The overall bond energy trends for the second row metal hydrides correspond fairly well between experiment and theory but the actual quantitative values differ more substantially than for the first row. Although the experimental and theoretical results for YH^+ and ZrH^+ are within 1 kcal/mol, the average difference between the present results and the experimental values is 6.7 kcal/mol. However, we should emphasize two points. First, inclusion of f functions on the metal (tested in the case of MoH^+) can increase the theoretical values by as much as 3 kcal/mol. Second, the experimental bond energies for these systems involve analysis of the threshold for $M^+ + H_2 \rightarrow MH^+ + H$ and require correction for excited M^+ in the beam. As a result, reanalysis of the experiments for the first row metal hydrides has led to decreases of up to 5 or even 10 kcal/mol in some of the experimental values. Thus, the present results, representing a consistent set of calculations for all of the second row metals, may help with the analysis of experimental results (which are less complete than for the first row counterparts).

Other theoretical bond dissociation energies have been reported for SrH^+

(81.6 kcal/mol versus our value of 45.0 kcal/mol),[6] CdH^+ (33.9 kcal/mol versus our value of 42.9 kcal/mol and the experimental value of 49.3 kcal/mol),[6] and AgH^+ (6.7 kcal/mol versus our value of 3.0 kcal/mol and an experimental value of 15±3 kcal/mol).[7] Recent calculations by Pettersson et al.[11] on YH^+ through AgH^+ yield bond dissociation energies that are very comparable for the early metal hydrides. For the later metal hydrides their bond energies are from 4–7 kcal/mol larger than those in the present study.

Analysis of the Metal Hydrogen Bond. The major factors affecting the bonding of hydrogen to the second row metal ions are:

1) the orbital character of the low-lying metal electronic states;

2) the relative sizes of the metal s and d orbitals;

3) the intrinsic bond strengths to pure s or d orbitals;

4) the effects of changes in exchange energy of the nonbonding d orbitals; and

5) the effects of metal orbital hybridization.

Low-lying Metal Electronic States. To analyze the low-lying electronic states we start with the orbital configuration of the ground electronic state of the ion. This generally involves either a d^n or $d^{n-1}s^1$ valence electronic configuration.[12] Our working hypothesis is that the ground configuration or a low lying excited configuration must have a singly occupied s orbital in order to make an s-like bond or a singly occupied d orbital to make a d-like bond (for Y^+, the ground state electronic configuration is s^2 but the ^3D state (s^1d^1) is only 0.16 eV higher in energy).[11] Figure 5 shows the relative difference in energy between the lowest electronic states formed from the $4d^n$ and $4d^{n-1}5s^1$ configurations for the second row transition metals. The general trend is for the state with the d^n configuration to be stabilized, with respect to the state with the $d^{n-1}s^1$ configuration, as one proceeds from left to right. Starting with Tc^+ the d^n configuration requires doubly occupying one of the d orbitals leading to an increase of electron-electron repulsion energy and a jump in the $d^n - d^{n-1}s^1$ separation.

Figure 5: Trends in the difference in energy between the lowest metal electronic states arrising from $4d^n$ and $4d^{n-1}5s^1$ configurations for the second row transition metal monopositive ions.[12] $\Delta E = E_{d^n} - E_{d^{n-1}s^1}$.

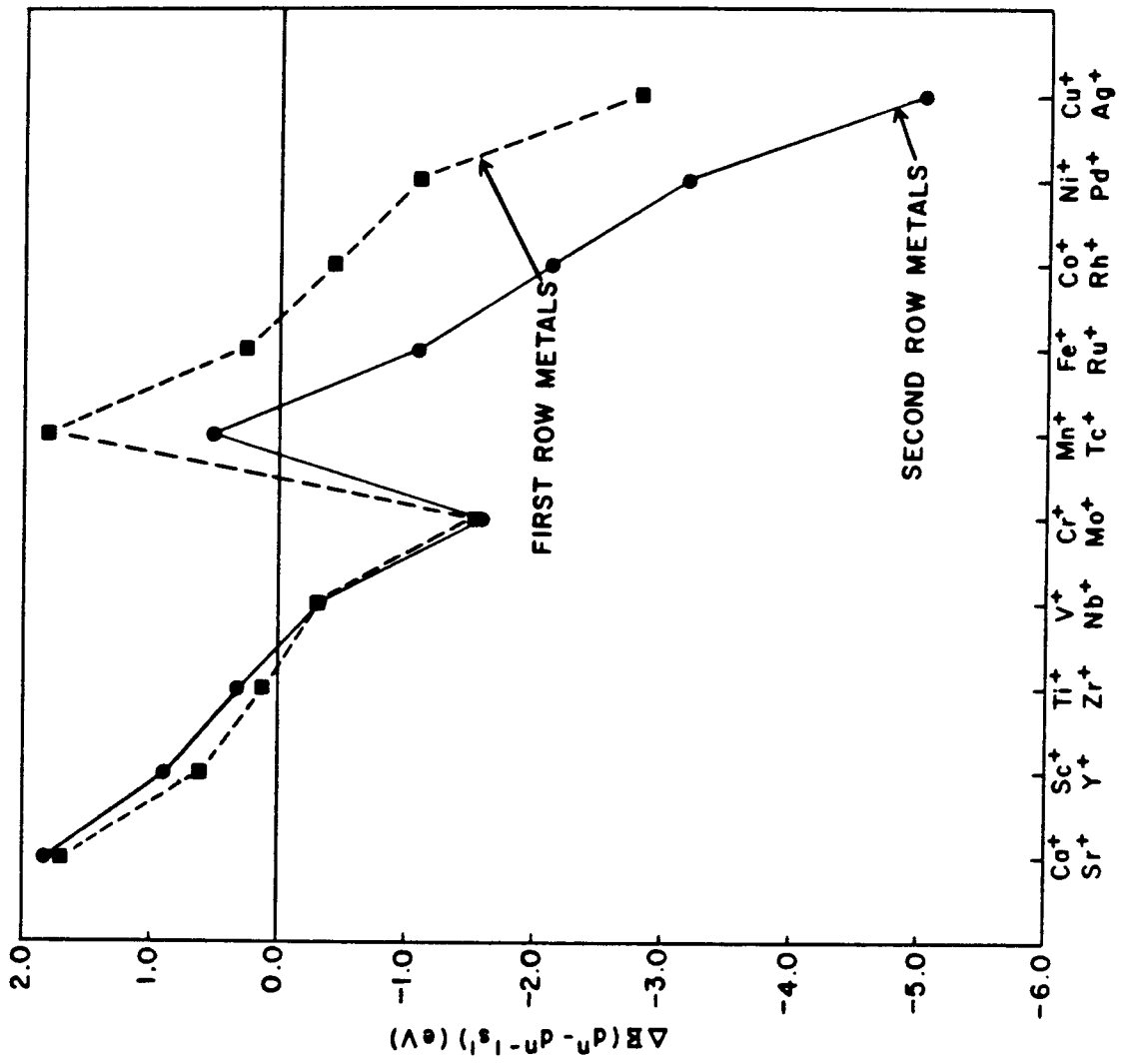
FIRST ROW METALS
SECOND ROW METALS
ΔE(d^n - d^{n-1}s^1) (eV)
2.0
1.0
0.0
-1.0
-2.0
-3.0
-4.0
-5.0
-6.0
Ca+ Sc+ Ti+ V+ Cr+ Mn+ Fe+ Co+ Ni+ Cu+
Sr+ Y+ Zr+ Nb+ Mo+ Tc+ Ru+ Rh+ Pd+ Ag+

The 5s orbital is more stable than 4d at the left of the row, but proceeding to the right leads to continuous stabilization of the d orbitals with respect to the s orbital due to differential shielding effects of 4d versus 5s. The d^n configurations are also stabilized due to larger d-d exchange energies as compared to s-d exchange. These exchange effects are greatest for the half-filled (d^5) and fully-filled (d^{10}) shells. Thus, for Ag^+, the ^1S (d^{10}) state is over 5 eV lower in energy than the ^3D (d^9s^1) state.

Metal Orbital Sizes. The size of the metal orbitals is intimately related to the shielding by electrons in other orbitals (the effective nuclear charge) and thus to the electronic configuration and relative energies of the electronic states. The relative energy between the lowest electronic states with d^n and $d^{n-1}s^1$ configurations for the late transition metals of the second row increases much more rapidly than for the first row. This is largely due to the reduced electron-electron repulsion resulting from the increased size of the second row d orbitals.

The size of the metal orbital also affects its overlap with a neighboring H atom, which should also affect the bond energies. Table III shows the root mean square radii found from Hartree-Fock wavefunctions for the atomic metal ions. As expected, both s and d orbitals contract in size going from left to right along the row, but the d orbitals contract faster. The ratio of size (R_s/R_d) for Sr^+ is 1.23 while for Ag^+ it is 2.18. In comparison, the first row metals Ca^+ and Cu^+ have size ratios of 1.33 and 2.81, respectively.[5] This results in average differences between orbital sizes for first and second row metals of 0.13 Å for s orbitals and 0.30 Å for d orbitals (second row orbitals larger). Thus, for the second row, the size of d orbitals with respect to s is larger than for the first. As shown in Table III, the bond distances of MH^+ track very well with changes in the size of the metal s orbitals. Thus, for SrH^+ through PdH^+ (all of which have significant d character), the MH^+ bond distance averages about 0.17 Å shorter than the size of the s orbital. For CdH^+ with *no* d character, the bond is 0.11 Å larger than the size of the s orbital. Similarly, for YH^+ through PdH^+, the bond distance

averages about 0.62 Å larger than the size of the d orbital.

Intrinsic Bond Strengths. It is useful to establish an intrinsic bond strength for the MH^+ bond by making corrections for the energy required to promote the metal to the bonding state and for the exchange energy changes due to the nonbonding orbitals. In order to establish the trends in bond energy to s and d orbitals, we carried out calculations on the metal hydrides in which the mixing of s and d character in the bond was not allowed. The results are tabulated in Table V and presented graphically in Figure 6. The intrinsic s bond is fairly constant over the whole range of metals, increasing approximately 10 kcal/mol between SrH^+ and CdH^+. The discontinuities seen between MoH^+ and TcH^+ and again between AgH^+ and CdH^+ are due to occupation of a $d\sigma$ nonbonding orbital to which the bond pair must become orthogonal. The intrinsic d bonding, on the other hand, varies considerably with a value of 75.0 kcal/mol for SrH^+ versus 30.8 kcal/mol for PdH^+. The decreasing intrinsic d bond strength on moving across the row seems to indicate that the optimum size for a d orbital for bonding H is at least 1.9 Å. The intrinsic s bond trend implies that the optimum size of a 5s orbital for bonding H is smaller than that of Cd^+ (less than 1.6 Å). It should be emphasized here that to exact such the intrinsic bond energies we used GVB-PP(1/2) calculations; thus, the relative values and trends should be reliable, but quantitative values should be too small by ~10–15 kcal/mol.

Exchange Energy Considerations. Loss of exchange energy plays an important role in moderating the bond energies to high spin species.[13] When a singly-occupied orbital of a high-spin atom is used in a bond, the spin coupling in the new bond is such that this orbital has the same spin as the nonbonding orbitals only one-half the time. Thus, approximately one half of the exchange energy between the bonding electron and the other high spin electrons on the atom is lost, effectively lowering the bond energy. This effect is largest for elements with the highest numbers of high-spin coupled electrons, i.e. toward the middle of the row.

Table V

Intrinsic Bond Dissociation Energies[a]

Molecule	s-Bond (kcal/mol)	d-Bond (kcal/mol)
SrH^+	26.8	75.0
YH^+	29.7	61.2
ZrH^+	28.9	54.5
NbH^+	29.5	48.5
MoH^+	32.7	40.7
TcH^+	21.1	39.0
RuH^+	23.0	33.9
RhH^+	23.8	32.7
PdH^+	25.2	30.5
AgH^+	25.6	0.0
CdH^+	36.4	0.0

[a] The trends in these numbers should be valid. However, in order to extract separate contributions, restrictions were made in the wavefunctions that make all numbers too low by ~10–15 kcal/mol.

Figure 6: Intrinsic bond strengths of H to metal 5s (circles) and 4d (squares) orbitals from GVB-PP(1/2) calculations. The intrinsic bond energies are the diabatic bond dissociation energies of the complex (allowing no hybridization) adding back in any exchange energy lost on bonding.

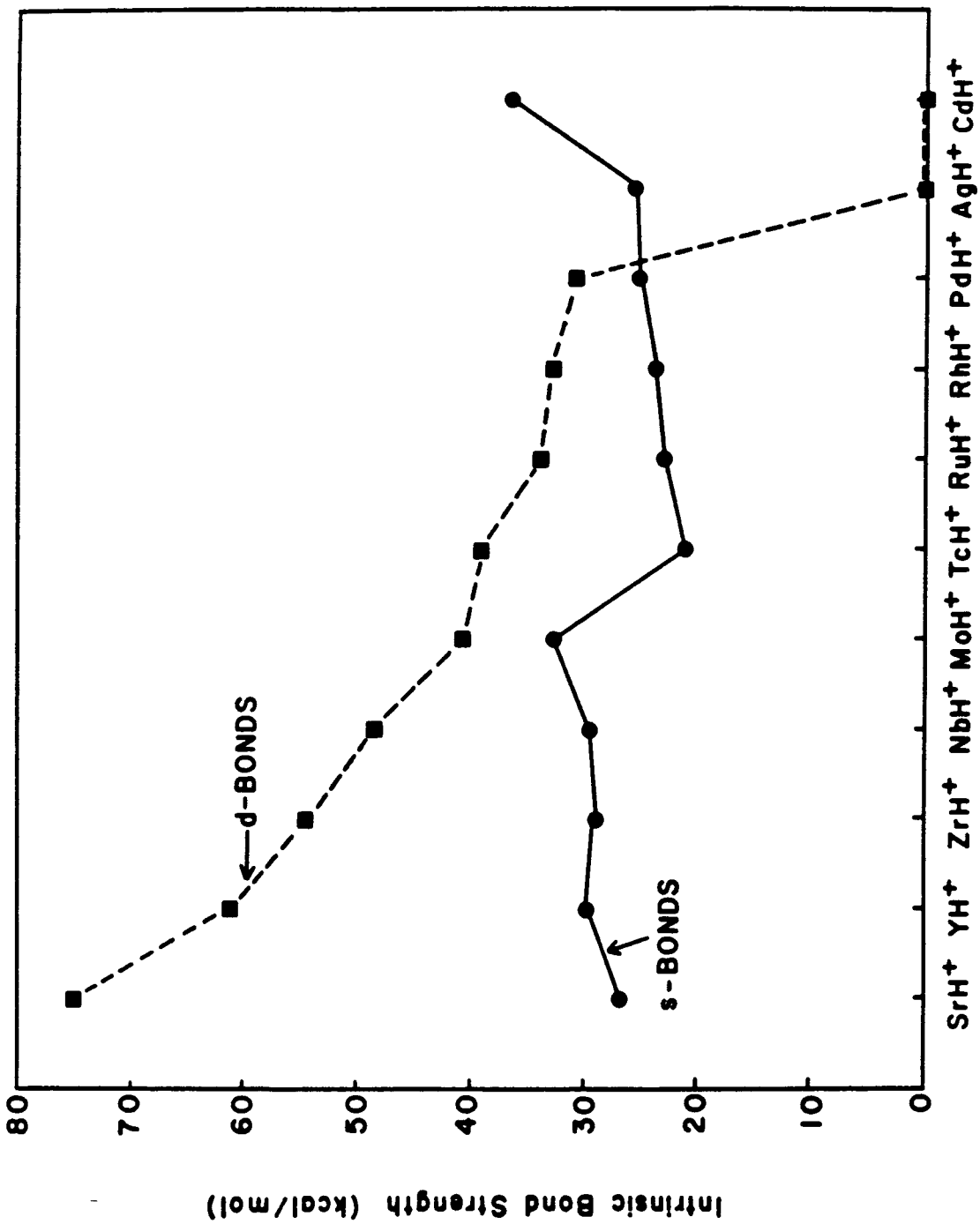
Intrinsic Bond Strength (kcal/mol)
80
70
60
50
40
30
20
10
0
d-BONDS
s-BONDS
SrH+ YH+ ZrH+ NbH+ MoH+ TcH+ RuH+ RhH+ PdH+ AgH+ CdH+

The exchange energy between two electrons is inversely proportional to the average distance between the electrons, and thus depends on the orbital sizes. The d-d exchange energies (K_{dd}) are consistently much larger than the s-d exchange energies (K_{sd}). Consider, for example, Y^+ and Pd^+. The ^3D (d^1s^1) state of Y^+ has K_{sd} = 9.87 kcal/mol, while the ^3F ($d\sigma d\delta$) state of Y^+ has K_{dd} = 11.65 kcal/mol. For the ^4F (d^8s^1) state of Pd^+, K_{sd} = 7.15 kcal/mol and $K_{d\sigma d\delta}$ = 21.14 kcal/mol. Thus, as the orbitals become smaller (with the d orbitals contracting faster), the K_{sd} values decrease, while the K_{dd} values increase. [As indicated in Table VI for Tc^+, the exchange energy also varies somewhat with orbital occupation.] Comparing the average K_{dd} and K_{sd} for the ^6S state of Tc^+ (K_{sd} = 8.28 kcal/mol, K_{dd} = 15.32 kcal/mol) to those of Mn^+ (K_{sd} = 4.81 kcal/mol, K_{dd} = 19.81 kcal/mol),[5] we see that for the second row, K_{sd} is larger and K_{dd} is smaller. The smaller d orbital size and larger K_{dd} for the first row is partly responsible for the dominance of s character in the metal-hydrogen bond. For the second row, Table VII shows the change in the intrinsic bond strengths due to loss of exchange energy. Lower K_{dd} values and higher K_{sd} values for the second row tend to favor bonding to d electrons.

Metal Orbital Hybridization. Table VIII shows the intrinsic bonding after correcting for exchange energy loss and the necessary promotion energies of the metals. We compare these values to those obtained from GVB-PP(1/2) calculations (which allow optimal metal orbital hybridization). For every case, the d-bond energy is larger then the s-bond energy. This coincides, for all cases except SrH^+, with the actual hybridizations shown in Table I. As expected, the bond energies for the hybridized species are greater than for the unhybridized species. For both the first and second row metals the strongest bonds are found for those metals whose admixture of s and d character is allowed by the ground state configuration while species where this is not possible tend to have weaker bonds.

Low-lying MH^+ Electronic States. For the first row metal hydrides,

Table VI

5s–4d and 4d–4d Exchange Energies for the ^6S and ^4D States of Tc^+

Orbitals	^6S ($5s^1 4d^5$)		^4D ($4d^6$)	
	Number	$\bar{K}$ (kcal/mol)	Number	$\bar{K}$ (kcal/mol)
s–d	5	8.28	0	
Ave. d–d	10	15.32	6	15.19
$d\sigma$–$d\pi$	2	11.76	2	11.20
$d\sigma$–$d\delta$	2	18.88	1	17.95
$d\pi$–$d\pi$	1	16.51	1	15.73
$d\pi$–$d\delta$	4	16.51	2	15.66
$d\delta$–$d\delta$	1	9.38	0	

Table VII

Intrinsic Bond Strengths after Correction for Exchange Energy Losses

Molecule	s-bond			d-bond		
	Exchange Loss		$D_s(M^+ - H)$[a]	Exchange Loss		$D_d(M^+ - H)$[b]
	K_{sd} Terms	Energy (kcal/mol)	(kcal/mol)	K_{dd} Terms	Energy (kcal/mol)	(kcal/mol)
SrH^+	0	0.0	26.8	0	0.0	75.0
YH^+	$\frac{1}{2}$	4.9	24.8	$\frac{1}{2}$	5.8	55.4
ZrH^+	1	9.1	19.8	1	10.8	43.7
NbH^+	$1\frac{1}{2}$	13.2	16.3	$1\frac{1}{2}$	16.8	31.7
MoH^+	2	16.9	15.8	2	26.9	13.8
TcH^+	$2\frac{1}{2}$	20.7	0.4	$1\frac{1}{2}$	20.2	18.8
RuH^+	2	14.8	8.4	1	15.3	18.6
RhH^+	$1\frac{1}{2}$	10.9	12.9	$\frac{1}{2}$	10.2	22.5
PdH^+	1	7.2	18.0	0	0.0	30.5
AgH^+	$\frac{1}{2}$	5.9	19.7	0	0.0	0.0
CdH^+	0	0.0	36.4	0	0.0	0.0

[a] $D_s(M^+ - H)$ = (intrinsic s-bond energy) − (Exchange energy lost on bonding to s orbital).

[b] $D_d(M^+ - H)$ = (intrinsic d-bond energy) − (Exchange energy lost on bonding to dσ orbital).

Table VIII

Comparison of s, d, and Hybridized Bonding in MH^+

Molecule	Intrinsic Bond Energies After Corrections for Exchange and Promotion Energies[a]		Calculated Bond Energies[b]
	s-bond (kcal/mol)	d-bond (kcal/mol)	(no restrictions) (kcal/mol)
SrH^+	26.8	32.8	37.1
YH^+	24.8	35.1	49.3
ZrH^+	19.8	36.6	44.9
NbH^+	8.7	31.7	39.3
MoH^+	−20.9	13.8	19.6
TcH^+	0.4	7.0	28.6
RuH^+	−16.9	18.6	18.6
RhH^+	−36.2	22.5	22.5
PdH^+	−55.6	30.5	30.5
AgH^+	−95.9	0.0	0.0
CdH^+	36.4		36.4

[a] Bond Energy = (Intrinsic Bond Strength) − (Exchange Energy Lost on Bonding) − (Metal Promotion Energy). [b] GVB Perfect Pairing wavefunction with no restrictions on orbital hybridization.

one can predict the ground state configuration by spin pairing the H to a sigma electron of the lowest metal state with a $4s^13d^{n-1}$ configuration and then taking into account the intraatomic electrostatic interaction of the nonbonding valence electrons.[5] This predicts the correct ground state even for species in which the lowest metal ion state does not have a $4s^13d^{n-1}$ configuration (e.g. CoH^+ and NiH^+). The increased importance of the d orbitals for the second row metals shows up as changes in the metal orbital hybridizations and also in the relative energies of some of the MH^+ low-lying electronic states.

As a illustrative example of differences between the first and second row metal hydrides we compare TcH^+ and MnH^+. Both of these metals have a ^7S ground state with a d^5s^1 valence electronic configuration. The ^5D (d^6) state for Tc^+ is 0.51 eV higher in energy while for Mn^+ this state is 1.81 eV above the ground state. Both metal hydrides have $^6\Sigma^+$ ground states, however, the metal bond orbital hybridizations are quite different. The d character in the metal bonding orbitals is seen to be 52.5% and 11.2% for Tc^+ and Mn^+ respectively. This difference can be attributed to the factors discussed previously. Comparing the lower limits for the s and d intrinsic bonding in TcH^+ we find that the intrinsic d bond is on the order of 19 kcal/mol stronger than an s bond. If the hydrogen atom is bonded to the s electron of ^7S Tc^+, there will be a loss of approximately 20.7 kcal/mol of exchange energy, while if a bond is formed to a d electron, approximately 34.8 kcal/mol of exchange energy is lost. Taking into account both the difference in exchange energy lost and the difference in intrinsic bond strengths, one would predict close to a 50–50 s/d hybridization. For MnH^+, the lower limit for the intrinsic s bond is 28.2 kcal/mol while the lower limit for the d bond is 18.8 kcal/mol. Thus, there is a reversal between the two bonds for the first and second row species. Again looking at bonding H to the ^7S state, one would predict a loss of 12 kcal/mol on bonding to an s electron and 42 kcal/mol on bonding to a d_{z^2} electron. Thus, for Mn^+, s character in the bond is overwhelmingly favored from the standpoint of both the intrinsic bond

Table IX
Relative Energies for Some Low-Lying Metal Hydride Electronic States

Molecule	State	Nonbonding Configuration dσ dπ dδ	R_e (Å)	ω_e (cm^{-1})	Force Constant[a] (hartrees/Å^2)	Relative Energy (kcal/mol)
SrH^+	$^1\Sigma^+$	0 0 0	2.079	1346	0.2457	0.0
YH^+	$^2\Sigma^+$	1 0 0	1.892	1639	0.3645	0.0
	$^2\Delta^\pm$	0 0 1	1.954	1554	0.3275	8.3
	$^2\Pi^\pm$	0 1 0	1.949	1530	0.3176	15.2
ZrH^+	$^3\Phi^\pm$	0 1 1	1.857	1658	0.3731	0.0
	$^3\Delta^\pm$	1 0 1	1.843	1680	0.3830	1.5
	$^3\Sigma^-$	0 2 0 0 0 2	1.866	1658	0.3729	2.3
	$^3\Pi^\pm$	0 1 1 1 1 0	1.856	1655	0.3717	3.8
NbH^+	$^4\Delta^\pm$	0 2 1	1.764	1805	0.4425	0.0
	$^4\Pi^\pm$	0 1 2 1 1 1	1.788	1763	0.4220	1.9
	$^4\Sigma^-$	1 2 0 1 0 2	1.808	1673	0.3800	8.7
	$^4\Phi^\pm$	1 1 1	1.780	1719	0.4012	10.0
MoH^+	$^5\Sigma^+$	0 2 2	1.708	1826	0.4536	0.0
	$^5\Delta^\pm$	1 2 1	1.728	1752	0.4170	25.1
	$^5\Pi^\pm$	1 1 2	1.730	1711	0.3977	37.2
TcH^+	$^6\Sigma^+$	1 2 2	1.719	1737	0.4099	0.0
	$^4\Delta^\pm$	0 2 3	1.664	1886	0.4831	24.0
	$^4\Pi^\pm$	0 3 2	1.641	1879	0.4796	26.4
RuH^+	$^3\Sigma^-$	0 4 2 0 2 4	1.581	1986	0.5361	0.0
	$^3\Phi^\pm$	0 3 3	1.601	1932	0.5070	0.2
	$^5\Delta^\pm$	1 2 3	1.696	1775	0.4283	6.7
	$^3\Pi^\pm$	0 3 3	1.614	1869	0.4747	9.0
	$^5\Pi^\pm$	1 3 2	1.664	1828	0.4541	9.0
	$^5\Sigma^+$	2 2 2	1.711	1733	0.4081	15.7
RhH^+	$^2\Delta^\pm$	0 4 3	1.539	2125	0.6138	0.0
	$^2\Pi^\pm$	0 3 4	1.588	1716	0.4002	19.5
PdH^+	$^1\Sigma^+$	0 4 4	1.512	2127	0.6323	0.0
AgH^+	$^2\Sigma^+$	1 4 4	2.428	372	0.0186	0.0
	$^2\Delta^\pm$	2 4 3	1.745	1587	0.3424	80.3
	$^2\Pi^\pm$	2 3 4	1.782	1553	0.3279	81.5
CdH^+	$^1\Sigma^+$	2 4 4	1.709	1696	0.3912	0.0

[a] Multiply by 4.359 to obtain mdyne/Å or by 627.5 to obtain (kcal/mol)/Å^2.

energies and the loss of exchange energy. An important point to note from the TcH^+ results is that s–d_{z^2} hybridization can and does take place when bonding an H atom to a metal state which contains singly occupied s and d_{z^2} orbitals. The two metal orbitals can be hybridized to form two orbitals, one of which has electron density primarily located along the z axis and the other of which has electron density located in a torus in the xy plane. Orbitals of this type can be seen in the orbital plots, Figures 1–3.

The lowest-lying electronic states for the two MH^+ species are quintet states formed by bonding the hydrogen to the d^6 configuration of the metal. For TcH^+, the $^5\Delta$ and $^5\Pi$ states are found at 25.1 and 37.2 kcal/mol, respectively, above the ground state. For MnH^+, the state splittings have not been calculated, however, due to the lower bond strength to the Mn d_{z^2} orbital and the 1.3 eV increase in the metal promotion energy, these states are expected to be much higher in energy than seen for the TcH^+ molecule.

The splitting between the lowest lying electronic states of Zr^+ (d^2), Nb^+ (d^3), and Mo^+ (d^4) is similar to that for Ti^+, V^+, and Cr^+ and as expected the ordering of states is similar. For these early transition metals, the bonding metal orbitals use large amounts of both s and d character (as seen in TcH^+). For metals where the difference in energy of states with d^n and s^1d^{n-1} configurations is fairly small, this hybridization will usually come from a mixing of the two configurations. For these configurations to be compatible, the s^1d^{n-1} configuration must have an empty d_{z^2} orbital, but this is possible for each of these metals. Indeed, even the order of the low lying excited states can often be predicted from examining the optimum states for the s^1d^{n-1} configurations of the ion and determining whether the d_{z^2} orbital is empty, as will be examined next.

For Zr^+, examining the d shell, the d^2 (^3F) configuration leads to seven states of ^3F symmetry, which, in terms of real d orbitals, can be written as

$$\Phi^+ : \quad [d_{xz}d_{x^2-y^2} - d_{yz}d_{xy}]$$

$$\Phi^- : \quad [d_{xz}d_{xy} + d_{yz}d_{x^2-y^2}]$$

$$\Delta^+ : \quad [d_{z^2}d_{x^2-y^2}] \qquad (1)$$

$$\Delta^- : \quad [d_{z^2}d_{xy}]$$

$$\Pi^+ : \quad \left\{(3/5)^{1/2}[d_{xz}d_{x^2-y^2} + d_{yz}d_{xy}] + (2/5)^{1/2}[d_{z^2}d_{xz}]\right\}$$

$$\Pi^- : \quad \left\{(3/5)^{1/2}[d_{xz}d_{xy} - d_{yz}d_{x^2-y^2}] + (2/5)^{1/2}[d_{z^2}d_{yz}]\right\}$$

$$\Sigma^- : \quad \left\{(4/5)^{1/2}[d_{xz}d_{yz}] + (1/5)^{1/2}[d_{x^2-y^2}d_{xy}]\right\}$$

Of these, only the $^3\Phi$ and $^3\Sigma^-$ states have an empty d_{z^2} orbital, and hence we expect them to be lower in energy. The $^3\Phi$ state should be lower since one nonbonded electron is always π-like and the other δ-like, while in the $^3\Sigma^-$ state 80% of the time the two electrons are both in the π orbitals (increasing the electron-electron repulsion with the bond pair) and 20% of the time they are both in the δ orbitals which place the two electrons in the same plane. Based on the d_{z^2} occupations, one would expect the $^3\Pi$ state next highest in energy, with the $^3\Delta$ state higher yet. This ordering is correct except that the $^3\Delta$ state is actually lower in energy than the $^3\Sigma^-$ state. The electronic configurations for the $^3\Delta$ states involve singly occupied s and d_{z^2} orbitals which can mix as seen in TcH^+. However, occupation of a nonbonding σ orbital leads to higher electron–electron repulsion with the bonding electrons. Thus, although the $^3\Delta$ states can add in d character without use of the excited state configuration, the increased electron-electron repulsion raises the energy sufficiently such that the $^3\Phi$ state is the ground state.

For Nb^+, the three electrons of the d shell lead to seven ^4F states:

$$\Phi^+ : \quad \{d_{z^2}[d_{xz}d_{x^2-y^2} - d_{yz}d_{xy}]\}$$

$$\Phi^- : \quad \{d_{z^2}[d_{xz}d_{xy} + d_{yz}d_{x^2-y^2}]\}$$

$$\Delta^+ : \quad [d_{xz}d_{yz}d_{xy}] \qquad (2)$$

$$\Delta^- : \quad [d_{xz}d_{yz}d_{x^2-y^2}]$$

$$\Pi^+ : \quad \left\{(3/5)^{1/2}\left[d_{z^2}\left[d_{xz}d_{x^2-y^2} + d_{yz}d_{xy}\right]\right] + (2/5)^{1/2}\left[d_{yz}d_{x^2-y^2}d_{xy}\right]\right\}$$

$$\Pi^- : \quad \left\{(3/5)^{1/2}\left[d_{z^2}\left[d_{xz}d_{xy} - d_{yz}d_{x^2-y^2}\right]\right] + (2/5)^{1/2}\left[d_{xz}d_{x^2-y^2}d_{xy}\right]\right\}$$

$$\Sigma^- : \quad \left\{(4/5)^{1/2}\left[d_{z^2}d_{x^2-y^2}d_{xy}\right] + (1/5)^{1/2}\left[d_{z^2}d_{xz}d_{yz}\right]\right\}$$

Here the ordering of states can be predicted on the basis of d_{z^2} occupation in the s^1d^{n-1} configurations ($^4\Delta^{\pm} < {}^4\Pi^{\pm} < {}^4\Sigma^- < {}^4\Phi^{\pm}$), leading to a $^4\Delta$ ground state. This sequence is the same as that for VH^+. The s–d_{z^2} hybridization seen for the $^3\Delta$ states of ZrH^+ and the $^6\Sigma$ state of TcH^+ is not important in NbH^+ due to the importance of the d-bonding and the presence of a d^4 configuration in the ground state of the metal ion.

For MoH^+, we analyze the bonding using the d orbital occupations for s^1d^4. The d hole can be either $d\sigma$, $d\pi$, or $d\delta$ leading to $^5\Sigma^+$, $^5\Pi^{\pm}$, and $^5\Delta^{\pm}$ states. The $^5\Sigma$ state is expected to be the ground state since this state can be formed by bonding the hydrogen to either the ground or first excited state of the metal and both d^5 and s^1d^4 configurations of the metal ion can readily mix. The $^5\Pi$ and $^5\Delta$ states are expected to be higher in energy since they cannot be formed by bonding hydrogen to ground state Mo^+ and require promotion to an excited state of the metal ion (^{6}D–1.59 eV higher in energy than the ^{6}S ground state of Mo^+) Indeed, the $^5\Delta$ state is found to be over 25 kcal/mol above the ground $^5\Sigma^+$ state with the $^5\Pi$ state at over 37 kcal/mol.

Y^+ is the only metal which does not have a ground state with either a d^n or s^1d^{n-1} electronic configuration. The Y^+ ground state configuration is $5s^2$ with no 4d electrons. One cannot form a bond to the Y^+ ground state without first uncoupling the two s electrons and adding in a higher electronic state of the metal such as the ^{3}P state (s^1p^1). We will thus analyze the bonding in a similar fashion to the other early metals. The ^{3}D (s^1d^1) state of Y^+ lies 0.16 eV above the ground state. The lowest state with a d^2 configuration is 0.88 eV

higher in energy. If one considers bonding hydrogen to ^{3}D Y^+, there are three possible symmetries $^2\Delta^{\pm}$, $^2\Pi^{\pm}$, and $^2\Sigma^+$ resulting from placing the nonbonding electron in either the dδ, dπ, or dσ orbitals. The energy ordering is expected to be $^2\Delta < {}^2\Pi < {}^2\Sigma$ as seen for ScH^+, which presumably results from the decreased electrostatic interaction of the δ orbital with the electrons of the bond pair. One might have expected the dσ to be stabilized because of less shielding, but it must also be orthogonalized to the bond pair. Table IX shows the energy ordering for these three states of YH^+. Although the $^2\Delta$ state is lower than $^2\Pi$, the ground state is $^2\Sigma^+$. There are two reasons for this difference between ScH^+ and YH^+. The most important is the presence of the ^{1}S (s^2) ground state of Y^+ which mixes into the $^2\Sigma$ wavefunction and lowers the energy. The lowest state of Sc^+ with an s^2 configuration is 1.44 eV above the ground state and thus does not play much of a role. The second factor is the importance of d character in the second row bonding and the ability to mix singly occupied s and d_{z^2} orbitals as seen for other second row metals. The bonding orbitals and singly occupied σ orbitals shown in Figures 1 and 3 show this hybridation. The nonbonding orbital shows very few contours in the region of the torous in the xy plane due to the very diffuse nature of the 5s orbital.

The second row group 8-10 hydrides exhibit much different bonding compared with their first row cogeners. This is basically a consequence of the greater stability of the d^n configuration with respect to the s^1d^{n-1} configuration for the second row (Figure 5). For the first row, the lowest state with an s^1d^{n-1} configuration is 0.25 eV above the lowest state with a d^n configuration for Fe^+. The ordering is reversed for Co^+ and Ni^+ with the d^n configuration lower in energy by 0.43 and 1.09 eV respectively. For all three second row metal ions, Ru^+–Pd^+, the d^n configuration is lower with energy differences of 1.09, 2.13, and 3.19 eV respectively. Due to the stronger intrinsic s bonds for the first row metals, they bond with an orbital predominantly s in character (the ground state for NiH^+ is the $^3\Delta$ state arriving from bonding to Ni^+ s^1d^8). The second row groups 8-10

metals bond primarily with d electrons (bonding is to the d^n metal configuration). For RuH^+, the d^7 (^3F) configuration leads to the same configuration of singly-occupied orbitals as in eq.(2), but now we want a singly-occupied d_{z^2} orbital for the bond. This leads to $^3\Sigma^-$ and $^3\Phi^\pm$ states that are within 0.1 eV. Other triplet states of RuH^+ are higher in energy (the $^3\Pi^\pm$ states are at 9.0 kcal/mol) since these have configurations with two electrons in the metal d_{z^2} orbital. The $^5\Delta$ state (the ground electronic state for FeH^+), expected to be the lowest of the quintet states, is found at 6.7 kcal/mol above the ground state. The $^5\Pi$ and $^5\Sigma$ states are found at 9.0 kcal/mol and 15.7 kcal/mol respectively. For RhH^+, the best Rh d^8 (^3F) configuration has singly-occupied d_{z^2} and $d\delta$ orbitals leading to a $^2\Delta$ state. For d^9 Pd^+, the only configuration with a singly-occupied d_{z^2} orbital leads to a $^1\Sigma^+$ state for PdH^+. The quartet states of RhH^+ and triplet states of PdH^+ are expected to be much higher in energy due to the large d^n to s^1d^{n-1} promotion energies (2.13 and 3.19 eV for Rh^+ and Pd^+, respectively).

Ag^+ has a ^1S (d^{10}) ground state, with the first excited state, ^3D (s^1d^9), 5.03 eV (116 kcal/mol) higher in energy. The states possible for AgH^+ from these two metal configurations are $^2\Sigma^+$, $^2\Pi^\pm$, and $^2\Delta^\pm$. The $^2\Pi$ and $^2\Delta$ states necessitate bonding to ^3D Ag^+. Although the $^2\Delta$ state has a bond of 38.3 kcal/mol with respect to dissociation to ^3D Ag^+ and ^2S H, this is 77.7 kcal/mol above the ground state fragments. The $^2\Pi$ states are even higher in energy. A $^2\Sigma^+$ state can be constructed by bonding the H either to a ^1S or ^3D configuration; however, the ^3D state is too high in energy to contribute. The difference in IP's of Ag (7.574 eV) and H (13.595 eV) also rules out a resonant three-electron bond. One is left with a bond arising from interaction of the Ag^+ ion and an induced hydrogen dipole, leading to a long (2.428 Å) weak bond of only 2.6 kcal/mol.

For Sr^+ and Cd^+, bonds involve primarily 5s character due to the high promotion energy in Sr^+ and the doubly occupied d_{z^2} orbital of Cd^+.

III. Calculational Details

Basis Sets. In these studies, the 28 electrons associated with the n=1, 2, and 3 metal core orbitals have been replaced with the the ab initio effective core potentials of Hay and Wadt[14] which include relativistic effects in the core electrons. Thus the 4s, 4p, 4d, 5s, and 5p electrons are considered explicitly (e.g., 14 electrons for Tc^+). The basis set is contracted valence triple zeta (5s,5p,4d/4s,4p,3d). For Sr^+, the published Hay and Wadt basis does not include d basis functions, and therefore a set of four 4d functions was added and contracted triple zeta (Table X).[15] For Cd^+ we also used the Hay and Wadt[16] effective core potential, where the full Kr core (36 electrons) was replaced by the EP (leaving 11 electrons to be considered explicitly), and this basis was contracted (3s,3p,4d/3s,3p,3d). Table XI shows a comparison between experimental and theoretical state splittings obtained using these basis sets. For hydrogen, we used the unscaled Dunning/Huzinaga[17] double zeta basis (4s/2s) supplemented with one set of p polarization functions. The p functions ($\alpha = 0.50$) are the same as those used for calculations of the first row metal hydrides.[5] No f polarization functions have been included on the metal ions. To estimate the effects on the bond dissociation energies of including f functions, one set of f functions was optimized for MoH^+ ($\alpha = 0.48$) at the optimum geometry and at the DCCI-GEOM level of calculation. The polarization functions were found to increase the bond dissociation energy by about 3 kcal/mol.[18] This same effect would also be expected for the other second row metal hydrides.

Wave Functions and Electronic Correlation. *Spectroscopic Parameters.* For the second row metal hydrides, the same calculational methods were used as for the first row metal hydrides. For the M^+–H bond dissociation energies we use the DCCI level of calculation (dissociation consistent configuration interaction). This involves starting with the configurations of a GVB-PP(1/2) wavefunction (where the bonding electrons form the GVB pair). From a restricted CI in bond pair orbitals (GVB-RCI(1/2)) we allow all single and double

Table X

The d basis for Sr^+.[a] Gaussian Primitive Functions with Exponents (α_i) and Contraction Coefficients (C_i).

α_i	C_i
8.186	-0.004582513
2.749	0.009945296
0.5851	1.000000000
0.09465	1.000000000

[a] From unpublished calculations by Rappé and Goddard, ref. 15.

Table XI

Low-lying $5s^14d^{n-1}$ and $4d^n$ States of Metal Cations:

Experimental and Theoretical State Splittings

Ion	$5s^14d^{n-1}$		$3d^n$				
	State	Configuration	State	Configuration	Relative Energy (eV)[a]		
					Exptl[b]	HF	DCCI
Sr^+	^2S	$5s^1$	^2D	$4d^1$	1.83	2.27	2.27
Y^+[c]	^3D	$5s^14d^1$	^3F	$4d^2$	0.88	0.86	0.83
Zr^+	^4F	$5s^14d^2$	^4F	$4d^3$	0.31	0.31	0.17
Nb^+	^5F	$5s^14d^3$	^5D	$4d^4$	−0.33	−0.31	−0.30
Mo^+	^6D	$5s^14d^4$	^6S	$4d^5$	−1.59	−1.82	−1.74
Tc^+	^7S	$5s^14d^5$	^5D	$4d^6$	0.51	1.48	1.22
Ru^+	^6D	$5s^14d^6$	^4F	$4d^7$	−1.09	−0.59	−0.82
Rh^+	^5F	$5s^14d^7$	^3F	$4d^8$	−2.13	−1.61	−1.83
Pd^+	^4F	$5s^14d^8$	^2D	$4d^9$	−3.19	−2.61	−2.64
Ag^+	^3D	$5s^14d^9$	^1S	$4d^{10}$	−5.03	−4.95	−4.90
Cd^+	^2S	$5s^14d^{10}$					

[a] Relative Energy of the $4d^n$ state with respect to the $5s^14d^{n-1}$ state. [b]Reference 12. The energies were calculated using a weighted average over J levels for each state. [c]The ground state of Y^+ is ^1S ($5s^2$) which is 0.16 eV lower in energy than the ^3D state. GVB(1/2) calculations puts the ^1S state 0.43 eV higher than the ^3D state.

excitations from the bond pair *times* all single excitations out of the nonbonded valence orbitals. The molecular calculation dissociates to a limit involving a free H atom plus a metal wavefunction having simultaneous single excitations out of the nonbonding orbitals and out of the metal σ bonding orbital. The equilibrium geometries and vibrational frequencies were determined at the DCCI-GEOM calculation level. This involves starting with the GVB-RCI(1/2) configurations and allowing all single and double excitations out of the bond pair *plus* all single excitations out of the nonbonding valence orbitals. This calculation dissociates to a Hartree-Fock hydrogen atom and a metal ion with single excitations from the nonbonding orbitals.

For molecular states involving several occupations of the nonbonding orbitals, the GVB calculation was altered to place an average number of electrons in each nonbonded d orbital and thus produce a set of cylindrically symmetric d orbitals. The CI calculation then started with configurations representing all possible occupations of these nonbonding orbitals, allowing the normal level of excitation and selecting for proper symmetry of the resultant configurations. This allows mixing in of the two or three major configurations necessary for the particular electronic state with no discrimination due to orbital shapes.

For the $^2\Sigma^+$ state of AgH^+, to allow the necessary polarization in the σ system, the calculations were modified. For this d^{10} configuration the GVB pair consists of in/out correlation of the d_{z^2} electrons rather than a "normal" bond pair and has the unpaired electron located on the hydrogen rather than in a metal d orbital. In order to not bias against other bonding configurations, the CI calculation for this molecule involves all triple and lower excitations from these three σ orbitals.

Bond dissociation energies are determined by dissociating the molecules diabatically to H atom and metal ion. For all cases except YH^+, the metal hydrides dissociate smoothly to ground state fragments and the bond dissociation energy is given by the difference in energy between the molecule at its equilibium geom-

etry and the energy of the separated atoms in their ground states. For YH^+, the diabatic dissociation limit is the ^3D (s^1d^1) state. The bond energy is thus taken to be this diabatic dissociation energy minus the experimental state splitting between the ^1S and ^3D states of Y^+. This allows for consistent dissociation of the molecule and cancellation of basis set errors plus the use of the correct metal state splitting.

Full DCCI calculations for RuH^+ were excessively large and were not performed. The bond energy for RuH^+ was obtained as follows. The difference between the DCCI-GEOM and DCCI bond energies for other largely "d bonded" species is 1.6 kcal/mol for PdH^+, 1.0 kcal/mol for RhH^+, and 0.9 kcal/mol for MoH^+ (with the DCCI-GEOM bond energies larger than the DCCI results). Thus, RuH^+ was assigned a difference of 0.5 kcal/mol which was subtracted from the DCCI-GEOM result.

Intrinsic Bond Dissociation Energies. To obtain intrinsic s-like or d-like bond dissociation energies, the mixing of s and d character must be restricted while allowing other orbital readjustments to occur. The calculation method thus depends on the particular system. For SrH^+–MoH^+, formation of an s-bond leads to an empty d_{z^2} orbital while formation of a d-bond leads to an empty s orbital. The calculations were thus carried out by eliminating the 5s or $4d_{z^2}$ basis functions. The bond length was then optimized under these conditions and the bond dissociation energy determined by dissociating the molecule to fragments where the same basis functions were removed from the metal ion calculation.

For TcH^+–CdH^+ the state involving an s-bond is complicated by the presence of nonbonding σ electrons. The d_{z^2} basis functions could thus not be removed. For TcH^+–AgH^+ the rehybridization process was effectively removed by placing one electron in a d_{z^2} orbital optimized for the corresponding state of the metal ion and freezing this orbital in the predetermined shape while allowing the other orbitals on the molecule to vary. The bonding orbital is thus forced to become orthogonal to the d_{z^2} orbital. For CdH^+ the GVB-PP(1/2) results are

used since very little d character is present. The d-bonding for TcH^+–PdH^+ is determined by bonding hydrogen to the d^n configuration of the metal, while for AgH^+ and CdH^+ there is effectively no d-bonding due to the full d^{10} shell.

These restricted calculations are at the GVB perfect pairing level and *not* the DCCI level used for reliable bond dissociation energies. Only the trends involved should be considered. The actual intrinsic bond energies presented in Table V are obtained from the GVB-PP calculations plus adding in the total amount of s-d or d-d exchange energy lost on bonding (determined from the metal ion exchange energies and the metal electronic configuration) and any electronic promotion energy.

MH^+ Electronic State Splitting Calculations. The relative energies of the low-lying electronic states of the metal hydride ions are determined by the difference in bond dissociation energies calculated for the various states at the DCCI-GEOM level of calculation. The relative bond dissociation energies were used as a measure of energy differences for the electronic states since the dissociation consistent nature of these calculations helps to remove errors inherent in the basis set representations of the metal ion states.

IV. Conclusion

The results presented here for the second row transition metal hydrides form a consistent and systematic set of data which should be helpful both for understanding the complex factors involved in metal bonding and as a contribution to the increasing data base of thermodynamic and spectroscopic values for metal compounds. The ideas used to discuss the bonding in the metal hydride diatomics are also applicable for other more complicated metal containing species. The consistent nature of the data for the entire row should be useful in helping to extract further reliable thermodynamic information from ion beam studies, increase understanding of the differences in reactivity of ground and excited states, and shed light on the reactivity differences of the different transition metals.

Acknowledgement. We thank the National Science Foundation (Grant Nos. CHE83-18041 and CHE84-07857) for partial support of this work.

References

(1) See, for example: (a) Armentrout, P. B.; Halle, L. F.; Beauchamp, J. L. *J. Chem. Phys.* **1982**, *76*, 2449. (b) Halle, L. F.; Crowe, W. E.; Armentrout, P. B.; Beauchamp, J. L. *Organometallics* **1984**, *3*, 1694. (c) Jacobson, D. B.; Freiser, B. S. *J. Am. Chem. Soc.* **1983**, *105*, 7492. (e) Jacobson, D. B.; Freiser, B. S. *J. Am. Chem. Soc.* **1983**, *105*, 5197. (f) Cassady, C. J.; Freiser, B. S. *J. Am. Chem. Soc.* **1985**, *107*, 1573. (g) Babinec, S. J.; Allison, J. *J. Am. Chem. Soc.* **1984**, *106*, 7718.

(2) See for example: (a) Larsen, B. S.; Ridge, D. P. *J. Am. Chem. Soc.* **1984**, *106*, 1912. (b) Jacobson, D. B.; Freiser, B. S. *J. Am. Chem. Soc.* **1983**, *105*, 736.

(3) See for example: (a) Halle, L. F.; Houriet, R.; Kappes, M. M.; Staley, R. H.; Beauchamp, J. L. *J. Am. Chem. Soc.* **1982**, *104*, 6293. (b) Houriet, R.; Halle, L. F.; Beauchamp, J. L. *Organometallics* **1983**, *2*, 1818. (c) Hanratty, M. A.; Paulsen, C. M.; Beauchamp, J. L. *J. Am. Chem. Soc.* **1985**, *107*, 5074.

(4) (a) Halle, L. F.; Armentrout, P. B.; Beauchamp, J. L. *J. Am. Chem. Soc.* **1981**, *103*, 962. (b) Elkind, J. L.; Armentrout, P. B. *J. Phys. Chem.* **1985**, *89*, 5626. (c) Elkind, J. L.; Armentrout, P. B. *J. Chem. Phys.* **1986**, *84*, 4862. (d) Elkind, J. L.; Armentrout, P. B. *J. Am. Chem. Soc.* **1986**, *108*, 2765.

(5) (a) Schilling, J. B.; Goddard, W. A., III; Beauchamp, J. L. *J. Am. Chem. Soc.* **1986**, *108*, 582. (b) Schilling, J. B.; Goddard, W. A., III; Beauchamp, J. L., submitted for publication.

(6) Pyykkö, Pekka *J. Chem. Soc., Faraday Trans. 2* **1979**, *75*, 1256.

(7) Stoll, H.; Fuentealba, P.; Dolg, M.; Flad, J.; Szentpály, L. v.; Preuss, H. *J. Chem. Phys.* **1983**, *79*, 5532.

(8) Huber, K. P.; Herzberg G. "Constants of Diatomic Molecules"; Van Nostrand Reinhold Co.: New York, 1979.

(9) Mandich, M. L.; Halle, L. F.; Beauchamp, J. L. *J. Am. Chem. Soc.* **1984**, *106*, 4403.

(10) Elkind, J. L.; Armentrout, P. B. *Inorg. Chem.* **1986**, *25*, 1080.

(11) Pettersson, L. G. M.; Bauschlicher, C. W., Jr.; Langhoff, S. R.; Partridge, H., private communication.

(12) Moore, C. E. "Atomic Energy Levels"; National Bureau of Standards: Washington, D. C., 1971; Vol. II and III.

(13) Goddard, W. A., III; Harding, L. B. *Annu. Rev. Phys. Chem.* **1978**, *29*, 363.

(14) Hay, J. P.; Wadt, W. R. *J. Chem. Phys.* **1985**, *82*, 299.

(15) Rappé, A. K.; Goddard, W. A., III, to be published.

(16) Hay, J. P.; Wadt, W. R. *J. Chem. Phys.* **1985**, *82*, 270.

(17) (a) Huzinaga, S. J. *J. Chem. Phys.* **1965**, *42*, 1293. (b) Dunning, T. H., Jr. *J. Chem. Phys.* **1970**, *43*, 2823.

(18) MoH^+ (at R_e) with one set of f functions ($\alpha = 0.48$) has a total energy of -67.22976 hartrees compared to -67.22531 hartrees without f functions (at the DCCI-GEOM calculation level. Thus, the increase in the bond dissociation energy is 2.8 kcal/mol.

CHAPTER VI

THEORETICAL STUDIES OF TRANSITION METAL HYDRIDES: IV. COMPARISON OF THE TRANSITION METAL DIHYDRIDE IONS CrH_2^+ AND MoH_2^+

Theoretical Studies of Transition Metal Hydrides: IV. Comparison of the Transition Metal Dihydride Ions CrH_2^+ and MoH_2^+

J. Bruce Schilling, W. A. Goddard III*, and J. L. Beauchamp

Contribution No. 7552 from the

Arthur Amos Noyes Laboratory of Chemical Physics

California Institute of Technology, Pasadena CA 91125

Abstract

The electronic and geometric structure of two transition metal dihydride cations, CrH_2^+ and MoH_2^+, has been studied theoretically using generalized valence bond and configuration interaction methods. MoH_2^+ is found to have two equally favorable geometries: $R_e = 1.705$ Å, $\theta_e = 64.6°$; and $R_e = 1.722$ Å, $\theta_e = 112.3°$. These lead to bond energies of $D_e(HMo^+–H)$ of 35.1 kcal/mol and 34.7 kcal/mol, respectively, compared with $D_e(Mo^+–H) = 33.8$ kcal/mol. CrH_2^+ leads to an open geometry with $R_e = 1.635$ Å and $\theta_e = 107.5°$. The bond energy is $D_e(HCr^+–H) = 19.4$ kcal/mol compared with $D_e(Cr^+–H) = 26.9$ kcal/mol.

I. Introduction

The gas phase activation of hydrocarbons by transition metal positive ions is an active area of research.[1-5] The proposed first step for most of these reactions after initial association is

$$M^+ + R-H \longrightarrow R-M^+-H \longrightarrow \text{Products} \qquad (1)$$

where the initial reaction step involves the insertion of the metal ion into a C–H bond. The initial intermediate thus involves two species sigma bonded to the metal ion. There is a growing amount of data, both experimental[2,3,6,7] and theoretical[8-10], dealing with the bond dissociation energies for single species bound to transition metal ions. Little is known, however, about the geometries of these metal insertion products or the strengths of the second bonds formed to the metals[11,12], both of which are important for an understanding of these metal ion reactions.

As a step toward understanding species formed on metal insertion into sigma bonds and to compare first and second row metal ions, we investigated the two species CrH_2^+ and MoH_2^+. The similarity of the Cr^+ and Mo^+ electronic states allows comparison of bonding differences due to orbital size differences of the two metals. The ground state symmetries, geometries, and bond strengths should be useful in helping to explain differences in the reactivities of the two metal ions. Extension can also be made to predict the geometries and bonding in other transition metal systems of the first and second transition series.

II. Calculational Details

A. Basis Sets. The basis sets for the present study are identical to those in previous work on metal hydride cations.[8] For Cr^+, the all-electron basis involved an optimized valence double zeta contraction (13s,10p,5d/5s,4p,2d).[13] For Mo^+, the Ni core was replaced with an ab initio effective core potential[14] so that Mo^+ has 13 explicitly treated electrons. A valence triple zeta contraction (5s,5p,4d/4s,4p,3d) of the ab initio basis was used. The hydrogen basis was the unscaled Dunning/Huzinaga double zeta basis[15] supplemented with one set of p polarization functions ($\alpha = 0.5$).[16]

B. Geometry Optimization. The geometries for the two metal dihydrides were optimized using a two step process. The metal-hydrogen bond lengths were fixed at the optimum value found for the diatomic ions (1.602 Å for Cr^+–H and 1.708 Å for Mo^+–H) and the H–M^+–H angle was varied to find the optimum angle. The metal-hydrogen bond lengths were then varied at the optimum bond angle for the complex. With this procedure, the optimum bond length for the dihyride complex was found to change only slightly from the value of the monohydride and thus the calculated geometries should be fairly close to the optimum geometries for the two complexes.

C. Wavefunctions. Four different types of wavefunction were used in this study of the bonding in CrH_2^+ and MoH_2^+: GVB-PP(2/4), GVB-RCI(2/4), RCI(2/4)$\times$[$D_{\sigma 1}$+$D_{\sigma 2}$+$S_{M^+,val}$], and $D_{\sigma 1}\times$[$D_{\sigma 2}$ + $S_{M^+,val}$]. These wavefunctions are described below.

1. GVB-PP(2/4). Generalized valence bond calculations allow the two electrons of each bond pair to use different (optimized) one-electron orbitals (generally these optimized orbitals are located primarily on opposite bonding centers), leading to a valence bond (VB) like wavefunction of the form

$$[\phi_l(1)\phi_r(2) + \phi_r(1)\phi_l(2)](\alpha\beta - \beta\alpha) \qquad (2)$$

where ϕ_l and ϕ_r are the optimized one-electron orbitals and α and β are spin

functions. In this simplest GVB wavefunction, only the two bond pairs are so correlated (with four orbitals total, hence 2/4) and the other electrons on the molecule are calculated self-consistently. Since the two bond pairs have the simple VB form (2) (one VB structure), this is referred to as the perfect-pairing (PP) wavefunction. As one M^+–H bond is broken, the molecule dissociates smoothly to a GVB-PP(1/2) description of MH^+ and an H atom.

2. GVB-RCI(2/4). The PP wavefunction does not allow the other spin couplings required to describe the high spin of the separated ions. To include such spin couplings and to allow instantaneous correlation between the electrons of different bond pairs, we allow the two electrons in each bond pair to occupy the two orbitals of this pair in all three possible ways, (nine spatial configurations for two bond pairs). This restricted configuration interaction (RCI) approximates the full GVB wavefunction in which spin coupling is optimized. This calculation level was used for the MH_2^+ geometry optimizations. For bond energy purposes it dissociates smoothly to a GVB-RCI(1/2) description of MH^+ and an H atom.

3. RCI(2/4)$\times[D_{\sigma 1} + D_{\sigma 2} + S_{M+,val}]$. Starting with the nine spatial configurations of the RCI wavefunction, we allow all single and double excitations from each metal-hydrogen bond pair to all virtual orbitals. All single excitations from the metal nonbonding valence orbitals (d orbitals) are also allowed. This calculation dissociates smoothly to the RCI(1/2)$\times[D_{\sigma}+S_{M+,val}]$ description of MH^+ (previously called DCCI-GEOM[8]) and an H atom.

4. $D_{\sigma 1} \times [D_{\sigma 2} + S_{M+,val}]$. For the metal hydrides, MH^+, a calculation level involving single and double excitations from the bond pair simultaneous with excitations from the valence orbitals ($D_{\sigma} \times S_{M+,val}$, also called DCCI[8]) was used to determine the metal hydride bond dissociation energies. Using the difference in first and second metal-hydrogen bond energies found in the calculation level described in 3 (for the metal dihydrides) and $D_e(M^+–H)$ from the DCCI calculations, we estimate $D_e(HM^+–H)$ for a calculation involving simultaneous single and double excitations from both bonds plus single and double excitations

from the bond being broken times single excitations from the nonbonding valence orbitals.

III. Results

Table I presents the main results for both the monohydrides and dihydrides including the optimum geometries, metal orbital hybridizations, and bond dissociation energies. Table II gives information on the configurations, total energies, and bond energies for the various levels of calculation performed on the metal species.

A. Metal Hydride Cations. The bonding of H to the first and second row transition metal hydrides has been described in previous papers.[8] The results obtained for CrH^+ and MoH^+ are summarized here.

1. CrH^+. The optimum bond length for the $^5\Sigma^+$ state of CrH^+ was found to be 1.602 Å and the vibrational frequency is 1818 cm^{-1}. The calculated bond dissociation energy is $D_e(Cr^+–H) = 26.9$ kcal/mol which corresponds to $D_0(Cr^+–H) = 24.3$ kcal/mol. These values are in good agreement with the recent "guided" ion beam experiments of Elkind and Armentrout[7] which give a bond dissociation energy of $D_0 = 27.7 \pm 2$ kcal/mol. Although the Cr^+ ion has a ground state valence electron configuration of $3d^5$ the metal hydride builds in more than 50% 4s and 4p character in the metal bonding orbital (40.6% s, 12.5% p, and 46.9% d).

2. MoH^+. MoH^+ is calculated to have an optimum bond length of 1.708 Å and a vibrational frequency of 1826 cm^{-1}. The theoretical bond dissociation energies are $D_e(Mo^+–H) = 33.8$ kcal/mol and $D_0(Mo^+–H) = 31.2$ kcal/mol. Ion beam experiments of Elkind and Armentrout give a value of $D_0(Mo^+–H) = 41 \pm 3$ kcal/mol.[7] The lowest-lying electronic state of Mo^+ is the same as that for Cr^+, however, the character of the metal bonding orbital in MoH^+ differs markedly from that of CrH^+. For MoH^+ there is less than 30% sp character in the metal bonding orbital (19.7% s, 7.0% p, and 73.3% d) compared to the greater

Table I

Geometries, Orbital Hybridization, Bond Energies for MH^+ and MH_2^+

Molecule	State	$R_e(M^+–H)$ (Å)	$\theta_e(H–M^+–H)$ (degrees)	Metal Orbital Hybridization[a] %s	%p	%d	$D_e(M^+–H)$[b] (kcal/mol)
CrH^+	$^5\Sigma^+$	1.602		40.6	12.5	46.9	26.9
MoH^+	$^5\Sigma^+$	1.708		19.7	7.0	73.3	33.8
CrH_2^+	$^4B_2$	1.635	107.5	20.4	9.5	70.1	19.4
MoH_2^+	$^4B_2$	1.705	64.6	13.0	5.4	81.6	35.1
MoH_2^+	$^4B_2$	1.722	112.3	15.4	7.7	76.9	34.7

[a] Taken from GVB-PP wave functions. [b] From $D_\sigma \times S_{M^+,val}$ (DCCI) calculations for MH^+. Using the difference between these values and RCI(1/2) $\times$ $[D_\sigma + S_{M^+,val}]$ (DCCI-GEOM) for MH^+, the bond energies for MH_2^+ are extrapolated from the known values from the RCI(1/2) $\times$ $[D_{\sigma 1} + D_{\sigma 2} + S_{M^+,val}]$ calculations.

Table II

Energy Information for Molecular and Atomic Species

Species	Calculation Level[a]	Total Energy (hartrees)	Configurations	Spin Eigenfunctions	Bond Energy (kcal/mol)
CrH_2^+	GVB(2/4)	−1042.98175	4	4	-4.6
$R_e = 1.635$ Å	GVB-RCI(2/4)	−1042.99926	9	34	4.1
$\theta_e = 107.5°$	RCI(2/4)×[$D_{\sigma 1} + D_{\sigma 2} + S_{M+,\Pi a l}$]	−1043.04388	1550	8472	17.8
MoH_2^+	GVB(2/4)	−67.73680	4	4	21.6
$R_e = 1.705$ Å	GVB-RCI(2/4)	−67.74483	9	34	24.3
$\theta_e = 64.6°$	RCI(2/4)×[$D_{\sigma 1} + D_{\sigma 2} + S_{M+,\Pi a l}$]	−67.78058	2636	15300	35.1
MoH_2^+	GVB(2/4)	−67.73832	4	4	22.8
$R_e = 1.722$ Å	GVB-RCI(2/4)	−67.74512	9	34	24.5
$\theta_e = 112.3°$	RCI(2/4)×[$D_{\sigma 1} + D_{\sigma 2} + S_{M+,\Pi a l}$]	−67.77987	2636	15300	34.7
CrH^+	GVB(1/2)	−1042.48981	2	2	8.9
$R_e = 1.602$ Å	GVB-RCI(1/2)	−1042.49351	3	7	11.2
	RCI(1/2)×[$D_\sigma + S_{M+,\Pi a l}$]	−1042.51595	148	444	25.3
	$D_\sigma \times S_{M+,\Pi a l}$	−1042.52762	1862	5966	26.9
MoH^+	GVB(1/2)	−67.20265	2	2	19.6
$R_e = 1.708$ Å	GVB-RCI(1/2)	−67.20676	3	7	22.2
	RCI(1/2)×[$D_\sigma + S_{M+,\Pi a l}$]	−67.22531	258	850	33.8
	$D_\sigma \times S_{M+,\Pi a l}$	−67.23292	5234	18826	33.8
Cr^+	HF	−1041.97641	1	1	
	$S_\sigma \times S_{\Pi a l}$[b]	−1041.98550	48	48	
Mo^+	HF	−66.67212	1	1	
	$S_\sigma \times S_{\Pi a l}$[b]	−66.67981	135	135	
H	HF	−0.49928	1	1	

[a] These calculations are described in section IIC of the paper. [b] Dissociation limit for MH^+ $D_\sigma \times S_{M+,\Pi a l}$ calculation.

than 50% seen for CrH^+. Figure 1 shows the GVB orbitals for the two metal hydrides. Both metal orbitals are seen to be polarized toward the hydrogen atom using atomic p character. The bonding lobe of the Cr^+ orbital is more diffuse than that for Mo^+ due to the larger amount of s character in the bond.

B. Metal Dihydride Cations. For purposes of discussion, we assume a C_{2v} geometry with the metal ion at the origin, the z axis is the symmetry axis, and the atoms are in the yz plane.

1. CrH_2^+. The ground electronic state of Cr^+ is ^6S ($3d^5$).[17] The lowest excited state, ^6D ($3d^44s^1$) lies 1.52 eV higher in energy. Bonding two atoms of hydrogen covalently to ^6S Cr^+, one is left with three unpaired 3d electrons on the metal. The bonding orbitals can use only combinations of the three orbitals in the yz plane, d_{z^2}, $d_{x^2-y^2}$, and d_{yz}, leaving unpaired a_2 (xy), b_1 (xz), and a_1 orbitals. This leads to a $^4B_2$ state of the molecule. For CrH^+ we found a large amount of 4s character in the metal-hydrogen bond and expect the same for CrH_2^+. This requires s^1d^4 (^6D) character, where the 4s electron must arise from excitation of an electron out of either the $3d_{z^2}$ or $3d_{x^2-y^2}$ orbital.

Figure 2 shows the angular energy dependence for C_{2v} CrH_2^+ with a Cr^+–H bond distance of 1.602 Å. The optimum angle found from the GVB-RCI(2/4) calculations is 107.5°. Optimization of the bond lengths at this angle yields a Cr^+–H bond length of 1.635 Å. The GVB orbitals for CrH_2^+ are shown in Figure 3 along with the nonbonding (singly-occupied) a_1 orbital. The Cr^+–H bonds are fairly covalent, with about 0.23 electrons transferred to the Cr^+. The bond pairs have an overlap of 0.617. The hybridizations of metal bonding orbitals are 20.4% s, 9.5% p, and 70.1% d character. Dissociation of CrH_2^+ to CrH^+ and H leads to $D_e(CrH^+–H)$ = 4.1 kcal/mol at the GVB-RCI calculation level and $D_e(CrH^+–H)$ = 17.8 kcal/mol at the RCI(2/4)×$[D_{\sigma 1}+D_{\sigma 2}+S_{M^+,val}]$ level as compared to $D_e(Cr^+–H)$ = 11.2 kcal/mol and $D_e(Cr^+–H)$ = 25.3 kcal/mol for the dissociation of the diatomic at the same calculation levels.

2. MoH_2^+. The ground state of Mo^+ is ^6S ($3d^5$).[17] The first excited state

Figure 1: GVB bond orbitals for CrH^+ (a) and MoH^+ (b). $R_e(Cr^+–H) = 1.602$ Å and the Cr^+ orbital is found to be 40.6% s, 12.5% p, and 46.9% d. $R_e(Mo^+–H) = 1.708$ Å and the Mo^+ bond orbital is 19.7% s, 7.0%p, and 73.3% d. On all plots long dashes indicate zero amplitude and the spacing between contours is 0.05 au.

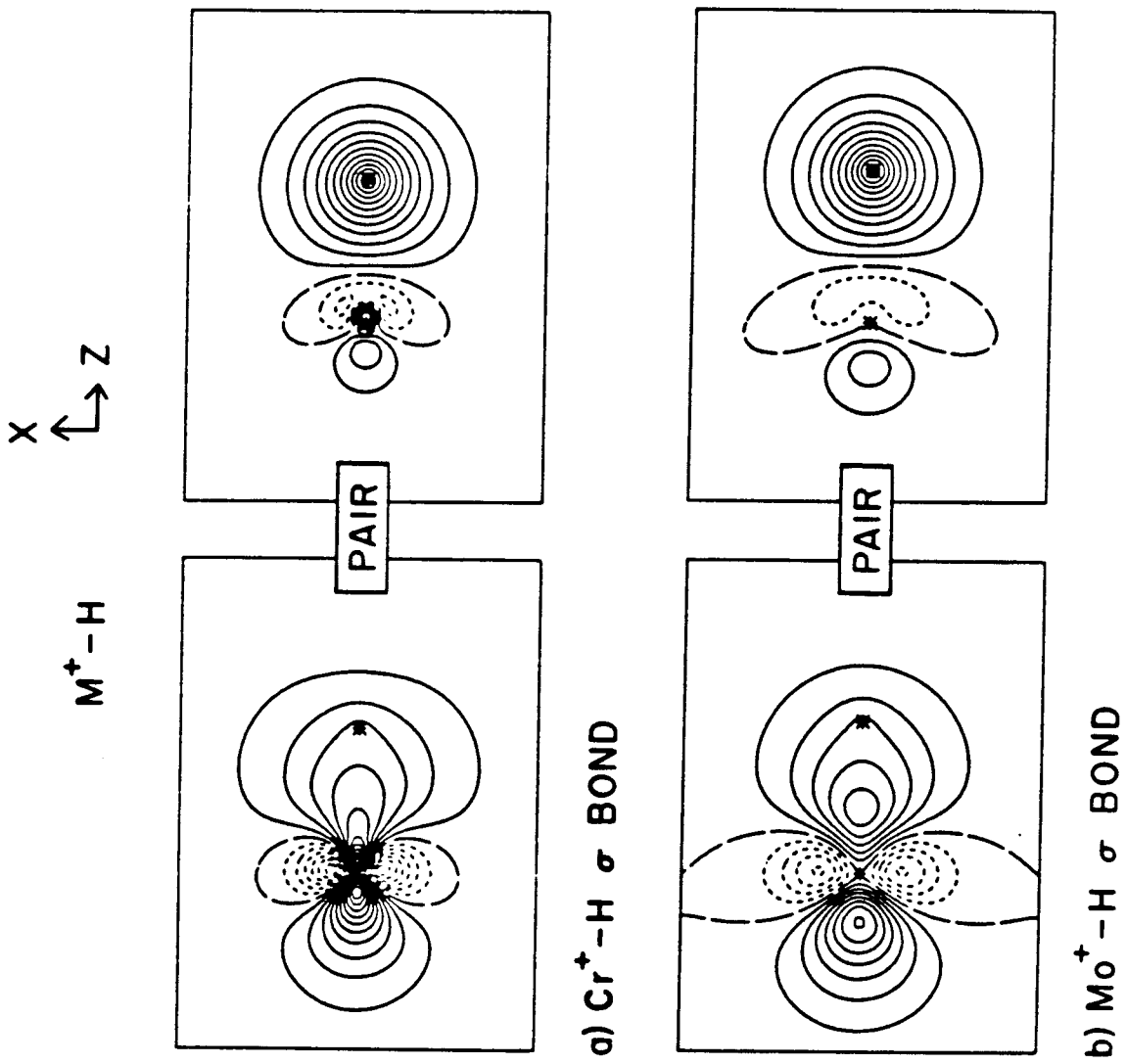
X
Z
M+-H
PAIR
PAIR
a) Cr+-H σ BOND
b) Mo+-H σ BOND

Figure 2: Dependence of the CrH_2^+ total energy (at the GVB(2/4) and GVB-RCI(2/4) levels) on the H–Cr^+–H bond angle. The Cr^+–H bond distance is fixed at 1.602 Å, the optimum value found for CrH^+. The optimum energy is found at 107.5°.

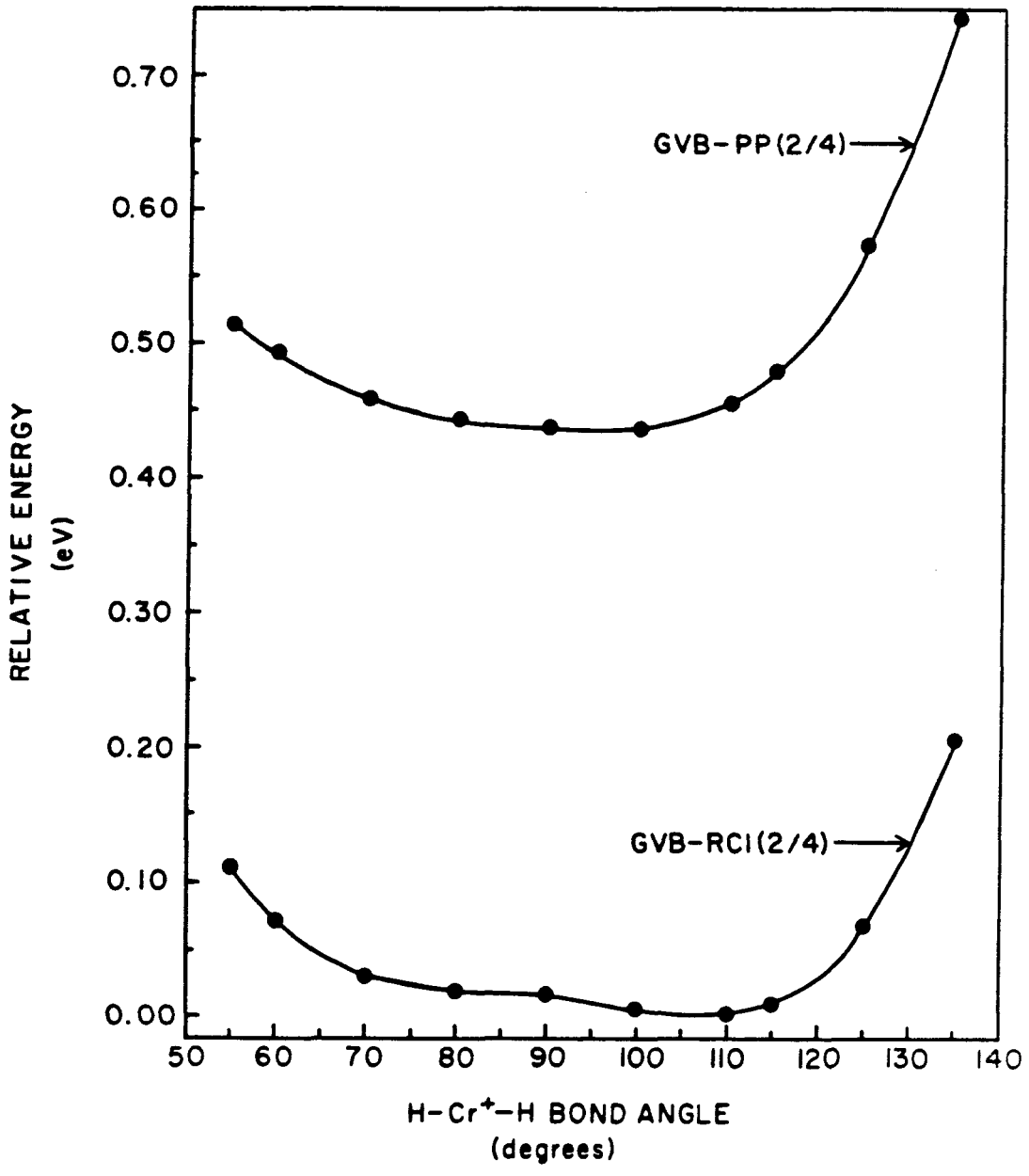
0.70
0.60
0.50
0.40
0.30
0.20
0.10
0.00
RELATIVE ENERGY
(eV)
GVB-PP(2/4)
GVB-RCI(2/4)
50
60
70
80
90
100
110
120
130
140
H-Cr+-H BOND ANGLE
(degrees)

Figure 3: (a) GVB bond orbitals for the Cr^+–H_1 bond pair. (b) GVB bond orbitals for the Cr^+–H_2 bond pair. (c) Cr^+ singly occupied a_1 orbital which is seen to be mostly d_{z^2} in character. The Cr^+ bond orbitals are found to be 20.4% s, 9.5% p, and 70.1% d.

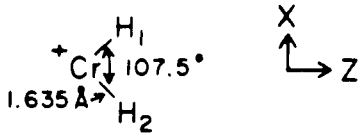

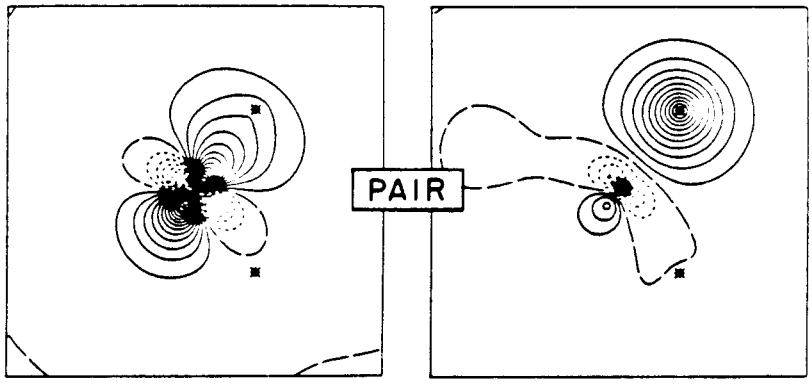

a) $Cr^+ - H_1$ BOND PAIR

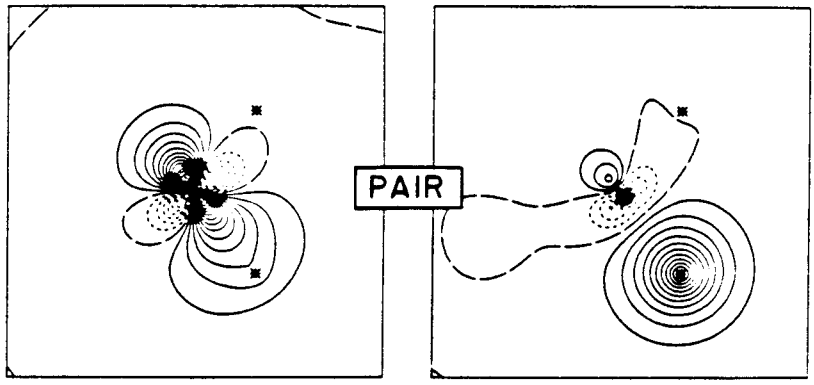

b) $Cr^+ - H_2$ BOND PAIR

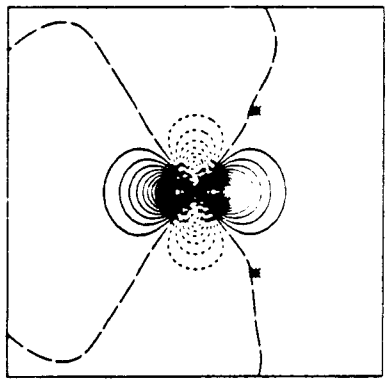

c) Cr^+ SINGLY OCCUPIED a_1 ORBITAL

is ^6D ($4d^45s^1$) at 1.59 eV, very close to the splitting for Cr^+. As with CrH_2^+, the ground state for MoH_2^+ is expected to be the $^4B_2$ state. Figure 4 shows the angular energy dependence for the molecule at the two levels of calculation. The MoH_2^+ molecule differs from its chromium counterpart by exhibiting two distinct minima, at 64.6° and 112.3°, with only a small energy barrier between them (transition state at 88.1° with a height of less than 1.5 kcal/mol, probably less than the zero point energy). Although CrH_2^+ has only one minimum (at 107°), it does have some bonding tendency at small angles. Due to the very flat nature of the potential wells observed for both CrH_2^+ and MoH_2^+, the bending and symmetric stretching vibrations of the two molecules should be quite strongly coupled. Bond length optimization at the two optimum angles gives bond lengths of 1.705 Å and 1.722 Å, respectively. The bond orbitals for these two geometries are shown in Figures 5 and 6. The bonding is fairly similiar for both minima in MoH_2^+. At 64.6°, the overlap of the bonding orbitals is 0.684, with 0.03 electrons transferred to each hydrogen. The hybridization for the Mo^+ bonding orbitals is 13.0% s, 5.4% p, and 81.6% d character. At the 112.3° geometry, the bond orbital overlaps are 0.687 with 0.06 electrons transferred from Mo^+ to each hydrogen. Here the metal orbital hybridization is 15.4% s, 7.7% p, and 76.9% d. The bond energy, $D_e(MoH^+–H)$, for the two cases is calculated to be 24.3 kcal/mol and 24.5 kcal/mol, respectively, at the GVB-RCI level and 35.1 kcal/mol and 34.7 kcal/mol respectively at the $RCI(2/4)\times[D_{\sigma 1}+D_{\sigma 2}+S_{M^+,val}]$ level of calculation. The bond dissociation energies for MoH^+, $D_e(Mo^+–H)$, at similar levels of calculation, are 22.2 kcal/mol and 33.8 kcal/mol.

Figure 4: Dependence of the MoH_2^+ total energy (at the GVB(2/4) and GVB-RCI(2/4) levels) on the H–Mo^+–H bond angle. The Mo^+–H bond distance is fixed at 1.708 Å and minima are found at 64.6° and 112.3° (GVB-RCI). The energy is seen to increase sharply as the bond angle is opened past 120°. Also shown is the angular energy dependence for d-bonded MoH_2^+ where the use of 5s and 5p functions is restricted. Optimum angles are found at 56.5° and 119.3°. Total energies should not be compared since the Mo^+ energy is higher due to the orbital restrictions in the d-bonding case.

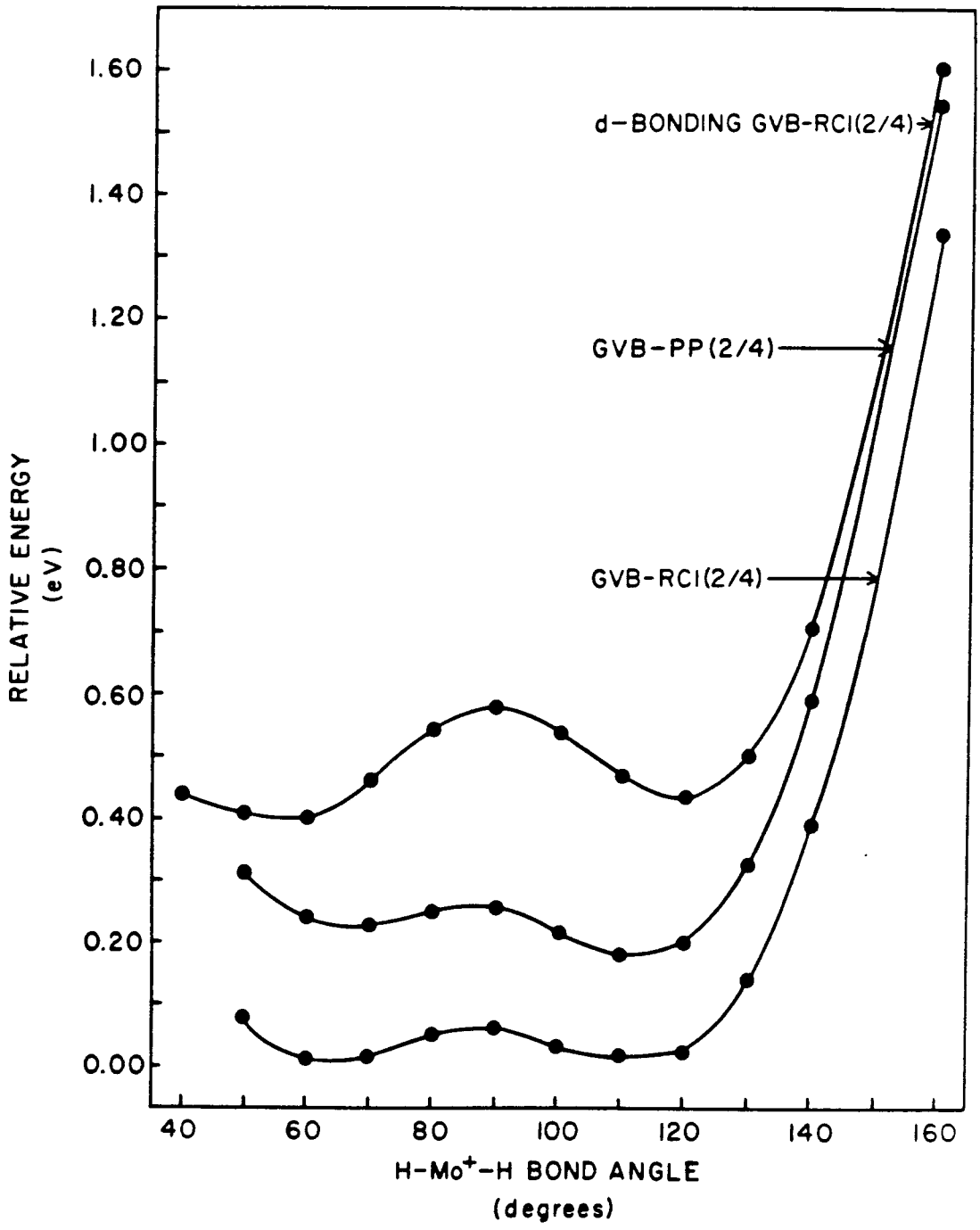
1.60
1.40
1.20
1.00
0.80
0.60
0.40
0.20
0.00
RELATIVE ENERGY
(eV)
d-BONDING GVB-RCI(2/4)
GVB-PP(2/4)
GVB-RCI(2/4)
40
60
80
100
120
140
160
H-Mo+-H BOND ANGLE
(degrees)

Figure 5: Orbital plots for small-angle MoH_2^+. (a) Mo^+–H_1 bond pair orbitals. (b) Mo^+–H_2 bond pair orbitals. (c) Singly occupied Mo^+ a_1 orbital showing d_{y^2} characteristics. The Mo^+ bond orbitals are hybridized 13.0% s, 5.4% p, and 81.6% d.

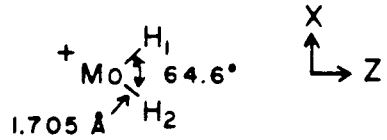

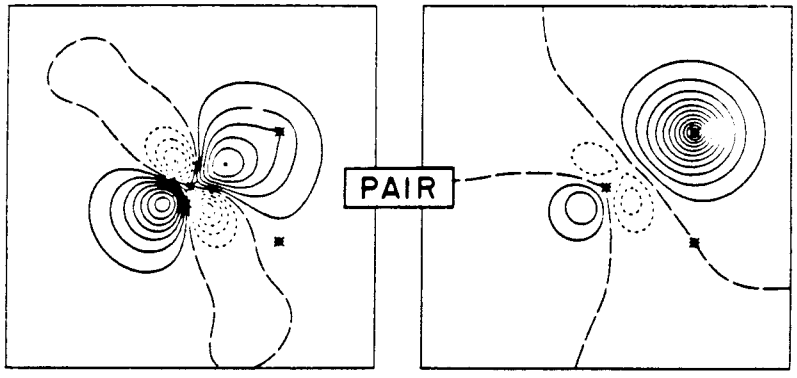

a) $Mo^+ - H_1$ BOND PAIR

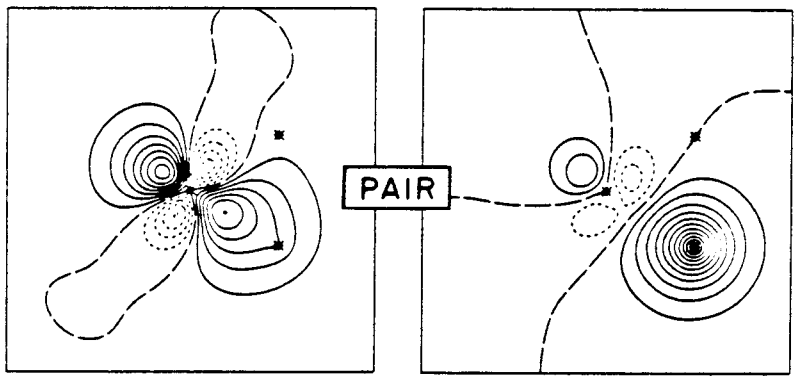

b) $Mo^+ - H_2$ BOND PAIR

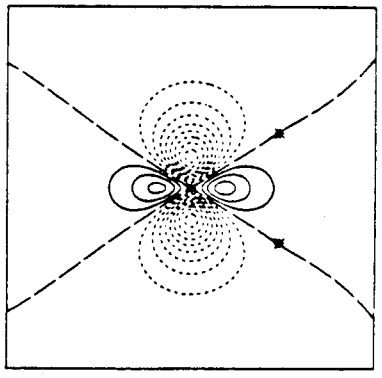

c) Mo^+ SINGLY OCCUPIED a_1 ORBITAL

Figure 6: Orbital plots for large-angle MoH_2^+. (a) Mo^+–H_1 bond pair orbitals. (b) Mo^+–H_2 bond pair orbitals. (c) Singly occupied Mo^+ a_1 orbital showing d_{z^2} characteristics. The Mo^+ bond orbitals are hybridized 15.4% s, 7.7% p, and 76.9% d.

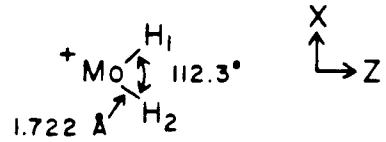

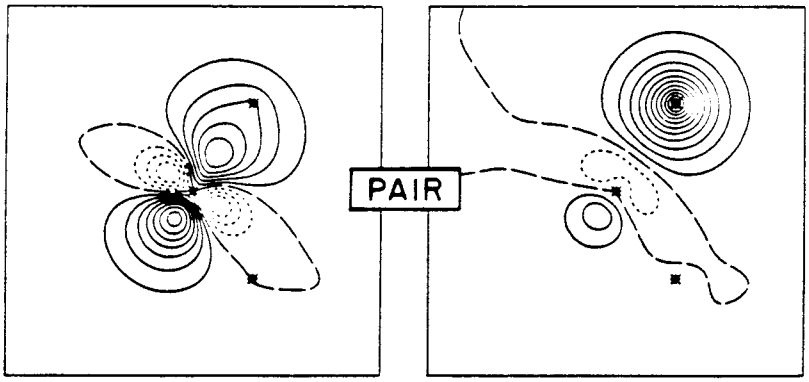

a) Mo^+-H_1 BOND PAIR

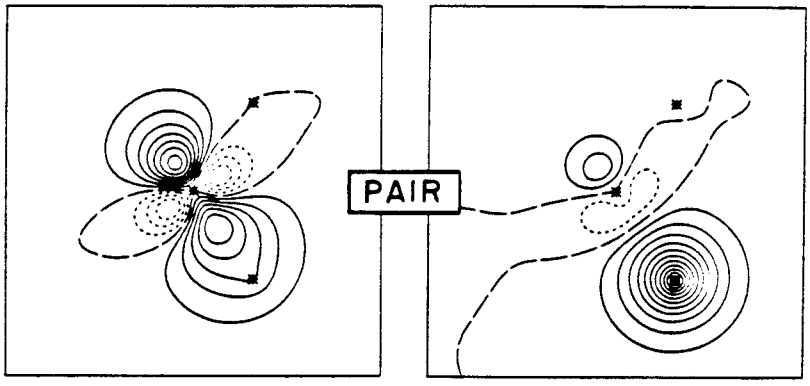

b) Mo^+-H_2 BOND PAIR

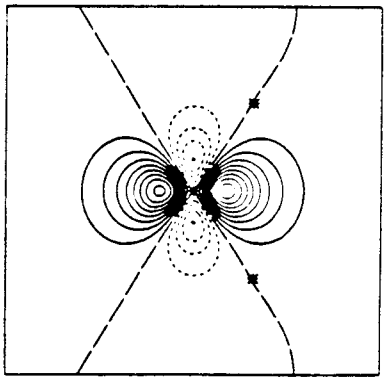

c) Mo^+ SINGLY OCCUPIED ORBITAL

IV. Discussion

The metal–H_2 interaction in CrH_2^+ and MoH_2^+ differs markedly from that seen in the saturated systems. Group 6 metal complexes involving two hydrogen atoms have been studied in rare gas matrices, rare gas solutions and in organic solvents. $Cr(CO)_5(H_2)$ has been observed in H_2–saturated hydrocarbon solution at room temperature[18,19] and in Ar matrices at 20 K.[20] $Cr(CO)_5(H_2)$, as well as $Mo(CO)_5(H_2)$ and $W(CO)_5(H_2)$, has also been produced in liquid xenon (at 70 K) by photolysis of $M(CO)_6$ in the presence of high pressures of H_2.[19,21] IR characterization of these molecules show them to be metal dihydrogen species with intact H–H bonds. η^2–bonded H_2 is also seen in $M(CO)_2(PR_3)_2(H_2)$ (M = Mo, W; R = Cy, i–Pr).[22] Neutron diffraction studies of $W(CO)_2(P\text{–}i\text{–}Pr_3)_2(H_2)$ give the H–H distance as 0.84 Å, slightly larger than for free H_2 (0.74 Å). Ab initio Hartree-Fock calculations on the model compound $W(CO)_3(PH_3)_2(H_2)$ yield an H–H distance of 0.79 Å.[23] Our calculations show that the unsaturated systems form two *covalent* metal hydrogen bonds rather than an η^2–H_2 complex. Thus, even in MoH_2^+, with a bond angle of 64.6°, the H–H distance is 1.822 Å.

For CrH^+ and MoH^+, we have shown that there are two important metal electronic configurations involved in bonding, d^5 and s^1d^4, where the optimum bond involves both $d\sigma$ and s character on the metal. These two configurations are also found to be important in the bonding of the metal dihydrides.

If the optimum bond of a hydrogen atom to a metal is to a d orbital, we expect the optimum bond to require a symmetric (d_{z^2} or $d\sigma$) orbital to get the largest overlap with the H.[24] Thus, two strong sigma bonds to two d orbitals of the d^5 metal configuration would require two orthogonal orbitals, each of which is $d\sigma$ about its bond axis. This requires bond angles of either 54.7° or 125.3°. [Two orthogonal orbitals of $d\sigma$ type can be formed in the yz plane by taking linear combinations of the d_{z^2}, d_{yz}, and $d_{z^2-y^2}$ atomic orbitals, leading to major axes at an angle of 54.7° (each orbital lying along one of the other's nodal surfaces).]

If the optimum bond of a hydrogen atom to a metal is to an s orbital,

the largest amount of s character can be incorporated in two metal hydrogen bonds by forming two sd hybrid orbitals (e.g., $s \pm d_{yz}$). This would yield an optimum H–M–H angle of 90°.[25] Factors other than optimum hybridization, such as hydrogen-hydrogen repulsion, will modify these bond angles. Examples of s-d and d-d metal hybrid orbitals are shown in Figures 7 and 8. In CrH_2^+ and MoH_2^+, the four orbitals (s, d_{yz}, $d_{x^2-y^2}$, and d_{z^2}) overlapping the two hydrogens are mixed to yield the three orbitals required to describe the three electrons involved in the two metal-hydrogen bonds and the a_1 nonbonded d electron. The Mulliken population analysis indicates that for both species, the actual metal hybridization is somewhere in between the sd and dd hybrid limits.

Calculations on ScH_2^+ by Alvarado-Swaisgood et al.[12] found one minimum on the angular potential surface (optimum angle of 106.7°) and a metal hybridization with approximately 40% sp character. Our GVB-RCI calculations for CrH_2^+ (29.9% sp character) hint at a second well at small angle but indicate only one optimum geometry, 107.5°. The MoH_2^+ molecule (18.4% or 23.1% sp character at the two optimum geometries) shows the double well behavior. These observations support the models presented; sd hybridization leads to one minima near 90° while two bonds to pure dσ orbitals would lead to a double well angular potential with optimum bonding at angles near 54.7° and 125.3°. The optimum bond angles for MoH_2^+ are 64.6° and 112.3°. Both calculated angles are shifted towards 90° from the pure d-d values. To test whether this shift is due to the 4s and 4p character in the wavefunction, calculations were performed where the three outermost s and p basis functions were removed. [Other s and p basis functions cannot be removed due to the presence of the 4s and 4p core electrons; thus, some amount of s and p character can still be used in the wavefunctions]. Figure 4 shows the results of these calculations. Again, a double well in the angular potential is found with the optimum angles of 56.5° and 119.3° shifted toward the values (54.7° and 125.3°) of the d-d model.

The bond in MoH^+ involves a Mo orbital with 73.3% d character (compared

Figure 7: Cr^+ hybrid orbitals. (a) $s \pm d_{yz}$ hybrid orbitals which point at 90° from each other. (b) d–d hybrids made up using the d_{z^2}, d_{yz}, and $d_{x^2-y^2}$ orbitals. Each orbital is d_{z^2}-like with respect to its axis, leading to an angle between their major axes of 54.7°. The s–d hybrids are more diffuse than the d–d hybrids due to the larger size of the s orbital.

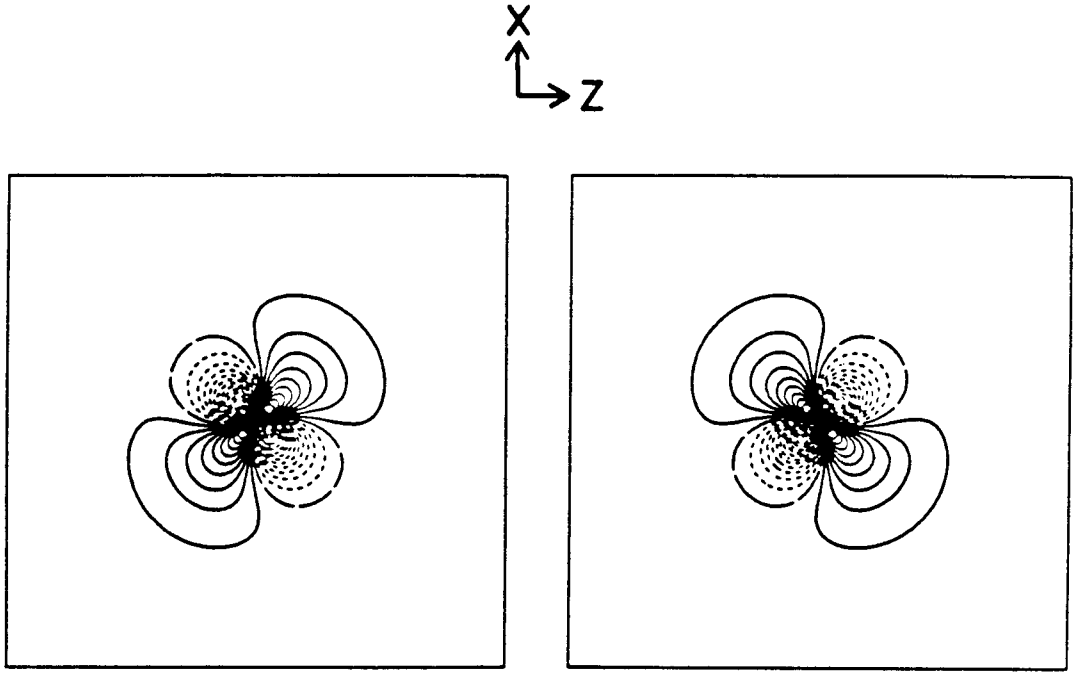

a) Cr^{+} s-d HYBRID ORBITALS

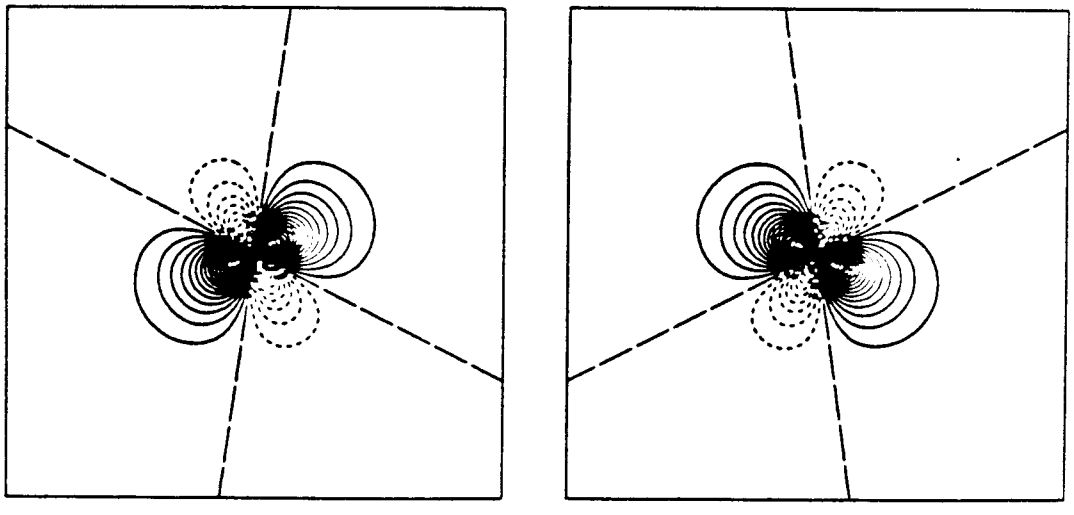

b) Cr^{+} d-d HYBRID ORBITALS

Figure 8: Mo^+ hybrid orbitals. (a) $s \pm d_{yz}$ hybrid orbitals pointing at 90° from each other. (b) d–d hybrids made up using the d_{z^2}, d_{yz}, and $d_{x^2-y^2}$ orbitals. Both orbitals are d_{z^2}-like and the angle between their major axes is 54.7°. The Mo^+ orbitals are seen to be more diffuse than the Cr^+ hybrid orbitals (Figure 7) due to their larger size.

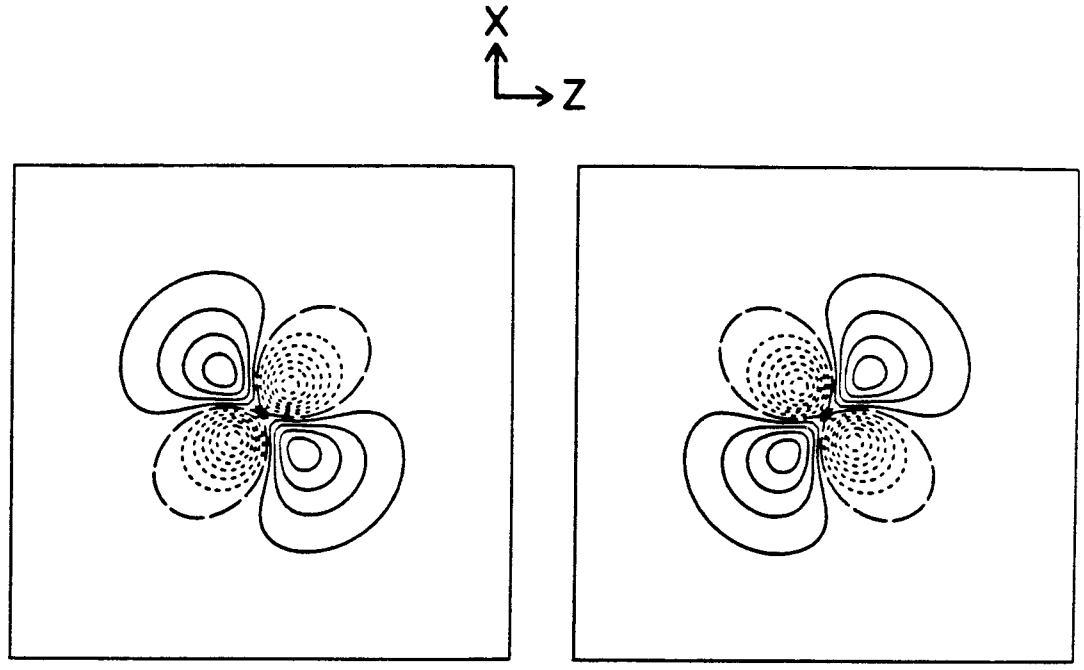

a) Mo^+ s-d HYBRID ORBITALS

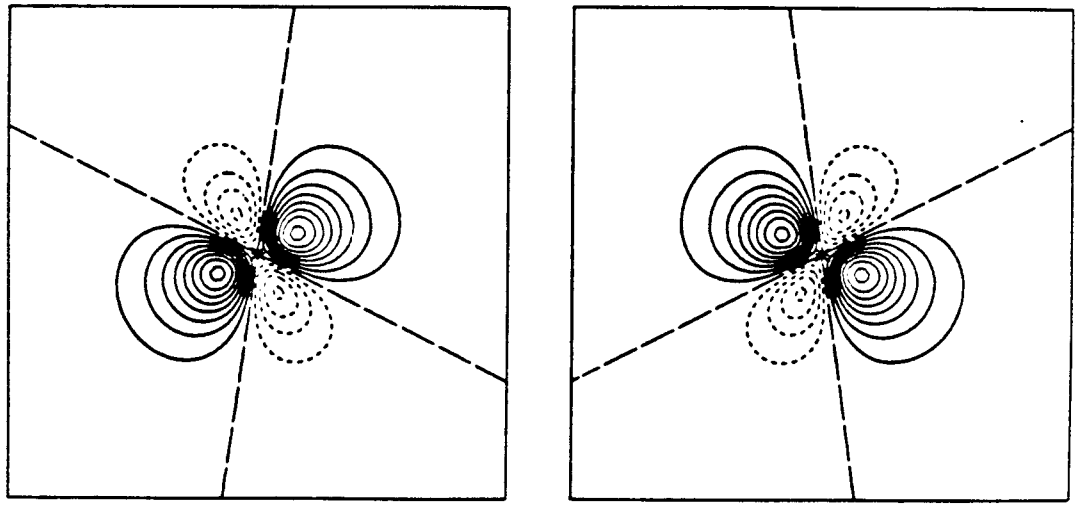

b) Mo^+ d-d HYBRID ORBITALS

with 46.9% for CrH^+). If the second metal-hydrogen bond was to a pure d orbital, the two resulting equivalent bonds would have 86.7% d character. The calculational results suggest that the actual values are in between these two results with slightly more s character present in the 112.3° geometry (76.9% d) than in the 64.6° geometry (81.6% d). The shape of the dihydride bond orbitals is thus seen to be quite close to that found for the monohydride with just slightly more d character. For Cr^+, on the other hand, a second metal-hydrogen bond to a pure d orbital would yield two equivalent bonds each with approximately 73% d character, very close to what is actually calculated.

Given the significant amount of sd hybridization in the bonds of MoH^+ and CrH^+, a second bond to a primarily d-like orbital would be expected to be weaker than the first metal–hydrogen bond. On the other hand, little electronic excitation energy is expected to be lost on formation of the second bond and, at the same time, the reduced overall spin for MoH^+ and CrH^+ relative to Mo^+ and Cr^+ would be expected to yield decreased exchange penalties. Table III presents the s–d and d–d exchange energies calculated for Cr^+ and Mo^+. Estimates of the energy lost on bonding to CrH^+ are 40 and 26 kcal/mol for the first and second hydrogens respectively[26] and for Mo^+, approximately 35 and 21 kcal/mol[27], leading to second bonds about 14 kcal/mol stronger. In fact, for MoH_2^+, we find the second bond is stronger than the first by about 1.3 kcal/mol, suggesting that these two factors are comparable.

Assuming that higher levels of electronic correlation will have the same effect on bond dissociation energies for both the first and second bonds (our calculations support this assumption to about 1 kcal/mol), we can estimate the best theoretical bond energies for the dihydrides using the best theoretical values calculated for the monohydrides. The monohydride values are 33.8 kcal/mol for $D_e(Mo^+–H)$, and 26.9 kcal/mol for $D_e(Cr^+–H)$, both at the $D_\sigma \times S_{M^+,val}$ level of calculation. This leads to estimated bond energies ($D_{\sigma 1} \times [D_{\sigma 2} + S_{M^+,val}]$) $D_e(MoH^+–H)$ of 35.1 kcal/mol and $D_e(CrH^+–H)$ of 19.4 kcal/mol. This can be

Table III

Cr^+ and Mo^+ Exchange Energies[a]

	Cr^+		Mo^+	
	^6S	^6D	^6S	^6D
$\overline{K}_{sd}$		5.12		8.47
$\overline{K}_{dd}$	16.54	18.20	13.44	14.20
$K_{\sigma\pi}$	12.51		10.29	
$K_{\sigma\delta}$	20.56		16.59	
$K_{\pi\overline{\pi}}$	17.88	19.88	14.49	15.40
$K_{\pi\delta}$	17.88	19.88	14.49	15.29
$K_{\delta\overline{\delta}}$	9.82	10.91	8.19	8.61

[a] Exchange energy values taken from Hartree Fock calculations on the atomic ions.

compared with $D_e(Sc^+–H) = 54.7$ kcal/mol and $D_e(ScH^+–H) = 51.7$ kcal/mol calculated by Alvarado-Swaisgood et al.[12] Thus, although the bonds in the Sc^+ systems are substantially stronger, the bond strength for the second hydrogen is calculated to be lower than for the first, as seen in CrH_2^+. As a check on the present calculations versus those of Alvarado-Swaisgood et al., we have also performed similar calculations on ScH_2^+. We obtain an optimum geometry with $R_e = 1.762$Å and $\theta_e = 105.8°$ (compared to 1.745 Å and 106.7°). Bond dissociation energies for the two levels of calculation, $RCI(2/4)\times[D_{\sigma 1}+D_{\sigma 2}+S_{M+,val}]$ and $D_{\sigma 1}\times[D_{\sigma 2} + S_{M+,val}]$ are 51.5 and 52.4 kcal/mol, respectively, in very good agreement with the Alvarado-Swaisgood et al. value of 51.7 kcal/mol.

What kind of predictions can be made about metal ion reactivity based on the geometric and energetic results for the metal dihydrides? The sum of the first and second metal-hydrogen theoretical bond dissociation energies for Cr^+ and Mo^+ are 46.3 kcal/mol and 68.9 kcal/mol, respectively. Since typical C–H or C–C bonds are worth 95–105 and 80–90 kcal/mol, respectively, these results suggest that neither metal in its ground state should insert into bonds of hydrocarbons. As a second estimate, we can use the theoretical differences in first and second bond strengths with the experimental values for the monohydrides to give estimates for the sums of the two bond energies of 48 kcal/mol and 83 kcal/mol for Cr^+ and Mo^+, respectively. Assuming that the metal-carbon bond is stronger than the metal-hydrogen bond (as reported for some metal species[3]) and that the metal-carbon bond increases in strength as the carbon chain length increases (better stabilization of metal charge), it is possible that ground state Mo^+ would react with hydrocarbons. The bond energies to Cr^+ are too low to expect insertion into normal C–C or C–H bonds. The presence of a potential minimum at low bond angle for Mo^+ would also help stabilize the intermediates as the reactant species come together, favoring insertion. Of equal importance with the energetics is the problem of spin conservation. The stable dihydrides have $S = 3/2$, whereas the reactants have $S = 5/2$. Since a change in total spin is

unlikely during a single collision, we expect that the observed chemistry involves either (i) excited S = 3/2 ions in the beam or (ii) formation of a long-lived complex involving nearly degenerate S = 3/2 and S = 5/2 states. The lowest excited S = 3/2 state is 56.7 kcal/mol and 44.0 kcal/mol[17] above the ground state for Cr^+ and Mo^+, respectively. The lower value for Mo^+, along with the increased spin orbit coupling for the heavier metal, also favors higher reactivity for Mo^+ versus Cr^+.

Current experimental ion beam studies on the reactions of Cr^+ and Mo^+ with alkanes and alkenes[28] are in agreement with these expectations. While Cr^+ beams produced by electron impact on $Cr(CO)_6$ (containing excited state Cr^+ ions) will react with methane,[29] ground state Cr^+ produced by surface ionization yields no exothermic products with alkanes of up to seven carbons in length. On the other hand, ground state Mo^+ reacts exothermically with straight chain alkanes, butane or larger, to give metal alkadiene ion products and hydrogen. Mo^+ is also seen to dehydrogenate alkenes while Cr^+ only reacts with larger alkenes such as the reaction with cyclohexene or cyclohexadiene to produce $Cr(benzene)^+$. Cr^+ insertion into C–H bonds in these cases is facilitated by the complexation due to the double bonds in addition to formation of the M–H and M–C sigma bonds.

The current results on Cr^+ and Mo^+ systems can also be used for predictions about other metal dihydrides. Bonds of hydrogen and carbon to first row transition metals involve the 4s orbitals. Thus, we expect that the metal dihydrides of the first row will tend to have geometries with bond angles slightly greater than 90°. Also, due to the fact that the second bond must be formed to an orbital having greater d character than for the first metal-hydrogen bond, the second bonds are expected to be weaker than the first (due to non-optimum hybridization and loss of d-d exchange energy). (Experimental results suggest $D(ScH^+–H)$ to be greater than $D(Sc^+–H)$ by 3.1 kcal/mol[30]). The second row metal ions form bonds principally with their 4d electrons rather than their 5s

electrons. We thus expect such second row metal dihydrides (YH_2^+ to RhH_2^+) to be similar to MoH_2^+ with two possible minima, one at small bond angle ($\sim$60°). This angle would be expected to vary depending on the electron configuration of the metal. As an example, theoretical calculations by Rappé and Goddard[31] on Cl_2TiH_2 show that the two hydrogen atoms bond to Ti d orbitals (the two Cl atoms effectively remove the two metal s electrons), leading to a bond angle of 74.9°. The optimum angle for two pure dσ-like orbitals is 54.7°, while the optimum placement of the two electrons in d orbitals from the standpoint of lowest electron-electron repulsion is dσdδ with the two electrons in orbitals at 90°. The resultant bond angle is thus a compromise between these two effects. Summarizing we find that for d-bonding situations the ground state metal electronic configuration plays an essential role in determining the geometry and energetics. Since both bonds to the second row metals are generally to d^n configurations, the second bonds should be comparable in strength or possibly stronger than the first (due to a smaller amount of exchange energy being lost, but tempered by non-optimum metal hybridization).

V. Summary

We find that for second row transition metals, hydrogen tends to bond to 4d orbitals rather than 5s. This differs dramatically from transition metal hydride cations of the first row which bond primarily using their 4s orbitals. This difference arises primarily from the difference in size of the s and d orbitals where for the second row the d orbitals are more diffuse and closer in size to the large s orbitals. These size differences affect the metal electronic levels, electron-electron repulsion and exchange energies, and the overlaps resulting from bonding. These effects play a similiar role in the dihydrides CrH_2^+ and MoH_2^+. The low-lying electronic states are similar, both having a d^5 electronic configuration in the ground state. However, MoH_2^+ has stronger overall bonds dominated with more d-bonding character than CrH_2^+, and leading to strong bonding at both small (65°) and large (112°) angles. The larger d–d exchange energies on Cr^+ and need for s character to produce stronger bonds causes the second Cr^+–H bond to be very weak. These general trends, along with consideration of the specific metal electronic states, should prove useful in predicting relative bond strengths and geometric structures for other metal species where the metal is sigma bonded to two hydrogen or alkyl ligands.

Acknowledgement. We thank the National Science Foundation (Grant Nos. CHE83-18041 and CHE84-07857) for partial support of this work.

References

(1) (a) Halle, L. F.; Armentrout, P. B.; Beauchamp, J. L. *Organometallics* **1982**, *1*, 963. (b) Hanratty, M. A.; Beauchamp, J. L.; Illies, A. J.; Bowers, M. T. *J. Am. Chem. Soc.* **1985**, *107*, 1788.

(2) Tolbert, M. A.; Beauchamp, J. L. *J. Am. Chem. Soc.* **1984**, *106*, 8117.

(3) Aristov, N.; Armentrout, P. B. *J. Am. Chem. Soc.* **1986**, *108*, 1806.

(4) (a) Jacobson, D. B.; Freiser, B. S. it J. Am. Chem. Soc. **1983**, *105*, 5197. (b) Jacobson, D. B.; Freiser, B. S. *J. Am. Chem. Soc.* **1983**, *105*, 7492.

(5) Larsen, B. S.; Ridge, D. P. *J. Am. Chem. Soc.* **1984**, *106*, 1912.

(6) (a) Armentrout, P. B.; Halle, L. F.; Beauchamp, J. L. *J. Am. Chem. Soc.* **1981**, *103*, 6501. (b) Stevens, A. E.; Beauchamp, J. L. *Chem. Phys. Lett.* **1981**, *78*, 291. (c) Mandich, M. L.; Halle, L. F.; Beauchamp, J. L. *J. Am. Chem. Soc.* **1984**, *106*, 4403. (d) Georgiadis, R.; Armentrout, P. B. *J. Am. Chem. Soc.* **1986**, *108* 2119. (e) Hettich, R. L.; Freiser, B. S. *J. Am. Chem. Soc.* **1986**, *108*, 2537.

(7) Elkind, J. L.; Armentrout, P. B. *Inorg. Chem.* **1986**, *25*, 1080.

(8) Schilling, J. B.; Goddard, W. A., III; Beauchamp, J. L. *J. Am. Chem. Soc.* **1986**, *108*, 582. (b) Schilling, J. B.; Goddard, W. A., III; Beauchamp, J. L. submitted for publication. (c) Schilling, J. B.; Goddard, W. A., III; Beauchamp, J. L. submitted for publication.

(9) Alvarado-Swaisgood, A. E.; Allison, J.; Harrison, J. F. *J. Phys. Chem.* **1985**, *89*, 2517.

(10) (a) Carter, E. A.; Goddard, W. A., III *J. Phys. Chem.* **1984**, *88*, 1485. (b) Carter, E. A.; Goddard, W. A., III *J. Am. Chem. Soc.* **1986**, *108*, 2180. (c) Mavridis, A.; Alvarado-Swaisgood, A. E.; Harrison, J. F. *J. Phys. Chem.* **1986**, *90*, 2584. (d) Harrison, J. F. *J. Phys. Chem.* **1986**, *90*, 3313.

(11) Halle, L. F.; Crowe, W. E.; Beauchamp, J. L. *Organometallics* **1984**, *3*, 1694.

(12) Alvarado-Swaisgood, A. E.; Harrison, J. F. *J. Phys. Chem.* **1985**, *89*, 5198.

(13) (a) Rappé, A. K.; Goddard, W. A., III to be published. (b) Rappé, A. K.; Smedley, T. A.; Goddard, W. A., III *J. Phys. Chem.* **1981**, *85*, 2607.

(14) Hay, P. J.; Wadt, W. R. *J. Chem. Phys.* **1985**, *82*, 299.

(15) (a) Huzinaga, S. J. *J. Chem. Phys.* **1965**, *42*, 1293. (b) Dunning, T. H., Jr. *J. Chem. Phys.* **1970**, *53*, 2823.

(16) The p polarization functions were optimized for $^6\Sigma^+$ MnH^+. See reference 8b.

(17) Moore, C. E. "Atomic Energy Levels"; National Bureau of Standards: Washington, D. C., 1971; Vol. I and II.

(18) Church, S. P.; Grevels, F.-W.; Hermann, H.; Schaffner, K. *J. Chem. Soc., Chem. Commun.* **1985**, 30.

(19) Upmacis, R. K.; Gadd, G. E.; Paliakoff, M.; Simpson, M. B.; Turner, J. J.; Whyman, R.; Simpson, A. F. *J. Chem. Soc., Chem. Commun.* **1985**, 27.

(20) Sweany, R. L. *J. Am. Chem. Soc.* **1985**, *107*, 2374.

(21) Upmacis, R. K.; Poliakoff, M.; Turner, J. J. *J. Am. Chem. Soc.* **1986**, *108*, 3645.

(22) Kubas, G. J.; Ryan, R. R.; Swanson, B. I. *J. Am. Chem. Soc.* **1984**, *106*, 451.

(23) Hay, P. J. *Chem. Phys. Lett.* **1984**, *103*, 466.

(24) Steigerwald, M. L. *Ph.D.* Thesis, California Institute of Technology, Pasadena, California (1984).

(25) Low, J. J.; Goddard, W. A., III *J. Am. Chem. Soc.* **1984**, *106*, 6928.

(26) Starting with the electronic excitation energy (d^5 to s^1d^4) plus the exchange energy lost on bonding to each electronic state, we multiply by the percentage of each metal electronic state determined from the metal hybridization (considering p character as equivalent to s character). Therefore, for the first bond in CrH_2^+, $2K_{dd}$ or approximately 33.08 kcal/mol of exchange energy is lost upon bonding to the d^5 state (which is present at 46.9%). $2K_{sd}$ or 10.24 kcal/mol of exchange energy and 35.05 kcal/mol electronic promotion

energy is lost on bonding to the d^4s^1 state which is present at 53.1%. Using these energies and percentages produces a total energy loss of approximately 39.6 kcal/mol. Exchange energy losses (1.5 K_{dd}) for the second M^+–H bond amount to approximately 26 kcal/mol.

(27) Using a similar argument as for CrH_2^+ in reference 25. The first bond in MoH_2^+ will lose 73% of the 26.88 kcal/mol lost on bonding to the d^5 state (K_{dd} exchange energy) and 27% of the 36.67 kcal/mol excitation energy and 16.94 kcal/mol s–d exchange energy lost on bonding to the d^4s^1 state. This leads to an overall loss of 34.1 kcal/mol. The second bond loses approximately 21 kcal/mol of exchange energy.

(28) Schilling, J. B.; Beauchamp, J. L. manuscript in preparation.

(29) Halle, L. F.; Armentrout, P. B.; Beauchamp, J. L. *J. Am. Chem. Soc.* **1981**, *103*, 962.

(30) Sunderlin, L.; Aristov, N.; Armentrout, P. B. *J. Am. Chem. Soc.* **1987**, *109*, 78.

(31) Rappé, A. K.; Goddard, W. A., III *J. Am. Chem. Soc.* **1982**, *104*, 297.

CHAPTER VII

THEORETICAL STUDIES OF TRANSITION METAL METHYL IONS, MCH_3^+

M = Sc, Cr, Mn, Zn, Y, Mo, Tc, Pd, AND Cd

Theoretical Studies of Transition Metal Methyl Ions, MCH_3^+: M = Sc, Cr, Mn, Zn, Y, Mo, Tc, Pd, and Cd

J. Bruce Schilling, William A. Goddard III*, and J. L. Beauchamp

Contribution No. 7553 from the

Arthur Amos Noyes Laboratory of Chemical Physics

California Institute of Technology, Pasadena, CA 91125

Abstract

Selected transition metal methyl cations have been studied using ab initio generalized valence bond and configuration interaction methods. We present equilibrium geometries and bond dissociation energies and analyze the character of the wavefunction for the ground state MCH_3^+ species. The present calculations are compared with previous studies of the corresponding MH^+ molecules. MCH_3^+ is similar to MH^+ from the standpoint of orbital hybridization, electron transfer, bond orbital overlap, and bond dissociation energy. Thus, we find bond energy differences, $D(M^+–CH_3) - D(M^+–H)$, ranging from -3.6 kcal/mol for M = Mo to $+6.0$ kcal/mol for M = Zn, whereas the total bond energy is calculated to range from 24 to 60 kcal/mol. Experimental estimates suggest that $D(M^+–CH_3)$ is, on the average, about 6 kcal/mol larger than $D(M^+–H)$.

I. Introduction

Bond dissociation energies are extremely important in chemistry for use in designing syntheses, predicting stable molecular structures, and predicting and analyzing reactions mechanisms and products. Although a large number of bond energies have been determined for organic compounds, relatively few are known quantitatively for organometallic compounds.[1-6] Even for these few, many of the bond energies are known only as averages of several metal–ligand bonds rather than as a bond energy for a particular metal–ligand bond. Recently, there have been a number of experimental determinations of bond energies for neutral[7,8] and ionic[9-14] gas-phase metal compounds. In the field of hydrocarbon activation, the important bonds are sigma bonds formed to the metal center by hydrogen and carbon atoms of the organic species. Experiments suggest that in saturated metal systems the metal hydrogen bonds tend to be much stronger (approximately 15-25 kcal/mol) than the metal carbon bonds.[15-18] In unsaturated metal systems, however, such as bare transition metal ions in the gas phase, metal methyl bond strengths have been found, experimentally, to be greater than or equal to those for the metal hydrides (differences of from 0 kcal/mol for Ti^+ to 14 kcal/mol for Pd^+) in all cases studied. The explanation for this difference between saturated and unsaturated metal systems is variously given as steric weakening of the metal alkyl bonds in saturated molecules[19] or as increased charge stabilization of the metal ion by the alkyl group, as compared with a hydrogen atom, in the unsaturated ionic systems.[12]

In order to help explain the difference in sigma bonding between a metal and either carbon or hydrogen, we have performed ab initio theoretical calculations on a series of MCH_3^+ species for representative metals of the first or second transition metal series. The metal ions used were chosen because they offer a wide variety of metal bond orbital sizes and hybridizations (from almost totally s-bonding for Zn^+ and Cd^+ to d-bonding with Pd^+). These results are compared with similar calculations on the metal hydrides.[20]

II. Results and Discussion

Bonding in the Metal Methyl Ions. The bond between between a transition metal ion and the methyl radical can be visualized as spin-pairing of an electron in a metal sigma orbital (a hybrid containing s, d_{z^2}, and p_z character) with the unpaired electron of CH_3 (in a carbon hybrid orbital containing s and p_z character). The interaction of the metal nonbonding electrons in the metal methyls was found to be very similar to that seen for the metal hydride ions, and we considered the electronic state corresponding to the ground state of MH^+. Under C_{3v} symmetry, the metal s and d_{z^2} orbitals are of a_1 symmetry while the d_{xy}, $d_{x^2-y^2}$, d_{xz}, and d_{yz} orbitals are of e symmetry. The hydrides of the metal ions in this study are all of Σ^+ symmetry (except ScH^+, which is Π), and the corresponding methyls have A_1 symmetry (E symmetry for $ScCH_3^+$).

Traditional oxidation state formalism describes the metal methyl species in terms of M^{2+} interacting with CH_3^-. However, a series[21,22] of generalized valence bond calculations suggests the alternative (GVB) formalism where one starts with every ligand as neutral and bonds this ligand to the ground atomic configuration for the metal in the appropriate charge state of the metal (+1 in this case). This covalent view of the bonding to alkyl, aryl, and hydride ligands is supported by the ab initio GVB calculations. Thus, for $M^+(CH_3)$, we find a charge transfer of -0.26 e^- (Pd) to $+0.33$ e^- (Sc) from the M^+ to the neutral CH_3. The GVB bond orbitals (each with *one* electron) for various M^+–R species are shown in Figures 1–5. In each case the two GVB orbitals are localized with one on each of the two atoms. Each figure depicts the bond orbitals from both MCH_3^+ and MH^+ for the corresponding first and second row metals. The C-H orbitals for all species are essentially the same and are shown for only $PdCH_3^+$ (Fig. 5).

Geometries. The theoretically determined metal methyl geometries are given in Table I. The C–H bond lengths have been held at the value in CH_4[23], 1.094 Å, and we constrained the metal methyl ions to have C_{3v} symmetry (the

Figure 1: (a) GVB orbitals for ScH^+. The Sc^+–H bond length is 1.810 Å and the metal orbital hybridization is 46.2% s, 13.5% p, and 40.3% d. (b) GVB orbitals for YH^+. The Y^+–H bond length is 1.892 Å and the metal orbital hybridization is 31.9% s, 10.2% p, and 57.9% d. (c) GVB orbitals for the metal carbon bond in $ScCH_3^+$ with a metal carbon bond length of 2.233 Å and a metal-carbon-hydrogen angle of 111.0°. The orbital hybridizations are: Sc^+ – 45.7% s, 8.1% p, and 46.2% d; and C – 28.5% s 71.3% p, and 0.2% d. (d) GVB orbitals for YCH_3^+ with a metal carbon bond length of 2.298 Å and an M^+–C–H angle of 110.9°. The orbital hybridizations are: Y^+ – 25.5% s, 6.8% p, 67.7% d; and C – 27.5% s, 72.3% p, 0.2% d. For the orbital plots in this and the other figures positive contours are solid, negative contours are dotted, nodal lines are shown by long dashes, the atomic nuclei are indicated by asterisks, and the spacing between contours is 0.05 a.u.

$M^+ - H$

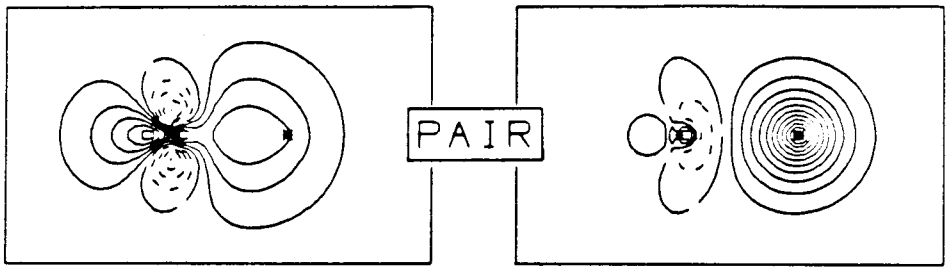

a) $Sc^+ - H$ SIGMA BOND

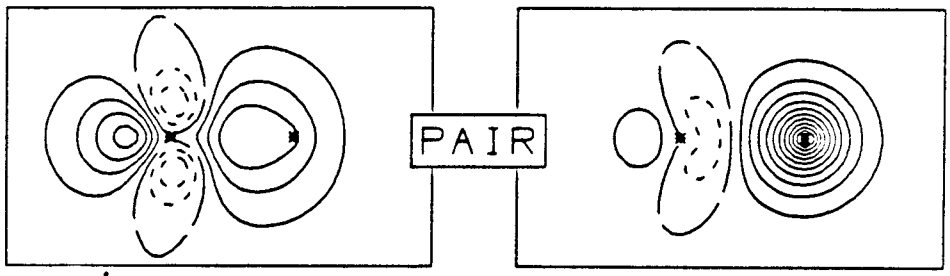

b) $Y^+ - H$ SIGMA BOND

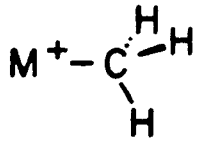

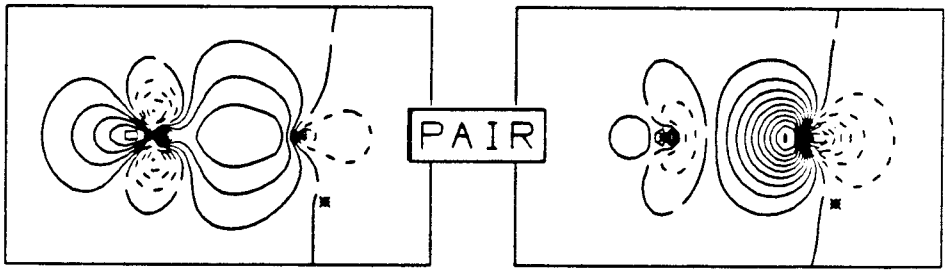

c) $Sc^+ - C$ SIGMA BOND

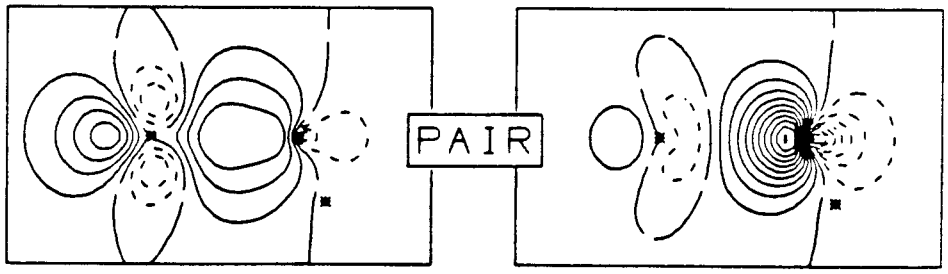

d) $Y^+ - C$ SIGMA BOND

Figure 2: (a) GVB orbitals for CrH^+. The Cr^+–H bond length is 1.602 Å and the metal orbital hybridization is 40.6% s, 12.5% p, and 46.9% d. (b) GVB orbitals for MoH^+. The Mo^+–H bond length is 1.708 Å and the Mo^+ orbital hybridization is 19.7% s, 7.0% p, 73.3% d. (c) GVB orbitals for the metal carbon bond in $CrCH_3^+$ with a metal carbon bond length of 2.074 Å and a metal–carbon–hydrogen angle of 108.4°. The orbital hybridizations are: Cr^+ – 41.9% s, 9.6% p, 48.5% d; and C – 15.3% s, 84.2% p, 0.5% d. (d) GVB orbitals for $MoCH_3^+$ with a metal carbon bond length of 2.201 Å and an M^+–C–H angle of 108.1°. The orbital hybridizations are: Mo^+ – 15.6% s, 3.3% p, 81.1% d; and C – 16.9% s, 82.7% p, 0.4% d.

$M^+ - H$

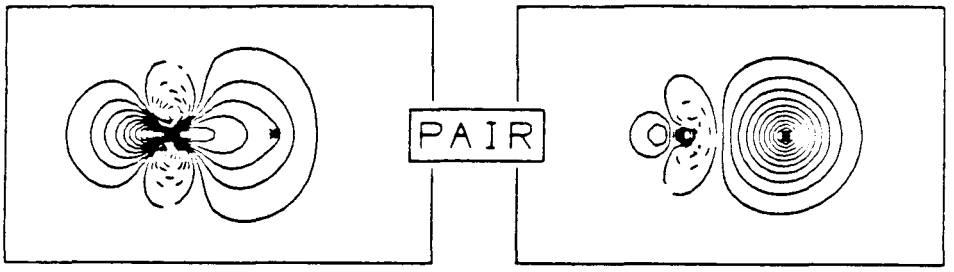

a) $Cr^+ - H$ SIGMA BOND

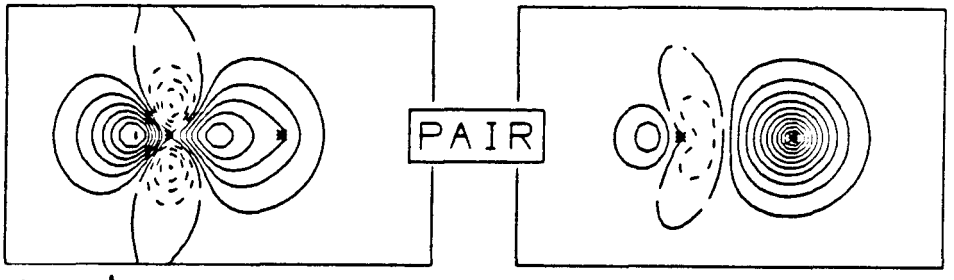

b) $Mo^+ - H$ SIGMA BOND

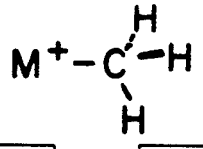

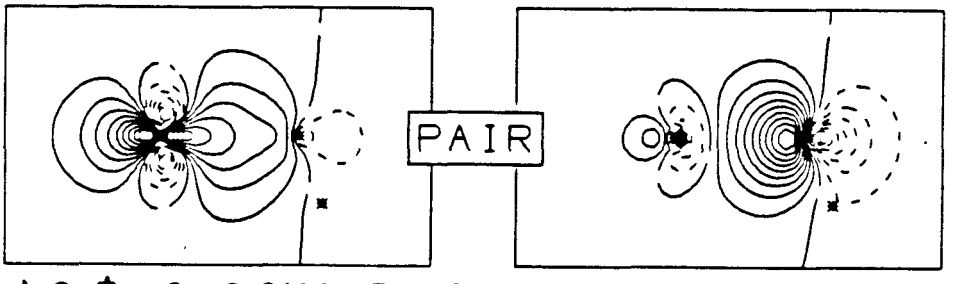

c) $Cr^+ - C$ SIGMA BOND

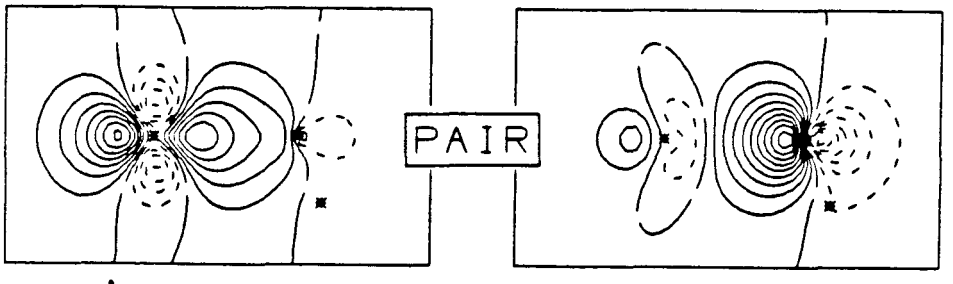

d) $Mo^+ - C$ SIGMA BOND

Figure 3: (a) GVB orbitals for MnH^+. The Mn^+–H bond length is 1.702 Å and the metal orbital hybridization is 76.3% s, 12.5% p, and 11.3% d. (b) GVB orbitals for TcH^+. The Tc^+–H bond length is 1.719 Å and the Tc^+ orbital hybridization is 40.5% s, 7.0% p, 52.5% d. (c) GVB orbitals for the metal carbon bond in $MnCH_3^+$ with a metal carbon bond length of 2.241 Å and a metal–carbon–hydrogen angle of 105.5°. The orbital hybridizations are: Mn^+ – 86.5% s, 6.2% p, 7.3% d; and C – 11.1% s, 88.5% p, 0.4% d. (d) GVB orbitals for $TcCH_3^+$ with a metal carbon bond length of 2.209 Å and an M^+–C–H angle of 107.7°. The orbital hybridizations are: Tc^+ – 40.2% s, 3.0% p, 81.1% d; and C – 21.4% s, 78.1% p, 0.5% d.

$M^+ - H$

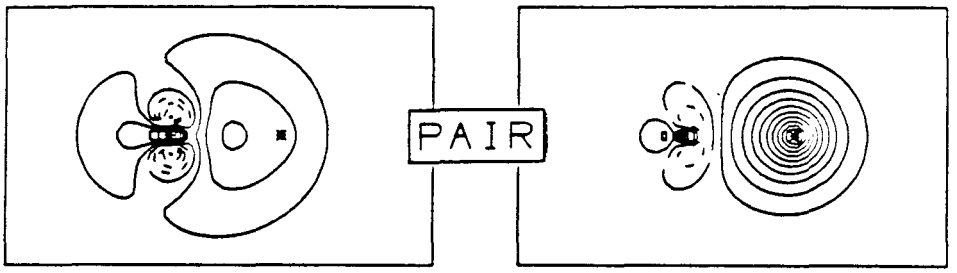

a) $Mn^+ - H$ SIGMA BOND

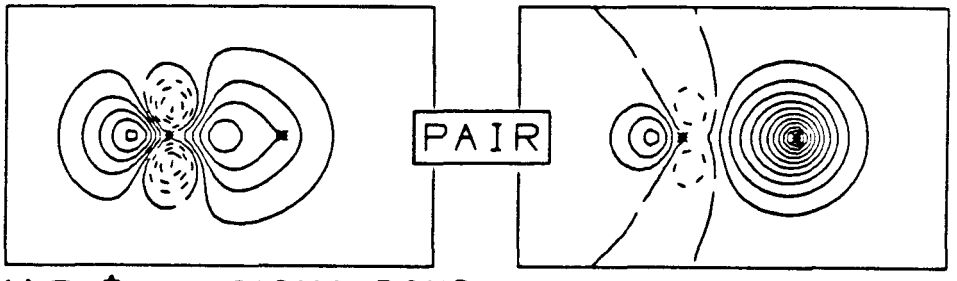

b) $Tc^+ - H$ SIGMA BOND

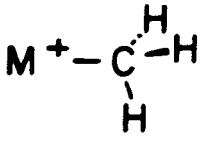

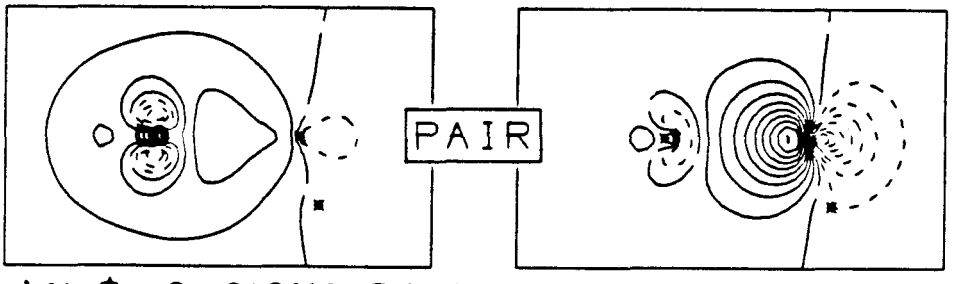

c) $Mn^+ - C$ SIGMA BOND

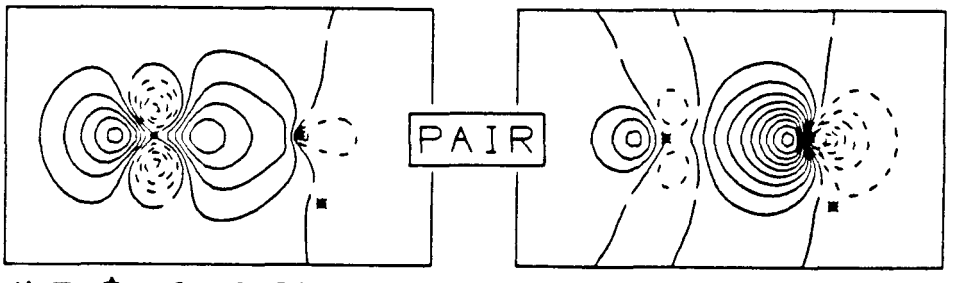

d) $Tc^+ - C$ SIGMA BOND

Figure 4: (a) GVB orbitals for ZnH^+. The Zn^+–H bond length is 1.545 Å and the metal orbital hybridization is 90.7% s, 8.9% p, and 0.4% d. (b) GVB orbitals for CdH^+. The Cd^+–H bond length is 1.709 Å and the Cd^+ orbital hybridization is 90.4% s, 9.2% p, 0.4% d. (c) GVB orbitals for the metal carbon bond in $ZnCH_3^+$ with a metal carbon bond length of 2.020 Å and a metal–carbon–hydrogen angle of 106.3°. The orbital hybridizations are: Zn^+ – 94.8% s, 4.7% p, 0.5% d; and C – 12.6% s, 86.9% p, 0.5% d. (d) GVB orbitals for $CdCH_3^+$ with a metal carbon bond length of 2.275 Å and an M^+–C–H angle of 104.5°. The orbital hybridizations are: Cd^+ – 95.6% s, 4.0% p, 0.4% d; and C – 9.9% s, 89.6% p, 0.5% d.

$M^+ - H$

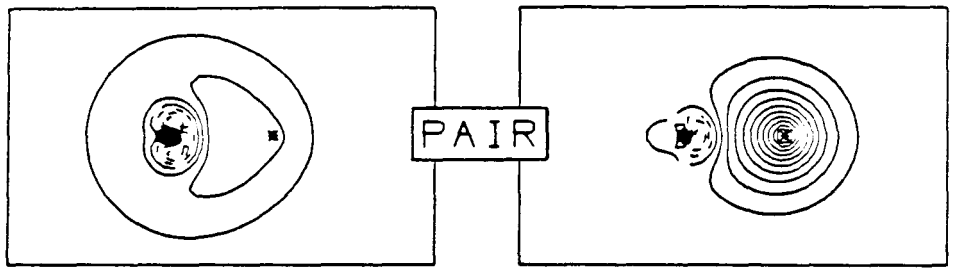

a) $Zn^+ - H$ SIGMA BOND

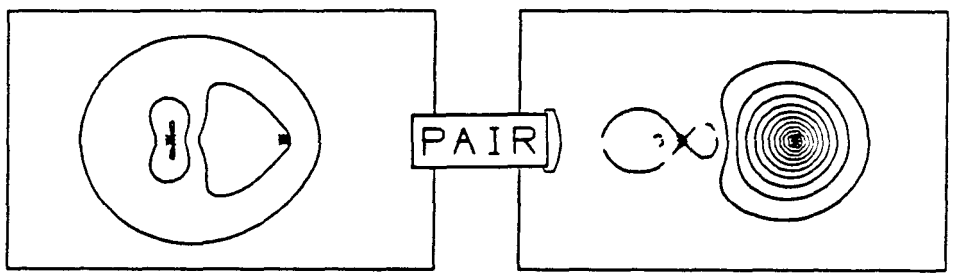

b) $Cd^+ - H$ SIGMA BOND

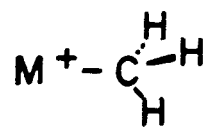

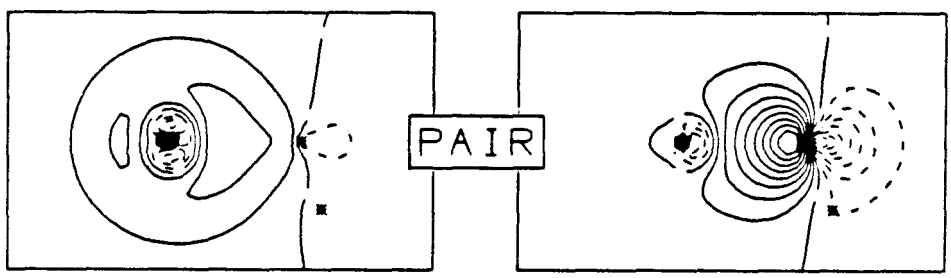

c) $Zn^+ - C$ SIGMA BOND

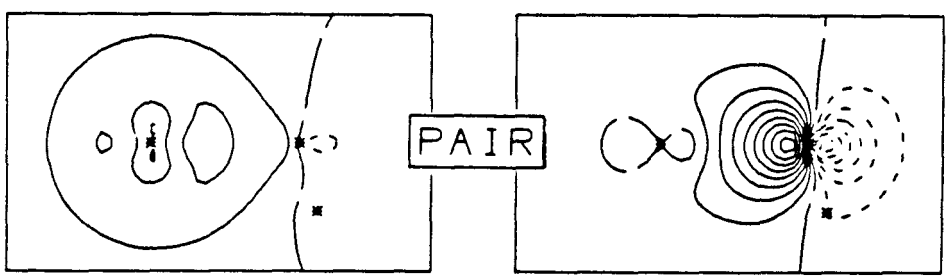

d) $Cd^+ - C$ SIGMA BOND

Figure 5: (a) GVB orbitals for PdH^+. The Pd^+–H bond length is 1.512 Å and the metal orbital hybridization is 5.1% s, 2.1% p, and 92.8% d. (b) GVB orbitals for the metal carbon bond in $PdCH_3^+$ with a metal carbon bond length of 2.123 Å and an M^+–C–H angle of 103.5°. The orbital hybridizations are: Pd^+ – 4.4% s, 1.9% p, 93.7% d; and C – 5.3% s, 93.5% p, 1.2% d. (c) GVB orbitals for the C–H bond in $PdCH_3^+$ with a C–H bond length of 1.094 Å.

$M^+ - H$

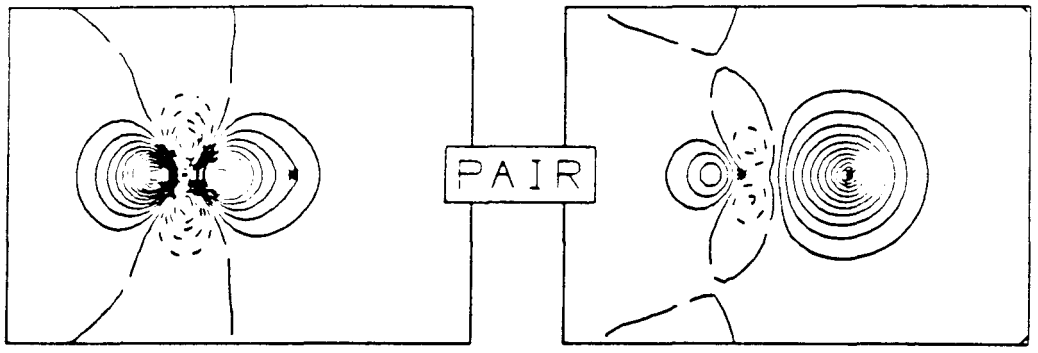

a) $Pd^+ - H$ SIGMA BOND

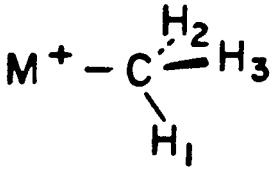

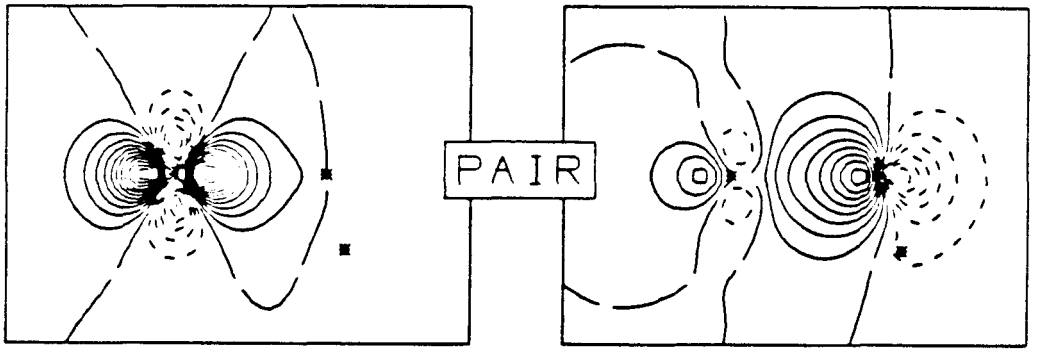

b) $Pd^+ - C$ SIGMA BOND

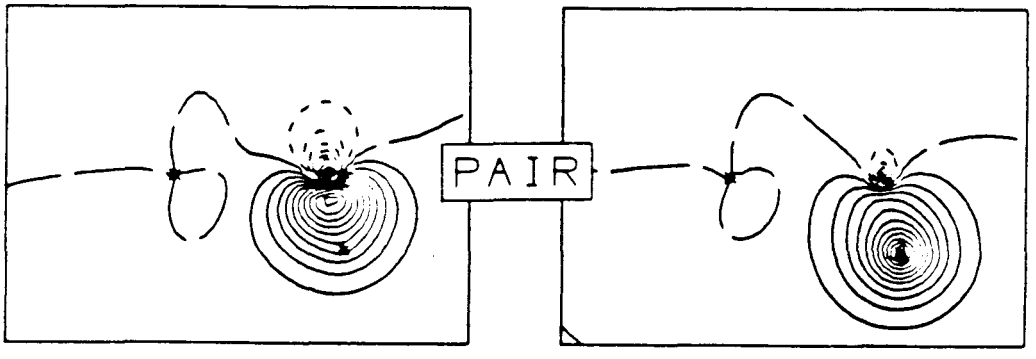

c) $C - H_1$ SIGMA BOND

Table I

Properties of Ground State MH^+ and MCH_3^+

Molecule	State	Geometry[a]		Force Constant		Overlap[d]	Charge Transfer	Hybridization[d]					
								M^+[e]			C[f]		
		$R_e(M^+-X)$ (Å)	$\angle(M^+-C-H)$ (Degrees)	M–R[b] (h/Å²)	M–C–H[c] (mh/Å²)		to Ligand[d]	% s	% p	% d	% s	% p	% d
ScH^+	$^2\Delta^{\pm}$	1.810		0.3571		0.763	0.225	46.2	13.5	40.3			
$ScCH_3^+$	^2E	2.233	111.0	0.3239	0.2194	0.765	0.333	45.7	8.1	46.2	28.5	71.3	0.2
CrH^+	$^5\Sigma^+$	1.602		0.4448		0.734	0.066	40.6	12.5	46.9			
$CrCH_3^+$	$^5A_1$	2.074	103.4	0.3547	0.1866	0.708	0.041	41.9	9.6	48.5	15.3	84.2	0.5
MnH^+	$^6\Sigma^+$	1.702		0.3321		0.718	0.079	76.3	12.5	11.3			
$MnCH_3^+$	$^6A_1$	2.188	106.1	0.1539	0.1807	0.662	0.014	84.7	6.7	8.6	12.8	86.8	0.4
ZnH^+	$^1\Sigma^+$	1.545		0.4713		0.690	0.069	90.7	8.9	0.4			
$ZnCH_3^+$	$^1A_1$	2.020	106.3	0.3718	0.2038	0.647	0.020	94.8	4.7	0.5	12.6	86.9	0.5
YH^+	$^2\Sigma^+$	1.892		0.3645		0.760	0.253	31.9	10.2	57.9			
YCH_3^+	$^2A_1$	2.298	110.9	0.3673	0.2110	0.762	0.288	25.5	6.8	67.7	27.5	72.3	0.2
MoH^+	$^5\Sigma^+$	1.708		0.4530		0.703	0.088	19.7	7.0	73.3			
$MoCH_3^+$	$^5A_1$	2.201	108.1	0.3306	0.2089	0.663	0.114	15.6	3.3	81.1	16.9	82.7	0.4
TcH^+	$^6\Sigma^+$	1.719		0.4099		0.752	0.107	40.5	7.0	52.5			
$TcCH_3^+$	$^6A_1$	2.209	107.7	0.3181	0.2111	0.722	0.128	40.2	3.0	56.8	21.4	78.1	0.5
PdH^+	$^1\Sigma^+$	1.512		0.6323		0.572	-0.115	5.1	2.1	92.8			
$PdCH_3^+$	$^1A_1$	2.123	103.5	0.2786	0.2200	0.475	-0.220	4.4	1.9	93.7	5.3	93.5	1.2
CdH^+	$^1\Sigma^+$	1.709		0.3912		0.674	0.036	90.4	9.2	0.4			
$CdCH_3^+$	$^1A_1$	2.275	104.5	0.2371	0.1850	0.599	-0.063	95.6	4.0	0.4	9.9	89.6	0.5

[a] The C–H bond length is set at 1.094 Å as in CH_4. [b] M–R stretch (hartrees/Å²). In MCH_3^+, the CH_3 geometry is held fixed. Multiply by 4.359 to obtain mdyne/Å and 627.5 to obtain (kcal/mol)/Å². [c] M–C–H symmetric bend (umbrella mode) (millihartrees/degree²). Multiply by 0.6275 to obtain (kcal/mol)/Å² or by 2.060×10^3 to obtain (kcal/mol)/radian². [d] These properties are from the GVB-PP wavefunction. [e] Hybridization for the bonding orbital on M^+. [f] Hybridization of the carbon orbital used for bonding to M^+.

coordinate system is chosen with the carbon atom at the origin and the metal ion along the positive z axis). Figure 6 shows potential curves for MnH^+ and $MnCH_3^+$ for motion of the H or CH_3 group with respect to the metal ion. The geometry of the CH_3 group is kept fixed in a tetrahedral arrangement so that dissociation is to a pyramidal methyl structure rather than the ground state planar geometry. Curves are shown for both the GVB-RCI(1/2) and RCI(1/2)$\times[D_\sigma + S_{M+,val}]$ levels of calculation. The geometry found using the latter calculation level involves an Mn^+–C distance of 2.124 Å and an Mn^+–C–H angle of 107.3 degrees (compared to 2.188 Å and 106.1° for the GVB-RCI(1/2) calculations). The bond thus shows the normal contraction with higher levels of electron correlation (a change of 0.064 Å) and the angle opens up by about one degree. Similar effects are expected if this level of correlation were to be used for the other metal methyl species. The metal-carbon bond length is found to vary considerably from metal to metal, depending upon the size and hybridization of the metal orbital. The second row metals tend to show a longer metal-carbon bond length than the first row metals of the same column, with the difference ranging from 0.25 (Cd) to −0.04 (Tc). However, the bond lengths tend to emphasize the difference in metal orbital hybridization between the two rows more than the differences in metal orbital size, although both are important.

M–C–H angles are largest (111°) for the early metals (Sc and Y), with the most charge transfer to the ligand (0.33 and 0.29), and smallest (104°) for the metals (Pd and Cd), with charge transfer to the metal (−0.22 and -0.06) (Cr is a slight exception). The hybridization of the carbon bond orbital varies also with the charge transfer (28% s for Sc and Y and 5 to 10% s for Pd and Cd). Bond trends are consistent with a more tetrahedral geometry for the CH_3 anion and a more planar geometry for the CH_3 cation.

"Agostic" interactions[24] between C–H sigma bonds and metals have been shown to be important in some metal complexes. These interactions require empty metal orbitals which can interact with the doubly occupied sigma C–H

Figure 6: Potential energy curves showing energy versus M^+–R bond distance for: (a) MnH^+; and (b) $MnCH_3^+$. Curves are shown for both the GVB-RCI(1/2) and RCI(1/2)$\times[D_\sigma + S_{M^+,val}]$ levels of calculation. For $MnCH_3^+$, the H–C–H angles remain fixed at 109.5° for the entire potential curve. Thus the molecule dissociates to pyramidal CH_3 rather than the lowest energy planar configuration. The curves should thus not be used for obtaining values for the Mn^+–CH_3 bond dissociation energy.

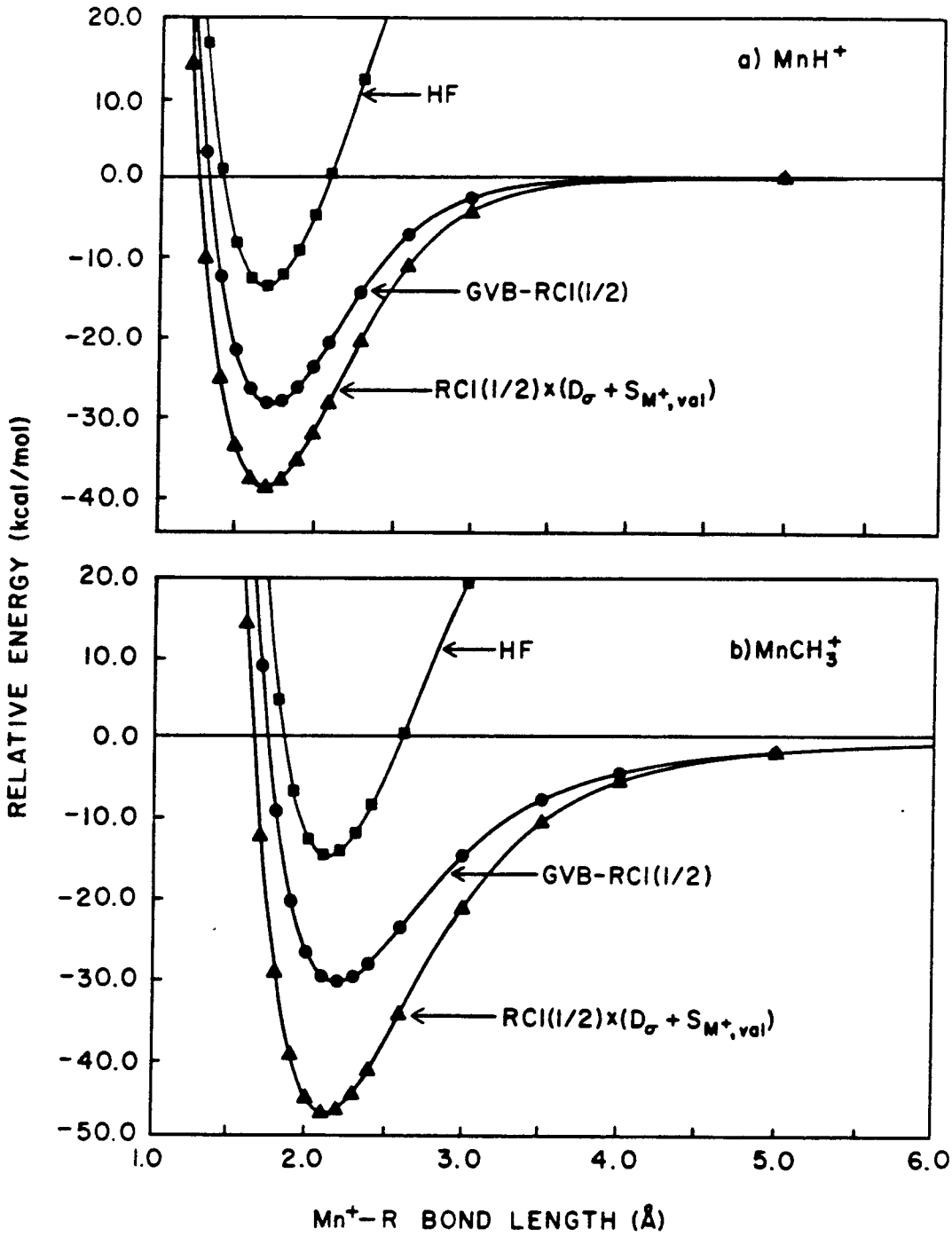
a) MnH+
HF
GVB-RCI(1/2)
RCI(1/2)x(Dσ + SM+,val)
b) MnCH3+
HF
GVB-RCI(1/2)
RCI(1/2)x(Dσ + SM+,val)
RELATIVE ENERGY (kcal/mol)
Mn+–R BOND LENGTH (Å)
20.0
10.0
0.0
-10.0
-20.0
-30.0
-40.0
-50.0
1.0
2.0
3.0
4.0
5.0
6.0

orbital. We thus feel that if agostic interactions are important in the present systems, they should be seen in the early metal systems where there are the largest number of empty metal d orbitals. We have thus performed test calculations on $ScCH_3^+$. Three levels of calculation (GVB(1/2), GVB-RCI(1/2), and RCI(1/2)$\times$[$D_\sigma + S_{M^+,val}$]) were used. Symmetry was restricted to C_s and the H–C–H angles were kept fixed. The geometry was changed by changing the Sc^+–C–H angle in the xz plane. These test calculations show the C_{3v} symmetry to be lowest in energy and we thus conclude that agostic interactions are not important in these ionic systems.

Bond Orbital Hybridization. We find the bonding in the metal methyl and metal hydride systems to be quite similar, with metal orbital hybridizations (Table I) generally changing only a few percent upon replacing CH_3 for H. For all cases, the amount of p character in the metal methyl bond is about half that of the hydrides. This seems to result from the directional nature of the carbon bonding orbital (sp hybrid). The metal adds in p character to polarize the bond in the direction of the ligand. With the nondirectional hydrogen 1s orbital, this effect is more important than with the directional carbon 2p orbital. For the first row metal ions the 4s orbital is more important in bonding than the $3d_{z^2}$ orbital, while for the second row metals the 4d orbitals are more important than the 5s. The general trend in sd hybridization is that, for metal-carbon bonds, the dominant orbital in the hybrid becomes even more dominant as the p character is decreased. The hybridization of the carbon orbital is governed by the charge transfer and the metal atomic configuration. Thus, $ScCH_3^+$ and YCH_3^+ with charge transfers to CH_3 of 0.29 and 0.33 lead to 28% s character in the C orbital, (much like the CH_3 anion), whereas $PdCH_3^+$ and $CdCH_3^+$ with transfers of 0.22 and 0.06 *away* from CH_3 lead to 5 and 10% s character (much like CH_3 radical). The atomic character on the metal ion plays a dominant role. Thus Zn^+ and Cd^+ (both strongly $d^{10}s^1$) lead to bonds with 95% s character. Similarly, Mn^+ (which strongly prefers d^5s^1) leads to 87% s character in the bond. On the other hand,

Mo^+ (strongly d^5) and Pd^+ (strongly d^9) lead to 81% and 94% d character in the bond. For Y^+ and Tc^+, the $d^{n-1}s^1$ to d^n state splittings are 0.88 eV and 0.51 eV[25] respectively (the Y^+ ground state is ^1S (s^2), 0.16 eV below the ^3D (s^1d^1) state), however, the strong d bonding in the second row leads to d character of 68% and 57% in the bonds. Cr^+, like Mo^+, is strongly d^5, however, loss of high spin exchange energy and strong first-row s bonds decrease the d character to 49%. For Sc^+, the $d^{n-1}s^1$ to d^n state splitting is only 0.6 eV and the s and d character in the bond is similar, ~46%.[25]

Bond Energies. We used MnH^+ and $MnCH_3^+$ as the prototypes for studying the effects of various levels of electron correlation on bond energy. Table II shows the bond dissociation energies for these molecules at various levels of calculation. [The generalized valence bond and configuration interaction (CI) wavefunctions are described in the Calculational Details section of the paper.] Major points are:

(1) Proper dissociation: Electron correlation in the bond being formed is essential for proper dissociation to fragments [cf. HF to GVB-PP(1/2)] (see Figure 6).

(2) Spin coupling on the metal: Some triplet character in the bond is induced by spin coupling to the d^5 nonbonding configuration [cf. GVB-PP(1/2) to GVB-RCI(1/2)]. This leads to a 2–3 kcal/mol increase in bond energy for both cases.

(3) M–C and C–H correlations: For $MnCH_3^+$, the correlation in the three C–H bonds adjacent to the Mn^+–C bond is important [cf. GVB-RCI(1/2) to GVB-RCI(4/8)]. It is the instantaneous motion of the two electrons in the M–C bond simultaneously with two electrons in the C–H bond

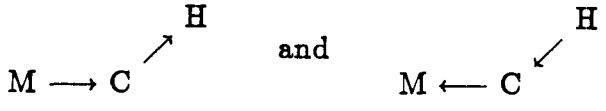

that is important, since there is no difference between GVB-PP(1/2) and GVB-PP(4/8). This is worth 3.6 kcal/mol for the M^+–CH_3 case (there is

Table II

Electron Correlation Effects on the Mn^+–H and Mn^+–CH_3 Bond Dissociation Energies

Calculation Level[a]	Configs/SEFS[b]	$D_e(Mn^+–H)$ (kcal/mol)	Configs/SEFS[b]	$D_e(Mn^+–CH_3)$ (kcal/mol)
HF	1/1	13.6	1/1	8.9
GVB-PP(1/2)	2/2	25.9	2/2	23.2
GVB-PP(4/8)	(2/2)[c]	(25.9)[c]	16/16	23.0
GVB-RCI(1/2)	3/8	28.0	3/8	26.2
GVB-RCI(4/8)	(3/8)[c]	(28.0)[c]	80/1736	29.8
GVB-RCI(1/2)×D_σ	93/333	37.6	333/1463	32.0
RCI(1/2) × [$D_\sigma + S_{M+}$]	168/523	38.7	563/2053	33.2
RCI(1/2) × [$D_\sigma + S_{M+,val}$]	168/523	38.7	726/3896	40.3

[a] See the calculational details section of the text for an explanation of the various calculations. [b] Number of configurations and spin eigenfunctions in the wavefunction. [c] GVB-PP(4/8) and GVB-RCI(4/8) calculations are not possible for MnH^+. The numbers in parentheses are thus from the comparable GVB-PP(1/2) and GVB-RCI(1/2) calculations on MnH^+.

no effect in MH^+).

(4) Full correlation of bond pair: The fully correlated bond pair (within the basis) is obtained with RCI(1/2)×D_σ. This increases the bond energy by 9.6 kcal/mol for MH^+ and 5.5 kcal/mol for MCH_3^+. This does *not* allow for instantaneous correlations in either the metal d electrons or the C–H bonds.

(5) M–R and Md correlations: The -RCI(1/2)×[$D_\sigma + S_{M+}$] allows for readjustment of the metal d orbitals simultaneous with correlation of the electrons in the bond pair. This increases the bond energy 1.1 kcal/mol for M^+–H and 1.2 kcal/mol for M^+–CH_3.

(6) M–R and C–H correlations: The RCI(1/2)×[$D_\sigma + S_{M+,val}$] improves upon (5) by allowing readjustment in all valence electrons simultaneously with correlation in the M–C pair [as in (3)] leading to a 7.1 kcal/mol effect for MCH_3^+.

(7) The M–H and M–C bond energies are very similar with M–C about 1.7 kcal/mol stronger.

(8) The simplest wavefunction with accurate *relative* bonding energies is GVB-RCI(4/8) (only 81 spatial configurations) which leads to a 1.8 kcal/mol stronger M^+–C bond.

The best bond energy estimates come from the RCI(1/2)×[Dσ + $S_{M+,val}$] calculations which involve correlation of both the C–H and M valence electrons and are equivalent to the DCCI-GEOM[20] calculations used for geometry optimization and state splitting calculations on the MH^+ species. For methane this calculation level[26] leads to, $D_e(H - CH_3)$ = 110.5 kcal/mol, only 1.7 kcal/mol below the experimental value of D_e = 112.2 ± 0.5 kcal/mol. This calculation level was used for all bond energy discussions of MH^+ and MCH_3^+.

Table III contains the calculated total energies for several calculation levels for MCH_3^+, MH^+, M^+, CH_3, and H (at the equilibrium geometries for the molecular species). The calculated bond dissociation energies $D_e(M^+–CH_3)$ are presented in Table IV. The bond energies cover a range 35 kcal/mol with a high

Table III

Total Energies for Ground State MCH_3^+, M^+, and CH_3[a]

Species	State	Total Energy (hartrees)[b]				
		GVB(1/2)	GVB-RCI(1/2)	GVB(4/8)	GVB-RCI(4/8)	RCI(1/2)×[$D_\sigma + S_{M^+,\Pi_d}$]
$ScCH_3^+$	^2E	−798.28870	−798.28886	−798.33245	−798.35002	−798.31969
Sc^+	^3D	−758.66317	−758.66317	−758.66317	−758.66317	−758.66317
$CrCH_3^+$	$^5A_1$	−1081.54159	−1081.54681	−1081.58493	−1081.60558	−1081.58053
Cr^+	^6S	−1141.97641	−1141.97641	−1141.97641	−1141.97641	−1141.97641
$MnCH_3^+$	$^6A_1$	−1187.96360	−1187.96851	−1188.00724	−1188.02821	−1188.00024
Mn^+	^7S	−1148.36628	−1148.36628	−1148.36628	−1148.36628	−1148.36628
$ZnCH_3^+$	$^1A_1$	−1815.19427	−1815.19427	−1815.23824	−1815.25403	−1815.22284
Zn^+	^2S	−1775.55652	−1775.55652	−1775.55652	−1775.55652	−1775.55678
YCH_3^+	$^2A_1$	−76.90519	−76.90534	−76.94860	−76.76562	−76.93698
Y^+[c]	^3D	−37.26855	−37.26855	−37.26855	−37.26855	−37.26855
$MoCH_3^+$	$^5A_1$	−106.25144	−106.25742	−106.29466	−106.31573	−106.28996
Mo^+	^6S	−66.67212	−66.67212	−66.67212	−66.67212	−66.67212
$TcCH_3^+$	$^6A_1$	−118.75863	−118.76612	−118.80229	−118.82549	−118.80124
Tc^+	^7S	−79.16302	−79.16302	−79.16302	−79.16302	−79.16302
$PdCH_3^+$	$^1A_1$	−165.24332	−165.24332	−165.28731	−165.29901	−165.27419
Pd^+	^2D	−125.62886	−125.62886	−125.62886	−125.62886	−125.62941
$CdCH_3^+$	$^1A_1$	−85.91881	−85.91881	−85.96305	−85.97796	−85.94760
Cd^+	^2S	−46.29916	−46.29916	−46.29916	−46.29916	−46.30065
CH_3	$^2A_1$	−39.56032	−39.56032	−39.60427	−39.61440	−39.56966

[a] Energies are for molecules at their equilibrium geometries. [b]For MCH_3^+ the total energies are for the calculation levels shown while the M^+ and CH_3 total energies are for the calculation levels to which these MCH_3^+ molecules dissociate (see Calculational Details Section of text). [c]The $^2A_1$ state of YCH_3^+ does not dissociate to ground state Y^+ (^1S) but to ^3D Y^+ as shown here.

Table IV

A Comparison of Theoretical and Experimental MH^+ and MCH_3^+ Bond Dissociation Energies[a]

Metal	Theory						Experiment			
	$D_e(M^+-H)$		$D_e(M^+-CH_3)$		ΔD_e[d]		$D_{298}(M^+-H)$[e]	$D_{298}(M^+-CH_3)$[f]	ΔD_{298}[g]	$\Delta(\Delta D)$[h]
	RCI[b]	CI[c]	RCI[b]	CI[c]	RCI	CI			EXP	
Sc	47.5	56.6	45.5	54.5	-2.0	-2.1	56.2±2.0	59±3	2.8	4.9
Cr	11.2	25.3	9.2	24.1	-2.0	-1.2	27.7±2.0	30±5	2.3	3.5
Mn	28.0	38.7	29.8	40.3	1.8	1.7	48.4±1.4	51±2	2.6	0.9
Zn	44.4	54.7	52.2	60.7	8.8	6.0	57.7[i]	70.6±3.2	12.9	6.9
Y	49.4	58.8	48.2	58.3	-1.2	-0.5	59±3	64±7	5.0	5.5
Mo	22.2	33.8	18.3	30.2	-3.9	-3.6	42±3			
Tc	32.0	44.4	30.2	43.0	-1.8	-1.4				
Pd	30.5	45.3	35.0	47.1	4.5	1.8	45±3[j]	59±5[j]	14.0	12.2
Cd	36.3	45.6	40.4	48.5	4.1	3.8				

[a] All values are given in kcal/mol. [b] RCI represents GVB-RCI(1/2) for MH^+ and GVB-RCI(4/8) for MCH_3^+. [c] CI represents the RCI(1/2)×[D_σ + $S_{M+,val}$] calculation. [d] ΔD_e is defined as $D_e(M^+-CH_3)$ − $D_e(M^+-H)$ for the two levels of calculation. [e] From Reference 13, unless otherwise noted. The values in the reference are given as D_0 and have been changed to D_{298} by addition of 0.9 kcal/mol. [f] From Reference 14, unless otherwise noted. [g] ΔD_{298} is defined as $D_{298}(M^+-CH_3)$ − $D_{298}(M^+-H)$ for the experimental values. [h] $\Delta(\Delta D) = \Delta D_{298}(EXP) - \Delta D_e(CI)$. [i] From Reference 4. [j] From Reference 12.

of 60.7 kcal/mol for $ZnCH_3^+$ and a low of 24.1 kcal/mol for $CrCH_3^+$. As with the metal hydrides, the variation in bond dissociation energies is due to several interrelated factors. The methyl group can be thought of as having a certain "intrinsic" bond energy when bonded to pure metal s, p, or d orbitals. The "intrinsic" bond energies are then moderated by: (1) the energy gained from orbital hybridization; (2) the promotion energy cost to promote the metal ion to an electronic state having the proper metal orbital for bonding to the ligand; and (3) the amount of energy lost due to loss of atomic electron exchange energy (favoring high spin) upon decoupling one metal electron from the others to form the bond.

"Intrinsic" bond energy trends for the metal hydrides[20] indicate that as one moves from left to right in a given row of transition metals, the bond energy to a metal s orbital slowly increases as the s orbital size decreases while the bond energy to a metal d orbital decreases rapidly as the d orbital size decreases. Due to the larger size of the orbitals of the second row metals, s-bonds tend to be slightly weaker and d-bonds (at least toward the later metals) tend to be stronger than for the first row. The general trends are expected to be similar for the metal methyl molecules. This is partially born out by the fact that the strongest bonds are formed by very early (e.g. Sc^+ and Y^+) or very late (e.g. Zn^+ and Cd^+) metals, where the early metals use significant amounts of d character and Zn^+ and Cd^+ use almost all metal s character

The strong bonds formed to the early metals are also due to the presence of low-lying metal electronic states allowing extensive s–d hybridization. This is complimented by the small amounts of exchange energy lost on bonding. The low bond energies for $CrCH_3^+$ and $MoCH_3^+$ (both d^5) are due to the large amount of exchange energy lost on bonding and by the inaccessability of the metal ^6D (d^4s^1) state, which is over 1.5 eV above the ^6S (d^5) ground state.[25]

One must be careful in comparing theoretical and experimental differences between metal hydride and metal methyl bond dissociation energies. The theo-

retical bond energies are D_e values while the experimental values are generally determined at ~298 K. Thus we must estimate the difference between D_e and D_{298} for MH^+ and MCH_3^+. Assuming an ideal gas with only translational and rotational degrees of freedom active, the differences in bond dissociation energies between 0 K and 298 K are: $D_0(M^+–H) = D_{298}(M^+–H) - 0.9$ kcal/mol and $D_0(M^+–CH_3) = D_{298}(M^+–CH_3) – 1.5$ kcal/mol. Our calculations yield the metal-hydrogen or metal-carbon vibrational force constants and also the CH_3 umbrella mode force constant (see Table I), but we did not allow other metal methyl motions in our calculations. The average zero point energy for the hydrides of the nine metal ions in this study is $D_e - D_0 = 2.5$ kcal/mol. Frequencies have been measured experimentally for $CuCH_3$[27], and $ZnCH_3$[28] (in a $BH_4^-ZnCH_3^+$ salt). CH_3Br and CH_3I[23] should also give good estimates for vibrational frequencies. Zero point energies for the four species vary from 21.2 to 22.6 kcal/mol with an average of 22.1 kcal/mol. The experimentally determined vibrational frequencies for the methyl radical[29] lead to a zero point energy of 18.2 kcal/mol. For the MCH_3^+ species, the zero point energy leads to $D_e - D_0 \sim 3.9$ kcal/mol. Thus, for MH^+, $D_{298} = D_e - 1.6$ and for MCH_3^+, $D_{298} = D_e - 2.4$. Thus $D_{298}(M^+–C) - D_{298}(M^+–H) = D_e(M^+–C) - D_e(M^+–H) - 0.8$.

By and large, the theory leads to similar $M^+–H$ and $M^+–C$ bond energies (average difference: 0.4 kcal/mol in favor of $M^+–C$). The values range from 3.6 kcal/mol weaker ($MoCH_3^+$) to 6.0 kcal/mol stronger ($ZnCH_3^+$). On the other hand, experimental studies[13,14,30] find metal methyl ion bond dissociation energies to be stronger than that for the corresponding metal hydrides by about 6 kcal/mol on the average. Indeed, using bond dissociation energies for $Sc^+–Mn^+$ from the most recent ion beam studies,[13,14] the average difference in metal methyl and metal hydrogen bond strengths is 1.7 kcal/mol. For Fe^+, Co^+, Ni^+, and Zn^+ the average experimental difference is 9.9 kcal/mol. Less is known experimentally about the second row transition metals. YCH_3^+ and $RhCH_3^+$ bond energies[12,14] are found to be 5 kcal/mol stronger than the respective hydrides,

while $RuCH_3^+$ and $PdCH_3^+$ are reported 13 and 14 kcal/mol stronger.[12]

Table IV compares the theoretical and experimental bond dissociation energies for various MH^+ and MCH_3^+. It should be pointed out that the CI values for $D_e(M^+–H)$ are for the $RCI(1/2)\times[D_\sigma + S_{M+,val}]$ (DCCI-GEOM calculations of reference 20) which correspond to the calculations on MCH_3^+ and not to the highest level of calculation performed on the metal hydrides (DCCI calculations of reference 20). The numbers presented here will thus be slightly different than the bond dissociation energies published elsewhere[20]. It should also be emphasized that there remain significant uncertainties in the experimental numbers. Most of the $M^+ + H_2$ reactions used for determining $D(M^+–H)$ have been extensively reevaluated to determine the role of excited state metal ions in the beam.[13] This has led to decreases in the experimental $M^+–H$ bond energies by up to 10 kcal/mol (in the case of FeH^+). Similar reevaluation has not been made for most of the metal methyl experiments (the values for VCH_3^+ and $ZnCH_3^+$ are probably the best) so that the experimental bond energies may yet be closer to the metal hydride bond energies (and closer to the theoretical values).

For saturated metal systems, the few molecules where directly comparable bond energies for $M–CH_3$ and M–H bonds have been determined, all lead to much stronger metal hydrogen bonds, with an average difference of 18 kcal/mol. The systems (differences in bond dissociation energies) are: Cp_2MoR_2 (23 kcal/mol),[15] Cp_2WR_2 (23 kcal/mol),[15] $Cp^*_2ThR_2$ (13 kcal/mol),[17] and $Mn(CO)_5R$ (15 kcal/mol)[16] where Cp is the cyclopentadienyl ligand, Cp* is the pentamethylcyclopentadienyl ligand, and R is CH_3 or H. Bond energies to larger alkyl fragments have generally been found to be quite weak (on the order of only 20 kcal/mol in some Co systems).[5] In general, the low M–C bond energies are attributed to steric factors, although it could also be due partly to the relaxation energies of the alkyl radical (which is absent in the M–H bond breaking process).

Several theoretical calculations comparing M–H and $M–CH_3$ bonds in neu-

tral metal systems have also been carried out. Low and Goddard[31] studied PdR_2 and PtR_2 (R = H, CH_3), finding average bond energy differences of 14.2 and 15.7 kcal/mol for Pd and Pt respectively (M–H stronger than M–C), whereas for $(PH_3)_2PdR_2$ and $(PH_3)_2PtR_2$ they find differences of 17.3 and 18.7 kcal/mol. These calculations did not correlate the CH bonds (although they did correlate the d orbitals) and hence may be biased against the M-C bonds. Carter and Goddard[26] studied several ClRu–R systems, which yielded Ru–H and Ru–CH_3 bond energies that are within 0.2 kcal/mol of each other when electron correlation is included between the M–C and C–H bond electrons, while the Ru–CH_3 bond energy is weaker than the Ru–H bond energy by 13 kcal/mol when this electron correlation is not included. Calculations on Cr^+–R *without* correlation of the C–H electrons[32] lead to a chromium methyl bond energy which is 7.1 kcal/mol lower than the chromium hydrogen bond energy while the present study (including this correlation) gives a bond energy difference of only 1.2 kcal/mol. Thus, for bond energy purposes, correlation of the C–H electrons with the electrons in the bond being broken is very important (5–13 kcal/mol). Summarizing, the calculations suggest that the M–C and M–H bonds are very similar in systems with little or no steric hindrance.

For the metal ion systems, the "increased" strength of the metal carbon bond is usually explained as due to stabilization of the ionic charge by either resonance effects

$$M^+—CH_3 \longleftrightarrow M—CH_3^+$$

or through an ion-induced dipole interaction. The latter effect can be estimated using

$$V(r) = \frac{-e^2\alpha}{2R^4} = \frac{166\alpha}{R_o^4} \text{ kcal/mol}$$

where R_o is the internuclear separation in Å, α is the ligand polarizability in $Å^3$, and e is the unit charge of the electron.[33] Average values of α for H and CH_3 are 0.4 $Å^3$ and 1.95 $Å^3$, respectively.[33,34] Although this equation does not

take into account covalent bonding interactions or electron-electron repulsion, it does give some idea as to the stability that could be imparted due to dipolar effects. Setting R_0 equal to the calculated bond lengths for the species, the average difference in V(r) for M^+–H and M^+–CH_3 is only 5.5 kcal/mol. Thus it is possible that ion-induced-dipole effects could play a small part in the bonding. However, the charge transfer from the metal to the ligand for MH^+ and MCH_3^+ is quite similar, and differences in charge transfer do not correlate with increased metal methyl bond energies.

III. Summary

We report ab initio theoretical calculations on MCH_3^+ for nine transition metal systems representing a variety of bonding conditions. In all instances the metal methyl bonds are very similar to the sigma bonds found in MH^+ systems. This similarity includes bond orbital overlaps, charge transfer, and metal orbital hybridization. A comparison of M^+–C and M^+–H theoretical bond energies also shows that the two types of sigma bond are very similar (the average difference for the nine metal systems being ~0.4 kcal/mol).

IV. Calculational Details

Basis Sets. The same metal basis sets have been used as in the previously published metal hydride calculations. The first row metals are described by the all electron valence double-zeta (VDZ) basis sets of Rappé and Goddard[35] (13s,10p,5d/5s,4p,2d). The second row metals, except Cd, are described using the effective potential basis sets of Hay and Wadt,[36] which treat the 4s, 4p, 5s, 4d electrons explicitly (5s,5p,4d/4s,4p,3d). The Cd basis is also a Hay and Wadt effective potential basis,[37] however, the 4s and 4p electrons are included in the effective core potential (3s,3p,4d/3s,3p,3d). The Dunning/Huzinaga[38] VDZ bases were used for C (9s,5p/3s,2p) and H (4s/2s), where $\zeta = 1.2$ for H bonded to C and $\zeta = 1.0$ for H bonded to M. One set of d polarization functions is included on C (ζ =0.64).[39]

Geometry Optimization. The metal methyl ion geometries were optimized at the GVB-RCI(1/2) level of calculation (generalized valence bond restricted configuration interaction). The geometry was optimized as follows. The orientation around the carbon was initially fixed (C_{3v} symmetry) using tetrahedral bond angles (109.5°) and the methane bond length (1.094 Å). The metal-carbon bond length was then optimized. Using this new M^+–C bond length the optimum M^+–C–H angle was found. If the bond angle changed by greater than 5°, a second bond length optimization was performed. The C–H bond distance remained fixed throughout the geometry optimization.

Wave Functions. Bond dissociation energies were calculated at the GVB-PP(1/2), GVB-PP(4/8), GVB-RCI(1/2), GVB-RCI(4/8), RCI(1/2) × D_σ, RCI(1/2)×[D_σ + S_{M+}], and RCI(1/2)×[D_σ + $S_{M+,val}$] levels of calculation. A comparison of the bond energies for MnH^+ and $MnCH_3^+$ at the various levels is presented in Table II. The CI bond energies presented in Table IV for all species is at the RCI(1/2)×[D_σ + $S_{M+,val}$] level, which allows the molecules to dissociate smoothly to the metal ion and the ground state of the ligand. All molecules dissociate to the ground electronic state of the metal ion except for

YCH_3^+ which dissociates to CH_3 and ^3D Y^+. In this case the bond energy is determined by subtracting the experimental state splitting between the ^3D and ^1S states from the diabatic dissociation energy. A description of the various SCF and configuration interaction calculations follows:

1) GVB-PP(1/2) and GVB-PP(4/8): In the perfect pairing (PP) approach to GVB, each bond pair is assumed to have pure singlet spin pairing (as in a simple VB spin function), but all orbitals are optimized. For N bond pairs, this leads to 2^N configurations.

2) GVB-RCI(1/2) and GVB-RCI(4/8): Restricted CI calculations allow the two electrons of each GVB bond pair to occupy the two orbitals in all three possible ways, allowing either covalent or ionic bonding. This allows all spin couplings (different VB structures), a particularly important effect for atoms with partially filled d configurations. For a wavefunction with N GVB pairs, this leads to 3^N configurations and hence three configurations for (1/2) and 81 configurations for (4/8). These calculations are dissociation-consistent: GVB-RCI(1/2) dissociates to a Hartree-Fock (HF) description of both M^+ and CH_3; GVB-RCI(4/8) dissociates to an HF description of M^+ and a GVB-RCI(3/6) description of CH_3. For the metal hydrides the GVB-RCI(1/2) calculations dissociate to HF fragments.

3) RCI(1/2)$\times D_\sigma$: From the three RCI configurations all single and double excitations are allowed out of the metal-ligand σ bond to all virtual orbitals. This calculation allows for all correlation between the two electrons of the bond pair. It dissociates to an HF$\times S_\sigma$ description for both the metal ion and the CH_3 fragments (the single excitation is from the s or d_{z^2} orbital on the metal, depending on which is used for bonding, and from the p_z orbital on CH_3). Metal hydrides dissociate to an HF$\times S_\sigma$ description of M^+ and an HF H atom.

4) RCI(1/2)$\times[D_\sigma + S_{M+}]$: To the configurations of (3) we add all those formed by starting with the RCI configurations and allowing single excitations from the metal nonbonding valence orbitals (to all occupied and virtual orbitals). This calculation dissociates to an HF calculation on the ligand and an all singles

CI for the metal valence orbitals.

5) RCI(1/2)×[D_σ + $S_{M^+,val}$]: This calculation is similar to (4) except that the single excitations are allowed out of all valence orbitals, not just those of the metal ion. For the metal hydrides the two calculations are the same. The metal methyls dissociate to an HF×S_{val} description on both fragments. This leads to an overcorrelation of the fragments in some cases (if single excitations on the metal lead to an energy lowering, e.g., $ZnCH_3^+$, $PdCH_3^+$, and $CdCH_3^+$) and hence to a calculated dissociation energy that may be slightly too low. This effect is not large and calculations by Carter and Goddard[22] on $RuCH_2$ involving a similar dissociation error show that the bond energy is underestimated by ~0.2 kcal/mol. We expect a similar error in our cases. As a test of the adequacy of this level of electron correlation, Carter and Goddard[26] performed a similar calculation breaking the C–H bond in CH_4. The theoretical bond dissociation energy was calculated at 110.5 kcal/mol in comparison to an experimental D_e of 112.2±0.5 kcal/mol. The calculated bond dissociation energy is thus only 1.7 kcal/mol lower than the experimental value, suggesting that our comparable calculations on MCH_3^+ species should be quite adequate.

Acknowledgement. We thank the National Science Foundation (Grant Nos. CHE83-18041 and CHE84-07857) for partial support of this work.

References

(1) Conner, J. A. *Top. Curr. Chem.* **1979**, *71*, 71.

(2) (a) Skinner, H. A. *Adv. Organomet. Chem.* **1964**, *2*, 49. (b) Skinner, H. A. *J. Chem. Thermodyn.* **1964**, *10*, 309.

(3) Gaydon, A. G. "Dissociation Energies and Spectra of Diatomic Molecules", Chapman and Hall, London, 1968.

(4) Huber, K. P.; Herzberg, G. "Molecular Spectra and Molecular Structure. IV. Constants of Diatomic Molecules", Van Nostrand Reinhold, New York, 1979.

(5) (a) Halpern, J. *Acc. Chem. Res.* **1982**, *15*, 238. (b) Halpern, J. *Inorg. Chim. Acta* **1985**, *100*, 41.

(6) (a) Yoneda, G.; Blake D. M. *J. Organomet. Chem.* **1980**, *190*, C71. (b) Yoneda, G.; Blake, D. M. *Inorg. Chem.* **1981**, *20*, 67.

(7) Sallans, L.; Kelley, R. L.; Squires, R. R.; Freiser, B. S. *J. Am. Chem. Soc.* **1986**, *107*, 4379.

(8) Tolbert, M. A.; Beauchamp, J. L. *J. Phys. Chem.* **1986**, *90*, 5015.

(9) (a) Hettich, R. L.; Freiser, B. S. *J. Am. Chem. Soc.* **1986**, *108*, 2537. (b) Hettich, R. L.; Jackson, T. C.; Stanko, E. M.; Freiser, B. S. *J. Am. Chem. Soc.* **1986**, *108*, 5086.

(10) (a) Armentrout, P. B.; Halle, L. F.; Beauchamp, J. L. *J. Chem. Phys.* **1982**, *76*, 2449. (b) Stevens, A. E.; Beauchamp, J. L. *Chem. Phys. Lett.* **1981**, *78*, 291.

(11) Armentrout, P. B.; Halle, L. F.; Beauchamp, J. L. *J. Am. Chem. Soc.* **1981**, *103*, 6501.

(12) Mandich, M. L.; Halle, L. F.; Beauchamp, J. L. *J. Am. Chem. Soc.* **1984**, *106*, 4403.

(13) (a) Elkind, J. L.; Armentrout, P. B. *Inorg. Chem.* **1986**, *25*, 1078. (b) Elkind, J. L.; Armentrout, P. B. *J. Am. Chem. Soc.* **1986**, *108*, 2765. (c) Elkind, J. L.; Armentrout, P. B. *J. Phys. Chem.* **1986**, *90*, 5736. (d)

Elkind, J. L.; Armentrout, P. B. *J. Phys. Chem.* **1986**, *90*, 6576.

(14) (a) Georgiadis, R.; Armentrout, P. B. *J. Am. Chem. Soc.* **1986**, *108*, 2119. (b) Aristov, N.; Armentrout, P. B. *J. Am. Chem. Soc.* **1986**, *108*, 1806. (c) Elkind, J. L.; Aristov, N.; Georgiadis, R.; Sunderlin, L.; Armentrout, P. B., to be published.

(15) Dias, A. R.; Salema, M. S.; Simões, J. A. M. *FJ. Organomet. Chem.* **1981**, *222*, 69.

(16) Conner, J. A.; Zafaroni-Moattar, M. T.; Bickerton, J.; El Saied, N. I.; Suradi, S.; Carson, R.; Al Takhin, G.; Skinner, H. A. *Organometallics* **1982**, *1*, 1166.

(17) Bruno, J. W.; Marks, T. J.; Morss, L. R. *J. Am. Chem. Soc.* **1983**, *105*, 6824.

(18) Simões, J. A. M.; Beauchamp, J. L., review submitted for publication.

(19) See, for example: Ng, F. T. T.; Rempel, G. L.; Halpern, J. *Inorg. Chim. Acta.* **1983**, *77*, L165.

(20) (a) Schilling, J. B.; Goddard, W. A., III; Beauchamp, J. L. *J. Am. Chem. Soc.* 1986 108 582 (b) Schilling, J. B.; Goddard, W. A., III; Beauchamp, J. L., submitted for publication. (c) Schilling, J. B.; Goddard, W. A., III; Beauchamp, J. L., submitted for publication.

(21) See, for example: (a) Rappé, A. K.; Goddard, W. A., III *J. Am. Chem. Soc.* **1977**, *99*, 3966. (b) Rappé, A. K.; Goddard, W. A., III, In "Potential Energy Surfaces and Dynamics Calculations", Truhlar, D. G., Ed., Plenum Press, New York, 1981. (c) Steigerwald, M. L. Ph.D. Thesis, California Institute of Technology, Pasadena, CA 91125, 1983. (d) Carter, E. A.; Goddard, W. A., III *J. Am. Chem. Soc.* **1984**, *88*, 1485.

(22) Carter, E. A.; Goddard, W. A., III *J. Am. Chem. Soc.* **1986**, *108*, 2180.

(23) Herzberg, G. "Molecular Spectra and Molecular Structure. III. Electronic Spectra of Polyatomic Molecules", Van Nostrand Reinhold, New York, 1966.

(24) Brookhart, M.; Green, M. L. H. *J. Organomet. Chem.* **1983**, *250*, 395.

(25) Moore, C. E. "Atomic Energy Levels", National Bureau of Standards, Washington, D.C., 1971, Vol. I, II, and III.

(26) Carter, A. E.; Goddard, W. A., III, manuscript in preparation.

(27) Adams, D. M. "Metal-ligand and Related Vibrations: A Critical Survey of the Infrared and Raman Spectra of Metallic and Organometallic Compounds", Edward Arnold Ltd., London, 1967.

(28) Nibler, J. W.; Cook, T. H. *J. Chem. Phys.* **1973**, *58*, 1596.

(29) (a) Holt, P. L.; McCurdy, K. E.; Weisman, R. B.; Adams, J. S.; Engel, P. S. *J. Chem. Phys.* **1984**, *81*, 3349. (b) Tan, L. Y.; Winer, A. M.; Pimentel, G. C. *J. Chem. Phys.* **1972**, *57*, 4028. (c) Amano, T.; Bernath, P. F.; Yamada, C.; Endo, Y.; Hirota, E. *J. Chem. Phys.* **1982**, *77*, 5284. (d) Snelson, A. *J. Phys. Chem.* **1970**, *74*, 537.

(30) Tolbert, M. A.; Beauchamp, J. L. *J. Am. Chem. Soc.* **1984**, *106*, 8117.

(31) (a) Low, J. J.; Goddard, W. A., III *J. Am. Chem. Soc.* **1984**, *106*, 6928. (b) Low, J. J.; Goddard, W. A., III *Organometallics* **1986**, *5*, 609. (c) Low, J. J.; Goddard, W. A., III *J. Am. Chem. Soc.* **1986**, *108*, 6115.

(32) Alverado-Swaisgood, A. E.; Allison, J.; Harrison, J. F. *J. Phys. Chem.* **1985**, *89*, 2517.

(33) Benson, S. W. "Thermochemical Kinetics", Wiley, New York, 1976.

(34) Hirschfelder, J. O.; Curtiss, C. F.; Bird, R. B. "Molecular Theory of Gases and Liquids", Wiley, New York, 1954.

(35) (a) Rappé, A. K.; Goddard, W. A., III, to be published. (b) Rappé, A. K.; Smedley, T. A.; Goddard, W. A., III *J. Phys. Chem.* **1981**, *85*, 260.

(36) Hay, J. P.; Wadt, W. R. *J. Chem. Phys.* **1985**, *82*, 299.

(37) Hay, J. P.; Wadt, W. R. *J. Chem. Phys.* **1985**, *82*, 270.

(38) (a) Huzinaga, S. J. *J. Chem. Phys.* **1965**, *42*, 1293. (b) Dunning, J. H., Jr. *J. Chem. Phys.* **1970**, *43*, 2823.

(39) Bair, R. A.; Goddard, W. A., III, unpublished results.